UNIVERSIDADE DE MOGI DAS CRUZES
MARIANA NASCIMENTO ROMERO TRUJILHO

ESTUDO DE RESÍDUOS CRUCIAIS PARA A MODULAÇÃO DE METACASPASES DE DIFERENTES ORGANISMOS

Mogi das Cruzes, SP
2025

UNIVERSIDADE DE MOGI DAS CRUZES

MARIANA NASCIMENTO ROMERO TRUJILHO

ESTUDO DE RESÍDUOS CRUCIAIS PARA A MODULAÇÃO DE METACASPASES DE DIFERENTES ORGANISMOS

Tese apresentada ao Programa de Pós-Graduação da Universidade de Mogi das Cruzes como parte dos requisitos para obtenção do grau de Doutor em Biotecnologia.

Área de concentração: Biologia Molecular

Orientador: Prof. Dr. Maurício Ferreira Marcondes Machado

Mogi das Cruzes, SP

2025

FINANCIAMENTO







Ficha catalográfica
Universidade de Mogi das Cruzes - Biblioteca Central

Trujilho, Mariana Nascimento Romero
T866e Estudos de resíduos cruciais para a modulação de metacaspases de diferentes organismos / Mariana Nascimento Romero Trujilho. -- Mogi das Cruzes, SP: Universidade de Mogi das Cruzes, 2025.
134 f. : il.

Tese (Doutorado em Biotecnologia) -- Universidade de Mogi das Cruzes, 2025.
Orientação: Prof. Dr. Mauricio Ferreira Marcondes Machado.
Inclui bibliografia.

1. Metacaspase 2. Saccharomyces cerevisiae 3. Trypanosoma brucei 4. Chalconas 5. Flavonoides 6. Tripanossomíase I. Machado, Maurício Ferreira Marcondes II. Universidade de Mogi das Cruzes III. Título

CDD 660.6

Elaborada por Maria Cristina Alves Silva Xavier – CRB-8/10077

ATAS

ATA DA SESSÃO PÚBLICA DE DEFESA DE TESE DE DOUTORADO EM BIOTECNOLOGIA DA UNIVERSIDADE DE MOGI DAS CRUZES.

Às quatorze horas e trinta minutos do dia três de fevereiro de dois mil e vinte e cinco, pela Universidade de Mogi das Cruzes, realizou-se a defesa da tese intitulada "ESTUDO DE RESÍDUOS CRUCIAIS PARA A MODULAÇÃO DE METACASPASES DE DIFERENTES ORGANISMOS" para obtenção do grau de doutor(a) pelo(a) candidato(a) **Mariana Nascimento Romero Trujilho**. Tendo sido o número de créditos alcançados pelo(a) mesmo(a) no total de 75 (setenta e cinco), a saber: 39 unidades de crédito em disciplinas e atividades na pós-graduação e 36 unidades de crédito no preparo da tese o(a) aluno(a) perfaz assim os requisitos para obtenção do grau de doutor(a). A comissão examinadora foi constituída pelos senhores professores doutores: Mauricio Ferreira Marcondes Machado, Wagner Alves de Souza Júdice, e Tatiane Faustino de Moraes, da Universidade de Mogi das Cruzes, e Vitor Marcelo Silveira Bueno Brandão de Oliveira, e Mirian Akemi Furuie Hayashi, da Universidade Federal de São Paulo, sob a presidência do primeiro, como orientador do(a) aluno(a). A sessão pública da defesa da tese foi aberta pelo senhor presidente da comissão que apresentou o(a) candidato(a). Em seguida o(a) candidato(a) realizou uma apresentação oral de seu trabalho, ao final da qual seguiram-se as arguições pelos membros da comissão examinadora. A seguir, a comissão, em sessão secreta, conforme julgamento discriminado por cada membro, considerou o(a) candidato(a)

aprovada (aprovado(a)/reprovado(a)) por UNANIMIDADE (unanimidade/maioria).

Mogi das Cruzes, 03 de fevereiro de 2025.

Comissão Examinadora	Julgamento
Prof. Dr. Vitor Marcelo Silveira Bueno Brandão de Oliveira	Aprovada (aprovado(a)/reprovado(a))
Profª Drª Mirian Akemi Furuie Hayashi	Aprovada (aprovado(a)/reprovado(a))
Prof. Dr. Wagner Alves de Souza Júdice	Aprovada (aprovado(a)/reprovado(a))
Profª Drª Tatiane Faustino de Moraes	Aprovada (aprovado(a)/reprovado(a))
Prof. Dr. Mauricio Ferreira Marcondes Machado	APROVADA (aprovado(a)/reprovado(a))

AGRADECIMENTOS

Agradeço primeiramente a Deus por me dar a vida, por me permitir ser tão rica com tanto amor e pessoas tão incríveis a minha volta, a minha vida é toda Dele, e quero sempre continuar sendo usada por Deus no meu caminho.

Agradeço ao meu noivo Felipe que a quase 10 anos me completa, me ensina a cada dia a ser uma pessoa melhor, me inspira, incentiva e me faz acreditar que juntos alcançamos tudo. Seu jeito único de enxergar e tratar o mundo faz com que tudo fique mais feliz e iluminado, te admiro muito.

Aos meus pais Marcos e Márcia que me ensinaram a ser quem eu sou, me mostraram que acima de tudo família é nossa maior riqueza. Sei o quanto se sacrificaram a vida toda para que eu tivesse o melhor estudo, inglês e que não faltasse nada. Eu valorizo muito e serei para sempre a filha companheira, que vai sempre retribuir com vários cafés da tarde, momentos que valorizamos tanto por estar ao redor da mesa juntos conversando.

A minha irmã e grude Manuela, que desde sempre foi tudo que eu pedia de Páscoa, natal ou aniversário. Sempre soube que compartilhar a vida com você seria a melhor coisa do mundo. Sou grata por ver você crescer e se tornar essa mulher tão linda e inteligente, continuarei cuidando e te irritando para sempre, afinal esse é meu papel como irmã mais velha.

Aos meus avós Evangelina, Antônio, Dina e Fernando (em memória) que sempre me deram o amor mais puro, e quando cansada me curaram com um bolo quentinho e uma boa conversa. Meu avô Fernando que antes mesmo de imaginar em fazer doutorado já me recebia com “Oi, doutora” e fazia meu dia. Vocês sempre enxergaram um potencial gigantesco em mim que nunca imaginei.

As minhas tias, Fernanda e Melissa, tios e primos que marcaram minha vida com temakis e caixas de twix, e deixavam a vida mais leve e divertida com momentos juntos jogando vôlei, taco na rua e jogos de tabuleiro, sou muito grata por viver esses momentos com vocês.

Ao meu orientador e professor Dr. Maurício Machado para sempre minha gratidão por ter mudado não só minha graduação, mas a minha vida. Me deu oportunidades sem igual permitindo que eu conhecesse a ciência, me apresentasse em congressos, usasse reagentes e equipamentos caros. Mas foi muito além e me deu conselhos de vida, amizade, dedicou seu tempo e me fez acreditar que aquela

menina de 18 anos poderia se tornar uma cientista, biomédica e futura doutora. Foi através dele que me encontrei na ciência, e nela vejo seu encanto em pelo menos uma fração de segundo descobrir algo que ninguém no mundo sabe.

Ao professor Dr. Wagner Júdice com quem tive conversas que orientaram minha vida profissional e pessoal, sei que sua bondade te acompanhará e te trará inimagináveis alegrias na vida.

Aos meus amigos do CIIB por fazerem essa trajetória ser mais leve e divertida, e em momentos de resultados negativos me levarem para tomar uma casquinha no shopping até surgirem ideias de como solucionar. Meu muito obrigada em especial a Taiz, Maffeis, João, Ane e Vitória.

Aos professores da graduação, que me inspiraram a continuar na vida acadêmica, vocês sempre serão grandes exemplos para mim.

Ao Professor Dr. Tarsis Gesteira que me recebeu em seu laboratório em Houston, e me deu oportunidade de conhecer a ciência em outro país.

Ao Professor Dr. Marcelo Marcondes por me receber em seu laboratório na UNIFESP e pelos ensinamentos sobre clonagem.

A Universidade de Mogi das Cruzes (UMC) pelo suporte e oportunidade ao longo desses 8 anos de instituição.

O presente trabalho foi realizado com o apoio da Coordenação de Aperfeiçoamento de Pessoal de Nível Superior - Brasil (CAPES) - Código de Financiamento 88887.609321/2021-00.

O presente trabalho foi realizado com o apoio da concessão da bolsa de mestrado processo nº 2022/06394-0, da Fundação de Amparo à Pesquisa do Estado de São Paulo (FAPESP).

EPÍGRAFE

“Eu sei que meu trabalho é uma gota no oceano,
mas sem ele o oceano seria menor”

Madre Teresa de Calcutá

RESUMO

As metacaspases são cisteíno-proteases da família C14, caracterizadas pela especificidade de clivagem pós-resíduos básicos e dependência de cálcio para ativação. Este estudo investigou a metacaspase tipo I de Saccharomyces cerevisiae (YCA1) e a metacaspase tipo II de Trypanosoma brucei (TbMCA2), destacando o papel de resíduos conservados na interação com cálcio e na regulação da atividade enzimática. Análises estruturais e funcionais identificaram a díade catalítica (Cys-His) e aspartatos críticos para a ligação ao cálcio. Experimentos de mutação sítio-dirigida demonstraram que o Asp283 é essencial para a estabilização e ativação da YCA1, enquanto mutações em Asp236, Asp252 e Asp253 impactaram marginalmente a função enzimática. A versão truncada YCA1-ΔN86 manteve atividade catalítica, sugerindo um mecanismo alternativo de ativação e diferenças na afinidade por cálcio mediadas pelo pró-domínio N-terminal. Adicionalmente, a triagem de compostos naturais revelou que quatro moléculas, incluindo derivados de chalcona e flavonoides, inibiram significativamente a TbMCA2, com três apresentando inibição competitiva e uma, inibição não competitiva. Estes achados reforçam a relevância dos resíduos de interação com cálcio na regulação das metacaspases e destacam novas perspectivas para o desenvolvimento de inibidores com potencial terapêutico contra a tripanossomíase humana africana. O estudo amplia a compreensão dos mecanismos moleculares de ativação e modulação das metacaspases, oferecendo subsídios para futuras aplicações biotecnológicas e farmacológicas.

Palavras-chaves: metacaspase; *Saccharomyces cerevisiae*; T*rypanosoma brucei*; chalconas; flavonoides.

ABSTRACT

Metacaspases are cysteine proteases of the C14 family, characterized by cleavage specificity after basic residues and calcium dependency for activation. This study investigated type I metacaspase from Saccharomyces cerevisiae (YCA1) and type II metacaspase from Trypanosoma brucei (TbMCA2), highlighting the role of conserved residues in calcium interaction and enzymatic activity regulation. Structural and functional analyses identified the catalytic dyad (Cys-His) and critical aspartates for calcium binding. Site-directed mutagenesis experiments demonstrated that Asp283 is essential for YCA1 stabilization and activation, while mutations in Asp236, Asp252, and Asp253 had marginal effects on enzymatic function. The truncated version YCA1-ΔN86 retained catalytic activity, suggesting an alternative activation mechanism and differences in calcium affinity mediated by the N-terminal pro-domain. Additionally, screening of natural compounds revealed that four molecules, including chalcone and flavonoid derivatives, significantly inhibited TbMCA2, with three exhibiting competitive inhibition and one displaying non-competitive inhibition. These findings reinforce the relevance of calcium-interacting residues in metacaspase regulation and highlight new perspectives for developing inhibitors with therapeutic potential against human African trypanosomiasis. This study enhances the understanding of the molecular mechanisms of metacaspase activation and modulation, providing insights for future biotechnological and pharmacological applications.

Keywords: metacaspase, *Saccharomyces cerevisiae*, *Trypanosoma brucei*, chalcones, flavonoids

LISTA DE ILUSTRAÇÕES

INTRODUÇÃO

Figura 1 - Principais subtipos de morte celular regulada.....20
Figura *2* - Via extrínseca e via intrínseca da morte celular por apoptose.....24
Figura 3 - Representação do conceito de exopeptidase e endopeptidase.....27
Figura 4 - Local de clivagem de substratos pelas exopeptidases e endopetidases....28
Figura 5 - Representação da interação dos sub-sítios de uma protease.....29
Figura 6 - Representação estrutural da papaína.....31
Figura 7 - Mecanismo esquemático de reação da cisteína protease mediada pela clivagem de uma ligação peptídica.....32
Figura 8 - Classificação das císteino-proteases em clãs e famílias.....33
Figura 9 - Mecanismo de ativação proposto para as caspases e metacaspases.....35
Figura 10 - Comparação das caspases e metacaspases: composição dos domínios e características bioquímicas.....36
Figura 11 - Estrutura cristalográfica da metacaspase de *Saccharomyces cerevisiae* (YCA1).....38
Figura 12 - Caracterização do sítio ativo da YCA1.....39
Figura 13 - Comparação estrutural entre Yca1 e TbMCA2.....40
Figura 14 - Imagens de microscopia eletrônica de varredura de células de *Saccharomyces* cerevisiae.....41

CAPÍTULO 1

Figura 1 - Mutação sítio dirigida por técnica de sobreposição de fragmentos.....64
Figura 2 - Eletroforese em gel de agarose 1% do produto da amplificação gerado na primeira etapa da reação de sobreposição de fragmentos.....65
Figura 3 - Eletroforese em gel de agarose 1% do produto da amplificação da segunda etapa da reação de sobreposição de fragmentos.....66
Figura 4 - Método *T5 exonuclease DNA assembly (TEDA)*.....67
Figura 5 – Eletroforese em gel de agarose 1% do produto da amplificação do vetor e da YCA1 com os primers TEDA. 68
Figura 6 - Eletroforese em gel de agarose 1% do produto da amplificação dos plasmídeos obtidos em colônias de E. coli *BL21(DE3)pLysS*.....69

CAPÍTULO 2

Figura 1 - Alinhamento da sequência primária da YCA1 íntegra com a sequência primária da TbMCA2.....82
Figura 2 - SDS-PAGE das frações eluídas na purificação por cromatografia de afinidade da YCA1..... 84
Figura 3 - SDS-PAGE das frações eluídas na purificação por cromatografia de afinidade da YCA1-ΔN86. 86
Figura 4 - *Western Blotting* da (A) YCA1 íntegra, (B) YCA1-ΔN86, (C) YCA1 íntegra e seus respectivos mutantes (D236A, D252A, D253A, D283A E D252/253) e (D) YCA1-ΔN86 e seus respectivos mutantes (D236A, D252A, D253A, D283A E D252/253) através de reconhecimento por anticorpo primário *anti-6XHis-tag*.....90
Figura 5 - Teste de maturação dos mutantes da YCA1 íntegra do sítio de cálcio na presença de cálcio.....97
Figura 6 - Teste de maturação dos mutantes da YCA1-ΔN86 do sítio de cálcio na presença de cálcio.....100

CAPÍTULO 3

Figure 1 - Screening of molecules on the activity of metacaspase-2 of *Trypanosoma brucei*……..118
Figure 2 - Inhibition kinetics of compound EM-1A against TbMCA2……120
Figure 3 - Inhibition kinetics of compound EM-1B against TbMCA2……121
Figure 4 - Inhibition kinetics of compound EM-1C against TbMCA2……...122
Figure 5 - Inhibition kinetics of compound EM-F12C against TbMCA2……122
Figure 6 - Molecular docking of the compound EM-F12C against TbMCA2……...127
Supplementary Figure S1 – Molecular Docking of the compound EM-1A against TbMCA2….....133
Supplementary Figure S3– Molecular Docking of the compound EM-1B against TbMCA2.....….133
Supplementary Figure S3– Molecular Docking of the compound EM-1C against TbMCA2….....134

LISTA DE TABELAS

CAPÍTULO 1

Tabela 1 - Primers utilizados na amplificação do gene da YCA1 para inserção da mutação pontual (em negrito o novo códon para troca do aminoácido e produção da mutação) 58

Tabela 2 - *Primers* projetados para amplificação do gene da *YCA1* utilizados na reação TEDA.....59

Tabela 3 - *Primers* projetados para amplificação do vetor pET28(a)+ utilizados na reação TEDA.....59

Tabela 4 - *Primers* utilizados para amplificação da região T7 (promotora e terminadora) que flanqueia o gene da YCA1.....59

Tabela 5 - Descrição dos *primers* usados na primeira etapa para inserção da mutação.....60

CAPÍTULO 2

Tabela 1 - *Primers* utilizados na amplificação do gene da YCA1 para inserção da mutação pontual nos resíduos do sítio de interação com o íon cálcio (em negrito o novo códon para troca do aminoácido e produção da mutação).....79

CAPÍTULO 3

Table 1 - Molecular structure of compounds derived from chalcones and flavonoids. 117

Table 2 - Inhibitory potential (IC_{50}) of compounds derived from chalcones and flavonols in modulating the enzymatic activity of TbMCA2…….119

Table 3 - Kinetic parameters of inhibition mechanisms and affinity values of compounds EM-1A, EM-1B, EM-1C, and EM-F12C……...123

Table 4 – Energy binding for interection of compounds EM-1A, EM-1B, EM-1C and EM-F12C with TbMCA2……..126

LISTA DE ABREVIATURAS E SIGLAS

AMPc	Adenosina Monofosfato Cíclico
AtMCA	Metacaspase de *Arabidopsis thaliana*
Ba^{2+}	Íon Bário
Ca^{2+}	Íon Cálcio
$CaCl_2$	Cloreto de cálcio
CaMCA	Metacaspase de *Candida albicans*
DMSO	Dimetil sulfóxido
DNA	Ácido desoxirribonucleico
DO_{600}	Densidade óptica
Fe^{2+}	Íon Ferro ferroso
Fe^{3+}	Íon Ferro férrico
K^{+}	Íon Potássio
KCl	Cloreto de potássio
KOH	Hidróxido de potássio
LB	Meio de cultura Luria Bertani
LmjMCA	Metacaspase de *Leishmania major*
MCR	morte celular regulada
Mg^{2+}	Íon Magnésio
$MgCl_2$	Cloreto de magnésio
MIPC	Manose-Inositol-Fosfo-Ceramida
Mn^{2+}	Íon Manganês
$MnCl_2$	Cloreto de manganês
MoMca	Metacaspase de *Magnaporthe oryzae*
Na_2HPO_4	Fosfato de sódio
NaCl	Cloreto se sódio
NaOH	Hidróxido de sódio
Ni^{2+}	Íon Níquel
OMS	Organização Mundial da Saúde
PARP	poli (ADP-ribose) polimerase
PCR	Reação em cadeia da polimerase

PKA	Proteína Quinase A
PKC	Proteína Quinase C
RNA	Ácido ribonucleico
SDS	Dodecil sulfato de sódio
Sm^{3+}	Íon Samário
SmAc	Acetato de semário
Sods	Superóxido Dismutases
TAE	Tampão TRIS-Acetato-EGTA
TbMCA	Metacaspase de *Trypanossoma brucei*
TEDA	*T5 exonuclease DNA assembly*
TNF	fator de necrose tumoral
UTI	Unidades De Terapia Ontensiva
YCA1	Metacaspase de *Saccharomyces cerevisiae*
YCA1-ΔN86	Metacaspase truncada (86 aminoácidos) de *Saccharomyces cerevisiae*
Zn^{2+}	Íon Zinco

ABREVIATURA DOS AMINOÁCIDOS

NOME DOS AMINOÁCIDOS	3 LETRAS	1 LETRA
Ácido aspártico	Asp	D
Ácido glutâmico	Glu	E
Alanina	Ala	A
Arginina	Arg	R
Asparagina	Asn	N
Cisteína	Cys	C
Fenilalanina	Phe	F
Glicina	Gly	G
Glutamina	Gln	Q
Histidina	His	H
Isoleucina	Ile	I
Leucina	Leu	L
Lisina	Lys	K
Metionina	Met	M
Prolina	Pro	P
Serina	Ser	S
Tirosina	Tyr	Y
Treonina	Thr	T
Triptofano	Trp	W
Valina	Val	V

SUMÁRIO

1 INTRODUÇÃO 19

1.1 MORTE CELULAR 19

1.1.1 Apoptose 21

1.2 PROTEASES 25

1.2.1 Classificação das proteases 27

1.2.2 Cisteíno-proteases 30

1.3 METACASPASE 34

1.4 METACASPASE DE *Saccharomyces cerevisiae* 37

1.5 *Saccharomyces cerevisiae* E SUAS APLICAÇÕES BIOTECNOLÓGICAS 40

1.6 *Trypanossoma brucei* – CICLO DE VIDA E METACASPASES 44

REFERÊNCIAS 46

CAPÍTULO 1- MUTAÇÕES SÍTIO-DIRIGIDAS NA METACASPASE DE *S. cerevisiae*: UMA ABORDAGEM METODOLÓGICA AVANÇADA PARA ESTUDOS ESTRUTURAIS E FUNCIONAIS 55

RESUMO 56

ABSTRACT 57

RESUMEN 57

INTRODUÇÃO 57

MATERIAIS E MÉTODOS 59

RESULTADOS E DISCUSSÃO 63

CONCLUSÕES 71

REFERÊNCIAS.....72

CAPÍTULO 2 - AVALIAÇÃO DE RESÍDUOS CHAVE PARA O FUNCIONAMENTO DA METACASPASE-1 DE *Saccharomyces cerevisiae (YCA1*) 74

RESUMO.....76

1 INTRODUÇÃO.....77

2 OBJETIVO.....78

2.1 OBJETIVO GERAL.....78

2.2 OBJETIVOS ESPECÍFICOS.....79

3 PROCEDIMENTOS EXPERIMENTAIS.....79

3.1 MUTAGÊNESE SÍTIO-DIRIGIDA DA YCA1.....79

3.2 EXPRESSÃO DE YCA1 SELVAGEM E MUTANTES 80

3.3 PURIFICAÇÃO DE YCA1 SELVAGEM E MUTANTES.....81

3.4 WESTERN BLOTTING DE YCA1 SELVAGEM E MUTANTES.....81

4 RESULTADOS E DISCUSSÃO 82

5 CONCLUSÃO 101

REFERENCIAS.....103

CAPÍTULO 3 - CHALCONE AND FLAVONOID DERIVATIVES AS MODULATING AGENTS OF METACASPASE-2 FROM *Trypanosoma brucei* (TbMCA2) **106**

ABSTRACT **108**

1 INTRODUCTION **109**

2 EXPERIMENTAL PROCEDURES **111**

2.1 Production of recombinant TbMCA2 ..... **111**

2.2 Purification of recombinant TbMCA2 ..... **111**

2.3 Peptide synthesis **112**

2.4 Screening of compounds as a TbMCA2 modulator **112**

2.5 Determination of IC50 values for inhibitor **113**

2.6 Enzyme kinetics and mechanism determination **113**

2.7 Molecular docking **113**

2.8 Molecular Dynamics Simulation in Desmond **114**

3 RESULTS **115**

3.1 Screening for the Inhibitory Activity of Compounds **115**

3.2 Inhibitory concentration (IC_{50}) **117**

3.3 Inhibition mechanisms of TbMCA2 by molecules derived from the class of chalcones and flavonoids **118**

4 DISCUSSION **123**

5 CONCLUSIONS **126**

REFERENCES.....128

ANEXO A – Cysteine proteases as potential targets for anti-trypanosomatid drug discovery 135

ANEXO B - Metacaspase of *Saccharomyces cerevisiae* (ScMCA-Ia) presents diferente catalytic cysteine in a processed and non-processed form**..... 147**

ANEXO C - Oximic compounds as potential inhibitors of metacaspase-2 (TbMCA2) of *Trypanosoma brucei***..... 153**

ANEXO D - N-terminal of metacaspase of *Candida albicans* as essential for calcium interaction..... 166

1 INTRODUÇÃO

1.1 MORTE CELULAR

A morte celular é considerada um dos processos essenciais responsáveis pela homeostase em organismos pluricelulares. Assim como a sobrevivência, proliferação e diferenciação celular, a morte celular regulada desempenha um papel primordial na manutenção do equilíbrio entre a vida e a morte das células, garantindo a remoção de células excessivas ou danificadas (GREEN; LLAMBI, 2015).

Embora estresse celular possa resultar na morte celular, a maioria dos casos de morte celular regulada (MCR) ocorrem de maneira ativa por vias de sinalização específicas. Esse processo está associado a um grupo de proteínas, as quais desencadeiam a morte da célula por destruição ordenada (GALLUZZI *et al*., 2018). É é altamente regulado e depende de uma maquinaria celular especializada (GALLUZZI *et al.,* 2018). Madeo, Fröhlich & Fröhlich (1997) identificaram que organismos unicelulares também experimentam o que conhecemos como MCR, e esse processo é mediado por uma protease com semelhança funcional e estrutural as caspases de mamíferos.

A princípio a morte celular foi classificada de três diferentes maneiras baseadas em alterações morfológicas: Tipo I (Apoptose), Tipo II (autofagia), e Tipo III (necrose). Porém, nos últimos anos houve uma maior dedicação a investigação desse fenômeno de morte celular, e assim foram identificados novos meios de classificações além das alterações morfológicas, como mecanismos moleculares, estímulos correspondentes e liberação de mediadores (D'ARCY, 2019; YAN, ELBADAWI & EFFERTH, 2020).

Dessa forma, temos atualmente dois grandes grupos para classificar os tipos de morte, a saber, a morte celular acidental e a morte celular regulada. Tal nomenclatura é decorrente, como já descrito, da necessidade de um novo tipo de classificação em decorrência do avanço dos estudos e a progressão de descobertas de novas vias de sinalização que levam a morte celular. A MCR abrange vários tipos de morte celular que podem apresentar morfologia necrótica e/ou apoptótica (Figura 1), entretanto cada uma com seu mecanismo molecular e particularidade. A classificação atual abrange os sub-tipos de morte: necroptose, ferroptose, piroptose, partanatos, morte celular entótica, morte celular NETótica, morte celular dependente de lisossomo (LDCD), morte celular dependente de autofagia (ADCD), morte celular imunogênica

(ICD), apoptose intrínseca, apoptose extrínseca e necrose induzida por transição de permeabilidade mitocondrial (MPT). Dentre os subtipos de morte regulada apresentados a apoptose é a principal via discutida na literatura (GALLUZZI, *et al.* 2018; D'ARCY, 2019).

Figura 1 - Principais subtipos de morte celular regulada. Classificação dos tipos de Morte Celular Regulada que podem apresentar morfologia apoptótica e/ou morfologia necrótica.

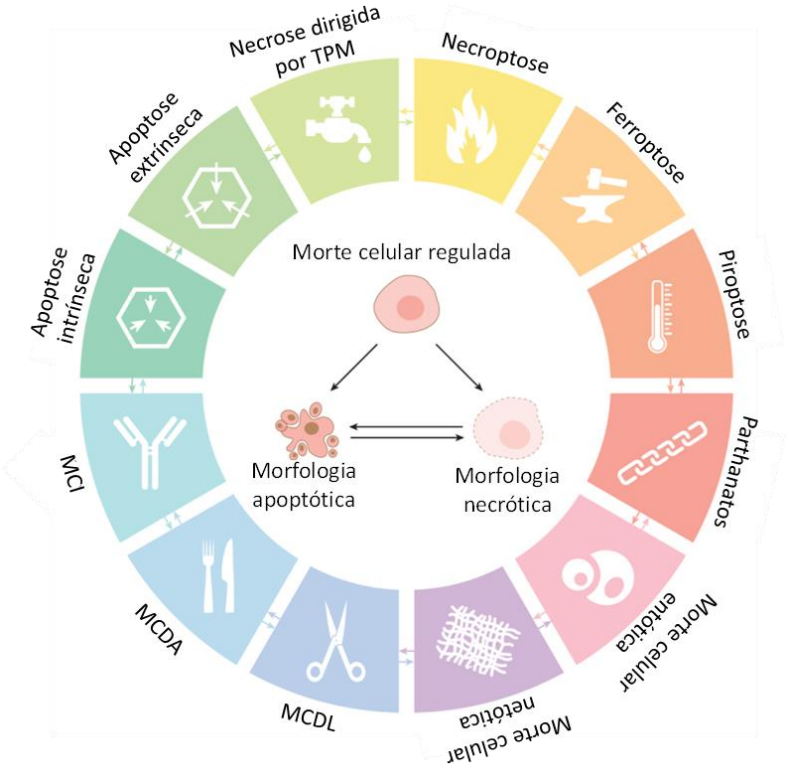

Fonte: Galluzzi *et al.,* 2018 (adaptação)

Büttner *et al.* (2006) descrevem que a morte celular, seja por envelhecimento ou dano que afeta sua capacidade metabólica, favorece a sobrevivência da população clonal.

Em ambos os cenários, a apoptose funciona como um mecanismo para eliminar células senescentes, com danos irreversíveis ou que apresentam disfunções prejudiciais à população de células fúngicas (VÁCHOVÁ E PALKOVÁ, 2005). O entendimento e caracterização dos mecanismos de morte vem ganhando foco no universo científico, permitindo que novos alvos sejam estudados para combater infeções.

1.1.1 Apoptose

O termo apoptose vem das palavras gregas, *apo* "a parte" e *ptose* “caído”. E foi usado pela primeira vez em 1972 pelos cientistas John F. R. Kerr, Andrew H. Wyllie & Alastair R. Currie, da Universidade de Edimburgo, para descrever uma forma de morte celular.

A apoptose é uma das modalidades de MCR que acontece durante o ciclo de desenvolvimento e envelhecimento celular (NORBURY & HICKSON, 2001), e tem um papel crucial na manutenção da homeostase de metazoários, o que permite a eliminação de células danificadas e/ou indesejadas. Este processo é gerenciado por uma complexa rede bioquímica, onde uma série de estímulos e circunstâncias, tanto fisiológicas quanto patológicas, podem provocar a apoptose (STELLER, 1995). Contudo, não é garantido que todas as células morrerão em resposta ao mesmo estímulo (ELMORE, 2007; DONEHOWER & BRADLEY, 1993).

Inicialmente, observa-se diminuição no volume celular, que é seguido de condensação da cromatina (picnose). Devido ao encolhimento celular, as células ficam menores, o citoplasma fica mais denso e as organelas mais compactadas. Estas alterações iniciais resultam no colapso celular, com a formação dos chamados corpos apoptóticos, que são rapidamente fagocitados para que não causem inflamação no tecido, assim como ocorre na morte celular por necrose (KERR; WYLLIE; CURRIE, 1972). Os corpos apoptóticos são então fagocitados de modo que não sejam liberados para as áreas circundantes, impedindo uma resposta inflamatória (KERR; WYLLIE; CURRIE*,* 1972; FLEISHER, 1997; GALLUZZI *et al.,* 2012). Além disso, a apoptose pode ou não ser acompanhada pela ativação de enzimas proteolíticas chamadas caspases (GALLUZZI *et al.,* 2012).

A princípio a apoptose foi descrita em organismos multicelulares (SILVA *et al*, 2005; EISENBERG *et al.,* 2010) e que esse fenômeno era exclusivo desse grupo de organismos (CARMONA-GUTIERREZ *et al.*, 2018). Contudo, em 1997 foi identificado e descrito as mesmas características de MCR só que em organismos unicelulares, o que permitiu um foco e grande desenvolvimento de pesquisas de apoptose em levedura (MADEO *et al.*, 1997).

A *Saccharomyces cerevisiae* é uma levedura que foi amplamente estudada e assim identificaram que as características apoptóticas presentes nela se assemelham as presentes em mamíferos, como os eventos de condensação da cromatina, a

ruptura do DNA, a externalização da fosfatidilserina para membrana externa da membrana plasmática, o acúmulo de espécies reativas de oxigênio (EROs) e a liberação de fatores pró-morte como, por exemplo, o citocromo *c* (MADEO *et al.*, 1999; MADEO *et al.*, 2002). Posteriormente em 2019, as mesmas características apoptóticas na levedura *S. cerevisiae* foram observadas para a levedura *Candida albicans* (LI *et al.*, 2019).

As enzimas proteolíticas que acompanham a ativação da cascata são chamadas de caspases, que são expressas como uma proenzima inativa que, quando ativada, pode ativar outras pró caspases, iniciando assim a cadeia de ativação das caspases. Esta cadeia proteica intensifica a via de sinalização apoptótica, conduzindo assim à MCR (ELMORE, 2007). As caspases possuem atividade de quebra de proteínas, com especificidades em resíduos de ácido aspártico. Foram identificadas dez caspases principais, categorizadas em iniciadoras (caspase-2, -8, -9, -10), efetoras (caspase-3,-6, -7) e inflamatórias (caspase-1, -4, -5). Entre outras caspases pode-se destacar a caspase-11, relacionada ao inflanossoma, a caspase-12, envolvida na apoptose endoplasmática, e a caspase-13 e caspase-14, com funções específicas em tecidos embrionários e adultos, respectivamente (KANG *et al.,* 2002).

Até o momento, foram descritas duas principais vias que desencadeiam a morte celular por apoptose: a via mitocondrial (intrínseca) e a via dependente do receptor de morte (extrínseca) (FLEISHER, 1997).

A via Intrínseca, ou via mitocondrial, é desencadeada após a perturbação da homeostase, como danos ao DNA, retirada do fator de crescimento, sobrecarga de espécies reativas de oxigênio (ERO's), exposição a toxinas, entre outros. Essa desordem gera a liberação de estímulos intracelulares, como as proteínas da família BCL-2 e proteínas BH3-only (homóloga de BCL-2), que ativam proteínas pró-sobrevivência ou pró-apoptóticas, as quais regulam a permeabilização da membrana externa da mitocôndria (D'ARCY, 2019; YAN, ELBADAWI & EFFERTH, 2020; LOMONOSOVA & CHINNADURAI, 2008; OBENG, 2021).

Após a liberação de proteínas pró-sobrevivência como BCL-2 (*B-cell lymphoma* 2), BCL-XL (*B-cell lymphoma - extra large*), BCL-W os lipídios mitocondriais e as proteínas interagem e regulam o fluxo metabólico bioenergético, impedindo a permeabilização da membrana mitocondrial (GREEN; KROEMER, 2004).

As proteínas da família BCL-2 desempenham um papel crucial na regulação da apoptose, controlando a permeabilidade da membrana externa da mitocôndria. Em

resposta a estímulos pró-apoptóticos, proteínas como BAX e BAK induzem a formação de poros nessa membrana, permitindo a liberação do citocromo c no citoplasma. O citocromo c, junto com APAF-1 (fator de ativação de protease apoptótica 1) e moléculas de ATP ou dATP, forma o apoptossomo, um complexo proteico essencial para a progressão da via apoptótica intrínseca (TAIT *et al.,* 2010; GALUZZI *et al.,* 2012).

O apoptossomo recruta e ativa a caspase-9, uma caspase iniciadora, que desempenha o papel central de ativar as caspases executoras, como as caspases-3 e -7. Essas caspases executoras degradam proteínas estruturais e regulatórias, levando à desestruturação celular característica da apoptose. Esse mecanismo em cascata é fundamental para a eliminação eficiente e programada de células danificadas (Figura 2) (YAN, ELBADAWI & EFFERTH, 2020; YUAN & AKEY, 2013; GORTAT *et al.,* 2015; CHENG *et al.,* 2016).

Figura *2* - **Via extrínseca e via intrínseca da morte celular por apoptose.** Ambas as vias de morte por apoptose, extrínseca e intrínseca, culminam na ativação da cascata de caspases, entretanto a indução é diferente em cada uma. Na via intrínseca, ou via mitocondrial, é ativada por algum tipo de lesão celular que desencadeia proteínas da família Bcl-2, iniciando com a ativação de moléculas pró-apoptóticas pela proteína BH3, a deficiência de proteínas reguladoras (antiapoptóticas) faz com que a membrana mitocondrial fique permeável a substâncias, como o citocromo c, que ao adentrar o citosol faz a ativação de caspases. Já a via extrínseca, ou via do receptor de morte, é caracterizada pela formação de um “complexo de sinalização indutor da morte” que é formado pela ligação de um ligante ao receptor, esse complexo ativa caspases e resulta na morte por apoptose, assim como na outra via.

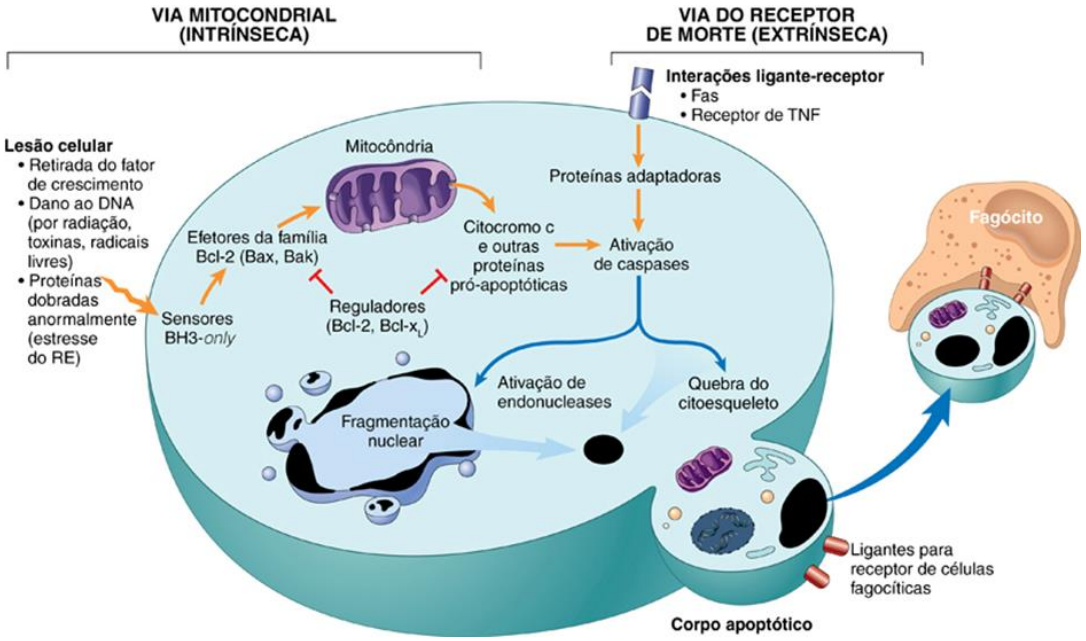

Fonte: Kumar, Abbas & Aster (2018)

Já a via extrínseca, ou via dependente de receptor de morte, ocorre por meio de estímulos externos à célula, tais como a oligomerização de proteínas transmembrana da superfamília de receptores de morte ou o aumento das concentrações extracelulares de determinados fatores. Isso leva à transmissão de sinais fatais ou ao acionamento de receptores dependentes (GALLUZZI *et al*., 2012; YAN, ELBADAWI & EFFERTH, 2020). Os receptores transmembrana da superfamília do fator de necrose tumoral (TNF) são então ativados (LOCKSLEY *et al*., 2001). Esses receptores apresentam similaridades em suas áreas extracelulares e possuem um "domínio da morte" citoplasmático essencial para a transmissão do sinal apoptótico. Os principais ligantes e receptores identificados são FasL/FasR (Ligante Fas/Receptor Fas), TNF-α/TNFR1 (*Tumor Necrosis Factor-alpha/ Tumor Necrosis Factor Receptor 1*), Apo3L/DR3 (*Apolipoprotein 3 Ligand/ Death Receptor 3*), Apo2L/DR4

(*Apolipoprotein 2 Ligand/ Death Receptor 4*) e Apo2L/DR5 (*Apolipoprotein 2 Ligand/* Death Receptor 5) (RUBIO-MOSCARDO *et al*., 2005; ELMORE, 2007).

Ambas proteínas adaptadoras aderidas ao receptor de morte associam-se a pró-caspase 8, fazendo com que ocorra a formação de um complexo de sinalização indutora de morte (DISC) que resultará na ativação da pró-caspase 8. O TNFR1 tem a capacidade de induzir apoptose dependente de FADD e da caspase 8 de forma indireta (ASHKENAZI, 1998). O receptor atrai proteínas ligadas à área de morte do TNFR1, que por sua vez recruta moléculas de sinalização como FADD, TRAF2 e RIP. Isso pode resultar na ativação da caspase 8 para induzir apoptose, além de ativar vias antiapoptóticas como NF-κB e JNK/AP-1 e desencadeará a cascata de caspases para que ocorra a morte da célula (GALLUZZI *et al.*, 2018; NAGATA, 2018; D'ARCY, 2019; OBENG, 2021).

Na etapa extrínseca da apoptose, ilustrada pelos modelos FasL/FasR e TNF-α/TNFR1, os receptores estabelecem conexões com os ligantes homólogos, dando origem ao Complexo de Sinalização Indutor de Morte (DISC). Depois de formar o DISC, a caspase-8 é ativada, o que provoca a ativação subsequente de outras caspases, como a caspase 3. Contudo, a conexão da caspase 8 com o FADD e a subsequente formação do DISC podem ser prevenidas se uma isoforma de um dos reguladores DR, denominada proteína inibitória celular FLICE-like (cFLIPs), se conectar ao FADD. Isso se deve ao fato de que uma dessas isoformas de cFLIP possui uma estrutura bastante parecida com a CASP8, com a única diferença do domínio catalítico ativo (HITOSHI *et al*., 1998; WAJANT, 2002; ELMORE, 2007).

1.2 Proteases

As proteases, ou também conhecidas como peptidases, proteinases ou enzimas proteolíticas, são enzimas que tem a função de hidrolisar as ligações peptídicas entre os aminoácidos, que unidos formam uma proteína (HOOPER, 2002; CASTRO *et al.*, 2011). Elas são específicas, logo possuem especificidade por determinados substratos e assim farão suas respectivas funções, as quais são essenciais para o desenvolvimento das células (RANI, RANA & DATT, 2012; SALVESEN, HEMPEL & COLL, 2016).

Essas enzimas proteolíticas desempenham um papel ativo em várias vias e processos biológicos, que ultrapassam a liberação de pequenos peptídeos e

aminoácidos originados na hidrólise de ligações peptídicas (RANI, RANA & DATT, 2012; SALVESEN, HEMPEL & COLL, 2016). Essas moléculas desempenham um papel crucial em vários processos biológicos, incluindo a coagulação sanguínea, o sistema complemento, a regulação do ciclo celular e a apoptose. Elas também desempenham um papel no metabolismo, no transporte de proteínas secretoras através das membranas e possuem a habilidade de fazer alterações e ativar proteínas por clivagem expressas como zimogênios (RANI, RANA & DATT, 2012; CHAKRABARTY *et al*., 2019).

Normalmente as peptidases são expressas na forma de zimogênios, que são inativos, e por isso dependem de uma etapa de ativação para que consigam efetuar suas funções. Essa etapa de ativação geralmente consiste em uma clivagem proteolítica com a finalidade de remover ou fazer um rearranjo de uma região da proteína que bloqueia o acesso ao sítio ativo. A atividade das proteases é altamente regulada, pois a falha pode levar a uma série de doenças, como por exemplo o desenvolvimento do câncer e a neurodegeneração (CHAKRABARTY *et al.*, 2019).

A interação da protease com seu substrato ocorre em uma região da cadeia da mesma denominada de sítio ativo. Este sítio ativo pode ser subdividido em diferentes sub-sítios, cada um com sua alta especificidade para um resíduo de aminoácido particular presente no substrato (MÓTYÁN e TŐZSÉR, 2013).

A investigação de proteases tem grande relevância científica e tecnológica devido à sua ampla aplicação em diversas áreas, incluindo o uso como reagentes em laboratórios de pesquisa, diagnósticos clínicos, indústrias e terapias médicas. O estudo detalhado de suas interações com substratos e inibidores é fundamental para o desenvolvimento de novos agentes terapêuticos, contribuindo significativamente para os avanços na área farmacêutica (MÓTYÁN, TÓTH & TÖZSÉR, 2013). Dada a diversidade funcional e estrutural das proteases, assim como sua participação em inúmeros processos fisiológicos, essas enzimas se destacam como alvos de grande interesse na biotecnologia. Pesquisas focadas na exploração de suas propriedades e no aprofundamento do conhecimento sobre estrutura e função são essenciais para ampliar as possibilidades de suas aplicações práticas e terapêuticas (RANI, RANA & DATT, 2012).

1.2.1 Classificação das proteases

As proteases são classificadas de acordo com a reação catalisada, mais precisamente do local da clivagem da ligação peptídica, natureza química do seu sítio catalítico, ou pela similaridade estrutural em sua estrutura primária (HOOPER, 2002; RANI, RANA & DATT, 2012). Em relação ao local de clivagem das enzimas proteolíticas, estas podem ser classificadas como exopeptidades ou endopeptidases, baseadas no local onde houve a hidrólise do substrato (Figura 3) (BARRETT, 1994).

Figura 3 - Representação do conceito de exopeptidase e endopeptidase. Endopeptidases clivam ligações peptídicas internas, já as exopeptidases clivam ligações peptídicas nas extremidades do substrato, podendo ser subdivididas em amino e carboxipeptidases de acordo com a posição da clivagem da ligação peptídica. As aminopeptidases clivam nas ligações amino-terminais (NH_2), enquanto as carboxipeptidases clivam nas ligações carboxi-terminais (COOH).

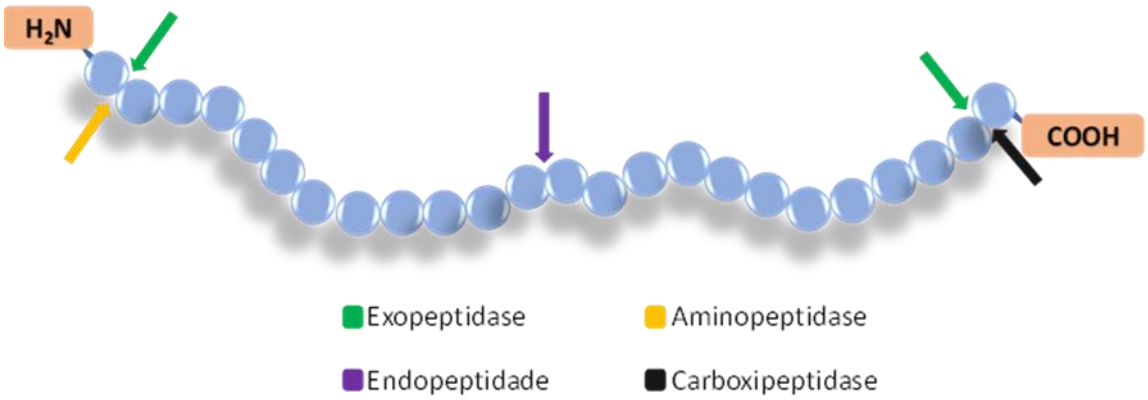

Fonte: LEHNINGER, NELSON e COX, 2018 (adaptação)

As exopeptidases são enzimas que hidrolisam seus substratos na extremidade da cadeia polipeptídica, nas porções amino-terminal (N-terminal) ou carboxi-terminal (C-terminal), sendo então denominadas como aminopeptidases e carboxipeptidases, respectivamente, de acordo com o local de ação (BARRETT, 1994; HOOPER, 2002; RANI, RANA & DATT, 2012).

As aminopeptidases clivam no N-terminal, e após a hidrolise há a liberação de algum resíduo de aminoácido (aminopeptidase), dipeptídeo (aminodipeptidase), tripeptídeo (aminotripeptidase), carboxipeptidases ou dipeptídeo (carboxidipeptidase) (Figura 4) (LEHNINGER, NELSON e COX, 2018). As carboxipeptidases ainda podem

ser classificadas de acordo com a natureza do resíduo que se encontra no sítio ativo da proteína, como por exemplo uma cisteíno-protease e serino-protease caso possuam cisteína ou serinas no seu sitio ativo, respectivamente BARRETT, 1994; MÓTYÁN e TŐZSÉR, 2013; RANI, RANA & DATT, 2012).

Figura 4 - Local de clivagem de substratos pelas exopeptidases e endopetidases

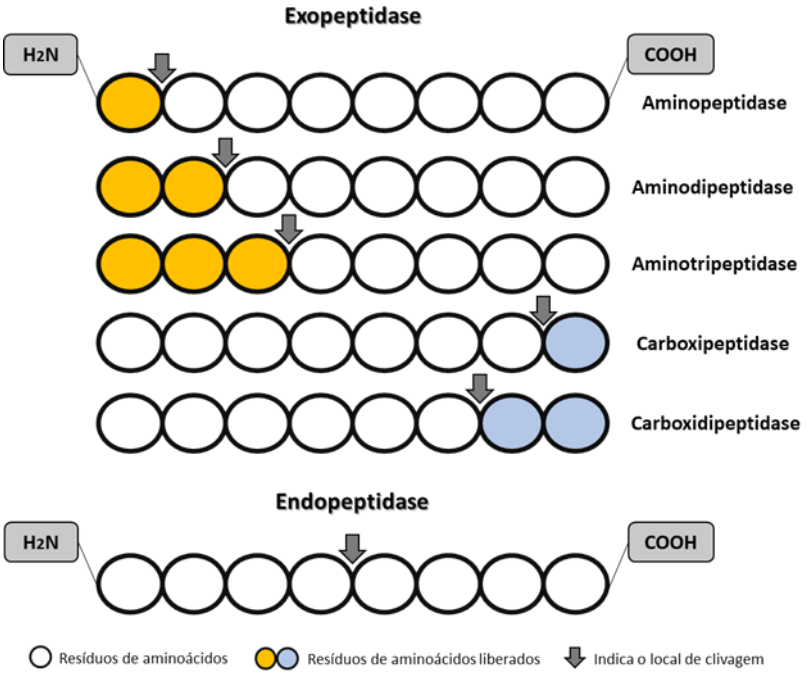

Fonte: Mahajan & Badgujar, 2010 (adaptação)

Já as endopeptidases são enzimas que clivam as ligações peptídicas localizadas nas regiões mais internas da cadeia polipeptídica, em locais centrais e afastadas das extremidades N-terminal e C-terminal (Figura 4). Elas clivam pequenos substratos denominados oligopeptidases (BARRETT, 1994; RANI, RANA & DATT, 2012).

A ligação da protease com o substrato ocorre em uma região específica denominada sítio catalítico, ou sítio ativo, que é o local na estrutura tridimensional da proteína onde o substrato se ligará para ocorrer a clivagem. O sítio ativo de cada enzima é dividido em diferentes sub-sítios, cada um com uma alta especificidade para determinado resíduo de aminoácido em uma posição do substrato (MÓTYÁN e TŐZSÉR, 2013).

Schechter e Berger em 1967, propuseram uma nomenclatura de classificação dos sub-sítios das proteases baseado no local de hidrólise e das extremidades

terminais. Foi adotado o P, de peptídeo, para resíduos de aminoácidos do substrato, e S para o sub-sítios do sítio ativo das proteases. A numeração adotada é de dentro para fora a partir do local de clivagem, assim, os aminoácidos hidrolisados a partir do sítio catalítico em direção ao N-terminal são denominados como P1, P2, P3, e assim por diante, e os sub-sítios que interagem com esses resíduos de aminoácidos são nomeados como S_1, S_2, S_3, e assim por diante. Já a identificação adotada dos resíduos de aminoácidos partir do sítio catalítico em direção ao C-terminal é P_1', P_2', P_3', e os sub-sítios correspondentes na protease são nomeados como S_1', S_2', S_3', e assim por diante (Figura 5) (SCHECHTER & BERGER, 1967; HOOPER, 2002; CHAKRABARTY *et al.*, 2019).

Figura 5 - Representação da interação dos sub-sítios de uma protease. Em azul é representado os sub-sítios de uma protease interagindo com os aminoácidos do substrato, identificados pelos círculos verdes. Porção aminoterminal (H_2N) e porção carboxiterminal (COOH).

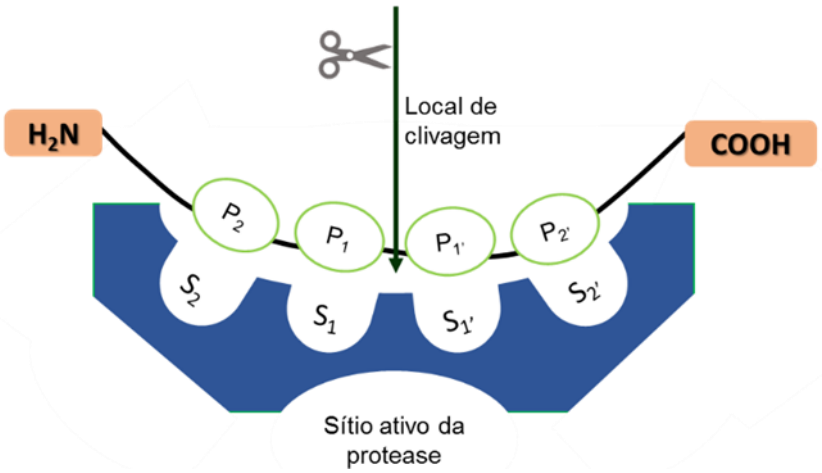

Fonte: Schechter & Berger 1967 (adaptação)

A partir do desenvolvimento das pesquisas com as proteases, surgiu a necessidade de classifica-las de forma mais detalhada de acordo com o grupo nucleofílico responsável do sítio catalítico, e assim em famílias e clãs. Essas classificações podem ser visualizadas no banco de dados MEROPS (https://www.ebi.ac.uk/merops/). A classificação baseada no resíduo do sítio catalítico, o qual é responsável por realizar o ataque nucleofílico no substrato, e assim permitiu que fossem identificadas pelo menos seis classes de proteases, sendo elas: cisteíno-proteases, serino-proteases, treonil-proteases, aspartil-proteases, metalo-proteases,

glutamato-proteases, e outras que possuem o sítio catalítico desconhecido ou que possuem mais de um sítio ativo (RAWLINGS, 2009; RAWLINGS *et al.*, 2018; CHAKRABARTY *et al.*, 2019).

1.2.2 Cisteíno-proteases

As cisteíno-proteases representam uma classe de enzimas de grande relevância biológica, desempenhando papéis cruciais em diversos processos fisiológicos, incluindo a morte celular programada. Devido à sua participação em mecanismos patológicos, essas enzimas são alvos estratégicos na pesquisa farmacêutica, com foco na descoberta de moléculas de potencial terapêutico para o tratamento de doenças graves, como o câncer, infecções por protozoários, tais como a malária, e infecções fúngicas, como a candidíase, entre outras condições que representam riscos significativos à saúde humana (HOOPER, 2002; RANI, RANA & DATT, 2012; VERMA, DIXIT & PANDEY, 2016).

Essas proteases estão presentes em todos os tipos de organismos vivos, abrangendo tanto eucariotos quanto procariotos, e recentemente foram identificadas em vários vírus, incluindo o SARS-CoV-2, agente etiológico da pandemia de COVID-19 (RANI, RANA & DATT, 2012; GAO *et al*., 2021). A ampla distribuição e a diversidade funcional das cisteíno-proteases tornam-nas foco central para o desenvolvimento de novos fármacos e estratégias terapêuticas.

A primeira cisteíno-protease identificada e caracterizada foi a papaína, que em 1937 foi extraída da *Carica papaya* (mamão). Anos depois, em 1968, sua estrutura tridimensional foi elucidada por Jansoniuns *et al.* e assim foi possível idetificar a presença de uma tríade catalítica composta pelos resíduos Cys^{25}, His^{159} e Asn^{175} (VERMA, DICXIT E PANDEY, 2016). A presença do resíduo de asparagina (Asn^{175}) conservado na proximidade da histidina catalítica (His^{159}), cria uma tríade de Cys-His-Asn considerada similar ao arranjo de Ser-His-Asp encontrado nas serino protease (Figura 6). A papaína serviu como modelo para estudo bioquímicos e moleculares da classe das cisteíno-proteases, sendo a enzima mais conhecida dentre todas as enzimas dessa classe (RANI, RANA & DATT, 2012; VERMA, DIXIT & PANDEY, 2016).

Figura 6 - Representação estrutural da papaína - Estrutura tridimensional da papaína, uma cisteíno-protease. Em verde são evidenciados os resíduos do seu sítio ativo constituído por Cys^{25}, His^{159} e Asn^{175}

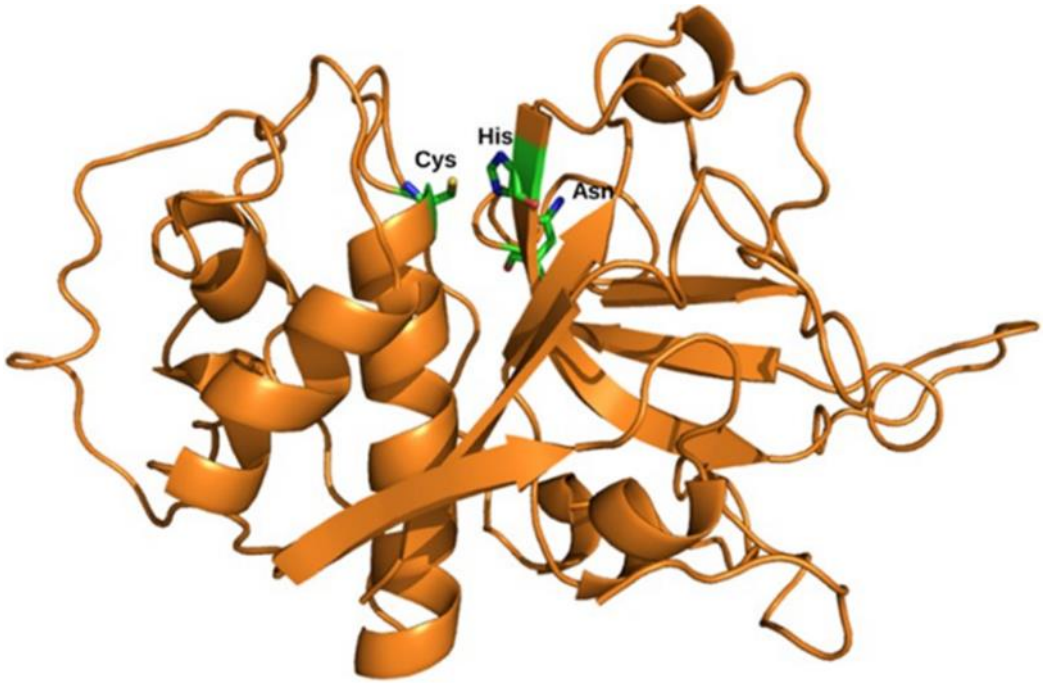

Fonte: Verma, Dixit & Pandey, 2016

Umas das características mais importantes das cisteíno-proteases é a dependência de uma díade catalítica, sempre composta por um resíduo de cisteína (Cys) e um resíduo de histidina (His) em seu sítio catalítico. A presença ou ausência de um terceiro elemento em seu sítio ativo, formando assim uma tríade catalítica, serve para garantir uma melhor orientação e estabilização do anel imidazólico da histidina no momento da hidrólise, como ocorre com o resíduo de asparagina no centro ativo da papaína (OTTO & SCHIRMEISTER, 1997; CASTRO *et al.*, 2011).

No momento da hidrólise, o resíduo de histidina do sítio ativo atua como doador de prótons, facilitando o ataque nucleofílico do resíduo de cisteína ao substrato. Esse ataque resulta na formação de um intermediário tetraédrico inicial, em que o resíduo de cisteína interage com o carbono da ligação peptídica alvo, promovendo a clivagem e a liberação do fragmento N-terminal do substrato. A estabilização desse intermediário ocorre por meio de interações de hidrogênio entre o substrato e um resíduo de glutamina presente no sítio ativo. Em seguida, a hidrólise subsequente da ligação tioéster gera um ácido carboxílico como produto final (Figura 7) (RANI, RACHITA & DATT, 2012; VERMA, DIXIT & PANDEY, 2016).

Figura 7 - Mecanismo esquemático de reação da cisteína protease mediada pela clivagem de uma ligação peptídica. No processo de clivagem catalisado por uma cisteíno protease, após a desprotonação de um tiol no sítio ativo pela histidina adjacente, ocorre um ataque nucleofílico ao substrato carbonilo pela cisteína desprotonada. Isso resulta na liberação de um fragmento do substrato e na formação de uma ligação intermediária tioéster. Em seguida, a histidina é restaurada à sua forma desprotonada, e o fragmento remanescente do substrato é hidrolisado, resultando na geração de um ácido carboxílico. Ao final do processo, a enzima é regenerada, pronta para participar de novas reações catalíticas.

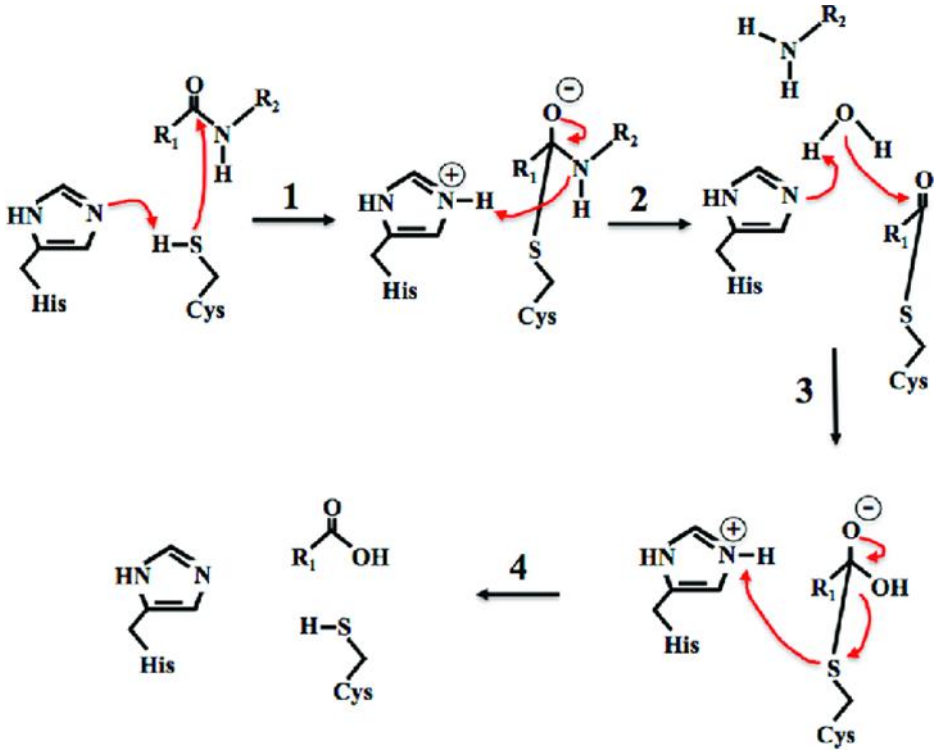

Fonte: RANI, RACHITA & DATT, 2012 (adaptação)

Segundo o banco de dados MEROPS, até o momento existem mais de 13 clãs da classe das cisteíno-proteases, que são classificados baseado em sua estrutura terciária das famílias presentes, as quais existem mais de 50 famílias (RAWLINGS *et al.,* 2018). Cada clã é organizado baseado na similaridade estrutural das famílias, como exemplo temos as caspases e as metacaspases que ambas são pertencentes ao clã CD e família C14 (Figura 8) (MININA, *et al.,* 2017).

Figura 8 - Classificação das císteino-proteases em clãs e famílias. Representação dos clãs, em azul, que compõem a classe de proteases que possuem como resíduo de catálise a cisteína nas cisteíno-proteases. Em verde, as letras representam os aminoácidos que junto a cisteína (C) são importantes para a catálise, como (D) ácido aspártico, (E) ácido glutâmico, (H) histidina, (N) asparagina, (T) treonina. Em vermelho, está o clã CD que possui a díade catalítica (His/Cys), e as famílias que o compõem. Em destaque, dentro da família C14, encontram-se as caspases e metacaspases.

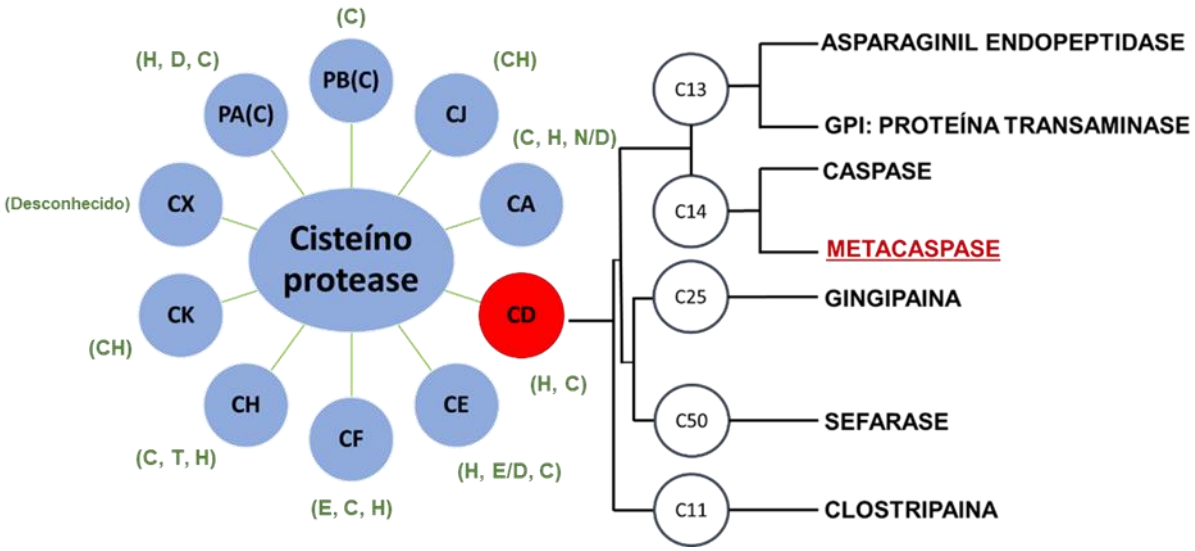

Fonte: Mottram *et al.,* 2003 (adaptação)

O clã CD se diferencia dos demais clãs por sua similaridade em sua estrutura terciária, sequência de aminoácidos, especificidade de hidrólise e funções catalíticas (MOTTRAM *et al.,* 2004). Esse clã tem sido amplamente estudado devido as proteases presentes nesse grupo terem se mostrado grandes potenciais farmacológicos (TSIATSIANI *et al.,* 2011).

Dentro do clã CD temos a família C14 temos as caspases e metacaspases que vem sendo cada vez mais estudadas devido sua suposta função de regulação entre as fases do ciclo celular em eucariotos simples (TSIATSIANI *et al.,* 2011). Esse clã compreende proteases dependentes de cisteína (Cys), com uma única dobra nas folhas α e β, que é constituída por uma subunidade grande (P_{20}) que contém a díade catalítica de Cisteína/Histidina (Cys/His), e uma subunidade pequena (P_{10}) (MININA *et al.*, 2017).

1.3 METACASPASE

Como destacado anteriormente, as peptidases ganharam foco em pesquisas por desempenharem importantes papeis na manutenção da homeostase, metabolismo e da fisiologia da célula, e vem se mostrando potenciais alvos farmacológicos no controle e combate de doenças infecciosas (VANDANA *et al.,* 2019). Assim foram descobertas as metacaspases, por Uren *et al.,* (2000), que através de ferramentas de bioinformática observou a influência da mesma na regulação da morte celular programada (UREN *et al.,* 2000).

As metacaspases possuem similaridades estruturais com as caspases, mas são encontradas em plantas, fungos e protozoários, diferente das segundas que são encontradas em mamíferos (UREN *et al.,* 2000). Elas são sintetizadas como zimogênios (pró enzimas inativas), possuem em seu sítio catalítico uma díade catalítica composta por Cys/His. São compostas por um pró-domínio que antecede as duas subunidades P_{20} (grande) e P_{10} (pequena), e tornam-se enzimaticamente ativas após sofrerem uma clivagem proteolítica após dois resíduos de ácido aspártico (D). Após a remoção do pró domínio, as caspases sofrem clivagem proteolítica liberando dois fragmentos peptídicos com pesos moleculares de 10 kDa e 20 kDa, as subunidades P_{10} e P_{20}, respectivamente. A subunidade P_{10} é necessária para a formação de heterodímeros, o que torna a caspase cataliticamente ativa (Figura 9) (MACKENZIE E CLAK, 2012; KLEMENČIČ & FUNK, 2019).

As metacaspases não necessariamente precisam conter um pró-domínio rico em prolina, glutaminas e asparaginas, e não necessitam passar pelo processo de dimerização para estarem ativas, pois já são ativas em sua forma de monômeros. Entretanto para estarem na forma de monômeros e poderem desempenhar sua função de regulação da MCR, elas sofrem a clivagem proteolítica que é dependente do íon cálcio como cofator (HILL & NYSTRÖM, 2015; KLEMENČIČ & FUNK, 2019). Comparado com as caspases que clivam seus substratos após resíduos de aspartato (aspartato-proteases) na posição P_1, as metacaspases possuem um subsítio S_1 altamente ácido, o que confere especificidade por substratos que contenham resíduos básicos (arginina ou lisina) na posição P_1 (MACHADO *et al.,* 2013; MOTTRAM *et al.,* 2003; GONZALEZ *et al.,* 2007; CARMONA *et al.,* 2010). Isso ocorre porque os aspartatos conservados estão localizados no sítio de especificidade, resultando na

clivagem após resíduos de aminoácidos carregados positivamente (VERCAMMEN *et al.,* 2004).

Figura 9 - Mecanismo de ativação proposto para as caspases e metacaspases. Figura A: Representação ilustrativa da estrutura da caspase durante sua clivagem, pró-domínio (pro), subunidade P_{20} (azul) e subunidade P_{10} (bege) resíduos de ácido aspártico (D). Figura B: Representação ilustrativa proposta para a metacaspase durante seu autoprocessamento. Todos os três tipos de metacaspases são compostas pelas subunidades P_{20} (rosa) onde está localizada a díade catalítica His/Cys (H e C) e P_{10} (bege), além de possuírem uma região rica em glutamina e asparagina (Q/N) na subunidade P_{20}. A metacaspase I possui a presença de um pró-domínio (pro).

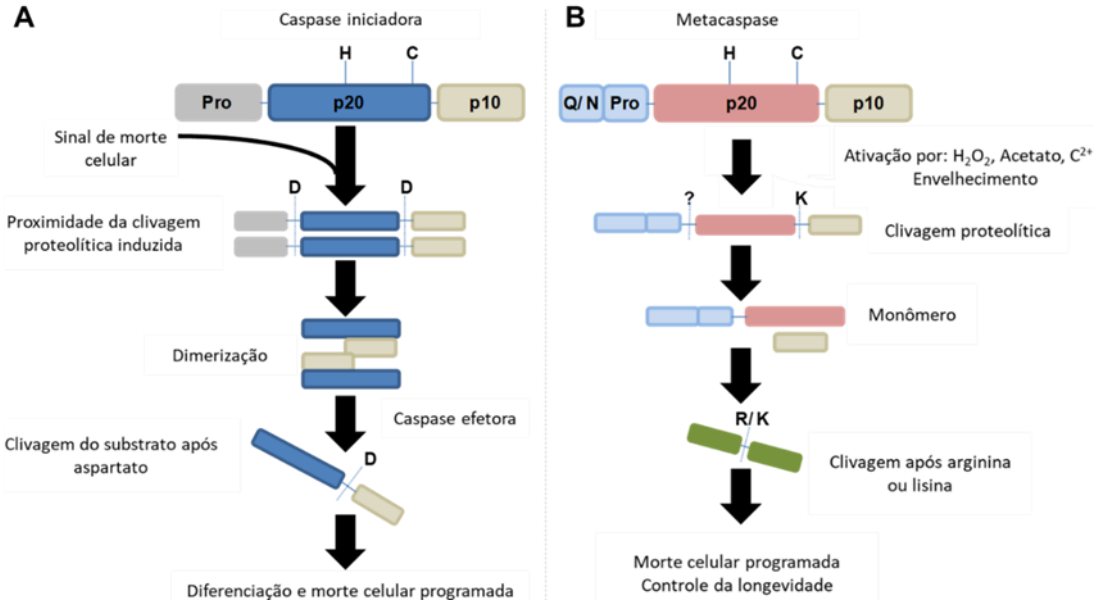

Fonte: MININA *et al.,* 2017 (adaptação).

As metacaspases são classificadas em três tipos: I, II e III, baseadas nas diferenças estruturais encontradas até o momento. As metacaspases do tipo I possuem um pró-domínio na porção N-terminal rico em prolina e uma região chamada de dedo de zinco. Já as metacaspases do tipo II não possuem a região do pró-domínio, porém possuem uma região de ligação constituída por aminoácidos que separam a subunidade P_{20} catalítica e P_{10} reguladora. Já nas metacaspases do tipo III a pequena subunidade P_{10} antecede a subunidade P_{20}, encontrando-se localizada no N-terminal (Figura 10) (MININA *et al*., 2017; KLEMENČIČ & FUNK, 2019).

Figura 10 - Comparação das caspases e metacaspases: composição dos domínios e características bioquímicas - Composição dos domínios e características das caspases e metacaspases. Em cinza o pró-domínio no N-terminal (pro) presente nas caspases e metacaspases do tipo I. A metacaspase do tipo II possui um domínio vinculador entre as subunidades P_{20} e P_{10}. Na metacaspase do tipo III a subunidade menor P_{10} antecede a subunidade grande P_{20}.

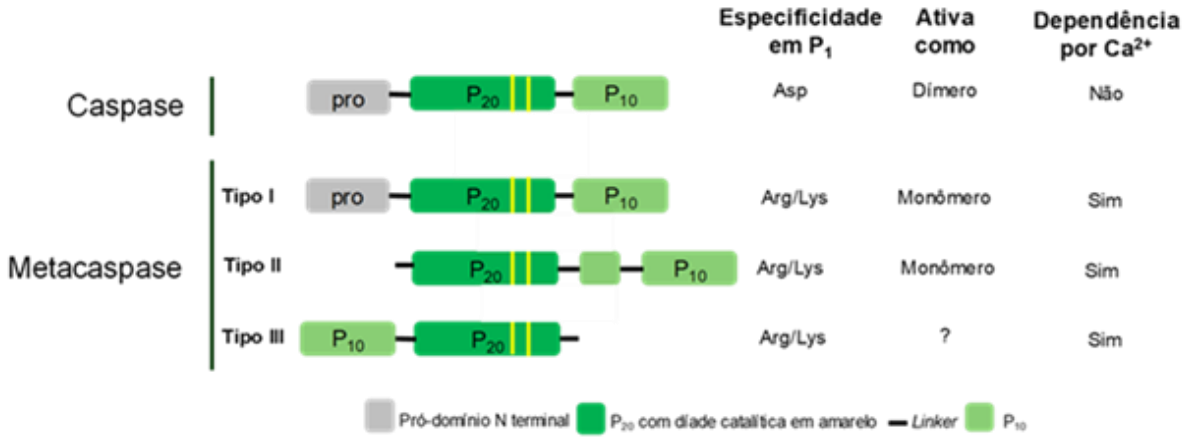

Fonte: Klemenčič & Funk, 2019 (adaptação)

Como já destacado anteriormente, a relação evolutiva e funcional entre caspases e metacaspases tem sido objeto de debate e ampla investigação no meio científico (McLUSKEY & MOTTRAM, 2015; GREEN & FITZGERALD, 2016). Um ponto central nessa discussão se diz respeito às diferenças nos mecanismos de ativação dessas proteases. Enquanto as caspases em metazoários necessitam de dimerização e da interação com proteínas adaptadoras para se tornarem ativas, as metacaspases diferem nesse aspecto, sendo capazes de ativação independente desses fatores (McLUSKEY & MOTTRAM, 2015). Essas distinções sugerem uma evolução funcional divergente, apesar de algumas semelhanças estruturais entre os dois tipos de proteases.

O estresse celular desencadeia a liberação de sinais que induzem a ativação das metacaspases, resultando em um processo de autoprocessamento (TSIATSIANI *et al*., 2011). Esse autoprocessamento é iniciado após a interação das metacaspases com íons de cálcio, embora essa interação não seja um requisito indispensável para a atividade enzimática dessas proteases (MOSS *et al*., 2007). Ainda que não seja determinante para a ativação, o autoprocessamento está diretamente associado a um aumento significativo da atividade catalítica, modulada pela concentração de cálcio (MACHADO *et al*., 2013). Estudos com a metacaspase tipo 2 de *Trypanosoma brucei*

demonstraram que essa etapa de autoprocessamento é crucial para a realocação do N-terminal, o que permite a exposição dos resíduos do sítio catalítico e viabiliza a ação da enzima sobre substratos proteicos de maior tamanho, além de oligopeptídeos (GILIO *et al*., 2017).

Com o passar dos anos foram identificados diversos genes codificadores de metacaspases em diferentes organismos. Em eucariotos simples, por exemplo, foram identificadas metacaspases com funções biológicas conhecidas, como metacaspases do tipo I nos gêneros *Leishmania spp. e Trypanossoma spp* em protozoários (TSIATSIANI *et al.,* 2011). No protozoário *Leishmania donovani*, por exemplo, foram encontrados genes que codificam duas metacaspases, LsMc1 e LsMc2, as quais tem papéis fundamentais na MCR do parasita induzida pelo estresse oxidativo (LEE *et al.,* 2007). Já no protozoário *Leishmania major* foi codificado uma única metacaspases, a LmjMCA, que sua função também tem interferência na regulação no ciclo celular na MCR (ZALILA *et al*., 2011).

1.4 METACASPASE DE *Saccharomyces cerevisiae*

A levedura *Saccharomyces cerevisiae* codifica uma única metacaspase, chamada de Yeast Caspase 1 (YCA1) (SHRESTHA *et al.*, 2019). Essa metacaspase tem sido amplamente estudada, pois pesquisas indicaram que seu nível de expressão está diretamente relacionado com a morte celular (apoptose) induzida por estresse oxidativo, regulação do ciclo celular, senescência celular e eliminação de agregados proteicos na levedura *Saccharomyces cerevisiae* (MADEO *et al.*, 2002; TSIATSIANI *et al*., 2011; SHRESTHA *et al.*, 2019).

Lee *et al.* (2008) comprovou a influência da YCA1 na regulação do ciclo celular na levedura *S. cerevisiae* que atua na transição da fase G1 para a fase S. Em estudos de comparação entre cepas selvagens (BY4741) de *S. cerevisiae* e cepas nocautes (ΔYCA1), quando não há o gene da YCA1 ou quando tem sua atividade inibida, foi observado uma transição tardia da fase G_1 para S do ciclo celular e desordem no *checkpoint* mitótico G2/M.

Novamente Lee *et al.* (2010) avaliou o envolvimento da YCA1 na remodelagem de agregados insolúveis proteicos, e foi observado mutantes com o gene YCA1 nocauteado apresentavam uma maior quantidade de proteínas insolúveis quando comparados com a levedura selvagem. Dados publicados por Hill *et al*. (2015)

observaram que a superexpressão da YCA1 prolonga a vida útil da replicação da levedura e reduz agregados de proteínas, formados durante o processo de envelhecimento celular e estresse, complementando os dados de Lee *et al.* (2010).

Estudos sobre a YCA1 mostraram que essa enzima também é importante no controle da proteostase, em situações de acúmulo de agregados proteicos que não podem ser atenuados, é usado um mecanismo de defesa da levedura em que durante a citocinese, esses agregados proteicos são distribuídos de forma assimétrica. Assim, a protease YCA1 é importante para garantir a assimetria e assegurar que a célula-filha esteja livre de proteínas insolúveis (KACZANOWSKI, SAJID & REECE, 2011), bem semelhante ao papel das caspases eucarióticas na regulação da divisão simétrica/assimétrica das células-tronco (BELL & MEGENEY, 2017).

A estrutura cristalográfica da YCA1 foi revelada por Wong, Yan & Shi (2012), e foi possível destacar a presença da subunidade grande (P_{20}) e pequena (P_{10}) como característica das metacaspases, e baseado em análises feitas por sequenciamento do N-terminal foi suposto que o autoprocessamento ocorra nas lisinas 331 e 334 na parte das extremidades carboxílicas. Baseado na estrutura cristalográfica da YCA1 é destacado em sua composição oito folhas β e cinco α-hélices (α1 a α5), três hélices localizadas em um lado (α1, α4 e α5) e duas hélices do outro (α2 e α3), com três alças ordenadas (L1, L2 e L4) (Figura 11), sendo que o resíduo catalítico (cisteína 276) está localizado na alça L2 (Figura 12) (WONG, YAN & SHI, 2012).

Figura 11 - Estrutura cristalográfica da metacaspase de *Saccharomyces cerevisiae* (YCA1). Estrutura tridimensional da YCA1, que consiste em cinco α-hélices (representadas em rosa) e oito folhas β (em azul), que se organizam para formar uma folha β central. Além disso, é identificado em colorido o resíduo catalítico Cys^{276}.

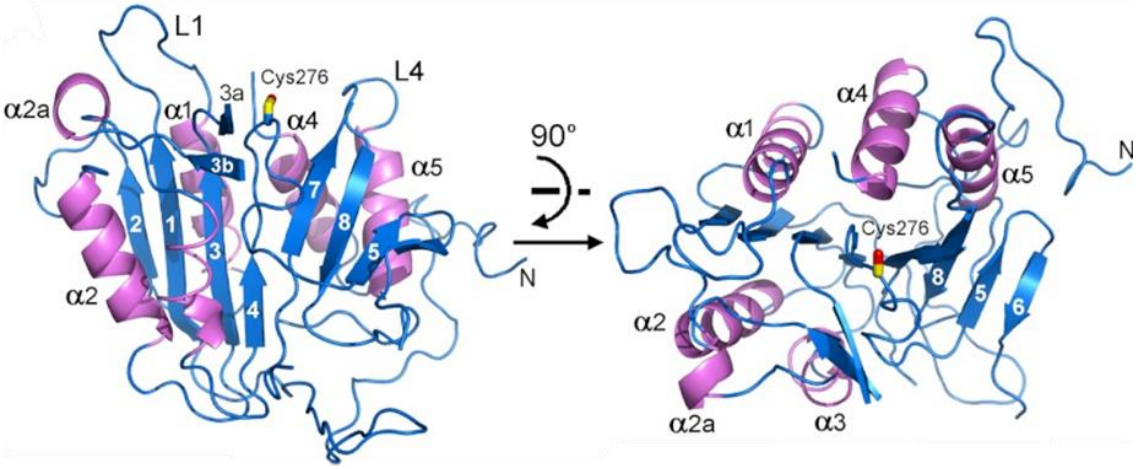

Fonte: WONG *et al.,* (2012).

Figura 12 - Caracterização do sítio ativo da YCA1. O sítio ativo é composto pelos resíduos: Cys276 His220.

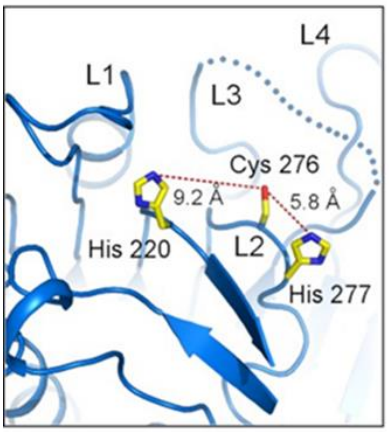

Fonte: WONG *et al.,* (2012).

Dados publicados por Wong, Yan & Shi (2012) a fim de avaliar o autoprocessamento da YCA1, realizaram estudos com a protease pura na presença do íon Ca^{2+} e concluíram que o processamento ocorre tanto no C-terminal quanto no N-terminal. Foi observado através de uma corrida eletroforética em SDS-PAGE que no primeiro processamento há a liberação de um pequeno fragmento, sendo possível observar um fragmento em torno de 14kDa chamado de subunidade pequena, e no segundo processamento há a liberação de um fragmento maior de em torno de 45kDa, denominada de subunidade grande (WONG, YAN & SHI, 2012).

Estudos realizados por Erhardt, Wegrzyn & Deuerling em 2010, revelaram que os aminoácidos que compõem a região do N-terminal da YCA1 interferem na capacidade da enzima de se precipitar, enfatizando que a região rica em glutamina e asparagina (Q/N) é fortemente relacionada a esse processamento.

A metacaspase 2 de *Trypanosoma brucei* (TbMCA2) quando comparada com a YCA1 traz semelhanças e diferenças. Apesar de apresentarem baixa identidade na sequência de aminoácidos, resíduos críticos para a interação com íons divalentes se mostraram preservadas. Uma vez que as sequencias de ambas foram alinhadas, foi possível destacar que a posição dos resíduos da díade catalítica se encontra invariável, Cys^{276} e His^{220} para a YCA1 e Cys^{213} e His^{158} para a TbMCA2. O mesmo ocorre com os quatro resíduos de aspartatos que são responsáveis pela interação com o íon cálcio, Asp^{236}, Asp^{252}, Asp^{253} e Asp^{283} para a metacaspase de *S. cerevisiae*, e Asp^{173}, Asp^{189}, Asp^{190} e Asp^{220} para a metacaspase de *T. brucei* (Figura 13). Além disso, como semelhanças estruturais pode-se destacar a alça L3, que forma a base do sulco de ligação ao substrato, está desordenada em ambas as estruturas.

Entretanto, enquanto a díade catalítica da YCA1 se encontra na alça L2, o sítio catalítico da TbMCA2 se encontra nas extremidades C-terminais das fitas β3 e β4 (WONG *et al.,* 2012).

Figura 13 - Comparação estrutural entre Yca1 e TbMCA2. Na sobreposição estrutural ao redor do sítio de ligação do samário na TbMCA2, os quatro resíduos que se ligam ao samário na TbMCA2 estão em parênteses (Asp^{173}, Asp^{189}, Asp^{190} e Asp^{220}) são invariantes na YCA1. Os quatro resíduos da Yca1 também estão presentes e são marcados.

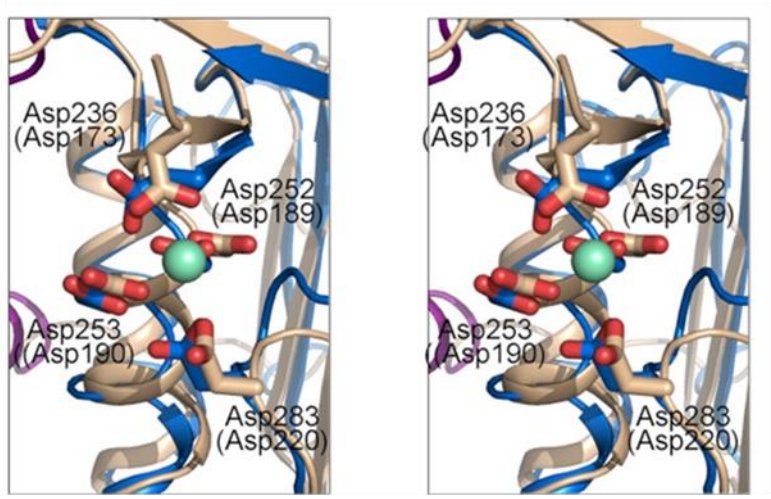

Fonte: WONG *et al.,* (2012).

A YCA1 quando comparada com a metacaspase de *Candida Albicans* (CaMCA) compartilha características estruturais importantes como a conformação das alças do sítio ativo e a presença de resíduos de ligação com o íon cálcio.

Artigos publicados sobre a investigação do processamento com íons divalentes destacaram que a YCA1 sofre um processamento adicional em fragmentos menores após incubação com Ca^{2+}, mas a concentração ideal ainda não foi estipulada. Outros íons divalentes foram testados e não tiveram efeito semelhante, o Ca^{2+} demonstrou ser específico na indução desse processamento na YCA1 (WONG *et al.,* 2012).

1.5 *Saccharomyces cerevisiae* E SUAS APLICAÇÕES BIOTECNOLÓGICAS

A *Saccharomyces cerevisiae* é uma levedura não patogênica pertencente ao reino dos fungos como um eucarioto unicelular, e é integrante do complexo *Saccharomyces sensu stricto*. É uma levedura que tem como característica realizar a fermentação gerando como produto etanol e dióxido de carbono, sendo assim o

principal micro-organismo utilizado na atualidade nos processos de fermentação alcoólica industriais de alimentos e bebidas (KURTZMAN, 2011; SICARD & LEGRAS, 2011; BORNEMAN & PRETORIUS, 2015).

Seu aspecto morfológico é ovoide e sua divisão é feita por brotamento (Figura 14) podendo ser haploide, diplóides ou poliplóides. Consiste em um micro-organismo aeróbico facultativo, que se ajusta metabolicamente quando há presença ou ausência de oxigênio, e sua duplicação se dá a cada 90 minutos sob temperatura de crescimento entre 20 e 30º C (GODDARD & GREIG, 2015; SALARI & SALARI, 2017; TULLIO, 2022).

Figura 14 - Imagens de microscopia eletrônica de varredura de células de *Saccharomyces cerevisiae*

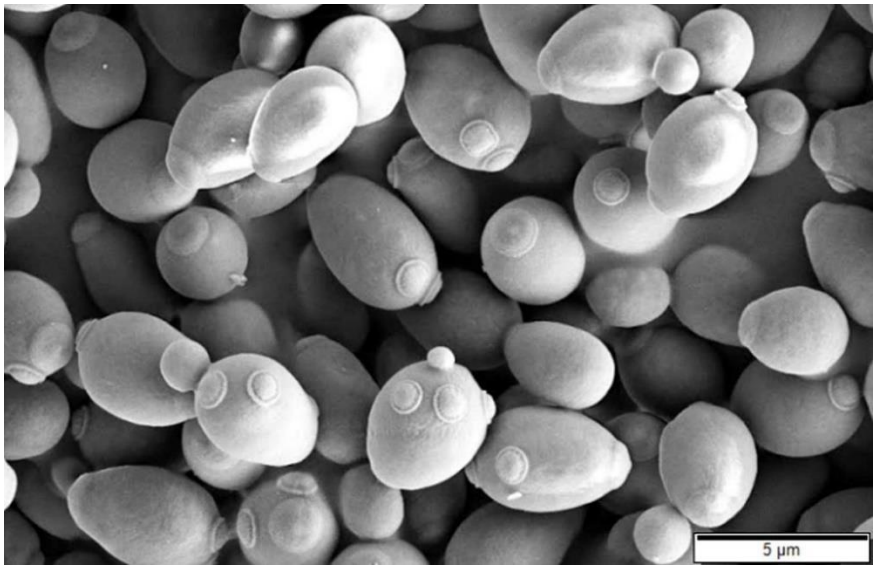

Fonte: MURTEY & RAMASAMY (2016)

Na década de 1980 os Estados Unidos da América realizaram um workshop com a intenção de avaliar os métodos existentes de detecção de mutações e nele surgiu a ideia de mapear o genoma humano completo, como uma forma de transformar a genética conhecida pela biologia. O projeto foi denominado Projeto Genoma Humano (HUGO). Logo, países como França, Europa e Japão se uniram para somar dados.

Anos depois, em 1996 a *S. cerevisiae* teve seu genoma totalmente sequenciado pelos pesquisadores Goffeau *et al*. como parte do projeto genoma e, a partir desse momento, ocorreu um avanço no desenvolvimento tecnológico voltado ao ramo da biotecnologia (GOFFEAU *et al.*, 1996). A levedura passou assim a ser um

modelo de referência, uma vez que havia informações concretas sobre suas características, como sua estrutura e sequência, o que forneceu base para aplicação em outros organismos, permitindo que diversas tecnologias fossem testadas com o modelo (CHERRY *et al.*, 2012).

Atualmente entre diversas espécies de organismos, a *S. cerevisiae* segue sendo amplamente utilizada para estudos e aplicações tecnológicas, desde pesquisas científicas até a utilização em produções industriais em larga escala. A evolução da levedura Saccharomyces cerevisiae comparada à história do desenvolvimento tecnológico e científico humano tem uma influência significativa no desenvolvimento de diversos estudos abordando aspectos biológicos, metabólicos, químicos e evolutivos desse micro-organismo (TULLIO, 2022).

Há mais de duas mil cepas de leveduras registradas em bancos de dados microbiológicos especializados. Dentre elas, a *Saccharomyces cerevisiae* é a espécie mais amplamente utilizada na nutrição de animais monogástricos e ruminantes, devido aos seus benefícios como probiótico e aditivo alimentar. Embora sua suplementação seja comum, *S. cerevisiae* não coloniza o trato digestivo de forma estável, devido à competição com a microbiota natural e a barreiras como o pH e o fluxo constante dos conteúdos digestivos (ELGHANDOUR *et al*., 2020).

Através da engenharia genética a levedura *S. cerevisiae* é largamente utilizada no ramo industrial desde a produção de fármacos até o ramo alimentício. Uma de suas aplicações é na produção de biofármacos, como na síntese de proteínas heterólogas, como por exemplo, a insulina e anticorpos monoclonais (DUARTE *et al.*, 2022; SUN *et al.*, 2022; TULLIO, 2022).

Estudos apontam que seu uso como suplemento alimentar permite a absorção de nutrientes que normalmente são pouco absorvidos como oligoelementos (zinco, ferro e selênio), além de regular a flora intestinal. Sua aplicabilidade também abrange rações para animais, uma vez que não é patogênica e ainda auxilia no equilíbrio da microbiota intestinal promovendo o crescimento de bactérias benéficas; estimulando o sistema imunológico e melhorando a digestão dos nutrientes, proteínas e aminoácidos (ELGHANDOUR *et al*., 2020).

A levedura *Saccharomyces sp.* é uma das únicas espécies de leveduras que é conveniente como alimento para animais e seres humanos, sendo assim amplamente utilizada na produção de etanol, rações para animais, produtos de panificação, e processamento de bebidas alcóolicas como cachaça, vinho e cervejas

(CABALLERO *et al*., 1997). Por não ser patogênica, o seu manuseio é simples, o que facilita no processo de cultivo e emprego no campo da ciência (SALARI & SALARI, 2017). Basicamente os produtos comercializados são compostos por leveduras vivas em meio de cultivo que foram previamente desidratadas para manterem suas funções de fermentação (ELGHANDOUR *et al*., 2020).

O uso da *S. cerevisiae* como modelo de estudo têm contribuído para a compreensão de processos biológicos oriundos de células eucarióticas, seja no ponto de vista bioquímico, molecular ou celular, auxiliando também na observação de processos ligados ao desenvolvimento de doenças em humanos (OSTERGAARD, OLSSON & NIELSEN, 2000; GODDARD & GREIG, 2015). Como exemplo, podemos citar os estudos relacionados ao processo de morte celular que utilizam como modelo a *S. cerevisiae*, e que foram úteis para o entendimento a respeito das vias de morte celular em organismos pluricelulares (CARMONA-GUTIERREZ *et al.,* 2010; CARMONA-GUTIERREZ *et al.*, 2018; SHRESTHA *et al.,* 2019).

Através de manipulação genética a *S. cerevisiae* ainda pode ser utilizada na produção de biocombustíveis, já que possui a aptidão de fermentar açúcar em etanol. Deste modo seu metabolismo pode ser modificado para que produza outros tipos de álcool com maiores características, como butanol e biodiesel. Outra grande aplicação da *S. cerevisiae* é na área de panificação da indústria alimentícia, onde atua como fermento biológico na produção de pães, esfihas, bolos e laticínios, como queijos e iogurtes (ABID *et al.*, 2022).

Graças a sua fácil manipulação, cultivo e crescimento essa levedura tem um futuro promissor quanto a perspectivas juntamente com o desenvolvimento das ferramentas genéticas aplicáveis. Visando sempre o desenvolvimento de tecnologias sustentáveis uma dessas possíveis futuras aplicações é através da agricultura celular, onde cepas da levedura geneticamente modificadas que produziriam a proteína do leite em larga escala, não sendo mais necessário a extração de leite de vacas. Essa nova abordagem pode garantir uma grande redução do impacto ambiental com menores emissões de gases de efeito estufa, redução de recursos hídricos e uso de terras, além de garantir uma produção em larga escala mais segura e controlada, podendo ainda gerar mais empregos com a inovação da indústria de alimentos e novas oportunidades de mercado (ELGHANDOUR *et al*., 2020; TULLIO, 2022).

Com base em todas as informações fornecidas sobre o impacto dos estudos em torno da *S. cerevisiae*, nosso trabalho teve como intuito aprofundar o

conhecimento sobre a YCA1, a única metacaspase encontrada na levedura considerada modelo, e que participa no processo de morte celular por apoptose. O mesmo processo ocorre em outros organismos patogênicos, assim corroborando para o entendimento do funcionamento das metacaspases, o que pode auxiliar no tratamento de doenças. Deste modo, esse trabalho teve como objetivo revelar, através de mutações sítio dirigidas, o impacto dos resíduos do sítio de cálcio na ativação enzimática e no autoprocessamento da YCA1.

1.6 *Trypanossoma brucei* – CICLO DE VIDA E METACASPASES

No genoma de *Trypanossoma brucei* foram encontrados 5 genes que codificam metacaspases (*TbMCA1* – *TbMCA5*) (MOTTRAM *et al.*, 2003). Os produtos da expressão desses genes dependem do estágio do ciclo de vida em que o parasita se encontra, vale, portanto, resumidamente explicar esse processo. A espécie *Trypanossoma brucei* (*T.brucei*) possui um ciclo de vida alternado entre um hospedeiro vertebrado e invertebrado, onde o protozoário passa por modificações que facilitam sua sobrevivência em cada fase do ciclo de vida (Domenicali Pfister *e cols.*, 2006; Fall, 2021). No hospedeiro vertebrado, ele apresenta-se na forma tripomastigota sanguínea, capaz de se proliferar através de divisão binária. Ao ser ingerido pelo inseto, no momento do repasso sanguíneo ele se diferencia na forma tripomastigota pró-cíclico (procyclic form- PCF), forma que permite sua sobrevivência no lúmen do sistema digestivo do vetor. Neste inseto infectado o ciclo de vida do parasita continua passando por uma série de mudanças, quando chega a glândulas salivares o tripomastigota pró-cíclico dá origem então a forma infectiva meta-cíclica, que é inoculada no hospedeiro vertebrado no momento do repasso sanguíneo. Quando em contato com a corrente sanguínea, as células meta-cíclicas (bloodstream form- BSF), que possui uma multiplicação assexuada se espalha pelo sangue, linfonodos, fluido espinhal e em um estágio mais avançado da infecção, pelo sistema nervoso central. No pico de parasitemia, algumas tripomastigotas sanguíneas se diferenciam em uma forma menor que é sugada pelo inseto vetor, reiniciando o ciclo de vida (Fall *et al*, 2022; Stuart *e cols.*, 2008).

A TbMCA2 e a TbMCA3 que são expressas somente na forma tripomastigota sanguínea possuem 89% de identidade entre si, diferença na verdade que se deve a uma extensão N-terminal presente na TbMCA3 que é uma região para ancoramento em membrana, enquanto a TbMCA2 que não possui esta extensão é citosólica (MACHADO *et al*., 2013). Estas peptidases, assim como outras metacaspases, possuem a díade catalítica de histidina e cisteína conservadas (MCLUSKEY *et al*., 2012). A TbMCA5 é expressa tanto na forma tripomastigota sanguínea como na forma pró-cíclica no inseto.

Os genes *TbMCA1* e *TbMCA4* codificam uma serina no lugar da cisteína catalítica, sugerindo então que estas enzimas sejam cataliticamente inativas, uma vez que experimentos de mutação sítio dirigida, já demonstraram que a troca da cisteína catalítica por serina em cisteíno peptidases resulta na inativação das mesmas MCLUSKEY *et al*., 2012).

REFERÊNCIAS

ABID, R.; WASEEM, H.; ALI, J. *et al.* Probiotic Yeast *Saccharomyces*: Back to Nature to Improve Human Health. **J Fungi (Basel)**, Suíça, v. 8, n. 5, p. 444, 2022.

ASHKENAZI, A.; DIXIT, V. M. Death receptors: Signaling and modulation. **Science**, v. 281 n. 1, p. 1305–1308, 1998.

BARRETT, A.J. Classification of Peptidases. *In:* ABELSON, J.; SIMON, M. **Methods in Enzymology**: Proteolytic Enzymes – Serine and Cysteine Peptidases, v. 244. 1. ed. Estados Unidos: Academic Press, 1994. cap. 1, p. 1-15.

BELL, R. A. V.; MEGENEY, L. A. Evolution of caspase-mediated cell death and differentiation: twins separated at birth. **Cell Death & Differentiation**, v. 24, n. 8, p. 1359-1368, 2017.

BORNEMAN, A. R.; PRETORIUS, I. S. Genomic insights into the Saccharomyces sensu stricto complex. **Genetics,** v. 199, p. 281–291, 2015.

BÜTTNER, S.; EISENBERG, T.; HERKER, E.; CARMONA-GUTIERREZ, D.; KROEMER, G.; MADEO, F. Why yeast cells can undergo apoptosis: death in times of peace, love, and war. **The Journal of cell biology**, v. 175, n. 4, p. 521–525, 2006.

CABALLERO-CÓRDOBA, Glenys M.; PACHECO, Maria Teresa B.; SGARBIERI, Valdemiro C. Composição química da biomassa de levedura integral (Saccharomyces sp.) e determinação do valor nutritivo da proteína em células íntegras ou rompidas mecanicamente. **Food Science and Technology**, v. 17, p. 102-106, 1997.

CARMONA-GUTIERREZ, D.; BAUER, M.A.; ZIMMERMANN, A. *et al.* Guidelines and recommendations on yeast cell death nomenclature. **Microbial Cell**, Áustria, v. 5, n. 1, p. 4-31, 2018.

CARMONA-GUTIERREZ, D.; FROHLICH, K.U.; KROEMER, G.; MADEO, F. Metacaspases are caspases. Doubt no more. **Cell Death Differ**, Reino Unido, v. 17, n. 3, p. 377-378, 2010.

CASTRO, H.C. *et al*. Looking at the proteases from a simple perspective. **J Mol Recognit**, Reino Unido, v. 24, n. 2, p. 165-181, 2011.

CHAKRABARTY, S.; KAHLER, J.P.; VAN DE PLASSCHE, M.A.T. *et al*. Recent Advances in Activity-Based Protein Profiling of Proteases. *In:* CRAVATT, B.; HSU, K.L.; WEERAPANA, E. (eds). **Current Topics in Microbiology and Immunology**, v. 420. Suíça: Springer, p. 253-281, 2019.

CHERRY, J.M.; HONG, E.L.; AMUNDSEN, C. *et al. Saccharomyces* Genome Database: the genomics resource of budding yeast. **Nucleic Acids Res**, Reino Unido, v. 40, n. D1, p. D700-705, 2012.

D’ARCY, M.S. Cell death: a review of the major forms of apoptosis, necrosis and autophagy. **Cell Biol Int**, Estados Unidos, v. 43, n. 6, p. 582-592, 2019.

DONEHOWER LA, BRADLEY A. The tumor suppressor p53. **Biochimica et Biophysica Acta**, v. 1155, n. 2, p. 181-205, 1993.

DUARTE, M.; OLIVEIRA, A.L.; OLIVEIRA, C. *et al.* Current postbiotics in the cosmetic market—an update and development opportunities. **Appl Microbiol Biotechnol**, Alemanha, v. 106, n. 18, p. 5879-5891, 2022.

ELGHANDOUR, M. M. Y. *et al*. Saccharomyces cerevisiae as a probiotic feed additive to non and pseudo-ruminant feeding: a review. **Journal of applied microbiology**, v. 128, n. 3, p. 658-674, 2020.

ELMORE, S. Apoptosis: a review of programmed cell death. **Toxicologic Pathology,** v. 35, n. 4, p. 495-516, 2007.

ERHARDT, M.; WEGRZYN, R.; DEUERLING, E. Extra N-terminal residues have a profound effect on the aggregation properties of the potencial yeast prion protein Mca1. **PLoS One**, v. 5, n. 3, p. e9929, 2010.

FLEISHER, T.A. Apoptosis. **Ann Allergy Ashthma Immunol**, Estados Unidos, v. 78, n. 3, p. 245-250, 1997.

GALLUZZI, L.; KEPP, O.; TROJEL-HANSEN, C.; KROEMER, G. Mitochondrial control of cellular life, stress, and death. **Circulation Research**, v. 111, n. 10, p. 1198–1207, 2012.

GALLUZZI, L.; VITALE, I.; AARONSON, S. A.; ABRAMS, J. M.; ADAM, D.; AGOSTINIS, P.; ALNEMRI, E. S.; ALTUCCI, L.; AMELIO, I.; ANDREWS, D. W.; ANNICCHIARICO-PETRUZZELLI, M.; ANTONOV, A. V.; ARAMA, E.; BAEHRECKE, E. H.; BARLEV, N. A.; BAZAN, N. G.; BERNASSOLA, F.; BERTRAND, M. J. M.; BIANCHI, K.; BLAGOSKLONNY, M. V.; BLOMGREN, K.; BORNER, C.; BOYA, P.; BRENNER, C.; CAMPANELLA, M.; CANDI, E.; CARMONA-GUTIERREZ, D.; CECCONI, F.; CHAN, F. K.; CHANDEL, N. S.; CHENG, E. H.; CHIPUK, J. E.; CIDLOWSKI, J. A.; CIECHANOVER, A.; COHEN, G. M.; CONRAD, M.; CUBILLOS-RUIZ, J. R.; CZABOTAR, P. E.; D'ANGIOLELLA, V.; DAWSON, T. M.; DAWSON, V. L.; DE LAURENZI, V.; DE MARIA, R.; DEBATIN, K. M.; DEBERARDINIS, R. J.; DESHMUKH, M.; DI DANIELE, N.; DI VIRGILIO, F.; DIXIT, V. M.; DIXON, S. J.; DUCKETT, C. S.; DYNLACHT, B. D.; EL-DEIRY, W. S.; ELROD, J. W.; FIMIA, G. M.; FULDA, .; GARCÍA-SÁEZ, A. J.; GARG, A. D.; GARRIDO, C.; GAVATHIOTIS, E.; GOLSTEIN, P.; GOTTLIEB, E.; GREEN, D. R.; GREENE, L. A.; GRONEMEYER, H.; GROSS, A.; HAJNOCZKY, G.; HARDWICK, J. M.; HARRIS, I. S.; HENGARTNER, M. O.; HETZ, C.; ICHIJO, H.; JÄÄTTELÄ, M.; JOSEPH, B.; JOST, P. J.; JUIN, P. P.; KAISER, W. J.; KARIN, M.; KAUFMANN, T.; KEPP, O.; KIMCHI, A.; KITSIS, R. N.; KLIONSKY, D. J.; KNIGHT, R. A.; KUMAR, S.; LEE, S. W.; LEMASTERS, J. J.; LEVINE, B.; LINKERMANN, A.; LIPTON, S. A.; LOCKSHIN, R. A.; LÓPEZ-OTÍN, C.; LOWE, S. W.; LUEDDE, T.; LUGLI, E.; MACFARLANE, M.; MADEO, F.; MALEWICZ, M.; MALORNI, W.; MANIC, G.; MARINE, J. C.; MARTIN, S. J.; MARTINOU, J. C.; MEDEMA, J. P.; MEHLEN, P.; MEIER, P.; MELINO, S.; MIAO, E. A.; MOLKENTIN,

J. D.; MOLL, U. M.; MUÑOZ-PINEDO, C.; NAGATA, S.; NUÑEZ, G.; OBERST, A.; OREN, M.; OVERHOLTZER, M.; PAGANO, M.; PANARETAKIS, T.; PASPARAKIS, M.; PENNINGER, J. M.; PEREIRA, D. M.; PERVAIZ, S.; PETER, M. E.; PIACENTINI, M.; PINTON, P.; PREHN, J. H. M.; PUTHALAKATH, H.; RABINOVICH, G. A.; REHM, M.; RIZZUTO, R.; RODRIGUES, C. M. P.; RUBINSZTEIN, D. C.; RUDEL, T.; RYAN, K. M.; SAYAN, E.; SCORRANO, L.; SHAO, F.; SHI, Y.; SILKE, J.; SIMON, H. U.; SISTIGU, A.; STOCKWELL, B. R.; STRASSER, A.; SZABADKAI, G.; TAIT, S. W. G.; TANG, D.; TAVERNARAKIS, N.; THORBURN, A.; TSUJIMOTO, Y.; TURK, B.; VANDEN BERGHE, T.; VANDENABEELE, P.; VANDER HEIDEN, M. G.; VILLUNGER, A.; VIRGIN, H. W.; VOUSDEN, K. H.; VUCIC, D.; WAGNER, E. F.; WALCZAK, H.; WALLACH, D.; WANG, Y.; WELLS, J. A.; WOOD, W.; YUAN, J.; ZAKERI, Z.; ZHIVOTOVSKY, B.; ZITVOGEL, L.; MELINO, G.; KROEMER, G. Molecular mechanisms of cell death: recommendations of the Nomenclature Committee on Cell Death 2018. **Cell Death & Differentiation,** v. 25, n. 3, p. 486 – 541, 2018.

GALLUZZI, L.; VITALE, I.; ABRAMS, J. M.; ALNEMRI, E. S.; BAEHRECKE, E. H.; BLAGOSKLONNY, M. V.; DAWSON, T. M.; DAWSON, V. L.; EL-DEIRY, W. S.; FULDA, S.; GOTTLEIB, E.; GREEN, D. R.; HENGARTNER, M. O.; KEPP, O.; KNIGHT, R. A.; KUMAR, S.; LIPTON, S. A.; LU, X.; MADEO, F.; MALORNI, W.; MEHLEN, P.; NÚÑEZ, G.; PETER, M. E.; PIACENTINI, M.; RUBINSZTEIN, D. C.; SHI, Y.; SIMON, H. U.; VANDENABEELE, P.; WHITE, E.; YUAN, J.; ZHIVOTOVSKY, B. Molecular definitions of cell death subroutines: Recommendations of the Nomenclature Committee on Cell Death. **Cell Death and Differentiation**, v. 19, n. 1, p. 107–120, 2012.

GAO, X.; QIN, B.; CHEN, P. *et al*. Crystal structure of SARS-CoV-2 papain-like protease. **Acta Pharm Sin B**, Holanda, v. 11, n. 1, p. 237-245, 2021.

GILIO, J. M.; MARCONDES, M. F.; FERRARI, D.; JULIANO, M. A.; JULIANO, L.; OLIVEIRA, V.; MACHADO, M. F. Processing of metacaspase 2 from Trypanosoma brucei (TbMCA2) broadens its substrate specificity. **Biochimica et Biophysica Acta**, Alemanha, v. 1865, n. 4, p. 388-394, 2017.

GODDARD, M.R.; GREIG, D. *Saccharomyces cerevisiae*: a nomadic yeast with no niche?. **FEMS Yeast Res**, Reino Unido, v. 15, n. 3, p. 1-6, 2015

GOFFEAU, A.; BARRELL, B.G.; BUSSEY, H. *et al.* Life with 6000 Genes. **Science**, Estados Unidos, v. 274, n. 5287, p. 546-567, 1996.

GONZALES, I. J.; DESPONDS, C.; SCHAFF, C.; MOTTRAM, J. C.; FASEL, N. Leishmania major metacaspase can replace yeast metacaspase in programmed cell death and has arginine-specific cysteine peptidase activity. **International Journal of Parasitology**, v. 37, p. 161–172, 2007.

GREEN, D. R.; FITZGERALD, P. Just So Stories about the Evolution of Apoptosis. **Current Biology**, v. 26, n. 13, p. R620-R627, 2016.

GREEN, D. R.; KROEMER, G. The pathophysiology of mitochondrial cell death. **Science**, v. 305, n. 5684, p. 626-629, 2004.

GREEN, D. R.; LLAMBI, F. Cell Death Signaling. **Cold Spring Harbor Perspectives in Biology,** v. 7, n. 12, p. a006080, 2015.

HILL, S. M.; NYSTRÖ, M T. The dual role of a yeast metacaspase: What doesn't kill you makes you stronger. **Bioessays,** v. 37, n. 5, p. 525–531, 2015.

HITOSHI, Y.; LORENS, J.; KITADA, SI.; FISHER, J.; LABARGE, M.; RING, H. Z.; FRANCKE, U.; REED, J. C.; KINOSHITA, S.; NOLAN, G. P. Toso, a cell surface, specific regulator of Fas-induced apoptosis in T cells. **Immunity**, v. 8, n. 1, p. 461–471, 1998.

HOOPER, N.M. Proteases: a primer. **Essays Biochem**, Reino Unido, v. 38, n. 1, p. 1-8, 2002.

KACZANOWSKI, S.; SAJID, M.; REECE, S. E. Evolution of apoptosis-like programmed cell death in unicellular protozoan parasites. **Parasites & Vectors,** v. 4, n. 44, p. 1-8, 2011.

KANG, S. J.; WANG, S.; KUIDA, K.; YUAN, J. Distinct downstream pathways of caspase-11 in regulating apoptosis and cytokine maturation during septic shock response. **Cell Death Differentiation,** v. 9, n. 10, p. 1115-1125, 2002.

KERR, J. F.; WYLLIE, A. H.; CURRIE, A. R. Apoptosis: a basic biological phenomenon with wide-ranging implications in tissue kinetics. **British Journal of Cancer,** v. 26, n. 4, p. 239-257, 1972.

KLEMENČIČ, M.; FUNK, C. Evolution and Structural Diversity of Metacaspases. **J Exp Bot**, Reino Unido, v. 70, n. 7, p. 2039-2047, 2019.

KLEMENČIČ, M.; FUNK, C. Type III metacaspases: calcium-dependent activity proposes new function for the p10 domain. **New Phytol**, Reino Unido, v. 218, n. 3, p. 1179-1191, 2017.

KUMAR, V.; ABBAS, A.K.; ASTER, J.C. **Robbins Patologia Básica**. 10ª ed. Rio de Janeiro: GEN | Editora Guanabara Koogan, 2018.

KURTZMAN, C. P. Discussion of Teleomorphic and Anamorphic Ascomycetous Yeasts and Yeast-like Taxa. In.: KURTZMAN, C. P.; FELL, J. W.; BOEKHOUT, T. The Yeasts a Taxonomic Study. 5ª ed. Elsevier, v. 2, p. 293–307, 2018.

LEE, N.; GANNAVARAM, S.; SELVAPANDIYAN, A.; DEBRABANT, A. Characterization of metacaspases with trypsin-like activity and their putative role in programmed cell death in the protozoan parasite Leishmania. **Eukaryot Cell**, v. 6, n. 61, p. 1745-57, 2007.

LEE, R. E. C.; BRUNETTE, S.; PUENTE, L. G.; MEGENEY, L. A. Metacaspase Yca1 is required for clearance of insoluble protein aggregates. **Proceedings of the National Academy of Sciences of the United States of America**, v. 107, n. 30, p. 13348-13353, 2010.

LEE, R. E.; PUENTE, L. G.; KAERN, M.; MEGENEY, L. A. A non-death role of the yeast metacaspase: Yca1p alters cell cycle dynamics. **PLoS One**, v. 3, p. e2956, 2008.

LEHNINGER, T. M.; NELSON, D. L.; COX, M. M. **Princípios de Bioquímica**. 8. ed. Porto Alegre: Artmed, 2019.

LI, X.; WU, X.; GAO, Y.; HAO, L. Synergistic Effects and Mechanisms of Combined Treatment With Harmine Hydrochloride and Azoles for Resistant *Candida albicans*. **Front Microbiol**, Suíça, v. 10, n. 2295, p. 1-12, 2019.

LOCKSLEY, R. M.; KILLEEN, N.; LENARDO, M. J. TNF receptor superfamilies and TNF: integrating mammalian biology. **Cell**, v. 104, n. 1, p. 487–501, 2001.

LOMONOSOVA, E.; CHINNADURAI, G. Bh3-only proteins in apoptosis and beyond: an overview. **Oncogene**, v. 27, n. S2, p. S2-S19, 2008.

LOMONOSOVA, Elena; CHINNADURAI, G. BH3-only proteins in apoptosis and beyond: an overview. **Oncogene**, v. 27, n. 1, p. S2-S19, 2008.

MACHADO, M. F.; MARCONDES, M. F.; JULIANO, M. A.; MCLUSKEY, K.; MOTTRAM, J. C.; MOSS, C. X.; JULIANO, L.; OLIVEIRA, V. Substrate specificity and the effect of calcium on Trypanosoma brucei metacaspase 2. **The FEBS Journal**, v. 280, n. 11, p. 2608-1621, 2013.

MACKENZIE, S.H; CLARK, A. C. Death by caspase dimerization. **Advances in Experimental Medicine and Biology**, v. 747, n. 54, p. 55-73, 2012.

MADEO, F.; FRÖHLICH, E.; FRÖHLICH, K. U. A yeast mutant showing diagnostic markers of early and late apoptosis. **Journal of Cell Biology,** v. 139, n. 3, p. 729-734, 1997.

MADEO, F.; HERKER, E.; MALDENER, C.; WISSING, S.; LÄCHELT, S.; HERLAN, M.; FEHR, M.; LAUBER, K.; SIGRIST, S. J.; WESSELBORG, S.; FRÖHLICH, K. U. A caspase-related protease regulates apoptosis in yeast. **Molecular Cell,** v. 9, n. 7, p. 911-917, 2002.

MADEO, F.; FRÖHLICH, E.; LIGR, M. *et al*. Oxygen Stress: A Regulator of Apoptosis in Yeast. **J Cell Biol**, Estados Unidos, v. 145, n. 4, p. 757-767,1999.

MADEO, F.; HERKER, E.; MALDENER, C. *et al.* A Caspase-Related Protease Regulates Apoptosis in Yeast. **Mol Cell**, Estados Unidos, v. 9, n. 4, p. 911-917, 2002.

MAHAJAN, R.T.; BADGUJAR, S.B. Biological aspects of proteolytic enzymes: A Review. **Journal of Pharmacy Research**, Índia, v. 3, n. 9, p. 2048-2068, set/2010.

MCLUSKEY, K.; MOTTRAM, J. C. Comparative structural analysis of the caspase family with other clan cysteine peptidases. **Biochem Journal**, v. 476, n. pt 2, p. 219-232, 2015.

MCLUSKEY, K.; RUDOLF, J.; PROTO, W. R.; ISAACS, N. W.; COOMBS, G. H.; MOSS, C. X.; MOTTRAM, J. C. Crystal structure of a Trypanosoma brucei metacaspase. **Proceedings of the National Academy of Sciences of the United States of America,** v.109, n. 19, p. 7469-7474, 2012.

MININA, E.A.; COLL, N.S.; TUOMINEN, H.; BOZHKOV, P.V. Metacaspases versus caspases in development and cell fate regulation. **Cell Death Differ**, Reino Unido, v. 24, n. 8, p. 1314-1325, 2017.

MOSS, C.X.; WESTROP, G.D.; JULIANO, L. *et al*. Metacaspase 2 of *Trypanosoma brucei* is a calcium-dependent cysteine peptidase active without processing. **FEBS Lett**, Estados Unidos, v. 581, n. 29, p. 5635-5639, 2007.

MOTTRAM, J.C.; HELMS, M.J.; COOMBS, G.H.; SAJID, M. Clan CD cysteine peptidases of parasitic protozoa. **Trends Parasitol**, Reino Unido, v. 19, n. 4, p. 182-187, 2003.

MOTTRAM, J.; COOMBS, G.; ALEXANDER, J. Cysteine peptidases as virulence factors of Leishmania. **Current Opinion in Microbiology,** v. 7, n. 4, p. 375-381, 2004.

MÓTYÁN, J. A.; TÓTH, F.; TŐZSÉR, J. Research applications of proteolytic enzymes in molecular biology. **Biomolecules**, v. 3, n. 4, p.923–942, 2013.

MURTEY, M. Das; RAMASAMY, Patchamuthu. Sample preparations for scanning electron microscopy–life sciences. **Modern electron microscopy in physical and life sciences**, v. 2, 2016.

NAGATA, S. Apoptosis and Clearance of Apoptotic Cells. **Annu Rev Immunol**, Estados Unidos, v. 36, n. 1, p. 489-517, 2018.

NORBURY, Chris J.; HICKSON, Ian D. Cellular responses to DNA damage. **Annual review of pharmacology and toxicology**, v. 41, n. 1, p. 367-401, 2001.

OBENG, E. Apoptosis (programmed cell death) and its signals – A review. **Braz J Biol**, Brasil, v. 81, n. 4, p. 1133-1143, 2021.

OSTERGAARD, S.; OLSSON, L.; NIELSEN, J. Metabolic Engineering of *Saccharomyces cerevisiae*. **Microbiol Mol Biol Rev**, Estados Unidos, v. 64, n. 1, p. 34-50, 2000.

OTTO, H.H.; SCHIRMEISTER, T. Cysteine Proteases and Their Inhibitors. **Chem Rev**, Estados Unidos, v. 97, n. 1, p. 133-171, 1997.

PROTO, W.R.; CASTANYS-MUNOZ, E.; BLACK, A. *et al.* Trypanosoma brucei metacaspase 4 is a pseudopeptidase and a virulence fator. **J Biol Chem**, Estados Unidos, v. 286, n. 46, p. 39914-39925, 2018.

RANI, K.; RANA, R.; DATT, S. Review on latest overview of proteases. **International Journal of Current Life Sciences**, India, v. 2, n. 1, p.12-18, 2012.

RAWLINGS, N.D. A large and accurate collection of peptidase cleavages in the MEROPS database. **Database (Oxford)**, v. 2009, n. bap015, p. 1-14, 2009.

RAWLINGS, N.D.; BARRETT, A.J. Evolutionary families of peptidases. **Biochem J**, Reino Unido, v. 290, n. 1, p. 205-218, 1993.

RAWLINGS, N.D.; BARRETT, A.J.; FINN, R. Twenty years of the MEROPS database of proteolytic enzymes, their substrates and inhibitors. **Nucleic Acids Res,** Reino Unido, v. 44, n. D1, p. D343-D350, 2016.

RAWLINGS, N. D.; BARRETT, A. J.; THOMAS, P. D.; HUANG, X.; BATEMAN, A. & FINN, R. D. The MEROPS database of proteolytic enzymes, their substrates, and inhibitors in 2017 and a comparison with peptidases in the PANTHER database. **Nucleic Acids Research**, 2018.

RUBIO-MOSCARDO, F.; BLESA, D.; MESTRE, C.; SIEBERT, R.; BALASAS, T.; BENITO, A.; ROSENWALD, A.; CLIMENT, J.; MARTINEZ, J. I.; SCHILHABEL, M.; KARRAN, E. L.; GESK, S.; ESTELLER, M.; DELEEUW, R.; STAUDT, L. M.; FERNANDEZ-LUNA, J. L.; PINKEL, D.; DYER, M. J.; MARTINEZ-CLIMENT, J. A. Characterization of 8p21.3 chromosomal deletions in B-cell lymphoma: TRAIL-R1 and TRAIL-R2 as Candidate dosage-dependent tumor suppressor genes. **Blood**, v. 106, n. 1, p. 3214–3222, 2005.

SALARI, R.; SALARI, R. Investigation of the Best *Saccharomyces cerevisiae* Groselvagemh Condition. **Electron Physician**, Irã, v. 9, n. 1, p. 3592-3597, 2017.

SALVESEN, G.S.; HEMPEL, A.; COLL, N.S. Protease signaling in animal and plant-regulated cell death. **FEBS J**, Reino Unido, v. 283, n. 14, p. 2577-2598, jul/2016SAMBROOK, J.; RUSSEL, D. W. **Molecular Cloning.** 3 editions. 3 vol. Cold Spring Harbor Laboratory Press, New York, 2001.

SCHECHTER, I.; BERGER, A. On the size of the active site in proteases. I. Papain. **Biochemical and Biophysical Research Communications,** v. 27, n. 2, p. 157-162, 1967.

SHRESTHA, A.; BRUNETTE, S.; STANFORD, W.L.; MEGENEY, L.A. The metacaspase Yca1 maintains proteostasis through multiple interactions with the ubiquitin system. **Cell Discov**, Reino Unido, v. 5, n. 6, p. 1-13, 2019.

SICARD, D.; LEGRAS, J-L. Bread, beer and wine: Yeast domestication in the Saccharomyces sensu stricto complex. C. R. Biologies, n. 334, p. 229–236, 2011.

SILVA, R.D.; SOTOCA, R.; JOHANSSON, B. *et al*. Hyperosmotic stress induces metacaspase- and mitochondria-dependent apoptosis in *Saccharomyces cerevisiae*. **Mol Microbiol**, Reino Unido, v. 58, n. 3, p. 824-834, nov. 2005.

STELLER H. Mechanisms and genes of cellular suicide. **Science,** v. 267, n. 5203, p. 1445-1449, 1995.

SUN, J.; XUM S.; DU, Y. *et al.* Accumulation and Enrichment of Trace Elements by Yeast Cells and Their Applications: A Critical Review. **Microorganisms**, Suíça, v. 10, n. 9, p. 1746, 2022.

TAIT, S. W. G.; GREEN, D. R. Mitochondria, and cell death: Outer membrane permeabilization and beyond. **Nature Reviews Molecular Cell Biology**, v. 11, n. 9, p. 621–632, 2010.

TSIATSIANI, L.; VAN BREUSEGEM, F.; GALLOIS, P.; ZAVIALOV, A.; LAM, E.; BOZHKOV, P. V. Metacaspases. **Cell Death & Differentiation**, v. 18, n. 8, p. 1279-1288, 2011.

TULLIO, V. Yeast Genomics and Its Applications in Biotechnological Processes: What Is Our Present and Near Future?. **J Fungi (Basel)**, Suíça, v. 8, n. 7, p. 752, jul/2022.

UREN, A. G.; O'ROURKE, K.; ARAVIND, L. A.; PISABARRO, M.T.; SESHAGIRI, S.; KOONIN, E.V.; DIXIT, V. M. Identification of paracaspases and metacaspases: two ancient families of caspase-like proteins, one of which plays a key role in MALT lymphoma. **Molecular Cell,** EUA, v. 6, n. 4, p. 961-967, 2000.

VÁCHOVÁ, L.; PALKOVÁ, Z. Physiological regulation of yeast cell death in multicellular colonies is triggered by ammonia. **The Journal of cell biology**, v. 169, n. 5, p. 711–717, 2005.

VERCAMMEN, D.; VAN DE COTTE, B.; DE JAEGER, G.; EECKHOUT, D.; CASTEELS, P.; VANDEPOELE, K.; VANDENBERGHE, I.; VAN BEEUMEN, J.; INZÉ, D.; VAN BREUSEGEM, F. Type II metacaspases Atmc4 and Atmc9 of Arabidopsis thaliana cleave substrates after arginine and lysine. **Journal of Biological Chemistry**, v. 279, n. 44, p. 45329-45336, 2004.

VERMA, S.; DIXIT, R.; PANDEY, K. C. Cysteine Proteases: Modes of Activation and Future Prospects as Pharmacological Targets, **Frontiers in Pharmacology**, v. 7, n. 107. p. 1-12, 2016.

WAJANT, Harald. The Fas signaling pathway: more than a paradigm. **Science**, v. 296, n. 5573, p. 1635-1636, 2002.

WONG, A. H.; YAN, C.; SHI, Y. Crystal structure of the yeast metacaspase Yca1. **Journal of Biological Chemistry**, v. 287, p. 29251-29259, 2012.

YAN, G.; ELBADAWI, M. EFFERTH, T. Multiple cell death modalities and their key features (Review). **World Academy of Sciences Journal,** v. 2, n. 2, p. 38 – 48, 2020.

ZALILA, H.; GONZÁLEZ, I. J.; EL-FADILI, A. K.; DELGADO, M. B.; DESPONDS, C.; SCHAFF, C.; FASEL, N. Processing of metacaspase into a cytoplasmic catalytic

domain mediating cell death in Leishmania major. **Molecular Microbiology**, v. 79, 2. 1, p. 222-239, 2011

CAPÍTULO 1

MUTAÇÕES SÍTIO-DIRIGIDAS NA METACASPASE DE *S. cerevisiae*: UMA ABORDAGEM METODOLÓGICA AVANÇADA PARA ESTUDOS ESTRUTURAIS E FUNCIONAIS

PREFÁCIO

Este capítulo trata da metodologia implantada para a clonagem da YCA1 selvagem e mutantes utilizadas no capítulo 2 desta tese, este trabalho foi publicado na revista UMC, como artigo completo apresentado na 1ª edição do SUMMIT – UMC.

Revista Científica UMC | RCUMC | ISSN: 2525-5150

Mutações sítio-dirigidas na metacaspase de *S. cerevisiae*: Uma abordagem metodológica avançada para estudos estruturais e funcionais

Site-directed mutations in *S. cerevisiae* metacaspase: An advanced methodological approach for structural and functional studies

Mutaciones dirigidas en el sitio de la metacaspase de *S. cerevisiae*: Un enfoque metodológico avanzado para estudios estructurales y funcionales.

Mariana Nascimento Romero Trujilho[1], Laura de Azevedo Maffeis Dalzoto[1], Taiz dos Reis Santos[1], Laura Helena Araújo, João Pedro Martins Silva Costa, Ane Caroline Moreira Duarte, Tatiane Faustino de Moraes[1], Wagner Alves de Souza Judice[1], Marcelo Ferreira Marcondes Machado[2], Maurício Ferreira Marcondes Machado[1,*].

RESUMO

Objetivo: As metacaspases são cisteína-proteases que requerem cálcio para atividade e se ativam por autoprocessamento, diferentemente das caspases. As metacaspases são categorizadas em tipos I, II e III, como a YCA1 em *Saccharomyces cerevisiae,* associada à apoptose. O estudo buscou clonar um YCA1 recombinante, com mutações específicas nos resíduos Cys155 e Cys276, expressando e purificando essas proteínas. Os mutantes foram obtidos com sucesso usando sobreposição de fragmentos e método TEDA de clonagem, expressos em E. coli e purificados por cromatografia de camada e exclusão molecular. A identificação da importância da cisteína Cys155 no autoprocessamento da YCA1 e a sugestão de um segundo processamento intermolecular entre metacaspases ativas, semelhante à ativação das caspases, foram resultados notáveis. Mostrou-se que os processamentos levam à forma ativa da enzima no C-terminal, diferente do descrito anteriormente. Concluindo, a presença de uma segunda cisteína catalítica na YCA1 foi evidenciada, trazendo uma nova perspectiva sobre sua ativação, com processamentos antes não descritos, tanto autoprocessamento quanto intermolecular.

Palavras-chave: Metacaspase, *Saccharomyces cerevisiae*, Mutação, Cisteína

[1] 1Centro Interdisciplinar de Investigação Bioquímica, Universidade de Mogi das Cruzes, Av Dr. Cândido Xavier de Almeida e Souza, 200, 08780-991, Mogi das Cruzes, Brazil.. *E-mail: mauriciomachado@umc.br

[2] Departamento de Biofísica, Universidade Federal de São Paulo, Rua Pedro de Toledo, 669, 7º andar, 04039-032, São Paulo. Brazil.

SUBMETIDO EM: XX/2023 | ACEITO EM: XX/2023 | PUBLICADO EM: XX/2023

Revista Científica UMC | RCUMC | ISSN: 2525-5150

ABSTRACT

Objective: Metacaspases are cysteine proteases that require calcium for activity and are activated through autoprocessing, unlike caspases. Metacaspases are categorized into types I, II, and III, such as YCA1 in Saccharomyces cerevisiae, associated with apoptosis. The study aimed to clone a recombinant YCA1, with specific mutations in residues Cys155 and Cys276, expressing and purifying these proteins. Mutants were successfully obtained using fragment overlap and the TEDA cloning method, expressed in E. coli, and purified through layer chromatography and molecular exclusion. The identification of the significance of cysteine Cys155 in YCA1autoprocessing and the suggestion of a second intermolecular processing between active metacaspases, akin to caspase activation, were significant findings. It was shown that the processings lead to the enzyme's active form in the C-terminal, contrary to previous descriptions. In conclusion, the presence of a second catalytic cysteine in YCA1 was demonstrated, presenting a new perspective on its activation, involving previously undescribed processes—both autoprocessing and intermolecular processing.

Key words: Metacaspase, *Saccharomyces cerevisiae*, Mutation, Cysteine

RESUMEN

Objetivo: Las metacaspasas son cisteína-proteasas que requieren calcio para su actividad y se activan a través del autoprocesamiento, a diferencia de las caspasas. Las metacaspasas se clasifican en tipos I, II y III, como la YCA1 en Saccharomyces cerevisiae, asociada a la apoptosis. El estudio tuvo como objetivo clonar una YCA1 recombinante, con mutaciones específicas en los residuos Cys155 y Cys276, expresando y purificando estas proteínas. Los mutantes se obtuvieron con éxito mediante la superposición de fragmentos y el método de clonación TEDA, expresados en E. coli y purificados mediante cromatografía en capa y exclusión molecular. La identificación de la importancia de la cisteína Cys155 en el autoprocesamiento de la YCA1 y la sugerencia de un segundo procesamiento intermolecular entre metacaspasas activas, similar a la activación de las caspasas, fueron hallazgos significativos. Se demostró que los procesos conducen a la forma activa de la enzima en el extremo C-terminal, en contraste con lo descrito anteriormente. En conclusión, se evidenció la presencia de una segunda cisteína catalítica en la YCA1, aportando una nueva perspectiva sobre su activación, con procesos antes no descritos, tanto autoprocesamiento como intermolecular.

Palabras clave: Metacaspasa, *Saccharomyces cerevisiae*, Mutación, Cisteína

INTRODUÇÃO

Uma cisteíno-protease com similaridade estrutural às caspases de mamíferos foi identificada em células eucariotas simples por Uren *et al*. (2000) utilizando-se de ferramentas de bioinformática. A metacaspase, como passou a ser chamada, foi então identificada em plantas, fungos e protozoários, mas notou-se sua ausência em mamíferos (21).

As caspases são sintetizadas como zimogênios e possuem uma díade catalítica His/Cys (H e C), assim como as metacaspases. São compostas por um pró-domínio que antecede as duas

Revista Científica UMC | RCUMC | ISSN: 2525-5150

subunidades p20 (grande) e p10 (pequena), e tornam-se enzimaticamente ativas após sofrerem uma clivagem proteolítica após dois resíduos de ácido aspártico (D). Após essa clivagem, ocorre a dimerização das duas subunidades tanto p20 quanto p10, resultando na chamada caspase efetora (6,8,21).

As metacaspases, diferentemente das caspases, podem ter a presença ou não de um pró-domínio rico em prolina e/ou de uma região rica em glutaminas e asparaginas, não sendo necessário passar pelo processo de dimerização para estarem ativas, pois são ativas na forma monomérica, entretanto carecem da presença do íon cálcio, que possui papel de cofator, para o desempenho de sua atividade (6,8). Diferente das caspases que clivam substratos após um resíduo de ácido aspártico, as metacaspases clivam seus substratos após resíduos básicos de arginina ou lisina na posição P_1 (12,22).

A metacaspase do tipo I contém um pró-domínio N-terminal rico em prolina e motivo dedo de zinco. A metacaspase tipo II não possui pró-domínio, porém, possui um domínio vinculador com vários resíduos de aminoácidos que separam a subunidade p20 catalítica e p10 reguladora. Já a metacaspase tipo III sofre um rearranjo diferente, a subunidade p10 antecede a subunidade p20 encontrando-se localizada no N-terminal (8,16,17).

O estresse celular leva a liberação de sinais de morte que induzem a ativação da metacaspase e resulta em um autoprocessamento (20). Esse autoprocessamento ocorre após a interação do cálcio com a metacaspase, porém, esse não é um pré-requisito para sua atividade enzimática (18). Apesar de não ser um fator determinante para a atividade da metacaspase, o seu autoprocessamento está diretamente relacionado com o aumento da sua atividade catalítica, influenciada pelos níveis de cálcio (12). Em estudos utilizando a metacaspase tipo 2 de *Trypanosoma brucei*, verificou-se que a etapa de autoprocessamento é essencial para a realocação do N-terminal a fim de expor os resíduos do sítio catalítico e permitir assim a ação da enzima sobre substratos proteicos grandes e não apenas em oligopeptídeos (5).

A *Saccharomyces cerevisiae* é uma levedura que codifica uma única metacaspase, denominada como Yeast Caspase 1 (YCA1) (19). A YCA1 é uma metacaspase do tipo I e diversos estudos demonstram que sua expressão está relacionada diretamente a morte celular (apoptose) induzida por estresse oxidativo e senescência celular, regulação do ciclo celular e a eliminação de agregados de proteínas na levedura S. cerevisiae (13,19,20). Foi demonstrado que a YCA1 regula ativamente o ciclo celular da levedura, atuando precisamente na transição da fase G1 para a fase S e, quando é inibida a atividade da enzima ou na ausência do gene nota-se uma transição de G1 para S tardia em estudos de comparação entre cepas nocautes (YCA1-ΔN86) e selvagens (BY4741) (10). Com o intuito de demonstrar o autoprocessamento dessa metacaspase, foram realizados ensaios utilizando a enzima pura na presença do íon Ca^{2+} e demonstraram que esse processamento ocorre no C-terminal

Revista Científica UMC | RCUMC | ISSN: 2525-5150

e no N-terminal, sendo que no primeiro é liberado um fragmento menor quando realizado uma análise eletroforética em gel de SDS-PAGE, evidenciando uma banda abaixo de 14 kDa chamado de subunidade pequena, e o segundo liberando um fragmento com banda em torno de 45 kDa chamada de subunidade grande (23).

Quando comparada a estrutura da YCA1 com a estrutura da metacaspase 2 de *Trypanosoma brucei* (TbMCA2), verifica-se que ambas possuem semelhanças como a presença dos resíduos de ligação do cálcio, a díade catalítica e os resíduos de lisina onde ocorre o autoprocessamento. Entretanto, algumas características únicas podem ser destacadas, como a estrutura do N-terminal na TbMCA2, caracterizado por um N-terminal alongado que circunda toda a proteína, influenciando diretamente no acesso ao seu sítio ativo, diferentemente do que se encontra na YCA1. Quando sobrepostas as estruturas tridimensionais dessas proteínas, é possível observar que os aminoácidos de ligação ao cálcio, dado por quatro ácidos aspárticos, ocupam posições quase idênticas, o que sugere que a região de ligação do cálcio é conservada entre as metacaspases (12,14,23).

MATERIAIS E MÉTODOS

Para amplificação do material foram desenhados primers baseados na sequência completa do gene da metacaspase YCA1localizada no site UniProt. Wong, Yan & Shi (2012) elucidaram a estrutura cristalográfica da YCA1 e com isso foi possível observar a localização de duas cisteínas catalíticas, assim, foram desenhados primers foward (5-3') e reverse (3'-5') que induziram a substituição das cisteínas por uma alanina (Tabela 1).

Tabela 1 - *Primers* utilizados na amplificação do gene da *YCA1* para inserção da mutação pontual (em **negrito** o novo códon para troca do aminoácido e produção da mutação)

Primer	Sequência
C155A *Forward*	5' AAATCAACTGCGTGGT**GCT**ATCAATGATGCTC 3'
C155A *Reverse*	5' GAGCATCATTGAT**AGC**ACCACGCAGTTGATTT 3'
C276A *Forward*	5' ACAGCATTGTTTGACTCT**GCT**CATTCGGGTACAGTGTTG 3'
C276A *Reverse*	5' CAACACTGTACCCGAATG**AGC**AGAGTCAAACAATGCTGT 3'

Também foram desenhados primers, chamados de primers TEDA, que amplificaram o gene da YCA1 já com a mutação realizada + o plasmídeo Pet28(a). Na Tabela 2 encontra-se a lista dos *primers* projetados.

Revista Científica UMC | RCUMC | ISSN: 2525-5150

Tabela 2 - *Primers* projetados para amplificação do gene da *YCA1* utilizados na reação TEDA

Primer	Sequência
YCA1 *Forward*	5’ CTGGTGCCGCGCGGCAGCCATATGTATCCAGGTAGTGGACGT 3’
YCA1 *Reverse*	5’ GTGGTGGTGGTGGTGGTGCTCGAGCTACATAATAAATTGCAGATTTAC 3’

Na Tabela 3 é apresentado a sequência dos *primers* utilizados para a amplificação do vetor pET28(a)+.

Tabela 3 - *Primers* projetados para amplificação do vetor pET28(a)+ utilizados na reação TEDA

Primer	Sequência
pET28 *Forward*	5’ CTCGAGCACCACCACCACCACCACT 3’
pET28 *Reverse*	5’ CATATGGCTGCCGCGCGGCAC 3’

Os *primers* amplificadores da região T7 (Tabela 4) foram projetados para a primeira etapa da reação da PCR da mutação, tanto quanto para as amplificações por PCR para confirmação, como a PCR de colônia.

Tabela 4 - *Primers* utilizados para amplificação da região T7 (promotora e terminadora) que flanqueia o gene da *YCA1*

Primer	Sequência
T7 *Forward*	5’ TAATACGACTCACTATAGGG 3’
T7 *Reverse*	5’ TAGTTATTGCTCAGCGGTGG 3’

Para realizarmos as mutações pontuais através dessa amplificação nos baseamos no protocolo de Ho *et al.* (1989) com modificações. A técnica de sobreposição de fragmentos consiste em amplificar o gene em duas etapas, gerando fragmentos que irão ser complementares, usando *primers* flanqueadores do gene (A e D) complementares a sequência alvo, que são os *primers* TEDA, e *primers* internos contendo a mutação desejada (B e C), que são os *primers* da mutação (Tabela 5), separadamente de forma que se hibridizem posteriormente.

Revista Científica UMC | RCUMC | ISSN: 2525-5150

Tabela 5 - Descrição dos *primers* usados na primeira etapa para inserção da mutação

Primer	**Função**	**Descrição**
C155A *Forward*	Inserir a mutação	B
C155A *Reverse*	Inserir a mutação	C
C276A *Forward*	Inserir a mutação	B
C276A *Reverse*	Inserir a mutação	C
T7 *FW*	Flanqueador do gene	A
T7 *Reverse*	Flanqueador do gene	D

Realizamos as reações em tubos distintos, uma para o sentido *forward* e outro para o *reverse*, denominadas como PCR-I *Forward*, na qual utilizou-se o *primer forward* da mutação e o *primer reverse* T7, e PCR-I *Reverse,* na qual utilizou-se o *primer reverse* da mutação e o *primer forward* T7, criando assim os fragmentos AC e DB, respectivamente. A reação foi realizada utilizando PCR Bio (PCR Biosystems), seguindo as orientações do fabricante, e foi realizada em um termociclador T100 *Thermal Cycler* (Bio-Rad) nas seguintes condições: (1) 1 ciclo a 98º C por 1 minuto (desnaturação inicial), (2) repetições de 30 ciclos de variações consecutivas de temperatura, 98º C por 30 segundos (desnaturação), 55º C por 30 segundos (anelamento) e 72º C por 45 segundos (extensão), e (3) 1 ciclo extra de 10 minutos a 72º C (extensão final).

O produto da amplificação foi analisado através de eletroforese em gel de agarose preparado a 1% (m/v) contendo 0,75 µg/mL de brometo de etídio em tampão TAE (TRIS 80 mM; Ácido Acético glacial 40 mM; EDTA 2,5 mM, em pH 8,3). Em seguida foi submetido a uma tensão de 80 V durante 30 minutos em cuba horizontal. Após migração, o gel foi analisado sob luz UV no fotodocumentador ChemiDoc™ MP Imaging System (Bio-Rad).

Após a confirmação da amplificação dos fragmentos da primeira etapa, seguimos para a segunda etapa da reação. Para a PCR II foram utilizados 10 ng de cada produto da reação anterior e os *primers* desenhados para a reação do TEDA, usando YCA1 *forward* e YCA1 *reverse)*. As extremidades complementares formadas na região de ligação dos *primers*, B e C, se hibridizam (Figura 1) neste segundo PCR para criar o produto final contendo a sequência mutada. As condições da reação

Revista Científica UMC | RCUMC | ISSN: 2525-5150

foram alteradas para: (1) 1 ciclo a 98º C por 30 segundos (desnaturação inicial), (2) repetições de 35 ciclos de variações consecutivas de temperatura, 98º C por 10 segundos (desnaturação), 62º C por 15 segundos (anelamento) e 72º C por 30 segundos (extensão), e (3) 1 ciclo extra de 10 minutos a 72º C (extensão final). A análise foi realizada da mesma forma descrita anteriormente.

Para a amplificação do pET28(a)+ foram desenhados *primers* específicos (Tabela 3) para a realização da reação do TEDA, esses *primers* inserem em torno de 15 bases nitrogenadas que formam as extremidades homólogas entre inserto e vetor. A reação foi construída utilizando 60 ng de DNA molde e 25 pmol de cada *primer forward* e *reverse* TEDA. A reação foi catalisada pelo PCR BIO(PCR Biosystems), seguindo as orientações do fabricante. As condições da amplificação compreenderam as seguintes etapas: (1) 1 ciclo a 98º C por 30 segundos (desnaturação inicial), (2) repetições de 35 ciclos de variações consecutivas de temperatura, 98º C por 20 segundos (desnaturação), 72º C por 2 minutos (anelamento e extensão), e (3) 1 ciclo extra de 10 minutos a 72º C (extensão final). A análise foi realizada da mesma forma descrita anteriormente.

Para a realização do procedimento de montagem de DNA com T5 exonuclease, em inglês T5 exonuclease DNA assembly (TEDA), nos baseamos no trabalho descrito por Xia *et al.* (2019). Este trabalho descreve um método que combina a ação da T5 exonuclease e os mecanismos de reparo da *E. coli*. Trata-se de um método eficiente e de baixo custo que pode ser utilizado para protocolos de clonagem e mutação sítio dirigida. A metodologia baseia-se na montagem de fragmentos de DNA com extremidades homólogas utilizando exclusivamente a ação da T5 exonoclease capaz de remover as bases nitrogenadas apenas na direção 5´- 3´ (XIA *et al.*, 2019).

A primeira etapa para realização do TEDA, foi a preparação da solução estoque 5X (0,5 M TRIS; 50 mM $MgCl_2$; 50 mM DTT; PEG 8000 0,25 g/mL^{-1}, em pH 7,5 ajustado com HCl). A solução foi armazenada em alíquotas de 1 mL no freezer a -80° C. Para o preparado da solução 5X TEDA + T5 exonuclease, acrescentou-se 10 unidades da T5 exonuclease (ThermoFisher) em uma alíquota de 1 mL e preparamos alíquotas de 100 µL. A reação foi preparada seguindo as orientações descritas por Xia *et al.* (2019) quanto as condições ótimas para a reação TEDA. A proporção da reação foi 1:4 (vetor/inserto). Utilizamos 100 ng do vetor pET28(a)+ linearizado, e para calcularmos a concentração do inserto, utilizamos a Equação 1 (Eq. 1) abaixo.

$$ng\ Inserto = \frac{ng\ Vetor\ x\ pb\ Inserto}{pb\ Vetor} \qquad \text{(Eq. 1)}$$

Revista Científica UMC | RCUMC | ISSN: 2525-5150

O vetor linearizado e os insertos foram obtidos por amplificação via PCR e as extremidades homólogas foram introduzidas na reação usando os *primers* específicos do TEDA. Ambos, vetor e inserto, foram purificados utilizando kit de purificação *Easypure PCR Purification* (Transgen Biotech). O vetor, posteriormente a purificação, foi tratado com a enzima de restrição DpnI, a fim de clivar o material molde, sob condições em termociclador: (1) 37º C por 3h e (2) 80º C por 20 minutos para inativação da enzima.

Para cada reação TEDA foi utilizado 4 µL da solução 5X TEDA + T5 exonuclease, na qual adicionou-se a solução à mistura dos fragmentos do inserto e vetor linearizado e completou a reação com água ultra pura para o volume final de 20 µL, a mistura preparada foi então homogeneizada e incubada a 30° C durante 40 minutos.

Procedemos com o protocolo de transformação através de choque térmico utilizando 7 µL da solução reacional para uma alíquota de 100 µL de células competentes *E. coli* DH5α. As células foram incubadas por 30 minutos em gelo, submetidas a choque térmico a 42° C por 90 segundos e depois transferidos para gelo durante 2 minutos, em seguida acrescentou-se 800 µL de meio LB. A suspensão foi incubada em um agitador a 37 °C durante 60 minutos. Após o tempo de incubação, o material foi centrifugado, descartou-se 700 µL do sobrenadante e o *pellet* formado foi ressuspendido nos 100 µL restantes. As alíquotas de 100 µL obtidas foram espalhadas em placas de LB contendo canamicina (50 µg/mL). As placas foram incubadas *overnight* a 37 °C.

RESULTADOS E DISCUSSÃO

As mutações sítio dirigidas realizadas neste trabalho foram baseadas na sequência do gene codificante da metacaspase de S. cerevisiae (YCA1) quando alinhada a sequência de aminoácidos da TbMCA-IIa de Trypanosoma brucei e em resíduos essenciais identificados na estrutura cristalográfica dessa enzima (14,23).

Como observado para todas as metacaspases, a cisteína catalítica é conservada, compondo o sítio ativo da enzima junto a um resíduo de histidina, sendo a cisteína 276 o resíduo conservado na YCA1 (Cys^{276}). Foi observado na estrutura da TbMCAIIa que esta enzima apresenta uma segunda cisteína que está ligada ao seu autoprocessamento, identificada como resíduos Cys92 (2), quando avaliamos as duas sequências dessas metacaspases, observamos que a YCA1 apresenta uma cisteína conservada na mesma posição a Cys155. A partir dessas informações e alinhamentos, identificamos os resíduos de interesse para esse estudo, e projetamos os primers para realizarmos as mutações da segunda cisteína (Cys155) e da cisteína catalítica (Cys276).

Revista Científica UMC | RCUMC | ISSN: 2525-5150

Existem diversas técnicas desenvolvidas ao longo dos anos para a realização das mutações sítio dirigidas empregando a reação em cadeia da polimerase (PCR) e que foram aprimoradas com o passar dos anos. A primeira estratégia traçada para realizar a mutação neste trabalho foi através datécnica mais conhecida e utilizada, a *QuikChange™ Site-Directed Mutagenesis System* (Stratagene), que consiste em utilizar em uma mesma reação de PCR pares de *primers* complementares contendo a troca do códon para a mutação, a fim de amplificar totalmente o plasmídeo realizando a mutação pontual no gene, entretanto, o uso dessa metodologia foi ineficiente durante os nossos experimentos, uma vez que a amplificação do plasmídeo total não foi eficaz (dados não mostrados). Acredita-se que isso pode ocorrer devido a hibridização dos *primers* que, por serem complementares, pode levar ao alinhamento e formação de “dímeros”, reduzindo o rendimento da reação (3).

Com o intuito de evitar esse problema, utilizamos uma técnica alternativa para a obtenção dos mutantes da YCA1, que consiste na metodologia de sobreposição de fragmentos (7). A estratégia se baseia na realização de reações de PCR utilizando os *primers forward* e *reverse* separadamente. Assim, essa metodologia permite que sejam realizadas mutações de inserção, deleção e/ou substituição. O tipo de mutação sítio dirigida escolhida para esse trabalho foi a de substituição, nesse sentido, realizamos a troca de pares de bases que codificam um aminoácido importante na estrutura da proteína por outro, no caso para as mutações foi escolhido a troca por uma alanina. A escolha do aminoácido alanina ocorreu devido a sua estrutura simples e comum em proteínas, além da sua cadeia lateral curta, características que não impõem modificações e perturbações na estrutura secundária e terciária da proteína (4).

A metodologia de amplificação através da sobreposição de fragmentos é realizada em duas etapas de PCR. Na primeira etapa (PCR I) ocorre a amplificação de fragmentos que serão complementares, entre eles, utilizando *primers* flanqueadores do gene e *primers* internos contendo a mutação desejada, conforme demonstrado na Figura 1.

Revista Científica UMC | RCUMC | ISSN: 2525-5150

Figura 1 - Mutação sítio dirigida por técnica de sobreposição de fragmentos.

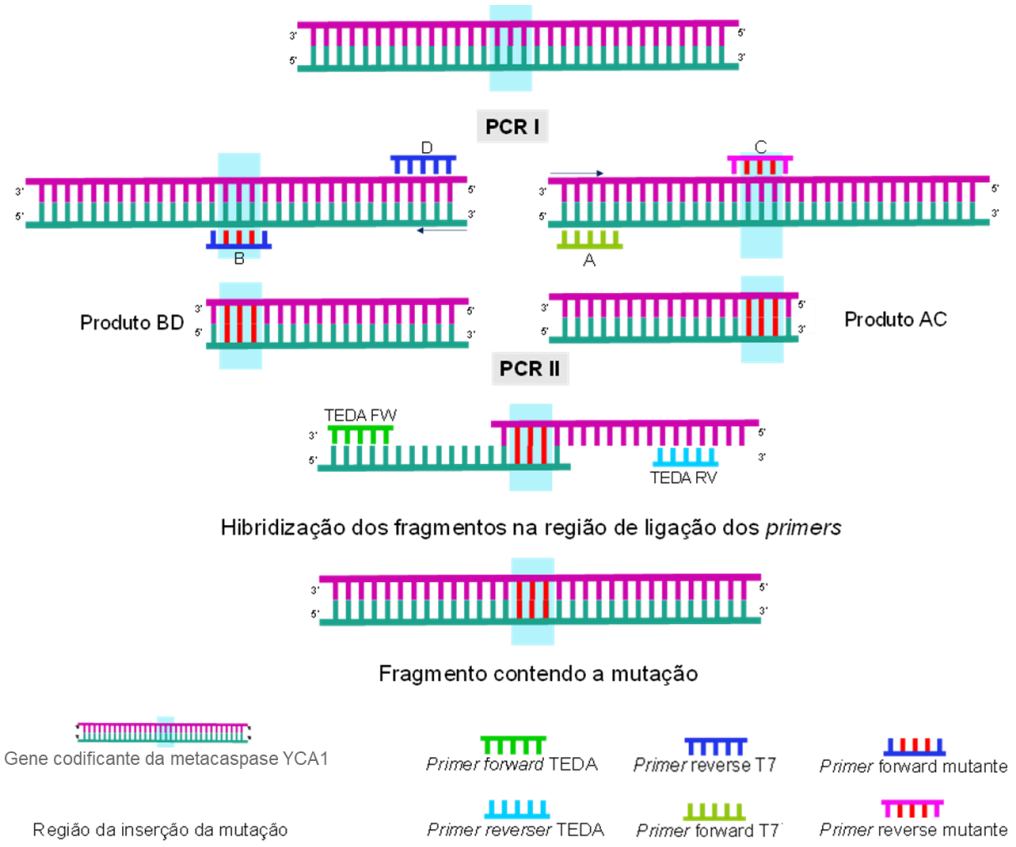

Fonte: Ho *et al.*, 1989 (adaptação)

Na PCR I ocorrem duas reações, utilizando os *primers* B/D (PCR I-FW) e A/C (PCR I-RV). B e C são os primers para mutação e irão substituir o códon original. Os fragmentos formados (BD e AC) são misturados para a PCR II, essa etapa utiliza os primers TEDA, que são projetados para inserir 15 bases nitrogenadas no sentido 5'-3' de cada fita. Com os fragmentos formados na primeira etapa são complementares, ocorre hibridização e a amplificação do fragmento completo, havendo a inserção da mutação.

Os *primers* B e C são responsáveis por realizar a troca do códon original pelo mutado, já que carregam essa alteração na sua sequência. Nessa primeira etapa, os fragmentos gerados desses mutantes são complementares entre si, um fator importante na segunda etapa dessa metodologia.

Como visto na Figura 1 as reações são realizadas usando os *primers* separadamente, criando assim os fragmentos AC e DB. O fragmento DB é correspondente a reação PCR-I *forward* (FW) e o fragmento AC é correspondente a reação PCR-I *reverse* (RV). Para essas reações de PCR, foram utilizados os *primers* da região T7, que flanqueiam o gene no plasmídeo pET28(a)+ (plasmídeo de escolha para clonagem), por esse detalhe somam-se as regiões amplificadas os pares de bases correspondentes a região T7, em torno de aproximadamente 150 pb. Na Figura 2 observamos as amplificações realizadas nessa primeira etapa para a mutação dos resíduos Cys^{155} e Cys^{276}.

Revista Científica UMC | RCUMC | ISSN: 2525-5150

Figura 2 - Eletroforese em gel de agarose 1% do produto da amplificação gerado na primeira etapa da reação de sobreposição de fragmentos.

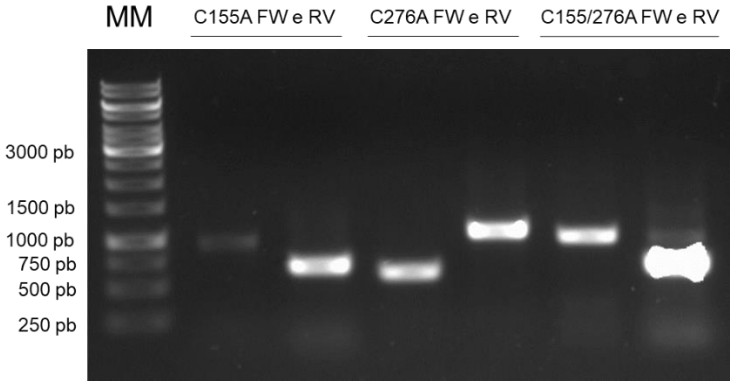

Linhas: (MM) marcador molecular *GeneRuler* 1kb; Produtos da amplificação da PCR I-FW e PCR I-RV do mutante C155A, apresentando 1001 pb e 659 pb, respectivamente; Produtos da amplificação da PCR I-FW e PCR I-RV do mutante C276A, apresentando 633 pb e 1027 pb, respectivamente; Produtos da amplificação da PCR I-FW e PCR I-RV do mutante C155/276A, apresentando 1001 pb e 659 pb, respectivamente.

Com os fragmentos gerados na primeira etapa (PCR I), prosseguimos para a segunda etapa de PCR (PCRII). Nessa reação ocorre a sobreposição das regiões complementares amplificadas através dos *primers* (B e C) da mutação. Para a PCR II utilizamos *primers* específicos para amplificação do gene da YCA1. Nas reações, foram usados na mesma proporção os fragmentos obtidos anteriormente, PCR-I FW e PCR-I RV. Os *primers* foram projetados visando a posterior reação do TEDA, acrescentando uma pequena sequência de pares de base para reconhecimento e clivagem pela T5 exonuclease – uma enzima com função de clivar o DNA no sentido 5'-3' – e que são complementares as extremidades da amplificação do plasmídeo pET28(a)+ na mesma região.

Como demonstrado na Figura 1, a região B e C se hibridizam nessa PCR e formam o molde para que os *primers* TEDA amplifiquem o gene contendo a mutação, gerando como produto um único fragmento. A Figura 3 demonstra os fragmentos obtidos na amplificação mutantes da YCA1.

Revista Científica UMC | RCUMC | ISSN: 2525-5150

Figura 3 - Eletroforese em gel de agarose 1% do produto da amplificação da segunda etapa da reação de sobreposição de fragmentos.

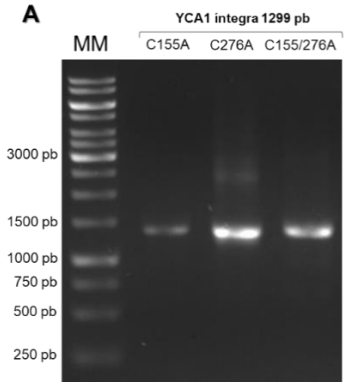

Linhas: (MM) marcador molecular *GeneRuler* 1kb; (A) PCR II dos mutantes íntegros, YCA1 C155A, YCA1 C276A e YCA1 C155/276A.

Através da análise das bandas obtidas confirmamos que a reação da PCR II ocorreu como esperado. Os fragmentos se hibridizaram e geraram os produtos finais no tamanho de ~1299 pb para os mutantes da YCA1.

O uso dos *primers* específicos do TEDA na segunda etapa de amplificação foi utilizado baseando-se na montagem do DNA através da reação com a enzima T5 exonuclease. O primeiro método desenvolvido para a realização de clonagens foi através da digestão com enzimas de restrição e posterior ligação dos fragmentos complementares com DNA ligase (2). Embora ainda seja o método mais utilizado, ao tentarmos aplicar não obtivemos eficiência no desenvolver do trabalho e optamos por seguir com técnicas mais recentes.

Diferentes métodos de clonagem foram desenvolvidos na última década, visando a melhoraria na eficiência e geração de protocolos mais rápidos, simples e econômicos. Métodos foram desenvolvidos aprimorando a técnica mais convencional, que geram fragmentos com extremidades coesivas, e outros foram projetados de modo a obter os produtos com princípios diferentes, como ocorre nas técnicas *in vivo* e *in vitro* que utilizam de sequências homólogas (1).

As técnicas voltadas à montagem de DNA *in vitro* em geral são métodos fáceis e confiáveis, entretanto com custos altos por conta do uso de várias enzimas, como ocorre no método de Gibson no qual utilizam-se três enzimas; a T5 exonuclease, Phusion DNA polimerase e a Taq DNA ligase (1,24).

O método T5 exonuclease DNA assembly (TEDA), foi projetado baseando-se na clonagem através de fragmentos de DNA com extremidades homólogas utilizando apenas uma enzima, a T5 exonuclease, que é capaz de clivar o DNA na direção 5’-3’. Assim, a T5 degrada a extremidade 5’ e gera fragmentos na extremidade 3’, passando de pontas cegas a pontas coesivas, que se hibridizam umas as outras. Portanto, quando o produto dessa incubação é transformado em células hospedeiras,

Revista Científica UMC | RCUMC | ISSN: 2525-5150

ocorre o reparo *in vivo* das lacunas pela ação das enzimas DNA polimerase e ligase, como demonstrado na Figura 4, onde a polimerase preenche os pares de base nas lacunas entre as fitas complementares e ligase faz a ligação fosfodiéster entre os fragmentos formados (24).

Figura 4 - Método T5 exonuclease DNA assembly (TEDA).

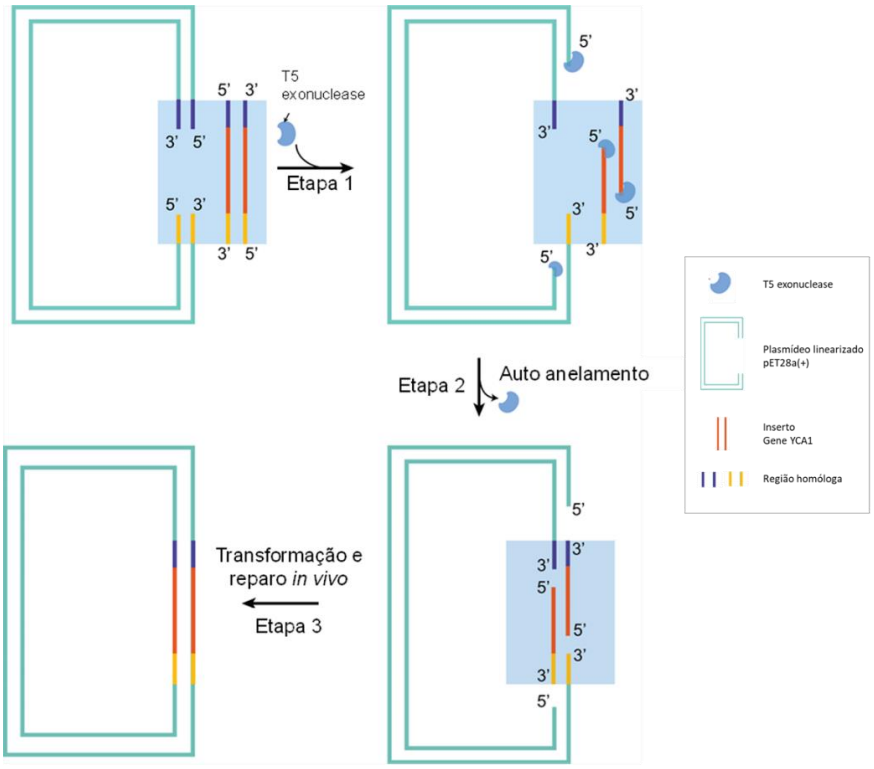

Fonte: Xia *et al.* (2019, p. 2 – com adaptação)

Representação da ação da T5 exonuclease na reação do TEDA. O retângulo de linha dupla com uma lacuna representa um plasmídeo linearizado. As linhas verticais duplas representam o inserto. Linhas com a mesma cor indicam a região homóloga. Na primeira etapa 1: a exonuclease T5 corta as extremidades 5' do plasmídeo linearizado e do inserto para gerar as extremidades complementares. Etapa 2: Os fragmentos se anelam por complementariedade e se ligam uns aos outros. Etapa 3: O DNA é transformado em células *E. coli* DH5α e as lacunas são reparadas *in vivo*.

Para realizar a clonagem através do TEDA é necessário obter o vetor linearizado no qual o gene será inserido, e para nosso trabalho utilizamos o pET28(a)+, que foi amplificado utilizando os *primers* do TEDA. Na Figura 5 A observamos o resultado dessa amplificação e por meio do tamanho do fragmento gerado, confirmamos a obtenção do plasmídeo linearizado.

Revista Científica UMC | RCUMC | ISSN: 2525-5150

Figura 5 – Eletroforese em gel de agarose 1% do produto da amplificação do vetor e da YCA1 com os primers TEDA.

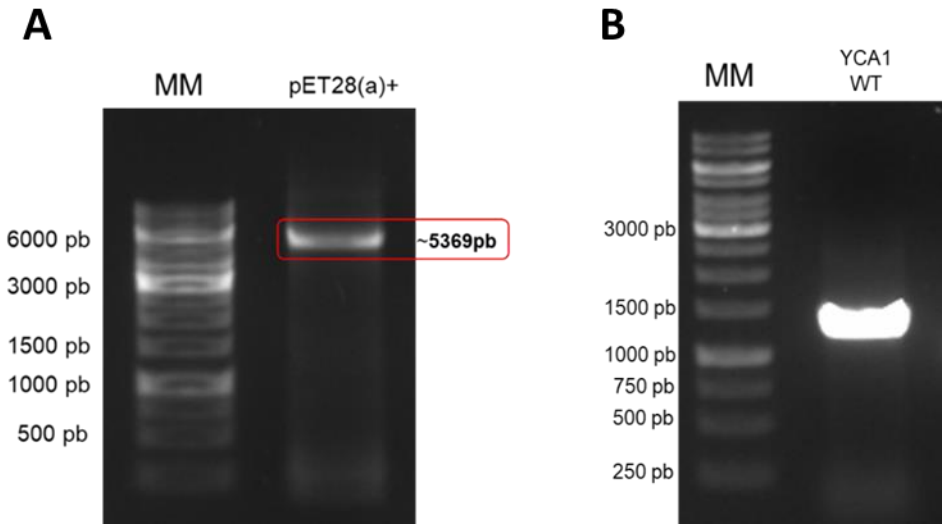

Linhas: **A:** (MM) marcador molecular *GeneRuler* 1kb; PCR de amplificação do vetor pET28(a)+ linearizado. **B:** (MM) marcador molecular *GeneRuler* 1kb; PCR de amplificação da YCA1.

O DNA utilizado como molde para a reação de amplificação do vetor é proveniente de *E. coli,* obtido através de extração por lise alcalina, e por esse motivo é metilado. A metilação do DNA é um processo realizado pelas bactérias afim de marcar e proteger seu próprio material genético contra a degradação quando, por exemplo, ocorre a invasão da célula por vírus. Assim, ocorre a distinção do DNA bacteriano comparado com o DNA viral com a marcação de um grupamento metil, portanto o material genético não marcado do vírus é degradado por enzimas de restrição de outras classes (11,15). Com base nisso, realizamos a etapa de digestão do produto da amplificação com a enzima de restrição DpnI, uma endonuclease utilizada para clivar o DNA metilado, com a finalidade de degradar o material molde utilizado na reação de amplificação e assim evitar que na próxima etapa esse plasmídeo não esteja presente nas nossas bactérias.

Após a digestão com DpnI, prosseguirmos com a reação de clonagem, realizando a purificação dos produtos amplificados. Com os produtos da PCRII realizamos a amplificação do gene da YCA1contendo as mutações pontuais, usando os *primers* TEDA, YCA1 *forward* e YCA1 *reverse*. Confirmamos a amplificação em gel de agarose (Figura 5 B). Como resultado, obtivemos bandas representando YCA1 com aproximadamente 1299 pb.

As amostras obtidas após purificação foram quantificadas em nanodrop. Os valores obtidos foram utilizados no cálculo de proporção para a reação do TEDA, que foram preparadas na proporção 1:4 de vetor/inserto. Prosseguimos com a incubação e após submetemos o produto a etapa de

Revista Científica UMC | RCUMC | ISSN: 2525-5150

transformação através de choque térmico em cepas de *E. coli* DH5α, a escolha dessa cepa foi baseada na sua capacidade em estabilizar e amplificar o DNA inserido (9).

Os clones foram selecionados através do crescimento em meio de cultura com antibiótico canamicina, uma vez que o pET28(a)+ confere resistência a este antibiótico. Escolhemos aleatoriamente algumas colônias para realizarmos uma PCR confirmatória e posteriormente selecionamos uma dessas colônias de cada para realizar a extração do plasmídeo através da lise alcalina.

Dentre os clones positivos, selecionou-se uma colônia de cada mutante para o preparo do pré-inóculo a fim de realizar a extração do DNA plasmidial por lise alcalina, obtido utilizando o kit comercial. Após a extração, o material adquirido foi submetido a uma amplificação utilizando os *primers* da região T7, assim como foi realizado anteriormente, para confirmamos a integridade dos plasmídeos.

Com a confirmação da clonagem, prosseguimos para submeter o produto da lise alcalina a etapa de transformação do produto em cepas de *E. coli* BL21(DE3)pLysS com o objetivo de prepararmos os ensaios para a expressão das proteínas. A transformação foi feita por choque térmico e após a obtenção das colônias, confirmamos através da amplificação com os *primers* da região T7 a obtenção dos clones dos mutantes nas cepas de expressão, assim como foi realizado anteriormente (Figura 6).

Figura 6 - Eletroforese em gel de agarose 1% do produto da amplificação dos plasmídeos obtidos em colônias de *E. coli* BL21(DE3)pLysS.

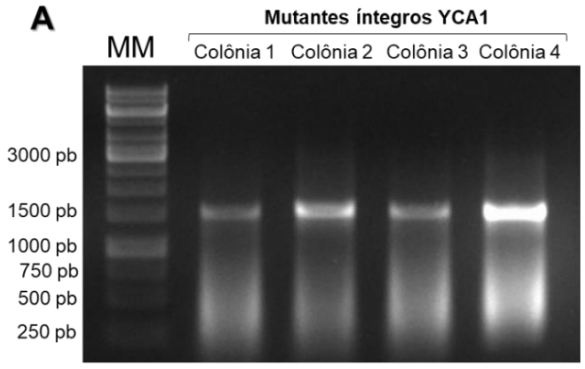

Linhas: (MM) marcador molecular GeneRuler 1kb; (A) PCR de colônia da YCA1 íntegra mutante, na figura como exemplo 4 colônias do mutante C155/276A; (B) PCR de colônia da YCA1-ΔN86 mutante, na figura como exemplo 4 colônias do mutante C276A.

O material oriundo da lise alcalina foi submetido a sequenciamento pela empresa Ludwig (dados não mostrados). Os resultados mostraram que nossos mutantes foram obtidos com êxito.

Revista Científica UMC | RCUMC | ISSN: 2525-5150

CONCLUSÕES

O presente trabalho descreve um processo meticuloso de mutação sítio-dirigida do gene codificante da metacaspase de *S. cerevisiae* (YCA1), utilizando como base a sequência de aminoácidos da TbMCA-IIa de *Trypanosoma brucei*, e levando em consideração os resíduos essenciais identificados na estrutura cristalográfica dessa enzima.

A análise revelou a conservação da cisteína catalítica, em particular a Cys^{276} na YCA1, que constitui o sítio ativo da enzima, juntamente com um resíduo de histidina. Adicionalmente, a TbMCA-IIa apresentou uma segunda cisteína (Cys^{92}) associada ao processo de autoprocessamento, o que implicou na mutação correspondente da Cys^{155} na YCA1.

Iniciamos com a estratégia *QuikChange™ Site-Directed Mutagenesis System*, amplamente utilizada, porém demonstrou ineficiência devido à hibridização dos primers, presumivelmente causando formação de dímeros e redução do rendimento da reação. Como alternativa, adotamos a técnica de sobreposição de fragmentos, permitindo mutações de substituição. Optamos pela alanina devido à sua estrutura e cadeia lateral simples, evitando perturbações na estrutura da proteína.

A amplificação por sobreposição de fragmentos foi realizada em duas etapas (PCR I e PCR II), gerando fragmentos complementares que serviram como matriz para a clonagem. A metodologia T5 *exonuclease DNA assembly* (TEDA) foi empregada, utilizando exclusivamente a T5 exonuclease para clivar o DNA na direção 5'-3', transformando extremidades coesivas em pontas cegas que se hibridizaram. O reparo *in vivo* das lacunas foi executado pela DNA polimerase e ligase da própria bactéria.

A digestão com DpnI foi crucial para degradar o DNA metilado empregado como molde na reação de amplificação, antes da clonagem no vetor linearizado pET28(a)+. A seleção dos clones foi conduzida com base na resistência à canamicina conferida pelo plasmídeo. A confirmação da clonagem foi realizada por PCR e subsequente sequenciamento.

Em seguida, procedeu-se com a transformação do produto em cepas de *E. coli* BL21(DE3)pLysS para a preparação dos ensaios de expressão das proteínas mutantes. O sequenciamento final atestou o sucesso na obtenção dos mutantes. O presente estudo apresenta uma abordagem metodológica robusta para a realização de mutações sítio-dirigidas em genes, com aplicabilidade potencial em investigações futuras sobre metacaspases.

Revista Científica UMC | RCUMC | ISSN: 2525-5150

REFERÊNCIAS

1. Chao R, Yuan Y, Zhao H. Recent advances in DNA assembly technologies. FEMS Yeast Res [Internet]. 2015 [zitiert 17. Januar 2023];15(1). Verfügbar unter: https://pubmed.ncbi.nlm.nih.gov/24903193/

2. Cohen SN, Chang ACY, Boyer HW, Helling RB. Construction of biologically functional bacterial plasmids in vitro. Proc Natl Acad Sci U S A [Internet]. 1973 [zitiert 17. Januar 2023];70(11):3240–4. Verfügbar unter: https://pubmed.ncbi.nlm.nih.gov/4594039/

3. Edelheit O, Hanukoglu A, Hanukoglu I. Simple and efficient site-directed mutagenesis using two single-primer reactions in parallel to generate mutants for protein structure-function studies. 2009; Verfügbar unter: http://www.biomedcentral.com/1472-6750/9/61

4. Gibbs CS, Zoller MJ. Identification of electrostatic interactions that determine the phosphorylation site specificity of the cAMP-dependent protein kinase. Biochemistry [Internet]. 1. Juni 1991 [zitiert 30. Oktober 2023];30(22):5329–34. Verfügbar unter: https://pubmed.ncbi.nlm.nih.gov/2036400/

5. Gilio JM, Marcondes MF, Ferrari D, Juliano MA, Juliano L, Oliveira V, u. a. Processing of metacaspase 2 from Trypanosoma brucei (TbMCA2) broadens its substrate specificity. Biochim Biophys Acta Proteins Proteom. 2017;1865(4).

6. Hill SM, Nyström T. The dual role of a yeast metacaspase: What doesn't kill you makes you stronger. BioEssays. 2015;

7. Ho SN, Hunt HD, Horton RM, Pullen JK, Pease LR. Site-directed mutagenesis by overlap extension using the polymerase chain reaction. Gene [Internet]. 15. April 1989 [zitiert 16. Oktober 2023];77(1):51–9. Verfügbar unter: https://pubmed.ncbi.nlm.nih.gov/2744487/

8. Klemenčič M, Funk C. Evolution and structural diversity of metacaspases. Journal of Experimental Botany. 2019.

9. Kostylev M, Otwell AE, Richardson RE, Suzuki Y. Cloning Should Be Simple: Escherichia coli DH5α-Mediated Assembly of Multiple DNA Fragments with Short End Homologies. PLoS One [Internet]. 8. September 2015 [zitiert 17. Januar 2023];10(9). Verfügbar unter: https://pubmed.ncbi.nlm.nih.gov/26348330/

10. Lee REC, Puente LG, Kærn M, Megeney LA. A non-death role of the yeast metacaspase: Yca1p alters cell cycle dynamics. PLoS One. 2008;

11. Lu L, Patel H, Bissler JJ. Optimizing DpnI digestion conditions to detect replicated DNA. Biotechniques [Internet]. 2002 [zitiert 17. Januar 2023];33(2):316–8. Verfügbar unter: https://pubmed.ncbi.nlm.nih.gov/12188183/12. Machado MFM, Marcondes MF, Juliano MA, McLuskey K, Mottram JC, Moss CX, u. a. Substrate specificity and the effect of calcium on Trypanosoma brucei metacaspase 2. FEBS Journal. 2013;280(11).

Revista Científica UMC | RCUMC | ISSN: 2525-5150

13. Madeo F, Engelhardt S, Herker E, Lehman N, Maldener C, Proksch A, u. a. Apoptosis in yeast: a new model system with applications in cell biology and medicine. Curr Genet [Internet]. 2002 [zitiert 31. Januar 2023];41(4):208–16. Verfügbar unter: https://pubmed.ncbi.nlm.nih.gov/12172961/

14. McLuskey K, Rudolf J, Proto WR, Isaacs NW, Coombs GH, Moss CX, u. a. Crystal structure of a Trypanosoma brucei metacaspase. Proc Natl Acad Sci U S A. 2012;

15. Mierzejewska K, Siwek W, Czapinska H, Kaus-Drobek M, Radlinska M, Skowronek K, u. a. Structural basis of the methylation specificity of R.DpnI. Nucleic Acids Res [Internet]. 29. Juli 2014 [zitiert 17. Januar 2023];42(13):8745–54. Verfügbar unter: https://pubmed.ncbi.nlm.nih.gov/24966351/

16. Minina EA, Coll NS, Tuominen H, Bozhkov P V. Metacaspases versus caspases in development and cell fate regulation. Cell Death and Differentiation. 2017.

17. Minina EA, Staal J, Alvarez VE, Berges JA, Berman-Frank I, Beyaert R, u. a. Classification and Nomenclature of Metacaspases and Paracaspases: No More Confusion with Caspases. Molecular Cell. 2020.

18. Moss CX, Westrop GD, Juliano L, Coombs GH, Mottram JC. Metacaspase 2 of Trypanosoma brucei is a calcium-dependent cysteine peptidase active without processing. FEBS Lett. 2007;

19. Shrestha A, Megeney LA. The non-death role of metacaspase proteases. Frontiers in Oncology. 2012.

20. Tsiatsiani L, Van Breusegem F, Gallois P, Zavialov A, Lam E, Bozhkov P V. Metacaspases. Cell Death and Differentiation. 2011.

21. Uren AG, O'Rourke K, Aravind L, Pisabarro MT, Seshagiri S, Koonin E V., u. a. Identification of paracaspases and metacaspases: Two ancient families of caspase-like proteins, one of which plays a key role in MALT lymphoma. Mol Cell. 2000;

22. Vercammen D, De Cotte B Van, De Jaeger G, Eeckhout D, Casteels P, Vandepoele K, u. a. Type II metacaspases Atmc4 and Atmc9 of Arabidopsis thaliana cleave substrates after arginine and lysine. Journal of Biological Chemistry. 2004;

23. Wong AHH, Yan C, Shi Y. Crystal structure of the yeast metacaspase Yca1. Journal of Biological Chemistry. 2012;

24. Xia Y, Li K, Li J, Wang T, Gu L, Xun L. T5 exonuclease-dependent assembly offers a low-cost method for efficient cloning and site-directed mutagenesis. Nucleic Acids Res. 2019;47(3).

CAPÍTULO 2 - AVALIAÇÃO DE RESÍDUOS CHAVE PARA O FUNCIONAMENTO DA METACASPASE-1 DE *Saccharomyces cerevisiae (YCA1*)

PREFÁCIO

Este capítulo tem como foco a metacaspase da levedura *Saccharomyces cerevisiae* na sua forma íntegra (YCA1) e com a deleção da porção N-terminal (YCA1-ΔN86) contendo as mutações sítio dirigidas nos sítios chave de interação com o íon cálcio Asp^{236}, Asp^{252}, Asp^{253}, Asp^{283}. Além de avaliar o impacto dos resíduos do sítio de cálcio na ativação enzimática e no autoprocessamento da YCA1.

Este capítulo está apresentado no formato de artigo científico para futura publicação no periódico Biochimie.

AVALIAÇÃO DE RESÍDUOS CHAVE PARA O FUNCIONAMENTO DA METACASPASE-1 DE *Saccharomyces cerevisiae (YCA1*)

Mariana Nascimento Romero Trujilho [a], Laura de Azevedo Maffeis Dalzoto [a], Taiz dos Reis Santos [a], Ane Caroline Moreira Duarte [b], Ana Júlia de Oliveira Machado [c], Wagner Alves de Souza Judice [a], Marcelo Ferreira Marcondes [c] and Maurício Ferreira Marcondes Machado [a, b, *].

[a] Centro Interdisicplinar de Investigação Bioquímica, Universidade de Mogi das Cruzes, Av Dr. Cândido Xavier de Almeida e Souza, 200, 08780-991, Mogi das Cruzes, Brasil.

[b] Núcleo de Pesquisas Tecnológicas, Universidade de Mogi das Cruzes, Av Dr. Cândido Xavier de Almeida e Souza, 200, 08780-991, Mogi das Cruzes, Brasil.

[c] Departamento de Biofísica, Universidade Federal de São Paulo, Rua Pedro de Toledo, 669, 7º andar, 04039-032, São Paulo. Brasil.

***Autor correspondente:**

Maurício Ferreira Marcondes Machado, Ph.D.

E-mail: mauriciomachado@umc.br

Centro Interdisciplinar de Investigação Bioquímica

Universidade de Mogi das Cruzes

Av Dr. Cândido Xavier de Almeida e Souza, 200, 08780-991, Mogi das Cruzes, Brasil.

RESUMO

As metacaspases são císteino-proteases pertencentes ao clã CD da família C14, caracterizadas por sua especificidade para clivagem após resíduos básicos (Arg/Lys) e pela dependência da interação com íons de cálcio para a atividade catalítica. Este estudo investiga a metacaspase do tipo I YCA1 de *Saccharomyces cerevisiae*, que apresenta autoprocessamento dependente de Ca^{2+}. Diferentemente das metacaspases do tipo II, a YCA1 possui um pró-domínio N-terminal hidrofóbico que precede uma região rica em glutamina e asparagina. A pesquisa se concentrou na clonagem, expressão e mutação sítio-dirigida da YCA1, visando os resíduos Asp^{236}, Asp^{252}, Asp^{253} e Asp^{283} para elucidar os mecanismos subjacentes ao seu autoprocessamento. Uma variante truncada, YCA1-ΔN86, sem os primeiros 86 aminoácidos do N-terminal, apresenta tanto autoprocessamento gradual quanto ativação intermolecular. Similarmente às caspases de mamíferos, a YCA1-ΔN86 é capaz de ativar outras moléculas, indicando uma ativação intermolecular que acelera a maturação. Sítios de ligação distintos para as formas completa e truncada destacam o papel da região N-terminal na modulação da afinidade pelo cálcio e revelam padrões diferenciados de processamento. Alterações estruturais e funcionais, incluindo a deleção do N-terminal e mutações sítio-específicas nos resíduos de ligação ao cálcio, fornecem informações cruciais sobre a regulação da atividade enzimática e do autoprocessamento da YCA1. Esses resultados avançam nossa compreensão dos mecanismos moleculares que governam a ativação e a funcionalidade das metacaspases.

1 INTRODUÇÃO

Proteases são proteínas que desempenharem funções na manutenção da homeostase, metabolismo e da fisiologia da célula. As metacaspases são enzimas envolvidas na morte celular programada descobertas através de ferramentas de bioinformática [1].

As metacaspases possuem similaridades estruturais com as caspases, mas são encontradas em plantas, fungos e protozoários, diferente das segundas que são encontradas em mamíferos [1]. Elas são sintetizadas como zimogênios (pró enzimas inativas), possuem em seu sítio catalítico uma díade catalítica composta por Cys/His. São compostas por um pró-domínio que antecede as duas subunidades P20 (grande) e P10 (pequena), e tornam-se enzimaticamente ativas após sofrerem uma clivagem proteolítica após dois resíduos de ácido aspártico (D). Após a remoção do pró domínio, as caspases sofrem clivagem proteolítica liberando dois fragmentos peptídicos com pesos moleculares de 10 kDa e 20 kDa, as subunidades P_{10} e P_{20}, respectivamente. A subunidade P_{10} é necessária para a formação de heterodímeros, o que torna a caspase cataliticamente ativa [2,3].

As metacaspases não precisam conter um pró-domínio rico em prolina, glutaminas e asparaginas, e não necessitam passar pelo processo de dimerização para estarem ativas, pois já são ativas em sua forma de monômeros. Entretanto para estarem na forma de monômeros e poderem desempenhar sua função de indução da MCR, elas sofrem a clivagem proteolítica que é dependente do íon cálcio como cofator [3,4].

Comparado com as caspases que clivam seus substratos após resíduos de aspartato (aspartato-proteases) na posição P_1, as metacaspases possuem um subsítio S_1 altamente ácido, o que confere especificidade por substratos que contenham resíduos básicos (arginina ou lisina) na posição P_1 [5–8]. Isso ocorre porque os aspartatos conservados estão localizados no sítio de especificidade, resultando na clivagem após resíduos de aminoácidos carregados positivamente [9].

A levedura *S. cerevisiae* codifica uma única metacaspase, a YCA1. Por ser do Tipo I, tem como particularidade um pró-domínio N-terminal, que, assim como a CaMCA e as metacaspases tipo I de Arabidopsis thaliana (AtMC, AtMC2 e AtMC3), apresentam uma região rica em glutaminas e asparaginas (Q/N) [10].

Estudos anteriores já descreveram a relação da composição dessa região com a indução de precipitação e agregação dessa enzima. Esse pró-domínio também está presente em caspases iniciadoras de mamíferos e pode ser responsável por interações proteína-proteína entre metacaspases ou outros componentes oligomerizantes de diferentes complexos de sinalização, resultando na ativação da metacaspase de forma gradual e lenta, o que justificaria o fato de a ausência do N-terminal, YCA1-ΔN86, se processar de forma mais rápida, resultando em autodegradação [9].

As metacaspases do tipo I de Arabidopsis, bem como a CaMCA e YCA1, possuem como característica a presença do pró-domínio N-terminal, também são sintetizadas como zimogênios inativos e são ativadas por auto processamento. Diferente daquelas do tipo II (AtMC4, AtMC5, AtMC6, AtMC7, AtMC8, AtMC9), que possuem ativação semelhante às caspases iniciadoras. Provavelmente, este fato se deve à presença do N-terminal [9].

Assim, além de avaliarmos a YCA1 na sua forma íntegra contendo 432 aminoácidos, utilizamos a enzima em sua forma truncada (YCA1-ΔN86), que possui a deleção de 86 aminoácidos da porção N-terminal. A construção desta forma da enzima truncada foi baseada na elucidação da estrutura cristalográfica da YCA1 [11]. Neste trabalho apresentamos os resultados referentes a clonagem, expressão e purificação da metacaspase de *S. cerevisiae* em sua forma íntegra, com destaque para a deleção do N-terminal (YCA1-ΔN86) e com as mutações sítio-dirigidas nos resíduos do sítio de ligação do cálcio (Asp^{236}, Asp^{252}, Asp^{253} e Asp^{283}). O propósito deste estudo foi investigar os impactos dessas mutações no sítio de cálcio na estrutura e na função da YCA1.

2 OBJETIVO

2.1 OBJETIVO GERAL

Produzir a metacaspase de *Saccharomyces cerevisiae* na sua forma íntegra (YCA1) e com a deleção da porção N-terminal (YCA1-ΔN86) contendo as mutações sítio dirigidas nos sítios chave de interação com o íon cálcio Asp^{236}, Asp^{252}, Asp^{253},

Asp^{283}. Além de avaliar o impacto dos resíduos do sítio de cálcio na ativação enzimática e no autoprocessamento da YCA1.

2.2 OBJETIVOS ESPECÍFICOS

Neste trabalho propomos obter as metacaspases YCA1 e YCA1-ΔN86 contendo mutações pontuais baseadas na estrutura cristalográfica dessa enzima (WONG, YAN & SHI, 2012), e estudar a influência desses resíduos na ativação da proteína. Para isso foi necessário:

Realizar a produção dos mutantes da YCA1 e YCA1-ΔN86 D236A, D252A, D253A, D283A, além do duplo mutante D252/253A

Submeter o produto da amplificação a reação com a enzima T5 exonuclease e clonar em células de *Escherichia coli* DH5α;

Extrair o DNA mutado e transformar em células de *Escherichia coli* BL21(DE3)pLysS;

Expressar, purificar as proteínas obtidas e confirmar por *western blotting*;

Realizar experimentos de *SDS-PAGE* para avaliação do processo de autoprocessamento das enzimas mutadas;

3 PROCEDIMENTOS EXPERIMENTAIS

3.1 MUTAGÊNESE SÍTIO-DIRIGIDA DA YCA1

Para realizarmos as mutações sítio-dirigidas na YCA1 (Tabela 1), seguimos um protocolo desenvolvido por Ho *et al*. (1989) com modificações [16]. Todas as PCRs foram realizadas usando a polimerase Pfu (Thermo) com primers específicos. Os produtos da PCR do inserto e pET28(a)+ foram tratados com 10 U/mL de exonuclease T5 em um buffer contendo 500 mM Tris, 50 mM $MgCl_2$, 50 mM DTT, 0,25 g/mL PEG 800, pH 7.0. A proporção vetor/inserto foi de 1:4 [17], e a reação foi incubada a 37 °C por 3 horas. As reações resultantes foram então transformadas em Escherichia coli BL21(DE3) pLysS.

Tabela 1 - *Primers* utilizados na amplificação do gene da YCA1 para inserção da mutação pontual nos resíduos do sítio de interação com o íon cálcio (em negrito o novo códon para troca do aminoácido e produção da mutação)

Primer	**Sequência**
D236A *Forward*	5' GAA GAT GGG ATG GAT **GCT** GTT ATA TAT CCG GTC 3'
D236A *Reverse*	5' GAC CGG ATA TAT AAC **AGC** ATC CAT CCC ATC TTC 3'
D252A *Forward*	5' CAA GGG CCA ATT ATC **GCC** GAT GAA ATG CAC GAT 3'
D252A *Reverse*	5' ATC GTG CAT TTC ATC **GGC** GAT AAT TGG CCC TTG 3'
D253A *Forard*	5' CAA GGG CCA ATT ATC GAC **GCT** GAA ATG CAC GAT 3'
D253A *Reverse*	5' ATC GTG CAT TTC **AGC** GTC GAT AAT TGG CCC TTG 3'
D283A *Forward*	5' TCG GGT ACA GTG TTG **GCT** CTT CCA TAT ACC TAT 3'
D283A *Reverse*	5' ATA GGT ATA TGG AAG **AGC** CAA CAC TGT ACC CGA 3'
D252/253A *Forward*	5' CAA GGG CCA ATT ATC **GCC GCT** GAA ATG CAC GAT 3'
D252/253A *Reverse*	5' ATC GTG CAT TTC **AGC GGC** GAT AAT TGG CCC TTG 3'

3.2 EXPRESSÃO DE YCA1 SELVAGEM E MUTANTES

Bactérias contendo YCA1 tipo selvagem e mutantes, bem como YCA1-ΔN86 selvagem, foram inicialmente cultivadas em 10 mL de meio Luria Broth suplementado com canamicina (50 µg/mL) e incubadas a 37°C por aproximadamente 16 horas com agitação a 150 rpm. As culturas noturnas foram transferidas para 1 L de meio LB a 37°C e cultivadas até a densidade de cultura atingir DO600 de 0,4. A temperatura foi então reduzida para 20°C até a densidade celular atingir DO600 de 0,6-0,7. O isopropil-β-D-1-tiogalactopiranosídeo foi adicionado a uma concentração final de 0,5 mM, e as células foram incubadas a 20°C por 14-16 horas antes de serem colhidas por centrifugação a 4000 x g por 10 min a 4°C. O pellet foi subsequentemente armazenado a -70°C até ser necessário. O pellet celular foi ressuspenso em 20 mL de fosfato de sódio 50 mM pH 8,0, 500 mM NaCl, 20 mM imidazol, 1 mg/mL lisozima. Foi então incubado no gelo por 30 min antes da adição de 5 µg/mL de RNase, 5 µg/mL de DNase e 0,02% de Triton X-100. A solução foi incubada por mais 30 min no gelo antes de ser centrifugada a 26.000 × g por 20 min a 4°C e o sobrenadante foi recuperado. Os lisados foram centrifugados e filtrados através de uma membrana de 0,45 µm.

3.3 PURIFICAÇÃO DE YCA1 SELVAGEM E MUTANTES

O pellet celular foi ressuspenso em 20 mL de solução contendo 50 mM fosfato de sódio pH 8,0, 500 mM NaCl, 20 mM imidazol e 1 mg/mL lisozima. Esta mistura foi incubada no gelo por 30 min antes da adição de 5 µg/mL de RNase, 5 µg/mL de DNase e 0,02% de Triton X-100. Após uma incubação adicional de 30 min no gelo, a solução foi centrifugada a 26.000 × g por 20 min a 4°C e o sobrenadante foi coletado. Os lisados foram então centrifugados e filtrados através de uma membrana de 0,45 µm. O material resultante foi carregado em uma coluna HisTrap Ni2+ Sepharose (GE Healthcare) conectada a um cromatógrafo AKTA-Start (GE Healthcare). A coluna foi previamente equilibrada com um buffer de ligação composto por 50 mM Tris pH 7,5 e 100 mM NaCl, com uma taxa de fluxo de 1,0 mL/min. A coluna foi lavada com 5 mL de buffer de ligação e as proteínas recombinantes YCA1 SELVAGEM e mutantes foram purificadas e eluídas usando um gradiente de concentração de imidazol (50, 100, 200, 300 e 500 mM) no mesmo buffer. As proteínas recombinantes YCA1 SELVAGEM e mutantes eluíram entre 200 e 300 mM de imidazol (conforme confirmado pela análise SDS/PAGE) e as frações de proteínas foram combinadas. Para dessalinizar a proteína combinada, ela foi carregada em uma coluna HiTrap 26/10 Desalting de exclusão por tamanho, 5 mL (GE Healthcare) e equilibrada em um buffer contendo 50 mM Tris pH 7,4 e 100 mM NaCl (buffer NaCl/Tris). As frações eluídas foram analisadas por SDS/PAGE e as frações contendo YCA1 recombinante puro foram coletadas. Essas frações foram armazenadas em buffer NaCl/Tris contendo 30% de glicerol a -20°C. Para evitar qualquer diminuição na atividade de YCA1, ciclos de congelamento e descongelamento repetidos foram evitados.

3.4 WESTERN BLOTTING DE YCA1 SELVAGEM E MUTANTES

Para confirmar a presença de YCA1 nas formas processada e não processada, um ensaio de *western blotting* foi realizado usando um anticorpo 6x-His-tag (MA1- 21315-HRP – Thermo). O gel SDS-PAGE foi transferido para uma membrana PVDF (Bio-Rad) por 5 minutos em um Trans-Blot Turbo (Bio-Rad) seguindo as instruções do fabricante. A membrana PVDF foi subsequentemente lavada com um buffer PBS (10 mM Na2HPO4, 150 mM NaCl – pH 7,4) com a adição de 5% de BSA

e 0,01% de Tween 20 e deixada para incubar por 1 hora com agitação à temperatura ambiente.

Após isso, a membrana foi lavada três vezes com PBS e então incubada com o anticorpo 6x-His-tag (Thermo), que foi diluído na proporção de 1:30.000 em PBS com 5% de BSA e 0,01% de Tween 20. Esta incubação ocorreu por 18 horas a 4°C com agitação constante. Após a incubação com o anticorpo, a membrana foi lavada com PBS e desenvolvida com SuperSignal-West Pico (Thermo) em um fotodocumentador ChemiDoc MP Imaging System (Bio-Rad).

4 RESULTADOS E DISCUSSÃO

Para obtenção da YCA1 selvagem e YCA1-ΔN86 contendo mutações sítio dirigidas no inicialmente foi necessário identificar os resíduos de interesse através do alinhamento das sequências de aminoácidos da YCA1 com a metacaspase de TbMCA2 de *Trypanosoma brucei* (Figura 1) e em resíduos essenciais identificados na estrutura cristalográfica de ambas as enzimas [11,13].

Como uma das características conservadas entre os tipos de metacaspases, podemos destacar a presença da cisteína do sítio catalítico (em amarelo) que se encontra preservada entre as estruturas, sendo a cisteína 276 o resíduo conservado na YCA1 (Cys^{276}). Porém, ao elucidarem a estrutura cristalográfica da TbMCA2, McLuskey *et al.* (2012) perceberam uma segunda cisteína que está relacionada ao autoprocessamento dessa metacaspase, identificada como resíduos Cys^{92} (MCLUSKEY *et al.*, 2012), e quando comparadas as duas sequências dessas metacaspases, observamos que a YCA1 apresenta uma cisteína conservada na mesma posição a Cys^{155} (Figura 1).

Outra característica conservada entre as estruturas da YCA1 e da TbMCA2 são os resíduos de interação com o íon cálcio (em magenta) que se encontram conservados quando as sequencias são alinhadas, sendo Asp^{236}, Asp^{252}, Asp^{253} e Asp^{283} para a metacaspase de *S. cerevisiae*, e Asp^{173}, Asp^{189}, Asp^{190}, Asp^{220} para a metacaspase de *T. brucei*. A partir dessas informações e alinhamentos, identificamos os resíduos de interesse para esse estudo, e projetamos os *primers* para realizarmos as mutações dos aspartatos responsáveis pela interação com o íon de cálcio (Asp^{236},

Asp^{252}, Asp^{253} e Asp^{283}) através da técnica de mutações sítio dirigida, com o objetivo de investigar o impacto de cada um deles na interação com os sítios de cálcio.

```
YCA1     MYPGSGRYTYNNAGGNNGYQRPMAPPPNQQYGQQYGQQYEQQYGQQYGQQNDQQFSQQYA 60
TbMCA2    ----------------------MCSLI---------------------------------- 5

YCA1     PPPGPPPMAYNRPVYPPPQFQQEQAKAQLSNGYNNPN------VNASNMYGPPQNMSLPP 114
TbMCA2   -----------TQLC-----DAGQLADYVGLGWLNAVSSQPYLVQALGLQPPPRRVDVDA  49

YCA1     P--QTQTIQGTDQPYQYSQC-TGRRKALIIGINYIGSKNQLRGCINDAHNIFNFLTNGYG 171
TbMCA2   AFRDAKGLH-GHQPWVATPLPGQTVRALFIGINYYGTSAALSGCCNDVKQMLATLQK-KG 107

YCA1     YSSDDIVILTD-EDQNDLVRVPTRANMIRAMQWLVKDAQPNDSLFLHYSGHGGQTEDLDG 229
TbMCA2   LPINEAVILVDEDNFPGRTDQPTRDNIVRYMAWLVKDAKPGDVLFFHYSGHGTQCKSRG  166

YCA1     DEEDGMDDVIYPVDFETQGPIIDDEMHDIMVKPLQQGVRLTALFDSCHSGTVLDLPYTYS 289
TbMCA2   DSDEKYDQCIAPVDFQKSGCIVDDDIHKLLFSRLPEKVRLTAVFDCCHSGSIMDLPFTYV 226

YCA1     TKGIIKEPNIWKDVGQDGLQAAISYATGNRAALIGSLGSIFKTVKGGMGNNVDRERVRQI 349
TbMCA2   CSGGEQASGTP----------------------------------------HMKRIREG 245

YCA1     KFSAADVVMLSGSKDNQTSADAVEDGQ------NTGAMSHAFIKVMTLQ-PQQSYLSLLQ 402
TbMCA2   NDVLGDVMMISGCADEQTSADVKNTATFGTGSTGAGGAATQCITCMLMNNQSLSYGKLLI 305

YCA1     NMRKEL-AGKYSQKPQLSSSHPIDVNLQFIM-----------     432
TbMCA2   ETRDMLKRKGFKQVPQLSASKAIDLDQTFSLTEMFSVDRSIQ     347
```

Figura 1 - Alinhamento da sequência primária da YCA1 íntegra com a sequência primária da TbMCA2. Comparação da estrutura primária da metacaspase YCA1 de *S. cerevisiae* com a TbMCA2 da *T. brucei*. Na primeira linha a YCA1, contendo em sea composição 432 aminoácidos e na segunda linha a TbMCA2, contendo em sua composição 347 aminoácidos. Os resíduos da díade catalítica de cisteína e histidina são representados em amarelo e os resíduos do sítio de interação com o ìon cálcio são identificados em magenta.

A sequência de aminoácidos da YCA1 quando alinhada com a metacaspase de *Candida Albicans* (CaMCA) também tem seus resíduos do sítio catalítico e do sítio de interação com o cálcio conservados, apesar da segunda não ter sua estrutura cristalográfica elucidada. Entretanto, ambas as enzimas são metacaspases do tipo I que apresentam a porção hidrofóbica em seu N-terminal [11].

Um estudo publicado por Erhardt *et al.,* (2010), demonstrou que a composição da porção N-terminal da metacaspase YCA1 da levedura *S. cerevisiae* detém uma grande influência na capacidade de precipitação desta protease, uma vez que essa região é rica em glutamina e asparagina. Semelhante a YCA1 e CaMCA, foi descrito que as metacaspases de *M. oryzae* (MoMca1 e MoMca2) também apresentam um N-

terminal rico em resíduos de Q/N, sugerindo ser uma característica comum entre as metacaspases do tipo I [14].

Uma característica da YCA1 é ser expressa como uma pró-enzima constituída por um pró-domínio em seu N-terminal, uma subunidade grande (P_{20}) e uma subunidade pequena (P_{10}) [15]. E assim Wong, Yan & Shi (2012) deram indícios de que o autoprocessamento da metacaspase YCA1 resulta na clivagem de seus dois domínios, o N-terminal e C-terminal, de uma maneira que inicialmente são liberados dois fragmentos no momento do primeiro autoprocessamento, sendo uma subunidade grande (~43 kDa) e uma subunidade pequena (~12 kDa), respectivamente. Logo após ocorre um segundo processamento, porém este mais lento, na sua subunidade grande que é responsável por gerar um novo fragmento com tamanho de ~31 kDa.

O autoprocessamento da metacaspase está relacionado diretamente com o aumento da sua atividade catalítica, permitindo que a enzima tenha ação sobre substratos proteícos grandes e não apenas oligopeptídeos [16,17]. A forma íntegra, quando processada, libera os fragmentos com peso molecular em torno de 43 kDa e 12 kDa, e a forma truncada libera os fragmentos com peso molecular em torno de 31 kDa e 12 kDa.

A liberação desses fragmentos, resultantes do autoprocessamento, é demonstrada para os mutantes nas imagens após purificação, que ocorrem de forma diferente, mas sendo possível destacar um deles que teve o processamento de forma bem mais lenta que os demais. Vale destacar também que foi notório a diferença na velocidade dos processamentos entre a enzima em sua forma selvagem e a com deleção no N-terminal.

Na Figura 2 são demonstrados os resultados dos mutantes da YCA1 íntegra após o processo de purificação por cromatografia de afinidade. A análise desses mutantes em relação à interação com íons de cálcio, e consequente ativação enzimática que evidencia o papel distinto dos resíduos Asp^{236}, Asp^{252}, Asp^{253} e Asp^{283} na funcionalidade da metacaspase. A YCA1 íntegra, eluida com aproximadamente 55 kDa, é ativada na presença de cálcio, resultando no processamento da proteína em fragmentos de 43 kDa e 12 kDa, o que faz referência ao autoprocessamento dependente desse íon.

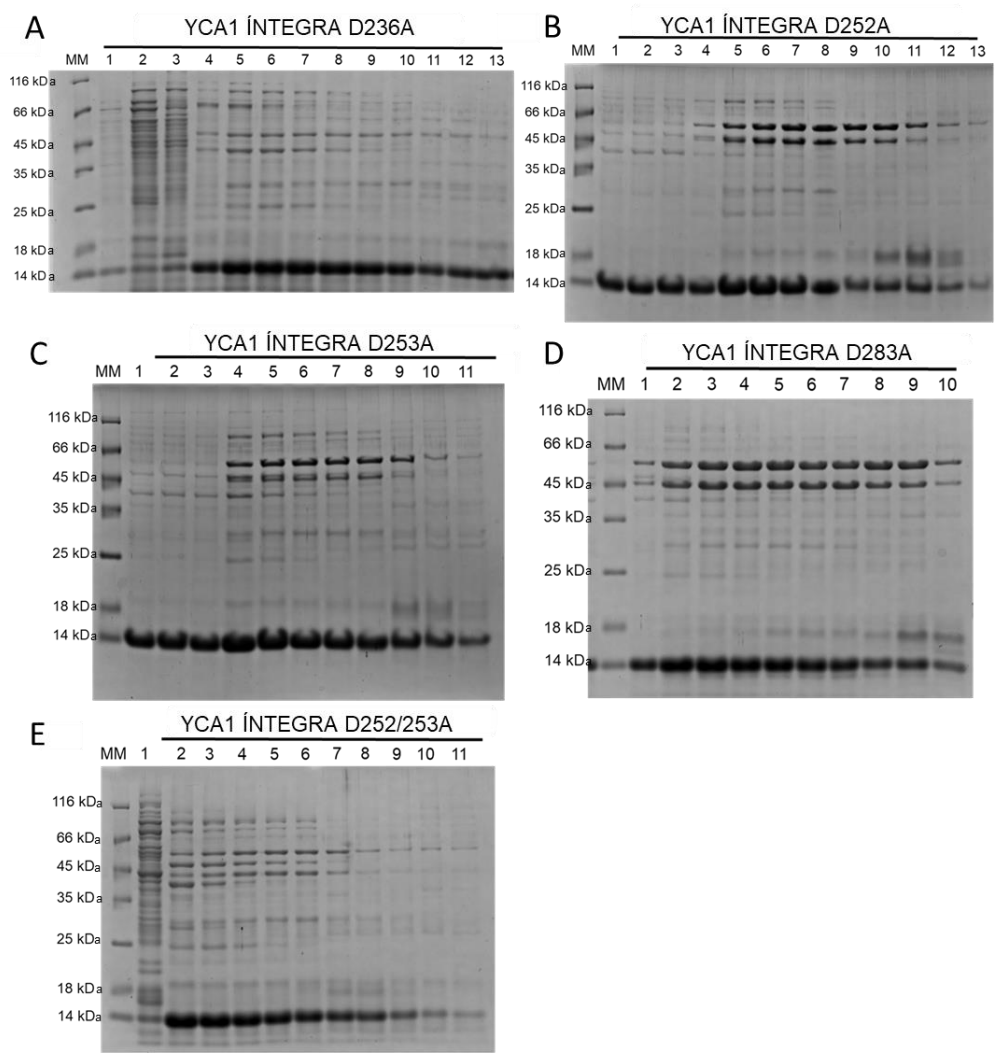

Figura 2 - SDS-PAGE das frações eluídas na Purificação por cromatografia de afinidade da YCA1 íntegra. Sendo (A) YCA1 Íntegra D236A; (B) YCA1 Íntegra D252A; (C) YCA1 Íntegra D253A; (D) YCA1 Íntegra D283A; (E) YCA1 Íntegra D252/253A.

O mutante YCA1 íntegra D236A (Figura 2A), ao ser analisado, apresentou bandas processadas (~43 kDa e ~12 kDa) além da forma não processada (~55 kDa), além de várias outras bandas provenientes de possíveis processamentos. Esse padrão sugere que o resíduo Asp^{236} participa da ativação da metacaspase, embora sua ausência não impeça o processamento ocorra. Sua presença pode facilitar a interação com o íon cálcio, favorecendo a clivagem da enzima em seus fragmentos ativos, mas não é essencial para a ativação plena da YCA1.

No caso do mutante D252A (Figura 2B), observou-se uma ligeira redução na intensidade da banda processada, indicando que o resíduo Asp^{252} contribui para a eficiência do processamento enzimático. Embora sua ausência comprometa parcialmente a clivagem da metacaspase, a enzima ainda consegue ser ativada, sugerindo que este resíduo favorece a estabilização da conformação ativa, mas sem ser essencial para o processamento.

O mutante D253A (Figura 2C), por outro lado, apresentou uma diminuição na banda processada, com a forma não processada predominando. Isso indica que o resíduo Asp^{253} exerce um papel regulador mais forte sobre o processamento, e sua mutação retarda a ativação da metacaspase. O resíduo Asp^{253} parece ter uma função estabilizadora, onde sua ausência compromete mais significativamente a ativação catalítica. Diferente do Asp^{252}, cuja ausência causa um impacto menos intenso, a falta de Asp^{253} pode afetar o equilíbrio entre as formas processadas e não processadas, sugerindo uma importância moderada na estabilidade da enzima ativa.

Para o duplo mutante D252/253A (Figura 2E), observou-se um diversas frações de processamentos além das frações processadas e não processadas. Apesar da mutação ser em dois resíduos o que faria com que a enzima interagisse menos com o cálcio, mostrou que os resíduos Asp^{252} e Asp^{253} não são os mais importantes para interação com o íon, já que sem eles a enzima continua interagindo com o cálcio e se processando. Embora ambos contribuam para o processamento, eles podem exercer papéis compensatórios, com suas funções individuais se complementando na regulação do autoprocessamento da YCA1.

Por fim, o mutante D283A (Figura 2D) se mostrou em maior concentração na forma não processada (~55 kDa), e posteriormente em sua forma processada (~43kDa), indicando que o resíduo Asp^{283} é essencial para a interação com o íon cálcio e para o autoprocessamento da metacaspase. A ausência de Asp^{283} dificulta a interação com o cálcio e assim a ativação da enzima retardando o processamento, sugerindo que esse resíduo desempenha um papel indispensável na conformação ativa da metacaspase.

Baseado nos resultados obtidos da purificação com as mutações sítio-dirigidas nos resíduos Asp^{236}, Asp^{252}, Asp^{253} e Asp^{283} da metacaspase YCA1 íntegra, o mesmo foi realizado com a YCA1-ΔN86. Vale ressaltar que cada uma dessas mutações foi

projetada para investigar a relevância dos respectivos resíduos na ativação e processamento da enzima, cujo peso molecular na forma truncada é de aproximadamente 43 kDa, com fragmentos processados em torno de 31 kDa e 12 kDa (Figura 3).

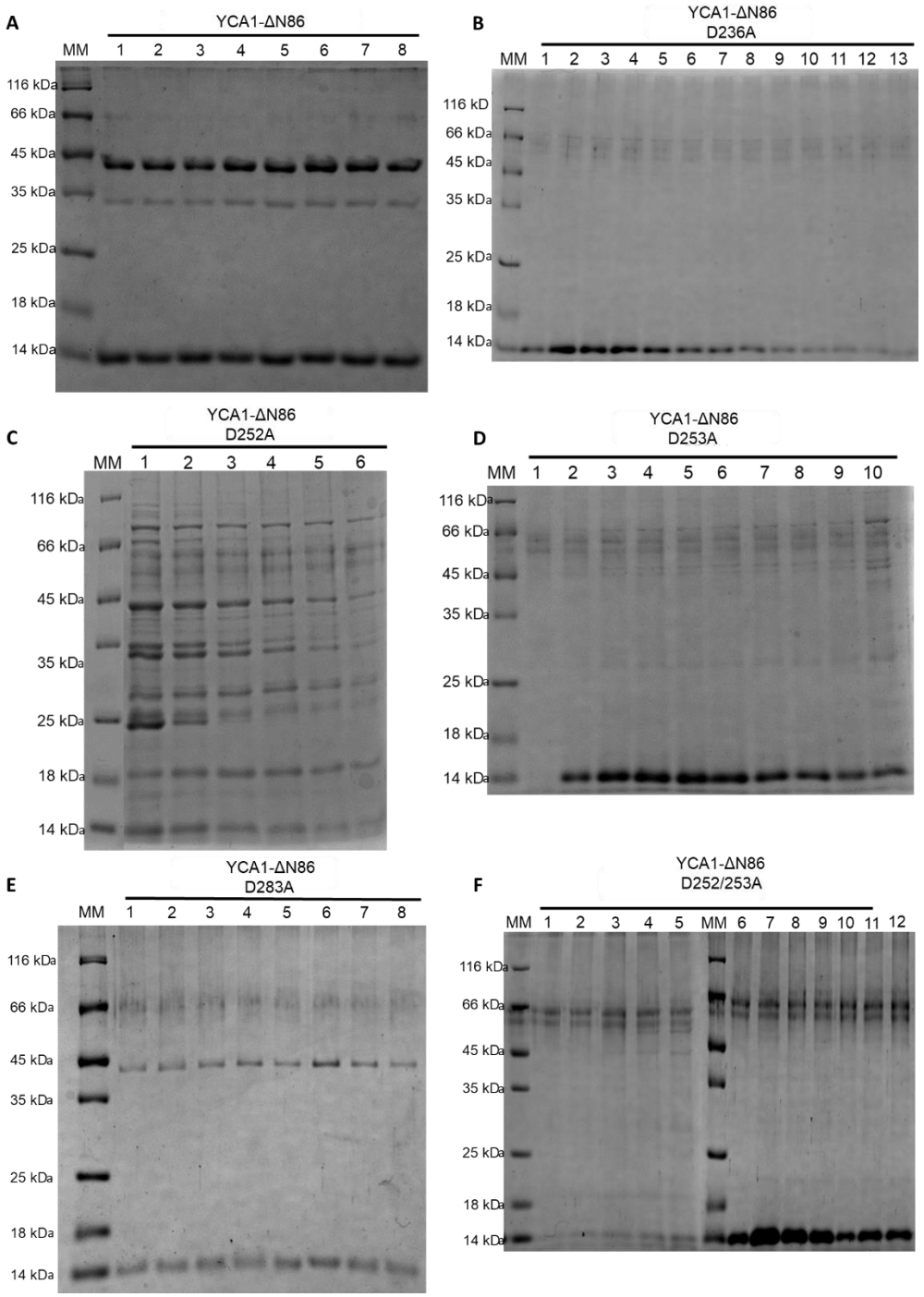

Figura 3 - SDS-PAGE das frações eluídas na purificação por cromatografia de afinidade da YCA1-ΔN86. Sendo (A) YCA1-ΔN86; (B) YCA1-ΔN86 D236A; (C) YCA1-ΔN86 D252A; (D) YCA1-ΔN86 D253A; (E) YCA1-ΔN86 D283A; (F) YCA1-ΔN86 D252/253A.

Nas amostras correspondentes a mutação D236A (Figura 3B), praticamente não se observa a formação dos fragmentos de 43 kDa e 31 kDa, apenas a formação do fragmento de aproximadamente 12kDa. Isso indica que a mutação de D236A interfere significativamente na ativação e no processamento da YCA1-ΔN86, sugerindo que este resíduo desempenha um papel importante na ligação do cálcio ou na estabilidade conformacional necessária para a atividade catalítica. A ausência das bandas dos fragmentos sugere que a mutação de Asp^{236} compromete a funcionalidade da enzima de forma intensa levando a um autoprocessamento mais acelerado. Quando comparado o mesmo mutante da YCA1 íntegra e YCA1-ΔN86, é possível observar que o processamento ocorre de forma bem mais rápida na enzima truncada, já que não é possível acompanhar as etapas do processamento e a enzima já aparece em ~12kDa, diferente do que ocorre na metacaspase íntegra.

Para a mutação D252A (Figura 3C), os resultados mostram uma pequena diminuição na intensidade das bandas de 43 kDa e 31 kDa em comparação com a enzima YCA1- ΔN86 sem mutação, mas a ativação e o processamento ainda ocorrem em algum grau. Isso sugere que Asp^{252} tem uma contribuição parcial para a atividade catalítica e a interação com o cálcio, mas seu papel não é tão crucial quanto o de Asp^{236}. A presença dos fragmentos processados indica que outros sítios de ligação de cálcio podem compensar parcialmente a função deste resíduo.

Na amostra mutada D253A (Figura 3D), observa-se uma diminuição intensa na geração dos fragmentos de 43 kDa e 31 kDa. Esse padrão sugere que Asp^{253} é importante para a ativação, mas, similar a Asp^{236}, levando a um autoprocessamento mais acelerado. Assim, a diminuição nas bandas dos fragmentos indica que a mutação neste resíduo afeta a interação com o cálcio e, consequentemente, a conformação necessária para a atividade proteolítica, uma vez que a banda mais intensa é a de 12kDa.

A amostra mutada no resíduo Asp^{283} (Figura 3E) exibem um perfil único, com uma inibição completa da formação do fragmento de 31 kDa. Esse resultado sugere que Asp^{283} é um dos sítios críticos para a ativação da YCA1-ΔN86, possivelmente essencial para a ligação do cálcio ou para a estabilização da enzima na conformação ativa. A ausência de processamento da enzima indica que, sem a interação deste

resíduo com o cálcio, a YCA1-ΔN86 não é capaz de atingir a conformação cataliticamente ativa.

Os resultados obtidos com as mutações nos quatro resíduos analisados sugerem diferentes graus da influência de cada sítio na ativação e processamento da YCA1-ΔN86. A mutação em D283A resultou na inibição quase completa do processamento da enzima, evidenciando que esse resíduo pode ser considerado crítico para a interação com o cálcio e essencial para a conformação ativa da metacaspase.

Em contraste, as mutações em D236A, D252A e D253A (Figura 3B, 3C e 3D) mostraram efeitos mais moderados, indicando que esses resíduos contribuem para a interação com o cálcio, mas não são indispensáveis para o processamento da enzima. Isso sugere que podem ter papéis secundários ou de estabilização que auxiliam na interação com o cálcio e na ativação da enzima.

Em uma comparação entre os resíduos mutados D236A, D252A, D253A e D283A é possível evidenciar que Asp^{283} pode ser os principais resíduos de interação com o cálcio necessário para a ativação e processamento da YCA1-ΔN86, enquanto os demais resíduos têm papéis auxiliaries de ligação com o íon. A diferença dos processamentos da mesma enzima na presença de mutações sítio dirigidas mostram a importância de múltiplos resíduos de ligação ao cálcio na regulação da atividade catalítica das metacaspases, sendo Asp^{283} crucial para a ativação e funcionalidade da YCA1-ΔN86.

Durante a expressão em sistema heterólogo em *E. coli*, uma sequência de seis histidinas foi introduzida na YCA1 por meio do vetor pET28(a)+. A detecção da YCA1 marcada com histidina foi realizada utilizando um anticorpo específico contra a sequência de histidina. Neste experimento, utilizamos o anticorpo Anti-6xHis da *Thermo Fisher Scientific* (Figura 4).

Todos os mutantes da YCA1 íntegra e YCA1-ΔN86 foram identificados, mas apresentando características distintas. Para os mutantes YCA1 íntegra observa-se no mutante D252A que a intensidade do fragmento processado (~43 kDa) foi pouco superior à não processada (~55 kDa), o que ocorre totalmente o inverso no mutante D253A apresentando uma maior intensidade na fração não processada. Os mutantes D283A e D252/253A apresentaram intensidades iguais nas duas frações da proteína, e já no mutante D236A apenas o fragmento processado foi detectado.

Já para os mutantes YCA1-ΔN86 todos foram majoritariamente detectados na forma não processada (~43 kDa). O mutante D236A apresentou a banda não processada (~43kDa), e outras duas formas processadas ~31kDa e ~12kDa. Os mutantes D252A, D253A e o duplo mutante D252/253A apresentaram padrões muito similares quanto aos processamentos e intensidades das bandas. Somente o mutante D283A foi observado apenas na forma não processada (Figura 4).

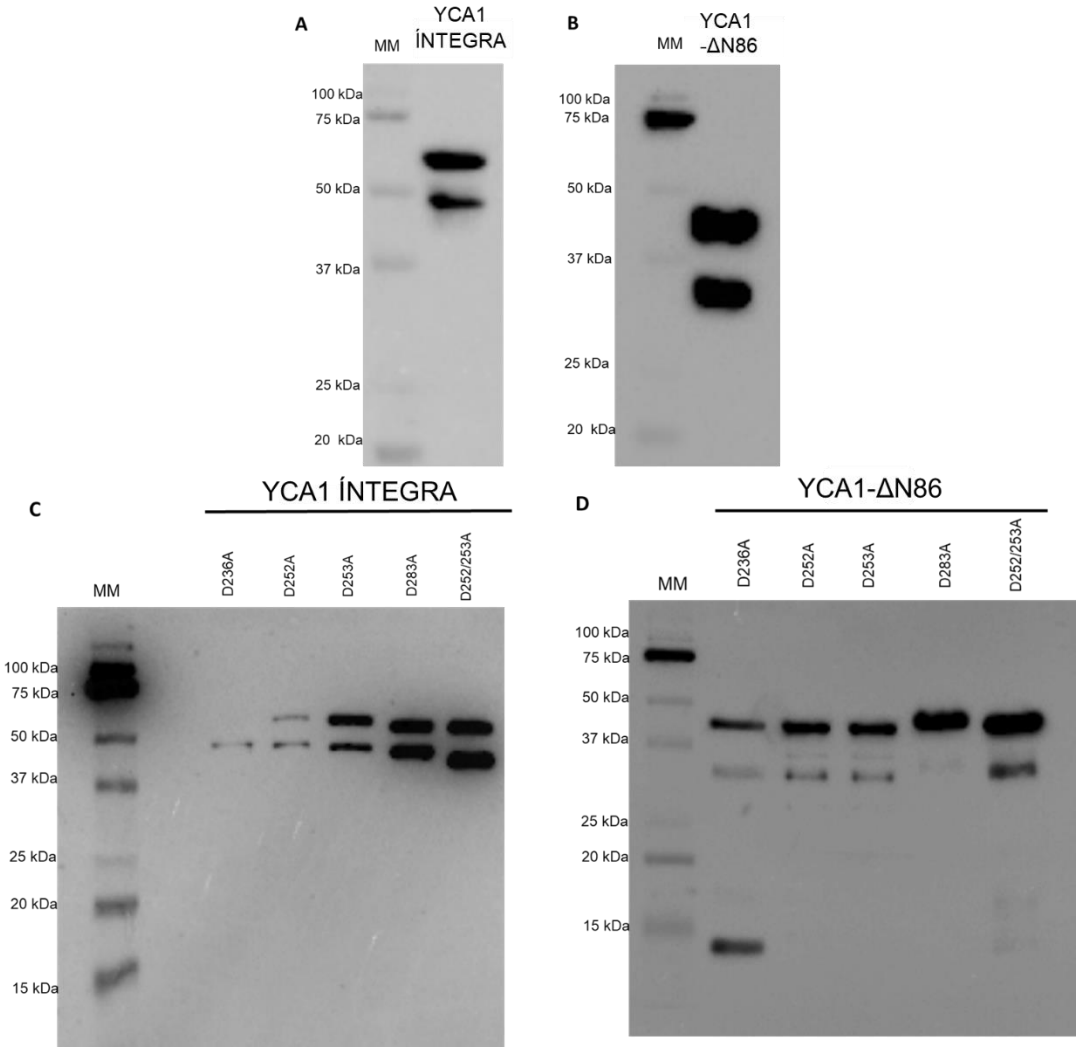

Figura 4: *Western Blotting* da YCA1 íntegra e YCA1-ΔN86. Onde, (A) YCA1 íntegra, (B) YCA1-ΔN86, (C) YCA1 íntegra e seus respectivos mutantes (D236A, D252A, D253A, D283A E D252/253) e (D) YCA1-ΔN86 e seus respectivos mutantes (D236A, D252A, D253A, D283A E D252/253) através de reconhecimento por anticorpo primário anti-6X*His*-tag.

Através dos resultados observados no *western blotting* para detectar a YCA1 em sua forma íntegra, truncada e seus respectivos mutantes foi possível observar variações no processamento de cada uma dessas formas.

Na figura 4A, observa-se a presença de duas bandas distintas, uma de aproximadamente 55 kDa e outra em torno de 43 kDa, o que sugere que o primeiro autoprocessamento ocorre no C-terminal, uma vez que ambas as frações foram detectadas pelo anticorpo anti-6X*His*-tag. A banda de 55 kDa corresponde à forma íntegra da YCA1 não processada. A presença desta banda indica que parte da proteína permanece em sua conformação inicial, sem passar pelo processo de ativação enzimática. A segunda banda, de aproximadamente 43 kDa, representa a forma processada da YCA1 íntegra, sugerindo que a proteína foi parcialmente processada, liberando fragmentos menores. Esse processamento indica que a YCA1 na sua forma íntegra pode sofrer clivagem e gerar uma forma ativa menor, evidenciando a possibilidade de autorregulação e processamento na presença de condições específicas que favorecem a ativação [18].

Como nosso anticorpo trata-se de um anti-6XHis-Tag, e nossas enzimas possuem uma cauda de histidina no N-terminal, chegamos à conclusão que, diferentemente do que foi descrito por Wong, Yan & Shi (2012), a YCA1 se autoprocessa no seu C-terminal, uma vez que foi possível observar a proteína com peso molecular em torno 43 kDa, se o processamento ocorresse no N-terminal não seria possível visualizar a banda nesse tamanho (Figura 4A). Curiosamente, para a YCA1-ΔN86 observamos que o processamento na forma truncada também ocorre no C-terminal, e pode ser evidenciado por uma terceira banda mais fraca com peso molecular de aproximadamente 31 kDa.

Na figura 4B as duas bandas observadas estão em torno de 43 kDa e 31 kDa. A banda de 43 kDa corresponde à YCA1-ΔN86 em sua forma não processada. Essa forma já é um produto da clivagem inicial da YCA1 íntegra e representa a versão encurtada, possivelmente com perda de regiões regulatórias ou domínios dispensáveis para a atividade catalítica. A segunda banda, de aproximadamente 31 kDa, indica a forma processada da YCA1-ΔN86, representando um fragmento adicional gerado pela clivagem. Essa forma processada sugere que a YCA1-ΔN86 ainda possui atividade auto catalítica ou é susceptível a processamento adicional, gerando fragmentos ativos menores.

Esses resultados indicam que tanto a YCA1 íntegra quanto a truncada podem sofrer processamento para formar versões menores, que provavelmente correspondem a formas que foram ativadas. Durante o primeiro processamento a forma íntegra (55 kDa) é processada para 43 kDa, o que sugere a remoção de um segmento e possível exposição do sítio catalítico. Já a YCA1 truncada (43 kDa) ao ser processada em 31 kDa aponta para uma clivagem posterior.

Como observado nas bandas do *western blotting* pode-se destacar que a YCA1 é depende de ativação auto catalítica, a qual é mediada por cálcio, para atingir sua funcionalidade. A análise comparativa entre a YCA1 íntegra e truncada reforça a importância do primeiro processamento como mecanismo de ativação da enzima.

Na figura 4C, observamos o perfil da YCA1 íntegra com mutações pontuais em cada um dos resíduos de interação com o íon cálcio, nomeadamente D236A, D252A, D253A e D283A. Estas mutações sítio-dirigidas foram realizadas para avaliar a importância de cada resíduo na ativação e no processamento auto catalítico da enzima. A YCA1 íntegra não processada apresenta uma banda em torno de 55 kDa, enquanto sua forma processada é identificada por uma banda de aproximadamente 43 kDa, assim como ocorre na enzima em sua forma selvagem.

A mutação no resíduo D236A mostra a presença de uma única banda, sendo essa a forma processada de 43 kDa, e não apresenta a forma de 55 kDa sem o processamento. A mutação desse resíduo pode ter deixado mais exposto o sítio de clivagem da enzima, abrindo o caminho do cálcio com outro resíduo mais importante para a atividade catalítica da enzima. Deste modo, a YCA1 é clivada de forma mais acelerada, não deixando uma quantidade da fração de 55kDa para ser detectada. Isso sugere que o resíduo Asp^{236} tenha uma função menos crítica no processo de ativação, atuando como secundário e não sendo tão essencial para a ativação enzimática e formação da banda processada, uma vez que em sua ausência o processamento ocorre na mesma forma.

Já na mutação D252A é possível observar a presença de ambas as formas não processadas e a processada, de 55 kDa e 43 kDa, respectivamente, mostrando que sua mutação não compromete o processamento. Há uma ligeira intensidade maior da banda processada do que da banda não processada, sugerindo que há uma importância desse resíduo para a interação com o cálcio e na eficiência do processamento, além da estabilidade conformacional da proteína. O aumento da

intensidade da banda de 43 kDa indica que, no contexto da mutação D252A, a YCA1 se encontra preferencialmente em sua forma processada. Essas características sugerem que D252A exerce uma função moduladora no controle do estado não processado, e sua ausência reduz a estabilidade desta forma. Isso reforça a hipótese de que Asp^{252} pode estar envolvido na estabilização da enzima na sua forma não processada, e sua mutação altera o equilíbrio conformacional, favorecendo o processamento.

Para o mutante D253A observamos que há uma maior intensidade relativa da banda correspondente à forma não processada (~55 kDa) em comparação à forma processada (~43 kDa), o que sugere que a mutação no resíduo Asp^{253} interfere no processamento eficiente da YCA1. Essa alteração pode desestabilizar a configuração necessária para o reconhecimento e clivagem pelo sistema proteolítico, retardando o processamento da enzima. Logo, esse resíduo afeta mais diretamente a capacidade da enzima de se processar, apontando para um papel crítico deste resíduo na interação com o cálcio para a ativação da YCA1. Como resultado da mutação do resíduo Asp^{253}, a YCA1 tende a permanecer preferencialmente na sua forma não processada, acumulando-se nesta conformação e gerando uma banda de 55 kDa com maior intensidade.

No mutante D283A, a presença de bandas de intensidade semelhante tanto para a forma não processada (~55 kDa) quanto para a forma processada (~43 kDa) sugere uma alteração na eficiência de processamento da YCA1, mas sem impedir completamente a clivagem. Esse padrão pode indicar que o resíduo Asp^{283} desempenha um papel de equilíbrio entre as formas da enzima. A presença de ambas as formas em quantidades similares sugere que a estrutura global da enzima não foi significativamente desestabilizada pela mutação, permitindo que o processamento ocorra, embora de maneira menos eficiente.

Já o comportamento do mutante D252/253A apresenta características sobre o papel individual e coletivo dos resíduos Asp^{252} e Asp^{253} na ativação e processamento da YCA1. A análise revela que a mutação combinada destes dois resíduos resulta em uma intensidade equilibrada entre as formas processada (~43 kDa) e não processada (~55 kDa), um perfil que contrasta com as alterações observadas nas mutações individuais. No mutante D252A, a redução da forma não processada e o aumento da fração processada sugerem que o resíduo Asp^{252} contribui para manter o estado

inativo da enzima, de forma que sua ausência acelera o autoprocessamento. Em contraste, o mutante D253A apresenta uma diminuição da forma processada, retardando o autoprocessamento. Quando ambos os resíduos são mutados simultaneamente, a combinação dos efeitos não produz um resultado extremo. Em vez disso, o equilíbrio entre as formas processada e não processada no mutante D252/253A sugere uma interação entre D252 e D253, onde a ausência conjunta de ambos os sítios limita parcialmente tanto a ativação quanto o bloqueio do processamento. Essa resposta intermediária indica que D252 e D253 têm papéis sinérgicos, mas parcialmente compensatórios, no controle do autoprocessamento da YCA1.

Na figura 4D, temos a YCA1 truncada no N-terminal, com mutações pontuais nos sítios de interação com o íon cálcio (D236A, D252A, D253A, D283A e o duplo mutante D252/253A). Como demonstrado anteriormente a enzima truncada apresenta uma banda em torno de 43 kDa na forma não processada e outra em torno de 31 kDa na forma processada. Observa-se que todos são predominantemente detectados na forma não processada (~43 kDa), o que sugere uma limitação no autoprocessamento em função da remoção do N-terminal.

Na mutação D236A são observadas a fração não processada de ~43kDa em sua maioria, além da fração processada ~31kDa e uma fração adicional de ~12kDa, possivelmente indicando múltiplas etapas de clivagem, o que supõe um papel importante deste resíduo na estabilidade e processamento da enzima sem o N-terminal.

Em contrapartida, os mutantes D252A, D253A e o duplo mutante D252/253A exibiram perfis similares entre si, com intensidades e padrões de bandas processadas e não processadas comparáveis, sugerindo uma interdependência funcional entre os resíduos D252A e D253A, sem que um deles isoladamente promova ou iniba significativamente o autoprocessamento. A mutação dos resíduos individuais D252A e D253A apresentaram de forma mais intensa a fração não processada de ~43kDa, de forma mais fraca a fração 31kDa, além de uma nova fração entre elas de aproximadamente 35kDa, sugerindo mais uma etapa de clivagem diante da mutação desses resíduos. Este resultado pode indicar que ambos os resíduos contribuem para um equilíbrio dinâmico no controle da atividade proteolítica.

No mutante D283A, a banda de 31 kDa é praticamente ausente, o que indica que o processamento da proteína é severamente comprometido. Isso implica que o

resíduo Asp^{283} é crucial para a ativação e processamento, atuando como o principal resíduo de interação com o cálcio, e que sua alteração bloqueia o processamento e a ativação da YCA1-ΔN86. Sendo possível destacar que a contribuição de cada resíduo para o processamento enzimático sugere que a ausência do N-terminal altera a dinâmica das interações iônicas, promovendo uma configuração estrutural menos propensa ao processamento.

Os dados indicam que cada um dos aspartatos tem sua importância como sítio de interação com o cálcio para a forma truncada da YCA1. Sendo possível destacar que o resíduo Asp^{283} é essencial, pois sua mutação impede quase completamente o processamento da enzima. O Asp^{253} e Asp^{252} também são importantes, mas com um impacto menor comparado a Asp^{283}, enquanto Asp^{236} parece ter papel secundário, pois sua mutação permite o processamento, embora possam reduzir sua eficiência.

Uma vez que esses resíduos são caracterizados quanto as suas funções, esses contribuem para a compreensão dos mecanismos regulatórios do autoprocessamento da YCA1, com implicações potenciais na manipulação de metacaspases para estudos visando potenciais aplicações na biotecnologia e em estratégias terapêuticas direcionadas ao controle da apoptose e outras vias reguladas por proteases. A elucidação dessas funções específicas poderá orientar o desenvolvimento de abordagens inovadoras que explorem as caspases como alvos terapêuticos em doenças que envolvem desequilíbrios nos processos de morte celular programada.

A obtenção da forma truncada da YCA1 foi feita a partir da deleção dos 86 resíduos que compõem o N-terminal da proteína, composto em grande parte por resíduos de glutamina e asparagina que geram uma região hidrofóbica, influenciando diretamente na precipitação *in vitro* da YCA1. Como visto anteriormente, a YCA1 íntegra após sua purificação, apresenta a capacidade de se autodegradar. Em resultados obtidos anteriormente pelo grupo ao produzir a YCA1 truncada sem mutações observamos maior estabilidade relacionada a precipitação da enzima e um aumento do rendimento da proteína durante sua expressão, o que gera melhores condições para estudos cinéticos e bioquímicos.

Ao realizarmos a deleção do N-terminal retirando os primeiros 86 aminoácidos da enzima para obtermos a YCA1 truncada (YCA1-ΔN86), evidenciamos que ela apresenta um peso molecular com aproximadamente 43 kDa, peso similar ao observado após o primeiro processamento da YCA1 íntegra. O primeiro processamento foi descrito em literatura como ocorrendo no N-terminal da YCA1,

possivelmente após os resíduos Arg^{72} e Lys^{86} [11], entretanto resultados obtidos anteriormente pelo grupo em mutações sítio específicas nas cisteínas catalíticas observamos que a YCA1-ΔN86 e os mutantes YCA1-ΔN86 C155A e YCA1-ΔN86 C276A continuaram se processando. Esse processamento é referente a uma clivagem no C-terminal, visto que ocorreu a deleção dos aminoácidos onde aconteceria a clivagem e liberação da fração N-terminal.

Estudos anteriores do grupo demonstraram que o processamento da YCA1-ΔN86 seja intermolecular, diferentemente do primeiro processamento no qual a enzima cliva ela mesma classificando como um autoprocessamento. Desta forma a enzima ativa, YCA1-ΔN86, está clivando outras enzimas YCA1-ΔN86 não ativas, gerando o fragmento do segundo processamento com o peso molecular de aproximadamente 31 kDa. O mesmo observado no *western blotting* da YCA1-ΔN86 e seus mutantes do sítio de interação com íon cálcio. Um evento similar foi observado para a metacaspase de *Candida glabatra* [19], nos fornecendo através desse estudo dados que corroboram com a nossa hipótese.

Comparando com estudos das metacaspases do protozoário *T. brucei*, foi visto que a TbMCA3, classificada como tipo I, é capaz de processar *in vivo* a TbMCA4. Esses dados fornecem evidências de que a cascata proteolítica que acontece entre as caspases pode estar ocorrendo entre metacaspases, a fim de gerar as formas ativas da enzima [20,21].

Como dito anteriormente, a metacaspase é expressa como zimogênio, e sua forma madura é liberada quando ela sofre os dois processamentos. De acordo com nossos dados, verificamos que ambos ocorrem na porção C-terminal diferentemente do que foi demonstrado anteriormente por Wong, Yan & Shi (2012).

A fim de investigar qual o nível de influência do cálcio na enzima, foi realizado uma incubação com crescentes concentrações de cálcio (0 a 15mM). A incubação foi realizada de 0 a 120h em tampão Tris 50mM e NaCl 150mM em pH 7,4 em temperatura ambiente e foram posteriormente analisadas através de gel SDS-PAGE 15% (Figura 5). A enzima em sua forma íntegra sem mutações rapidamente sofre diversos processamentos até se encontrar em aproximadamente 12kDa, o que dificulta sua visualização no gel SDS-PAGE.

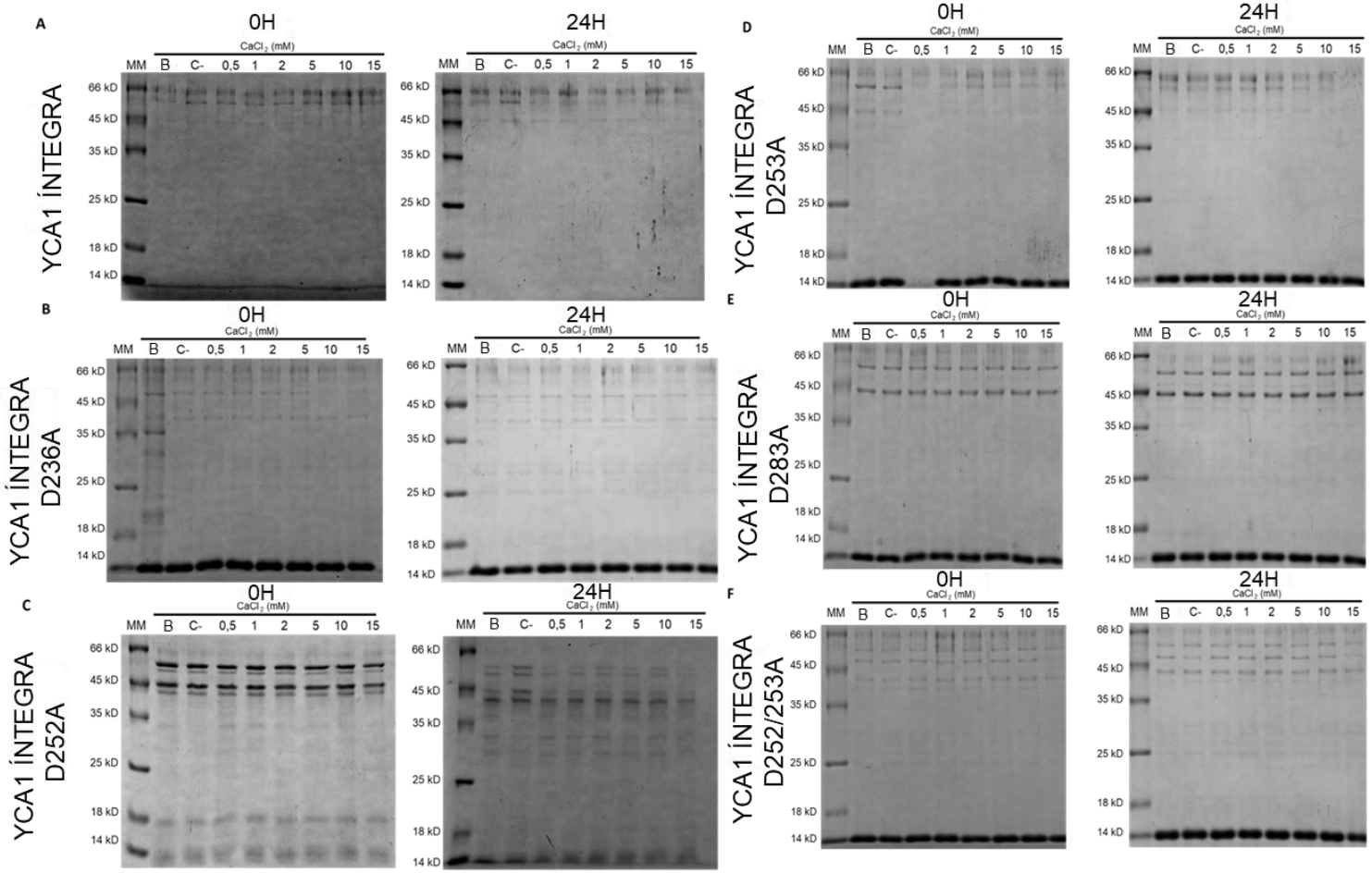

Figura 5 - Teste de maturação dos mutantes da YCA1 íntegra do sítio de cálcio na presença de cálcio. SDS-PAGE das amostras após a incubação na presença ou ausência de Ca^{2+} e EGTA. Na canaleta 1: marcador de peso molecular; na canaleta; 2 YCA1 Branco (enzima + tampão); na canaleta 3 YCA1 C- (enzima + tampão + EGTA); (A) YCA1 íntegra; (B) YCA1 íntegra D236A; (C) YCA1 íntegra D252A; (D) YCA1 íntegra D253A; (E) YCA1 íntegra D2833A; (F) YCA1 íntegra D252/253A.

Na Figura 5A é possível observar a YCA1 íntegra na sua forma não processada de 55kDa e sua forma processada de 43kDa imediatamente quando colocado na presença do íon cálcio. Nas maiores concentrações de cálcio, de 10mM e 15mM, a fração processada da enzima não se mostrou presente, tanto em 0H quanto 24H.

Já o mutante YCA1 íntegro D236A, Figura 5B, quando incubado com diferentes concentrações de cálcio apresentou processamento imediato (no tempo 0h de incubação), além do primeiro processamento em torno de 43kDa é possível observar outros processamentos.

O mesmo ocorre no tempo 0h de incubação para o mutante YCA1 íntegro D252A, Figura 5C, o qual apresenta processamento imediato. É possível observar um processamento logo após sua fração de ~55kDa (não processada) e seguida de outros. O processo de maturação se manteve após 24h, mas com uma menor intensidade da banda não processada, o que corrobora com o aparecimento de novas bandas provenientes de processamento. Bem parecido com o mutante YCA1 íntegro D252/253A, Figura 5F, onde a enzima se mostra com diversos processamentos mesmo em 0h, que vão se tornando mais fracos à medida que a concentração de cálcio vai aumentando.

Para o mutante íntegro YCA1 D253A, Figura 5D, só é possível observar o primeiro processamento e rapidamente a enzima aparece em sua fração mais processada em aproximadamente 14kDa. Apesar de Wong e colaboradores mostrarem que o mutante D252/253A seria o mais importante no processamento já que se encontra conservado em relação a metacaspase TbMCA2, porém nossos dados mostram que a mutação do resíduo de Asp^{283} é o resíduo crucial para interação com o cálcio e formação da fração cataliticamente ativa da YCA1 em sua forma íntegra e truncada.

Já o mutante YCA1 íntegro D283A, Figura 5E, se mostrou apenas nas formas não processadas de 55kDa e processada de 43kDa, além de se mostrar estável mesmo com altas concentrações de cálcio, possivelmente não interagindo tanto com o íon na ausência desse resíduo.

A enzima em sua forma íntegra e suas mutações apresentaram um baixo nível de estabilidade e mesmo armazenada nas condições ideais a mesma precipita, devido a sua porção hidrofóbica do N-terminal. Possivelmente induzindo a diversas etapas de processamento culminando ao processamento completo.

Baseado nos dados já obtidos com os mutantes íntegros e principalmente com o *western blotting* dos mutantes truncados, a mutação D283A ganhou destaque por não se processar. E assim a curva de maturação foi feita somente para a enzima YCA1-ΔN86 sem mutação, e YCA1-ΔN86 D283A (Figura 6A e 6B). As incubações foram realizadas das mesmas formas e concentrações como destacadas anteriormente, de 0h a 120h sendo de 0 a 15mM de cálcio, e os resultados também foram avaliados através de eletroforese SDS-PAGE 15%.

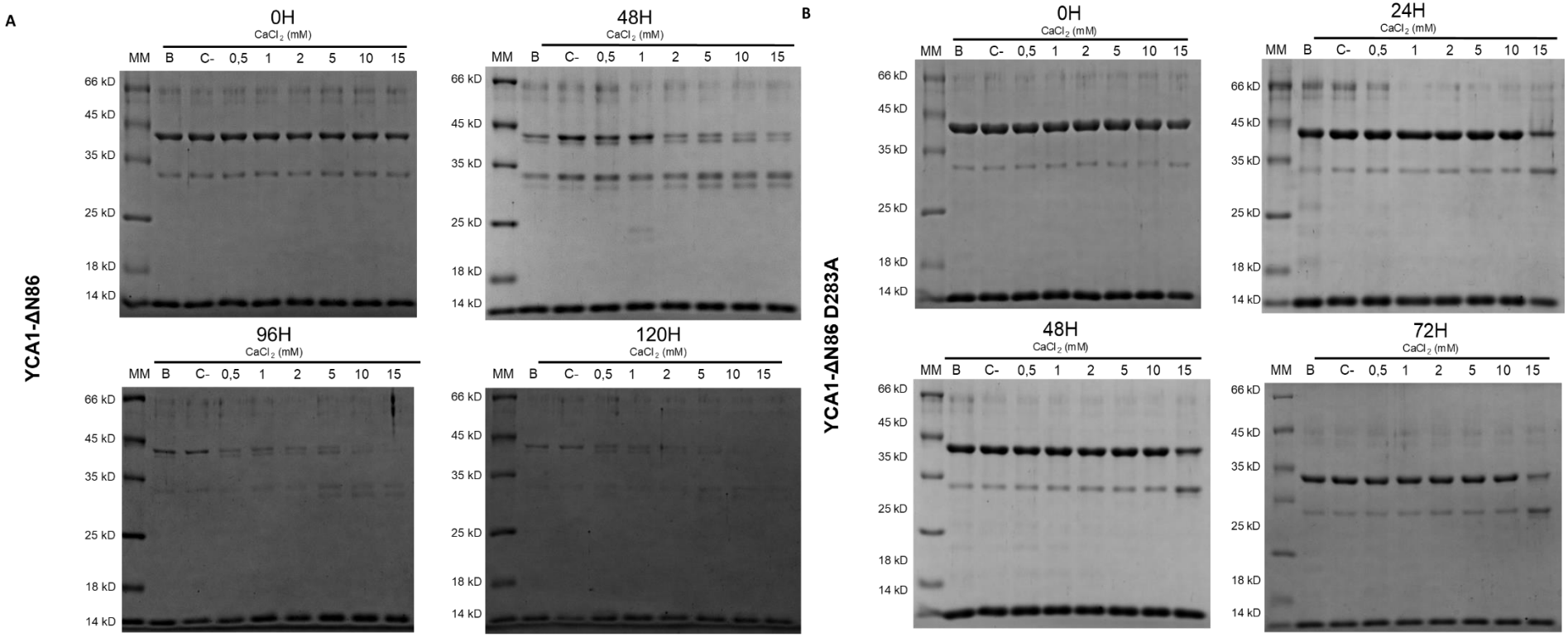

Figura 6 - Teste de maturação dos mutantes da YCA1-ΔN86 do sítio de cálcio na presença de cálcio. SDS-PAGE das amostras após a incubação na presença ou ausência de Ca^{2+} e EGTA. Na canaleta 1: marcador de peso molecular; na canaleta 2 Branco YCA1-ΔN86 (enzima + tampão); na canaleta 3 YCA1-ΔN86 C- (enzima + tampão + EGTA); (A) YCA1-ΔN86; (B) YCA1-ΔN86 D283A

Como observado na Figura 6A, a enzima YCA1-ΔN86 sem mutações foi a única que suportou a incubação com o íon cálcio com 120h e de maneira possível em visualizar no gel de SDS-PAGE, somente nas maiores concentrações de cálcio (10 e 15mM) que ela apresentava bandas mais fracas da enzima e a longo tempo se processou até atingir um peso de aproximadamente 14kDa.

O mesmo ocorreu para YCA1-ΔN86 D283A, Figura 6B que comparado com sua versão de mutação íntegra suportou muito mais o tem de interação com o íon cálcio, também apresentando duas frações mais fracas e mais sujeitas a processamento com 15mM do íon. Ainda em 48h é possível observar a fração não processada da enzima de aproximadamente 43kDa.

Em geral as enzimas truncadas, as quais não apresentam a porção hidrofóbica do N-terminal, suportaram por mais tempo a interação com o íon cálcio quando comparadas a enzima integra. Além de ser possível acompanhar cada etapa do processamento até chegar em uma única banda em 14kDa durante um longo tempo. Porém na concentração mais alta de 15mM de cálcio há uma maior indução da maturação da enzima, fazendo com que ela seja mais convertida da forma não processada para a forma cataliticamente ativa (processada).

A metacaspase YCA1 desempenha um papel crucial em processos celulares regulados, sendo sua ativação catalítica dependente de modificações estruturais e interações com cofatores. A enzima é inicialmente expressa em uma forma inativa, necessitando de um processamento autocatalítico que envolve a remoção de seu domínio N-terminal. O mesmo, presente na YCA1 íntegra impede o acesso ao sítio catalítico e, consequentemente, a atividade enzimática. A remoção do N-terminal desencadeia mudanças conformacionais que permitem a organização do sítio ativo fazendo que a YCA1 hidrolise outras proteínas. A YCA1-ΔN86 foi produzida experimentalmente sem o domínio N-terminal, representando a forma da enzima capaz de processar outras proteínas. A ausência desse domínio elimina a necessidade do processamento inicial, permitindo o estudo direto de sua atividade e interações [17,18].

O resíduo Asp283 identificado como crítico para a interação com o cálcio, desempenha um papel central na atividade da YCA1. Na enzima íntegra a interação entre o aspartato e o cálcio é essencial para o processamento autocatalítico inicial que gera a remoção do N-terminal. A mutação nesse resíduo interrompe essa interação, bloqueando a ativação da enzima e demonstrando que o cálcio não apenas facilita o

autoprocessamento, mas também regula a ativação estrutural. Na YCA1-TR a mutação no resíduo Asp^{283} não impede o processamento intermolecular que leva à ativação de outras metacaspases.

Essa diferença funcional entre a YCA1 íntegra e a YCA1-TR ressalta o papel do N-terminal e do resíduo de aspartato para ativação e funcionamento das diferentes isoformas da YCA1. O N-terminal regula o início da atividade enzimática onde o aspartato coordena a interação com o cálcio, sendo crucial tanto para a ativação inicial quanto para o processamento subsequente. Esse papel do N-terminal, bem como a importância da interação com o cálcio mostram um mecanismo de regulação, onde o processamento é intrinsecamente ligado a sinais celulares mediados pelo cálcio, destacando o papel central desse íon na funcionalidade da YCA1 [17,18].

Dados publicados pelo grupo anteriormente demonstraram que a ausência de uma das cisteínas catalíticas segura o primeiro processamento, impedindo que a enzima apresente outras isoformas. Os dados das mutações dos resíduos corroboram na sugestão de que a velocidade do processamento também seja regulada pela interação com os resíduos de cálcio, já que na avaliação da mutação individual apresentaram diferentes processamentos em tempos distintos, e o mutante D283A permitiu que o processamento ocorresse na presença de cálcio, porém de forma bem mais lenta de quando comparado a sua forma íntegra.

5 CONCLUSÃO

Os resultados obtidos neste estudo destacam o papel central do resíduo Asp^{283} na ativação e processamento da metacaspase YCA1. Entre os quatro resíduos analisados (Asp^{236}, Asp^{252}, Asp^{253} e Asp^{283}), a mutação no Asp283 resultou em uma perda significativa da capacidade da enzima de se processor ou apresentou um processamento consideravelmente mais lento, mesmo na presença de íons cálcio. Essa observação sugere que o Asp^{283} desempenha um papel estrutural e funcional indispensável na interação da enzima com o cálcio, enquanto os outros resíduos apresentam contribuições menos críticas. Os resultados elucidam o mecanismo de ativação da YCA1 e reforçam a importância de resíduos específicos para sua funcionalidade, fornecendo subsídios para o entendimento do papel do cálcio na

regulação de metacaspases e abrindo novas perspectivas para o desenho de moduladores enzimáticos.

REFERENCIAS

[1] A.G. Uren, K. O'Rourke, L. Aravind, M.T. Pisabarro, S. Seshagiri, E. V. Koonin, V.M. Dixit, Identification of paracaspases and metacaspases: Two ancient families of caspase-like proteins, one of which plays a key role in MALT lymphoma, Mol Cell (2000). https://doi.org/10.1016/s1097-2765(00)00094-0.

[2] S.H. MacKenzie, A.C. Clark, Death by caspase dimerization, Adv Exp Med Biol 747 (2012) 55–73. https://doi.org/10.1007/978-1-4614-3229-6_4.

[3] M. Klemenčič, C. Funk, Evolution and structural diversity of metacaspases, J Exp Bot (2019). https://doi.org/10.1093/jxb/erz082.

[4] S.M. Hill, T. Nyström, The dual role of a yeast metacaspase: What doesn't kill you makes you stronger, BioEssays (2015). https://doi.org/10.1002/bies.201400208.

[5] M.F.M. Machado, M.F. Marcondes, M.A. Juliano, K. McLuskey, J.C. Mottram, C.X. Moss, L. Juliano, V. Oliveira, Substrate specificity and the effect of calcium on Trypanosoma brucei metacaspase 2, FEBS Journal 280 (2013). https://doi.org/10.1111/febs.12248.

[6] J.C. Mottram, M.J. Helms, G.H. Coombs, M. Sajid, Clan CD cysteine peptidases of parasitic protozoa, Trends Parasitol (2003). https://doi.org/10.1016/S1471-4922(03)00038-2.

[7] I.J. González, C. Desponds, C. Schaff, J.C. Mottram, N. Fasel, Leishmania major metacaspase can replace yeast metacaspase in programmed cell death and has arginine-specific cysteine peptidase activity, Int J Parasitol (2007). https://doi.org/10.1016/j.ijpara.2006.10.004.

[8] D. Carmona-Gutierrez, K.U. Fröhlich, G. Kroemer, F. Madeo, Editorial: Metacaspases are caspases. Doubt no more, Cell Death Differ (2010). https://doi.org/10.1038/cdd.2009.198.

[9] D. Vercammen, B. Van De Cotte, G. De Jaeger, D. Eeckhout, P. Casteels, K. Vandepoele, I. Vandenberghe, J. Van Beeumen, D. Inzé, F. Van Breusegem, Type II metacaspases Atmc4 and Atmc9 of Arabidopsis thaliana cleave substrates after arginine and lysine, Journal of Biological Chemistry (2004). https://doi.org/10.1074/jbc.M406329200.

[10] M. Erhardt, R.D. Wegrzyn, E. Deuerling, Extra N-terminal residues have a profound effect on the aggregation properties of the potential yeast prion protein Mca1, PLoS One (2010). https://doi.org/10.1371/journal.pone.0009929.

[11] A.H.H. Wong, C. Yan, Y. Shi, Crystal structure of the yeast metacaspase Yca1, Journal of Biological Chemistry (2012). https://doi.org/10.1074/jbc.M112.381806.

[12] S.N. Ho, H.D. Hunt, R.M. Horton, J.K. Pullen, L.R. Pease, Site-directed mutagenesis by overlap extension using the polymerase chain reaction, Gene 77 (1989) 51–59. https://doi.org/10.1016/0378-1119(89)90358-2.

[13] K. McLuskey, J. Rudolf, W.R. Proto, N.W. Isaacs, G.H. Coombs, C.X. Moss, J.C. Mottram, Crystal structure of a Trypanosoma brucei metacaspase, Proc Natl Acad Sci U S A (2012). https://doi.org/10.1073/pnas.1200885109.

[14] J. Fernandez, V. Lopez, L. Kinch, M.A. Pfeifer, H. Gray, N. Garcia, N. V. Grishin, C.H. Khang, K. Orth, Role of Two Metacaspases in Development and Pathogenicity of the Rice Blast Fungus Magnaporthe oryzae, MBio 12 (2021) 1– 15. https://doi.org/10.1128/MBIO.03471-20.

[15] F. Madeo, S. Engelhardt, E. Herker, N. Lehman, C. Maldener, A. Proksch, S. Wissing, K.U. Fröhlich, Apoptosis in yeast: a new model system with applications in cell biology and medicine, Curr Genet 41 (2002) 208–216. https://doi.org/10.1007/S00294-002-0310-2.

[16] C.X. Moss, G.D. Westrop, L. Juliano, G.H. Coombs, J.C. Mottram, Metacaspase 2 of Trypanosoma brucei is a calcium-dependent cysteine peptidase active without processing, FEBS Lett (2007). https://doi.org/10.1016/j.febslet.2007.11.009.

[17] J.M. Gilio, M.F. Marcondes, D. Ferrari, M.A. Juliano, L. Juliano, V. Oliveira, M.F.M. Machado, Processing of metacaspase 2 from Trypanosoma brucei (TbMCA2) broadens its substrate specificity, Biochim Biophys Acta Proteins Proteom 1865 (2017). https://doi.org/10.1016/j.bbapap.2017.01.002.

[18] L. de A.M. Dalzoto, M.N.R. Trujilho, T. dos R. Santos, J.P.M.S. Costa, A.C.M. Duarte, W.A. de S. Judice, M.F. Marcondes, M.F.M. Machado, Metacaspase of Saccharomyces cerevisiae (ScMCA-Ia) presents different catalytic cysteine in a processed and non-processed form, Biochem Biophys Res Commun (2023) 149185. https://doi.org/10.1016/J.BBRC.2023.149185.

[19] L. Conchou, B. Doumèche, F. Galisson, S. Violot, C. Dugelay, E. Diesis, A. Page, A.L. Bienvenu, S. Picot, N. Aghajari, L. Ballut, Structural and molecular determinants of Candida glabrata metacaspase maturation and activation by calcium, Commun Biol 5 (2022). https://doi.org/10.1038/S42003-022-04091-4.

[20] W.R. Proto, E. Castanys-Munoz, A. Black, L. Tetley, C.X. Moss, L. Juliano, G.H. Coombs, J.C. Mottram, Trypanosoma brucei metacaspase 4 is a pseudopeptidase and a virulence factor, Journal of Biological Chemistry (2011). https://doi.org/10.1074/jbc.M111.292334.

[21] E.A. Minina, N.S. Coll, H. Tuominen, P. V. Bozhkov, Metacaspases versus caspases in development and cell fate regulation, Cell Death Differ (2017). https://doi.org/10.1038/cdd.2017.18.

CAPÍTULO 3 - CHALCONE AND FLAVONOID DERIVATIVES AS MODULATING AGENTS OF METACASPASE-2 FROM *Trypanosoma brucei* (TbMCA2)

PREFÁCIO

Este capítulo é uma continuidade do trabalho de doutorado da Dra. Laura Helena Araújo, onde para complementar os dados cinéticos foi realizado o docking e a dinâmica molecular, durante o período de Doutorado Sanduíche na University of Houston, Texas, Estados Unidos. Aqui estão apresentados tantos os dados da Dra. Laura quanto os dados obtidos através de bioinformática. Este artigo está prestes a ser submetido para análise na revista Biochemical Journal.

CHALCONE AND FLAVONOID DERIVATIVES AS MODULATING AGENTS OF METACASPASE-2 FROM *Trypanosoma brucei* (TbMCA2)

Mariana Nascimento Romero Trujilho[1,2,#], Laura Helena Araujo[1,#], Ane Caroline Moreira Duarte[3], Maria Aparecida Juliano[3], Wagner Alves de Souza Júdice[1], Denis Pires de Lima[4], Tarsis Ferreira Gesteira[2] and Maurício Ferreira Marcondes Machado[1,2,*].

[1]Interdisciplinary Center for Biochemical Research, University of Mogi das Cruzes, Av Dr. Cândido Xavier de Almeida e Souza, 200, 08780-991, Mogi das Cruzes, Brazil.
[2]College of Optometry, University of Houston, Houston, TX, United States.
[3]Technological Research Center, University of Mogi das Cruzes, Av Dr. Cândido Xavier de Almeida e Souza, 200, 08780-991, Mogi das Cruzes, Brazil.
[4]Department of Biophysics, São Paulo Federal University, Rua Pedro de Toledo, 669, 7º floor, 04039-032, São Paulo. Brazil.
[4]Federal University of Mato Grosso do Sul, Techonologic and Exates Science Center, Av. Filinto Müller, 155, 79074460 – Campo Grande, MS. Brazil.
Both authors contribute equally for this work

***Corresponding author:**
Maurício Ferreira Marcondes Machado, Ph.D.
Mail address: mauriciomachado@umc.br
Interdisciplinary Center for Biochemical Research
University of Mogi das Cruzes
Av. Dr. Cândido Xavier de Almeida e Souza, 200 - 08780-991 - Mogi das Cruzes, Brazil.

Author contributions:
LHA, JPMSC and ACMD – kinetic experiments and inhibitory tests for TbMCA2
MNRT, TFM and TFG – molecular docking
MFM and MAJ – expression and purification of *TbMCA2*
DPL – chalcone and flavonoid compound synthesis
WASJ - mathematics of inhibition mechanism of compounds
MFMM – design of experimental procedures and writing the manuscript.

Keywords: Chalcones, flavonoids, metacaspase, inhibition
Running Title: TbMCA2 inhibition by chalcone and flavonoid compounds.

ABSTRACT

African Human Trypanosomiasis (AHT) is a parasitic disease caused by the protozoan of the genus Trypanosoma. Its drug therapy remains a major challenge due to limited efficacy, disease complexity, potential side effects, and inaccessibility, necessitating the development of more effective and safer therapeutic approaches for treating the disease. Natural compounds have garnered interest in scientific research as they represent a potential source for developing new drugs and various pharmaceutical applications, such as chalcones and flavonoids, which have demonstrated anti-trypanosomal activity. In the present study, 9 compounds were evaluated, including 6 chalcone derivatives and 3 flavonoids, aiming to identify modulators of Trypanosoma brucei metacaspase-2. Screening of these molecules was performed at concentrations of 1 and 6 µM, followed by determination of their inhibitory potential. The results indicated inhibition capacity ranging from 2.2 to 7.6 µM, with notable IC50 values observed for compounds EM-1A, EM-1B, EM-1C, and EM-F12C (EM-1A = 2.14 ± 0.07 µM, EM-1B = 3.09 ± 0.09 µM, EM-1C = 3.02 ± 0.09 µM, and EM-F12C = 2.52 ± 0.13 µM). Mechanisms of inhibition were determined for these 4 molecules, revealing that 3 exhibited competitive inhibition profiles (EM-1A, EM-1C, and EM-F12C), while one showed a characteristic mechanism of non-competitive linear simple inhibition (EM-1B). Based on the findings of this study, chalcone and flavonoid derivatives are promising candidates for African Human Trypanosomiasis treatment, showing satisfactory inhibition of Trypanosoma brucei metacaspase-2 activity at micromolar scale. Further comprehensive investigations are crucial to assess both the efficacy and safety of these compounds.

1 INTRODUCTION

African Human Trypanosomiasis (AHT), also known as sleeping sickness, is a neglected tropical disease present in 36 countries of Sub-Saharan Africa, caused by subspecies of the parasitic protozoan *Trypanosoma brucei* and transmitted by the bite of the tsetse fly [1]. The disease progresses to the hemolymphatic and meningoencephalic stages, the latter characterized by an infection of the central nervous system after the parasite passes through the blood-brain barrier. This results in intense neuroinflammation and without treatment, this stage is fatal. However, available drugs are toxic and present complexities in administration [2, 3], which highlights the need for investigations to develop new drugs that are not only efficient, but also risk-free [4].

The family of chalcones, intermediate metabolites of flavonoids and isoflavonoids, stands out as an extensive group of bioactive natural products, presenting anticancer, anti-inflammatory, antimicrobial, antioxidant, and antiparasitic properties [5]. Research has focused on both synthetic and biosynthetic approaches as well as the broad biological activities of these substances. Chemically, chalcones are structured as 1,3-diaryl-2-propen-1-one, in which the two aromatic rings are connected by a three-carbon α,β-unsaturated carbonyl system [6], which allows the synthesis of various derivatives. Studies indicate that synthetic analogs of these molecules can present similar or even better activities than their natural counterparts, with potential therapeutic application in various diseases [5].

Flavonoids, a subclass of natural flavonoids, are widely distributed in fruits, herbs, stems, cereals, nuts, vegetables, flowers, and seeds [7]. With anticancer, antioxidant, anti-inflammatory, and antiviral properties, these phytochemical compounds are considered secondary metabolites and present a variety of chemical structures that consist mainly of a benzopyrone ring containing phenolic or polyphenolic groups in different positions, being classified into various types depending on their chemical structure, degree of unsaturation and oxidation of the carbon ring [8]. Flavonoids are valuable for being widely distributed in nature, being the target of research due to their proven efficacy for a variety of diseases, including antitrypanosomatid activity [9].

Parasitic proteases represent a vast and diversified group of enzymes that offer great potential to act as therapeutic targets for drug development [3]. In recent years, several research have been conducted on metacaspases (MCAs), which are cysteine proteases belonging to the CD clan, have a His-Cys catalytic dyad and perform the hydrolysis of peptide bonds after basic residues located at the P_1 position of the substrate, being present in plants, fungi, and protozoa [10, 11]. Among the most studied metacaspases, those found in trypanosomatids stand out, such as *Trypanosoma cruzi*, responsible for Chagas disease in South America, and *Trypanosoma brucei*, causing African sleeping sickness [12]. In the genome of *Trypanosoma brucei*, 5 types of metacaspases are encoded that differ in catalytic activity, with TbMCA2 being one of the enzymatically active variants that plays an important role in the regulation of self-processing and cellular activation events [13]. This specific metacaspase is dependent on calcium ions to initiate cleavage processes [14], since, through crystallographic analysis [15], it was possible to visualize a calcium binding site that is fundamental for the functional activity of TbMCA2[13–17].

The term “metacaspase” might cause confusion about the substrate specificity of these enzymes. While “caspase” stands for “Cysteine-ASpartate- ProteASE,” metacaspases tend to favor substrates with a basic residue (Arg or Lys) at the P_1 position. Therefore, a new system for classification and nomenclature has been suggested. The updated nomenclature uses the base symbol MCA, which is preceded by the species’ abbreviated Latin name, followed by a Latin numeral that represents the type of metacaspase, and a lowercase alpha character that indicates the homologous number of metacaspase in the genome [18].

The inherent link between autoprocessing and metacaspase activity is tied to the levels of Ca^{2+}. This relationship is defined by two distinct dissociation constants. The first, which has a higher affinity, is vital for the autoprocessing occurrence. Conversely, the second one, with a lower affinity, is instrumental in determining substrate specificity. [16, 17]. Calcium as important to release the autoprocessing of metacaspases, to reorder the N-terminal and C-terminal [14, 17].

Considering promising studies documented in the literature on chalcones and flavonoids, especially in the context of antiparasitic action, the present work aimed to evaluate compounds derived from these two classes of molecules to identify potential modulators of the activity of metacaspase-2 of *Trypanosoma brucei*.

2 EXPERIMENTAL PROCEDURES

2.1 Production of recombinant TbMCA2

The TbMCA2 clone was generously provided by Prof. Dr. Jeremy C. Mottram from York University. The expression of TbMCA2, which includes a N- terminal His-tag, has been previously documented [4].

Plasmids carrying the TbMCA2 gene were introduced into chemically competent *Escherichia coli* BL21(DE3)pLysS cells (Novagen, Darmstat, Germany). The cells were initially cultured in 20 mL of Luria broth medium with

50 µg/mL of kanamycin (supplemented LB, sLB) and incubated at 37°C for approximately 16 hours with shaking at 1,500 xg. The pre-inoculums were then transferred to 1 L of sLB medium and grown at 37°C until the culture density reached an OD_{600} of 0.4. The temperature was then lowered to 20°C, and isopropryl-β-D-1-thiogalactopyanoside (IPTG) was added to a final concentration of 0.5 mM. The cells were then incubated for an additional 16 hours before being collected by centrifugation at 3,000 xg for 20 min at 4°C. The resulting pellet was stored at -80°C as needed.

2.2 Purification of recombinant TbMCA2

The cell pellet was reconstituted in 20 mL of PBS (50 mM NaH_2PO_4, pH 8.0, 150 mM NaCl), enhanced with 20 mM imidazole and 1 mg/mL lysozyme. It was then chilled on ice for 30 minutes before adding 5 µg/mL RNase, 5 µg/mL DNase, and 0.02% Triton X-100. This mixture was further chilled for 30 minutes on ice before being centrifuged at 15,000 xg for 20 minutes at 4°C, and the supernatant was collected.

The supernatant from the cell lysis was introduced into a 1 mL HisTrap Ni^{2+}-Sepharose column (GE Healthcare, Armesham, UK) on an Akta Start system (GE Healthcare, Armesham, UK). The column had been previously balanced with a binding buffer composed of 20 mM NaH_2PO_4 at pH 8.0, 150 mM NaCl, and 20 mM imidazole, using a flow rate of 1.0 mL/min. The column was then rinsed with 5 mL of the binding buffer, and a recombinant TbMCA2 was purified and eluted using a step gradient of 5 mL of 50-, 150-, 300-, and 500-mM imidazole in the same buffer. TbMCA2 was eluted with 300 mM imidazole (as confirmed by SDS- PAGE analyses), and the collected fractions were combined.

To further purify and desalt the sample, the pooled protein was directly loaded onto a Sephadex G-75 size-exclusion column, prepacked with 100 mL of resin (GE Healthcare, Armesham, UK), and balanced in TBS buffer (50 mM Tris, pH 7.4, 150 mM NaCl). Elution fractions were analyzed using SDS-PAGE, and the fractions containing the recombinant TbMCA2 were collected. The purified TbMCA2 was stored in TBS buffer containing 30% glycerol and kept at -80°C.

2.3 Peptide synthesis

FRET peptides of the Abz-peptidyl-Gln-EDDnp, where Abz represents the fluorescent group ortho-aminobenzoic acid and EDDnp is the C-terminal quencher component N-(2,4-dinitrophenyl)-ethylenediamide, were produced via solid-phase synthesis (as outlined in [37]) using a PSSM-8 bench-top automated solid-phase peptide synthesizer (Shimadzu, Tokyo, Japan). The molecular weight and purity of the peptides were verified by an analytical Shimadzu HPLC 10AVP system (Shimadzu, Tokyo, Japan) and by MALDI-TOF MS using a microflex LT system (Brucker Daltonics, Bremen, Germany). Stock solutions of the peptide substrates were made in distilled water, and the concentration was determined spectrophotometrically at 365 nm using the molar extinction coefficient of the Dnp group of 17,300 $M^{-1}.cm^{-1}$.

2.4 Screening of compounds as a TbMCA2 modulator

Screening was carried out with 9 compounds, 6 of them belonging to the class of chalcones and 3 derivatives from the class of flavonoids. Initially, TbMCA2 was incubated for 5 minutes in 1 mL of TRIS buffer 50 mM, NaCl 100 mM, pH 7.4 containing 1mM $CaCl_2$ and 2.5 mM DTT, in the Hitachi F-2700 spectrofluorometer, configured at λ_{ex} = 320 nm and λ_{em} = 420 nm, excitation and emission slit 5 and 5 nm (700V) respectively. Shortly after, the control activity was measured by adding 10 µM of the FRET substrate Abz-KARSSAQ-EDDnp, performing the reading at a time of 300 seconds. The same procedure was followed for the analysis of the activity of each of the 9 compounds, performing readings at concentrations of 1 µM and 6 µM, these added along with the incubation time with the enzyme. The data obtained were plotted on the bar graph using the Grafit 5.0 program (Erithacus, UK), with the remaining activity subsequently analyzed in comparison with the activity of TbMCA2 without the influence of the compounds (control).

2.5 Determination of IC50 values for inhibitor

For the analysis of the inhibitory potential of molecules derived from chalcones and flavonoids, TbMCA2 was previously incubated in a final volume of 1 ml of TRIS buffer 50 mM, NaCl 100 mM - pH 7.4 containing 1 mM $CaCl_2$, 2.5 mM DTT, for 5 min at 25ºC, under constant agitation, in a quartz cuvette. Subsequently, increasing concentrations of the compounds were added. The reduction of enzymatic activity was measured with the help of the HITACHI F- 2700 spectrofluorometer (Hitachi, Tokyo, Japan), configured at the excitation and emission wavelengths of 320 and 420 nm, respectively, and excitation and emission slit of 5 and 5 nm (700 V), using the FRET substrate Abz-KARSSAQ- EDDnp. The calculation of IC_{50} was performed through non-linear regression, with the plot being carried out through the Grafit 5.0 program (Erithacus, UK), using the equation [y = Range/1+ (x/IC_{50})s].

2.6 Enzyme kinetics and mechanism determination

Studies related to the inhibition mechanisms of molecules that showed the best IC_{50} value against TbMCA2 were carried out through Michaelis-Menten kinetics, in the absence (control curve) and presence of the compounds, at their concentrations of 1, 2, 3, and 4 µM. For this, TbMCA2 was incubated with the compound for 10 minutes in a final volume of 1 ml of TRIS buffer 50 mM, NaCl
100 mM - pH 7.4 containing 1 mM $CaCl_2$, 2.5 mM DTT. Then, increasing concentrations of the FRET substrate Abz-TPTGRSTAGQ-EDDnp were added every 5 minutes. The HITACHI F-2700 spectrofluorometer (Hitachi, Tokyo, Japan) was adjusted for excitation and emission wavelengths of 320 and 420 nm, respectively, and excitation and emission slit of 5 and 5 nm (700 V). The data found were processed using the Grafit 5.0 program (Erithacus, UK) and linearized by plotting the double-reciprocal (Lineweaver-Burk) by the inverse of both the activity found and the substrate concentration. To determine the parameters of Ki and αKi, the replots of Slope versus [inhibitor] and Intercept versus [inhibitor], respectively, were used.

2.7 Molecular docking

To identify the binding sites between the target protein and the compounds, and to predict the optimal ligand conformation within the protein, molecular docking was performed using Webina, which is based on the AutoDock Vina software. The structures of the compounds were designed using the Ligand Reader & Modeler tool in CHARMM-

GUI. The PDB file of the protein was obtained from its amino acid sequence using the AlphaFold2 tool. With all receptor and ligand information prepared, CHARMM-GUI processed the data, and AutoDock Vina simulated and added the missing polar hydrogen atoms to the system. The docking box dimensions were set to 15x15x15 Å. The protein/ligand complex structures were analyzed using PyMOL and Visual Molecular Dynamics (VMD) software

2.8 Molecular Dynamics Simulation in Desmond

The molecular dynamics (MD) simulation was conducted using the Desmond software, integrated into the Maestro suite from Schrödinger. The initial system was built based on the three-dimensional structure of metacaspase 2 from Trypanosoma brucei (TbMCA2), obtained from the lowest energy docking pose. Subsequently, system preparation and parameterization were performed. For the preparation of the initial structure, the protein structure was pre-processed using the Protein Preparation Wizard module, correcting protonation states, adding missing hydrogen atoms, and removing unnecessary ligands or molecules. The ionization states of the side chains were adjusted to physiological pH (7.4) based on calculated pKa values. The simulation box was constructed by surrounding the system with an orthorhombic box of explicit water using the TIP3P water model. A 10 Å buffer was maintained between the protein and the edges of the box to ensure sufficient space for dynamics. Necessary ions (Na^+ and Cl^-) were added to neutralize the system's total charge, maintaining a 150 mM sodium chloride concentration to simulate physiological conditions. Force field parameters for the protein and other system molecules were assigned based on the OPLS_2005 force field, which is widely validated for biomolecular simulations. The system was then energy-minimized to relieve initial strains, using the steepest descent algorithm.

For equilibration, the system underwent a multi-stage process: Initial energy minimization (2,000 steps); molecular dynamics in the NVT ensemble (constant volume) at 10 K for 200 ps, with protein restraints; molecular dynamics in the NPT ensemble (constant pressure) at 300 K for 1 ns, to equilibrate density and pressure. Following equilibration, a production simulation was conducted for 100 nanoseconds in the NPT ensemble (constant pressure and temperature), maintaining the temperature at 300 K using the Nosé-Hoover thermostat and pressure at 1 atm using the Martyna-Tobias-Klein barostat. A time step of 2 fs was employed for the simulation, with bonds involving hydrogen atoms treated as constraints using the SHAKE

algorithm. The simulation conditions were defined as follows: Van der Waals and Coulombic interaction cutoffs set to 9.0 Å; long-range electrostatic interactions calculated using the Particle Mesh Ewald (PME) method; and system coordinates recorded every 10 ps for post-simulation analysis.

Binding free energy analysis was performed using the MM/GBSA (Molecular Mechanics/Generalized Born Surface Area) method implemented in Schrödinger Prime. For this, 500 frames were uniformly extracted from the 100- nanosecond MD trajectory. Each frame underwent free energy calculations, providing a reliable estimate of the interaction energy between the protein and the ligand throughout the simulation.

After the simulation, trajectory files were analyzed using the analysis module in Desmond. Properties such as RMSD (Root Mean Square Deviation), RMSF (Root Mean Square Fluctuation), potential energy, and structural variations were evaluated to interpret the system's stability and conformational events over time.

3 RESULTS

3.1 Screening for the Inhibitory Activity of Compounds

Through the plotting of the found values of control activity and remaining activity of TbMCA2 in relation to the 9 tested molecules derived from chalcones and flavonoids (Table 1).

Table 1 - Molecular structure of compounds derived from chalcones and flavonoids.

CHALCONES		
EM-1A	**EM-1B**	**EM-1C**
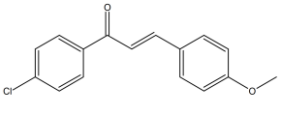	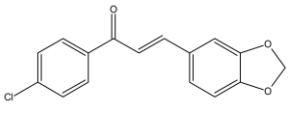	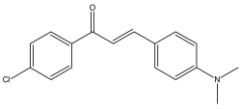
EM-2A	**EM-2B**	**EM-2C**
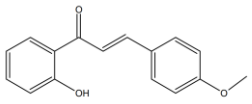	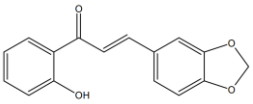	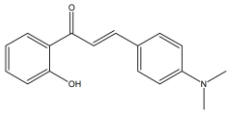
FLAVONOIDS		
EM-F12A	**EM-F12B**	**EM-F12C**
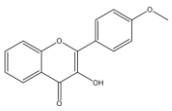	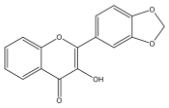	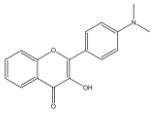

All inhibited the activity of the metacaspase, as shown in Figure 1, it is possible to visualize a more significant activity decay in the data referring to the concentration of 6 µM. Of the six compounds of the chalcone class (EM-1A, EM-1B, EM-1C, EM-2A, EM-2B, and EM-2C), the EM-2B molecule showed the greatest decrease in TbMCA2 activity when tested at a concentration of 1 µM, with a reduction of 17.4%. Already at the concentration of 6 µM, the EM-1A compound was the most effective, reducing the enzymatic activity by 87%, which corresponds to a remaining activity of 13%. The molecules derived from flavonoids (EM-F12A, EM-F12B, and EM-F12C) resulted in a percentage of remaining activity ranging from 74-87% at the concentration of 1 µM and from 24% to 58% at the concentration of 6 µM. This represents a reduction of activity from 13% to 26% for 1 µM and from 42% to 76% for 6 µM, with emphasis on the EM-F12C compound, which provided the greatest reduction of TbMCA2 activity (76%), with the remaining around 24%.

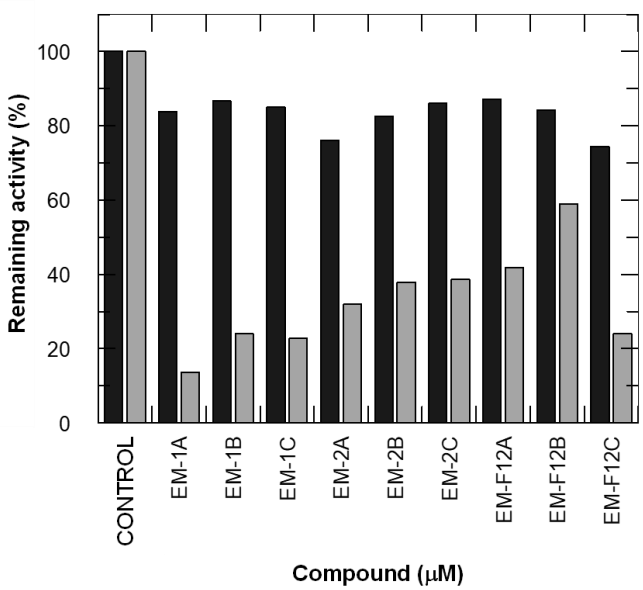

Figure 1 - Screening of molecules on the activity of metacaspase-2 of Trypanosoma brucei. Remaining activity of TbMCA2 with ( ) 1 μM and ( ) 6 μM of compounds from the classes of chalcones and flavonoids.

3.2 Inhibitory concentration (IC_{50})

Considering that all the compounds inhibited the activity of TbMCA2, the 9 molecules were subjected to inhibition assays to evaluate the inhibitory capacity of each one of them. For this, the enzyme was incubated for a period of 10 min at 25ºC, and subsequently, increasing concentrations of the compound were added. The evaluation of the activity was verified through the HITACHI F-2700 spectrofluorometer (Hitachi, Tokyo, Japan). After the inhibition assays were carried out, the IC_{50} values found for all tested molecules ranged from 2.14 to 7.55 μM, as shown in Table 2.

Table 2 - Inhibitory potential (IC_{50}) of compounds derived from chalcones and flavonols in modulating the enzymatic activity of TbMCA2.

COMPOUND	IC_{50} (µM)
EM-1A	2.14 ± 0.07
EM-1B	3.09 ± 0.09
EM-1C	3.02 ± 0.09
EM-2A	3.54 ± 0.19
EM-2B	4.06 ± 0.10
EM-2C	3.81 ± 0.13
EM-F12A	4.45 ± 0.17
EM-F12B	7.55 ± 0.41
EM-F12C	2.52 ± 0.13

The compound EM-1A presented the lowest concentration for a 50% reduction in the activity of TbMCA2, with 2.14 µM, and on the other hand, for the molecule EM-F12B, this reduction was only verified with a concentration equal to 7.55 µM, presenting the highest IC_{50} value. Regarding the compounds derived from chalcones, the molecule that showed the best inhibitory potential was EM-1A, with an IC_{50} equal to 2.14 ± 0.07 µM, followed by EM-1C, with 3.02 ± 0.09 µM, EM-1B (3.09 ± 0.09 µM), EM-2A (3.54 ± 0.19 µM), EM-2C (3.81 ± 0.13) and EM-2B (4.06 ± 0.10 µM). As for the derivatives of flavonoids, the compound with the highest inhibitory capacity was EM-F12C, exhibiting an IC_{50} value equal to 2.52 ± 0.13 µM, and the lowest inhibitory potential was verified in the molecule EM-F12B, with 7.55 ± 0.41 µM.

3.3 Inhibition mechanisms of TbMCA2 by molecules derived from the class of chalcones and flavonoids

After the IC_{50} assays, three molecules derived from chalcones (EM-1A, EM-1B, EM-1C) and one derived from the flavonoid class (EM-F12C) were selected for the study of the inhibition mechanism, along with the determination of the kinetic parameters K_i and αK_i. After performing Michaelis-Menten kinetics, both in the presence and absence of the compound, the linearization plot, and the slope and intercept replots, the inhibitory profile of each was analyzed.

The molecule EM-1A (Figure 2) showed a competitive inhibition mechanism, with a K_i value of 1.27 ± 0.06 µM. This means that increasing the inhibitor concentration increases the apparent value of the Michaelis-Menten constant (K_M), indicating direct competition with the substrate for the same active site on the enzyme. This type of inhibition does not affect the V_{max} parameter, as indicated by the intersection of the lines on the Y-axis in the double-reciprocal linearization.

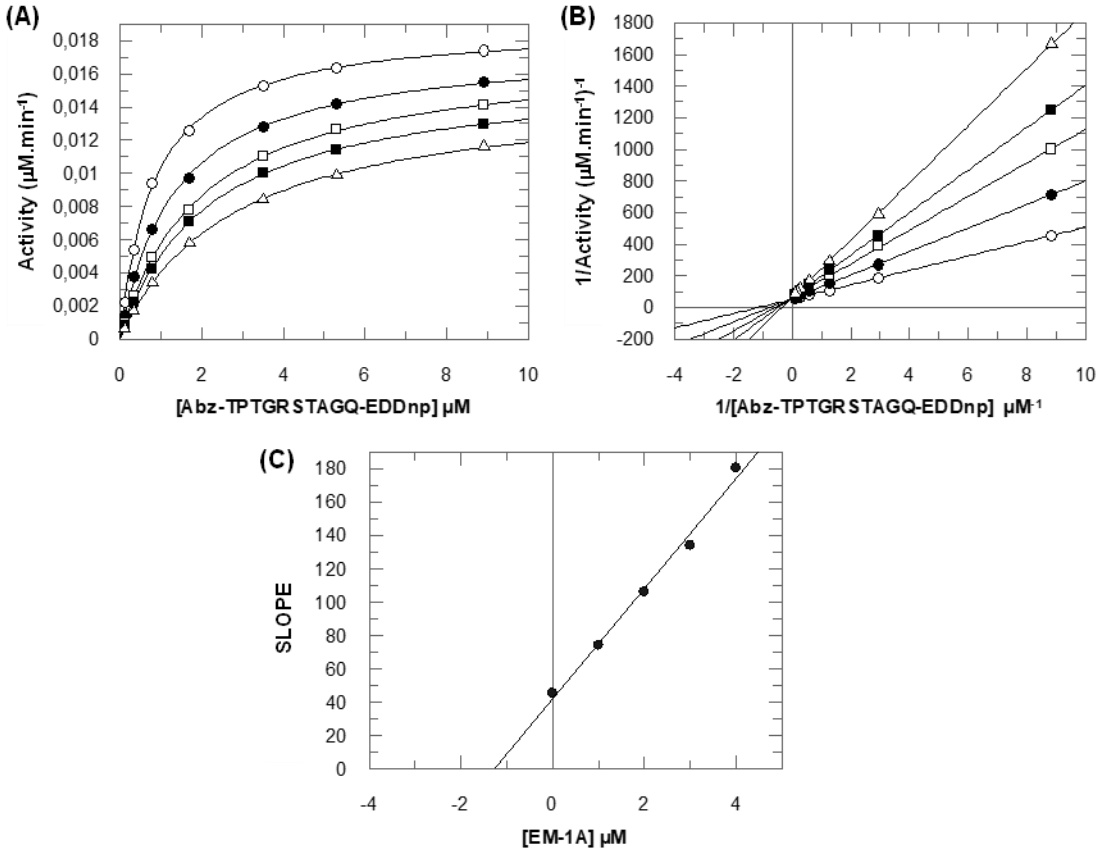

Figure 2: Inhibition kinetics of compound EM-1A against TbMCA2. (o) Control; (●) 1 µM; (□) 2 µM; (■) 3 µM; (Δ) 4 µM. (A) Michaelis-Menten plot, (B) Lineweaver-Burk, (C) Replot of the Slope, and (D) Replot of the Intercept

The molecule EM-1B showed a simple linear non-competitive inhibition pattern, with K_i and αK_i values of 2.69 ± 0.56 µM and 2.55 ± 0.36 µM, respectively. This type of inhibition mainly affects the V_{max} parameter, as illustrated in the Michaelis-Menten curve (Figure 3A) and confirmed by the convergence of the lines on the X-axis in the double-reciprocal plot (Figure 3B), using the line equation (y = ax + b). The Slope (Figure 3C) and Intercept (Figure 3D) analysis allowed the calculation of the K_i and αK_i parameters. The $K_i/\alpha K_i$ ratio equal to 1.0 indicates that the inhibition mechanism is simple linear non-competitive, suggesting that the inhibitor can bind to an allosteric site on the enzyme, not directly competing with the substrate for the active site.

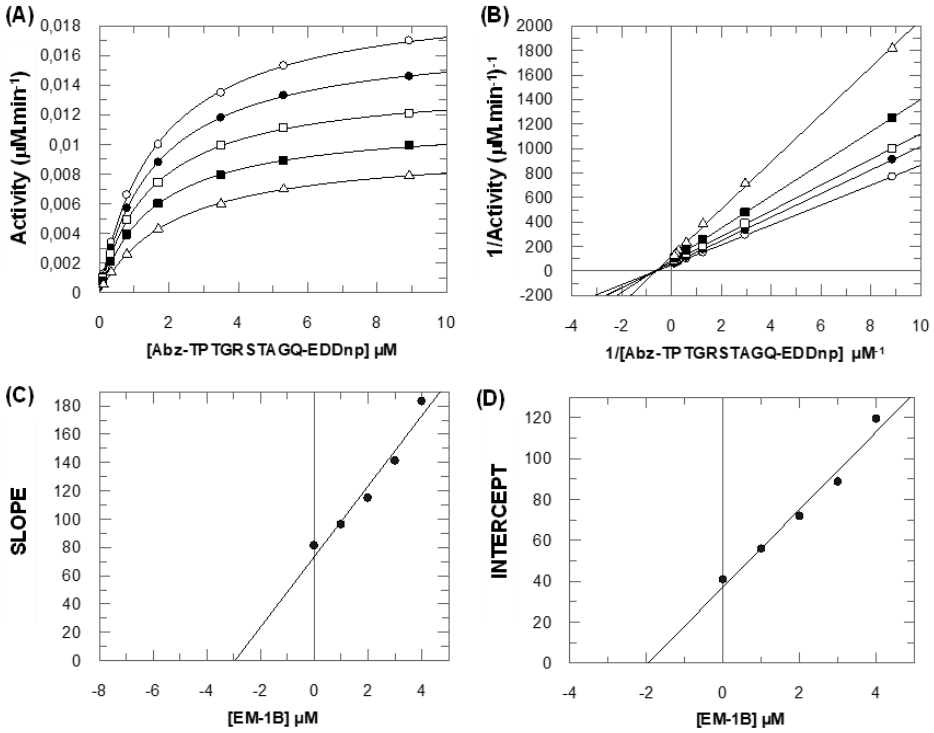

Figure 3: **Inhibition kinetics of compound EM-1B against TbMCA2.** (o) Control; (●) 1 µM; (□) 2 µM; (■) 3 µM; (Δ) 4 µM. (A) Michaelis-Menten plot, (B) Lineweaver-Burk, (C) Replot of the Slope, and (D) Replot of the Intercept

The compounds EM-1C (Figure 4) and EM-F12C (Figure 5) showed competitive inhibition like EM-1A. The K_i values were 1.56 ± 0.07 µM for EM-1C and 0.74 ± 0.18 µM for EM-F12C. These inhibitors do not affect the V_{max} parameter, as evidenced by the convergence of the lines on the Y-axis in the double-reciprocal plot, where the K_i value was determined.

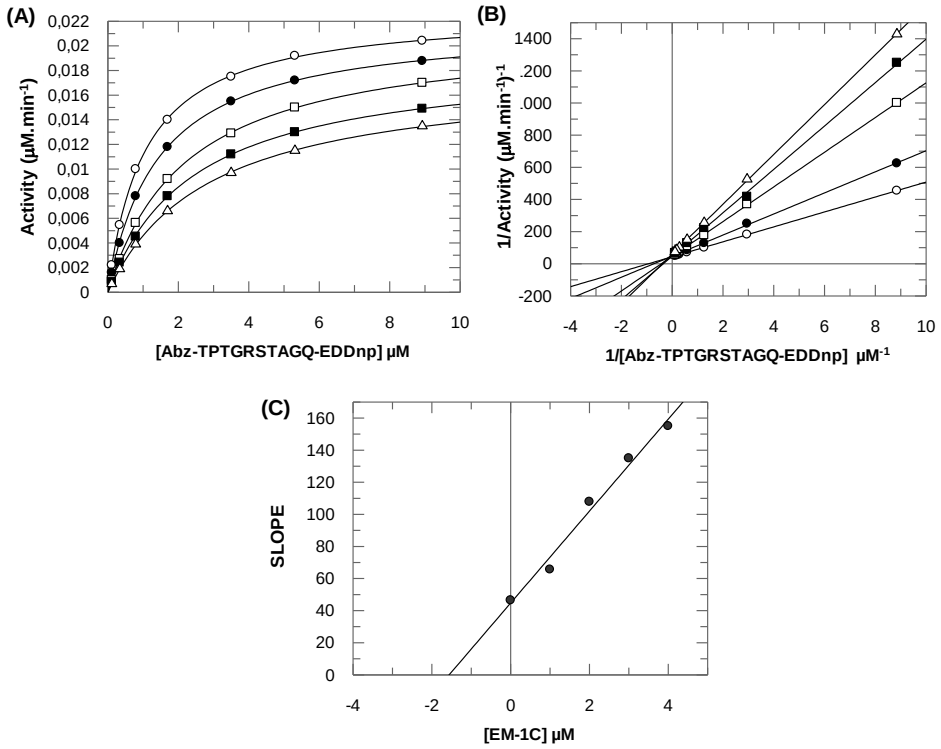

Figure *4*: Inhibition kinetics of compound EM-1C against TbMCA2. (o) Control; (●) 1 µM; (□) 2 µM; (■) 3 µM; (Δ) 4 µM. (A) Michaelis-Menten plot, (B) Lineweaver-Burk, (C) Replot of the Slope, and (D) Replot of the Intercept.

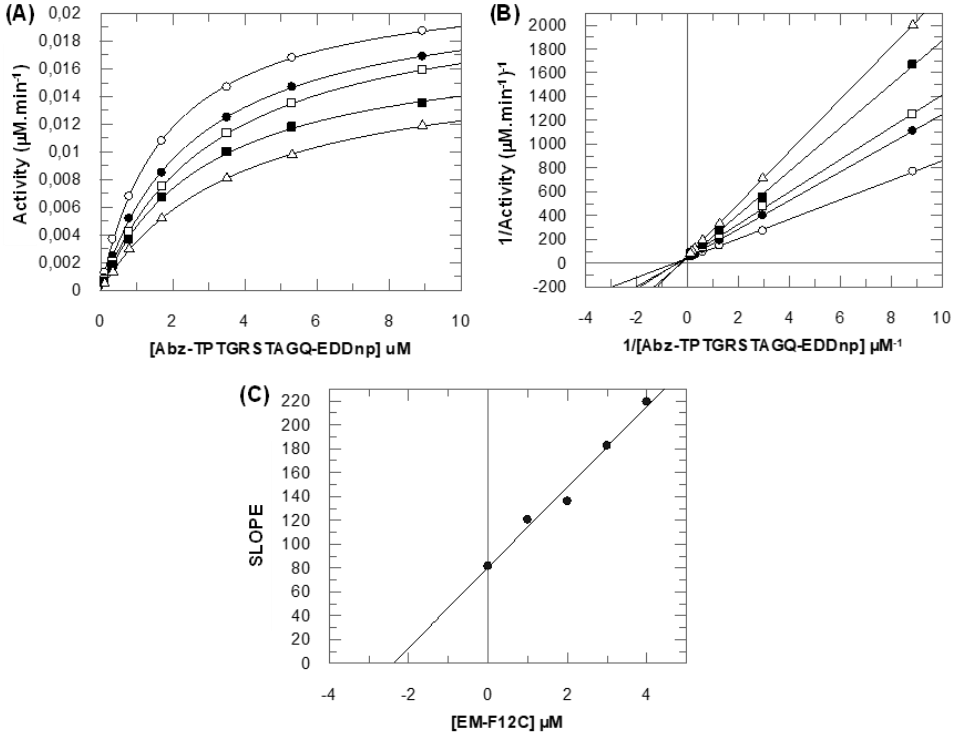

Figure 5: Inhibition kinetics of compound EM-F12C against TbMCA2. (○) Control; (●) 1 µM; (□) 2 µM; (■) 3 µM; (△) 4 µM. **(**A) Michaelis-Menten plot, (B) Lineweaver-Burk, (C) Replot of the Slope, and (D) Replot of the Intercept.

This indicates that both EM-1C and EM-F12C directly compete with the substrate for the same active site on the enzyme TbMCA2. The competitive inhibition reaction profiles of the compounds EM-1A, EM-1C, and EM-F12C and simple linear non-competitive inhibition of the molecule EM-1B.

Table 3 summarizes the results of the mechanisms found for all 4 inhibitors tested, as well as the structures of each evaluated compound.

Table 3: Kinetic parameters of inhibition mechanisms and affinity values of compounds EM-1A, EM-1B, EM-1C, and EM-F12C.

	EM-1A	**EM-1B**	**EM-1C**	**EM-F12C**
Inhibitor	C	NC	C	C
K_i (μM)	1.27 ± 0.06	2.69 ± 0.21	1.56 ± 0.07	0.74 ± 0.18
αK_i (μM)	-	0.417 ± 0.08	-	-
α	-	0.017	-	-

C: Competitive**; NC**: Non-competitive

4 DISCUSSION

Trypanosomatids, which are part of the Kinetoplastid order, include some species that are pathogens causing neglected diseases such as Chagas disease, sleeping sickness, and various forms of leishmaniasis. Although chemotherapies have been available for these diseases for many years, there are no vaccines against these protozoa. These drugs, however, have limitations as they can be toxic and may result in adverse side effects [3, 20–22]. Numerous efforts have been made to identify new therapeutic targets, with proteolytic enzymes emerging as promising candidates for the development of new drugs to treat trypanosomiasis [12, 23].

Metacaspases have been shown in recent years to play significant roles in various cellular processes within trypanosomatid parasites. These enzymes are crucial for cell cycle progression, differentiation, and homeostasis, all of which are essential for cell survival and development [14, 24–28]. The first evidence of the involvement of metacaspases in a programmed cell death pathway was observed in yeast [23]. Given their role in cell death pathways, metacaspases are an attractive target in the field of medically important trypanosomatids. It has been reported that *Trypanosoma brucei* contains five metacaspase genes (TbMCA1 – TbMCA-5), and three of these metacaspases are essential for the survival of the parasite's bloodstream form [24].

In this study, the screening of 9 compounds derived from chalcones and flavonoids showed that all molecules from both classes were able to reduce the activity of TbMCA2 at low concentrations. Among these 9 compounds, 3 belonging to the class of chalcones (EM-1A, EM-1B, and EM-1C) and one belonging to flavonoids (EM-F12C) stood out for having greater inhibitory efficacy, reaching a reduction level of up to 87% of enzymatic activity at a concentration of 6 µM.

The inhibitory potential tests carried out for the 9 evaluated molecules revealed IC_{50} values ranging between 2.14 and 7.55 µM. Among them, 4 reduced the activity of TbMCA2 by half, with emphasis on the compounds EM-1A, EM-1B, EM-1C, and EM-F12C which presented IC_{50} values equal to 2.14 ± 0.07 µM, 3.09 ± 0.09 µM, 3.02 ± 0.09 µM, and 2.52 ± 0.13, respectively. Of these molecules, three are derived from chalcones and one belongs to the class of flavonoids. It is

noteworthy that, when analyzing the chemical structure, the introduction of the chlorine element in carbon 3' of the compounds derived from chalcones (EM-1A, EM-1B, and EM-1C) resulted in a significant increase in the potential for inhibition of enzymatic activity, since these molecules presented the lowest IC_{50} values found in this class in question, indicating a positive impact on inhibitory efficacy. Was already recorded tests conducted on the cysteine proteases of *Leishmania mexicana* (rCPB2.8, rCPB3.0, and rH84Y) using the same compounds evaluated in the present work. In the work of Lourenço *et al*., the molecules that stood out with good inhibitory potentials against these enzymes were EM-F12A and EM-F12B, both derived from flavonoids, with inhibitory potential values of 3.85 µM and 5.23 µM, respectively [29]. When comparing these results with those obtained for the inhibition of metacaspase-2 of *Trypanosoma brucei*, it is observed that the values were even lower than those found by Lourenço *et al*., since the lowest IC_{50} for TbMCA2 was 2.14 µM, compared to 3.85 µM obtained for the cysteine proteases of *Leishmania mexicana*.

In addition, the inhibitory capacity of the EM-F12B compound against TbMCA2 was slightly superior to the test on the cysteine proteases of *Leishmania mexicana*, since the IC_{50} was 4.45 against 5.23 µM [29]. In the context of trypanosomatids, the literature presents tests conducted on *Trypanosoma brucei brucei*, in which libraries of chalcones based on indanone were used. The experiments carried out by Betteck *et al*. revealed IC_{50} values ranging between 0.5 and 8.9 µM [30]. This IC_{50} range is like that found in the tests carried out in this study, indicating that the class of chalcones has the potential to inhibit trypanosomes at relatively low concentrations of compounds.

Screening and IC_{50} tests were conducted using the FRET peptide Abz-KARSSAQ-EDDnp (K_M = 0.5 µM and k_{cat} 0.5 s^{-1}, [5]). Experiments to determine the inhibition mechanism were carried out with the enzymatic kinetic using the FRET peptide Abz-TPTGRSTAGQ-EDDnp (K_M = 5.5 µM and k_{cat} = 0.1 s^{-1}). This peptide was chosen due to its higher K_M and slower k_{cat}, which facilitated a more effective comparison of the kinetic parameters of TbMCA2 when performed with various compounds.

Among the four compounds selected to determine the inhibition mechanism (EM-1A, EM-1B, EM-1C, and EM-F12C), it was observed that the

molecules EM-1A, EM-1C, and EM-F12C exhibited a similar profile of competitive inhibition, and EM-1B presented a mechanism of simple linear non-competitive character. In the case of the competitive mechanism, the inhibitor tends to compete with the substrate for the active site of the enzyme, resulting in obtaining the value of K_i. Among the three tested molecules that follow this mechanism, the affinity values were: 1.27 ± 0.06 µM for EM-1A, 1.56 ± 0.07 µM for EM-1C, and 0.74 ± 0.18 µM for EM-F12C. These results indicate that EM-F12C has the lowest K_i, followed by EM-1A and then EM-1C, suggesting that the inhibitor derived from flavonoids has a higher affinity for the active site of the enzyme compared to the inhibitors of the chalcone class.

Regarding the EM-1B compound, since the K_i and αK_i parameters presented values equal to 2.69 ± 0.56 µM and 2.55 ± 0.36 µM, respectively, and the ratio of these data is equivalent to one unit, it is possible to verify that the mechanism of action of this molecule for inhibition of TbMCA2 is categorized as simple linear non-competitive, which demonstrates an equivalent preference for binding with the free enzyme and/or with the enzyme-substrate complex.

Interestingly, all compounds that exhibited competitive inhibition showed a higher binding energy with the residues of the catalytic site, particularly with the cysteine residue (Table 4, Figure 6, and Supplementary Figures S1, S2 and S3).

Table 4: Energy binding for interaction of compounds EM-1A. EM-1B. EM-1C and EM-F12C with TbMCA2

Compound	Energy binding
EM-1A	-6,4 kcal/mol
EM-1B	-5,0 kcal/mol
EM-1C	-6,9 kcal/mol
EM-F12C	-8,4 kcal/mol

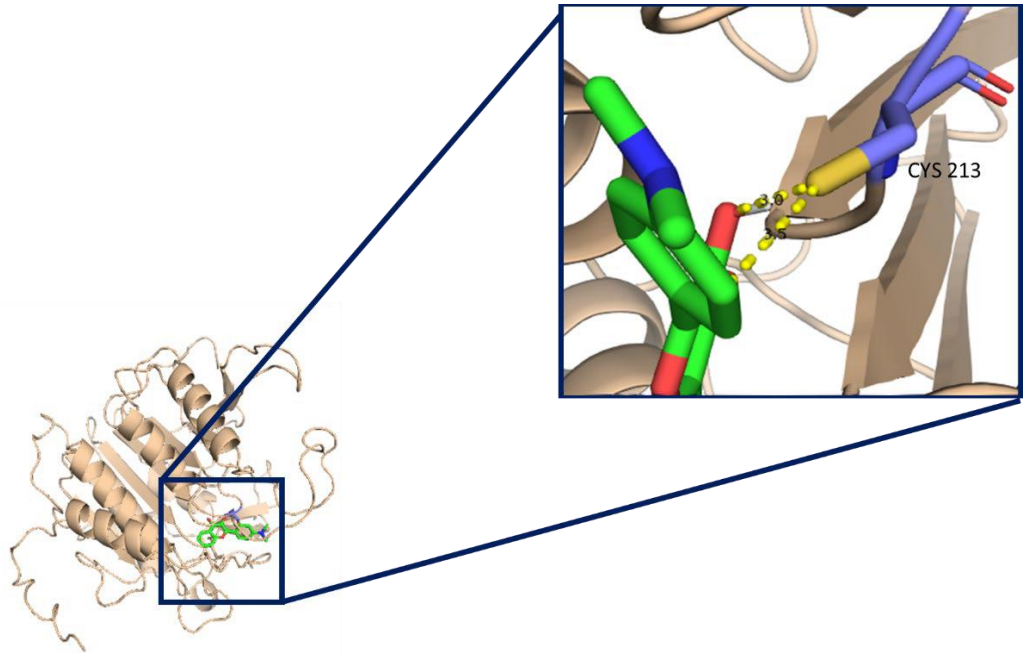

Figure 6 – Molecular Docking of the compound EM-F12C against TbMCA2. For the EM-F12C compound, carbons are shown in green, oxygens in red, and nitrogens in dark blue. For cysteine 213, sulfur is represented in yellow, carbons in light blue, and oxygens in red.

The compound EM-F12C, which has the lowest Ki value (0.74 µM), also exhibited the highest interaction energy of -8,4 kcal/mol (Figure 6), forming two hydrogen bond interactions with the Cys^{220} residue. Compound EM-1B presents a non-competitive mechanism; therefore, molecular dynamics were not performed.

5 CONCLUSIONS

This study demonstrated that compounds derived from chalcones, and flavonoids were effective in inhibiting metacaspase-2 of *Trypanosoma bruce*i at low concentrations. In the screening process of the 9 tested molecules, chalcones showed greater effectiveness in reducing enzymatic activity at a concentration of 6 µM, compared to compounds belonging to the class of flavonoids at the same concentration. The remaining activity generated by the EM-1A compound derived from chalcones was around 13% against 24% for the molecule derived from flavonoids (EM-F12C). The inhibitory capacity of the tested compounds was satisfactory in both classes, with the inhibitory potential in the range of 2.14 - 7.55µM, highlighting the molecules EM-1A, EM-1B, EM-1C, and EM-F12C, as they presented the lowest IC_{50} values. Regarding the inhibitory mechanisms, three compounds exhibited a competitive inhibition profile (EM-1A, EM-1C, and EM- F12C), in which the inhibitor

tends to compete with the substrate in the binding of the active site of the enzyme, and one of them (EM-1B) presented a characteristic profile of simple linear non-competitive inhibition, with similar values of K_i and αK_i, demonstrating equivalent preference of binding of this molecule with the free enzyme and/or with the enzyme-substrate complex.

In summary, the results showcased in this study offer encouraging outlooks for the creation of new therapeutic drugs aimed at metacaspases in trypanosomatids. This signifies a crucial progress in the fight against neglected diseases linked to these pathogens. It is essential to persist in this field of research to enhance the effectiveness and safety characteristics of these compounds. The objective is to provide more attainable and potent treatment options to communities impacted by these incapacitating diseases.

REFERENCES

[1] J.-M. Gao, Z.-Y. Qian, G. Hide, D.-H. Lai, Z.-R. Lun, Z.-D. Wu, Parasitology Human African trypanosomiasis: the current situation in endemic regions and the risks for non-endemic regions from imported cases, (n.d.). https://doi.org/10.1017/S0031182020000645.

[2] V. Lejon, M. Bentivoglio, J.R. Franco, Human African trypanosomiasis, Handb Clin Neurol 114 (2013) 169–181. https://doi.org/10.1016/B978-0-444-53490-3.00011-X.

[3] W.A.S. Judice, L.S. Ferraz, R. de M. Lopes, L. dos S. Vianna, F. da S. Siqueira, J.F. Di Iorio, L. de A.M. Dalzoto, M.N.R. Trujilho, T. dos R. Santos, M.F.M. Machado, T. Rodrigues, Cysteine proteases as potential targets for anti-trypanosomatid drug discovery, Bioorg Med Chem 46 (2021) 116365. https://doi.org/10.1016/J.BMC.2021.116365.

[4] A.A.M. Alkhaldi, Effects of Synthetic Ligustrazine-Based Chalcone Derivatives on Trypanosoma brucei brucei and Leishmania spp. Promastigotes, Molecules 28 (2023). https://doi.org/10.3390/MOLECULES28124652.

[5] H.A. Jasim, L. Nahar, M.A. Jasim, S.A. Moore, K.J. Ritchie, S.D. Sarker, Chalcones: Synthetic Chemistry Follows Where Nature Leads, Biomolecules 11 (2021). https://doi.org/10.3390/BIOM11081203.

[6] H. Sakagami, Y. Masuda, M. Tomomura, S. Yokose, Y. Uesawa, N. Ikezoe, D. Asahara, K. Takao, T. Kanamoto, S. Terakubo, H. Kagaya, H. Nakashima, Y. Sugita, Quantitative Structure-Cytotoxicity Relationship of Chalcones, Anticancer Res 37 (2017) 1091–1098. https://doi.org/10.21873/ANTICANRES.11421.

[7] T. Gervasi, A. Calderaro, D. Barreca, E. Tellone, D. Trombetta, S. Ficarra, A. Smeriglio, G. Mandalari, G. Gattuso, Biotechnological Applications and Health-Promoting Properties of Flavonols: An Updated View, Int J Mol Sci 23 (2022). https://doi.org/10.3390/IJMS23031710.

[8] A. Ullah, S. Munir, S.L. Badshah, N. Khan, L. Ghani, B.G. Poulson, A.H. Emwas, M. Jaremko, Important Flavonoids and Their Role as a Therapeutic Agent, Molecules 25 (2020). https://doi.org/10.3390/MOLECULES25225243.

[9] D. Ndjonka, L.N. Rapado, A.M. Silber, E. Liebau, C. Wrenger, Natural products as a source for treating neglected parasitic diseases, Int J Mol Sci 14 (2013) 3395–3439. https://doi.org/10.3390/IJMS14023395.

[10] A.G. Uren, K. O'Rourke, L. Aravind, M.T. Pisabarro, S. Seshagiri, E. V. Koonin, V.M. Dixit, Identification of paracaspases and metacaspases: Two ancient families of caspase-like proteins, one of which plays a key role in MALT lymphoma, Mol Cell (2000). https://doi.org/10.1016/s1097-2765(00)00094-0.

[11] M. Klemenčič, C. Funk, Type III metacaspases: calcium-dependent activity proposes new function for the p10 domain, New Phytologist (2018). https://doi.org/10.1111/nph.14660.

[12] B. Pérez, L.A. Bouvier, J.J. Cazzulo, F. Agüero, E. Salas-Sarduy, V.E. Alvarez, Screening and Identification of Metacaspase Inhibitors: Evaluation of Inhibition Mechanism and Trypanocidal Activity, Antimicrob Agents Chemother 65 (2021). https://doi.org/10.1128/AAC.01330-20.

[13] J.C. Mottram, M.J. Helms, G.H. Coombs, M. Sajid, Clan CD cysteine peptidases of parasitic protozoa, Trends Parasitol (2003). https://doi.org/10.1016/S1471-4922(03)00038-2.

[14] C.X. Moss, G.D. Westrop, L. Juliano, G.H. Coombs, J.C. Mottram, Metacaspase 2 of Trypanosoma brucei is a calcium-dependent cysteine peptidase active without processing, FEBS Lett (2007). https://doi.org/10.1016/j.febslet.2007.11.009.

[15] K. McLuskey, J. Rudolf, W.R. Proto, N.W. Isaacs, G.H. Coombs, C.X. Moss, J.C. Mottram, Crystal structure of a Trypanosoma brucei metacaspase, Proc Natl Acad Sci U S A (2012). https://doi.org/10.1073/pnas.1200885109.

[16] M.F.M. Machado, M.F. Marcondes, M.A. Juliano, K. McLuskey, J.C. Mottram, C.X. Moss, L. Juliano, V. Oliveira, Substrate specificity and the effect of calcium on Trypanosoma brucei metacaspase 2, FEBS Journal 280 (2013). https://doi.org/10.1111/febs.12248.

[17] J.M. Gilio, M.F. Marcondes, D. Ferrari, M.A. Juliano, L. Juliano, V. Oliveira, M.F.M. Machado, Processing of metacaspase 2 from Trypanosoma brucei (TbMCA2) broadens its substrate specificity, Biochim Biophys Acta Proteins Proteom 1865 (2017). https://doi.org/10.1016/j.bbapap.2017.01.002.

[18] E.A. Minina, J. Staal, V.E. Alvarez, J.A. Berges, I. Berman-Frank, R. Beyaert, K.D. Bidle, F. Bornancin, M. Casanova, J.J. Cazzulo, C.J. Choi, N.S. Coll, V.M. Dixit, M. Dolinar, N. Fasel, C. Funk, P. Gallois, K. Gevaert, E. Gutierrez-Beltran, S. Hailfinger, M. Klemenčič, E. V. Koonin, D. Krappmann, A. Linusson, M.F.M. Machado, F. Madeo, L.A. Megeney, P.N. Moschou, J.C. Mottram, T. Nyström, H.D. Osiewacz,

C.M. Overall, K.C. Pandey, J. Ruland, G.S. Salvesen, Y. Shi, A. Smertenko, S. Stael, J. Ståhlberg, M.F. Suárez, M. Thome, H. Tuominen, F. Van Breusegem, R.A.L. van der Hoorn, A. Vardi, B. Zhivotovsky, E. Lam, P. V. Bozhkov, Classification and Nomenclature of Metacaspases and Paracaspases: No More Confusion with Caspases, Mol Cell (2020). https://doi.org/10.1016/j.molcel.2019.12.020.

[19] I.Y. Hirata, M.H. Sedenho Cezari, C.R. Nakaie, P. Boschcov, A.S. Ito, M.A. Juliano, L. Juliano, Internally quenched fluorogenic protease substrates: Solid-phase synthesis and fluorescence spectroscopy of peptides containing ortho-aminobenzoyl/dinitrophenyl groups as donor-acceptor pairs, Letters in Peptide Science (1995). https://doi.org/10.1007/BF00119771.

[20] E. Schwartz, Tropical Diseases in Travelers, J Travel Med 17 (2010) 432–432. https://doi.org/10.1111/J.1708-8305.2010.00459.X.

[21] M.P. Barrett, R.J.S. Burchmore, A. Stich, J.O. Lazzari, A.C. Frasch, J.J. Cazzulo, S. Krishna, The trypanosomiases, Lancet 362 (2003) 1469–1480. https://doi.org/10.1016/S0140-6736(03)14694-6.

[22] B.L. Herwaldt, Leishmaniasis, Lancet 354 (1999) 1191–1199. https://doi.org/10.1016/S0140-6736(98)10178-2.

[23] F. Madeo, E. Herker, C. Maldener, S. Wissing, S. Lächelt, M. Herlan, M. Fehr, K. Lauber, S.J. Sigrist, S. Wesselborg, K.U. Fröhlich, A caspase-related protease regulates apoptosis in yeast, Mol Cell (2002). https://doi.org/10.1016/S1097-2765(02)00501-4.

[24] M.J. Helms, A. Ambit, P. Appleton, L. Tetley, G.H. Coombs, J.C. Mottram, Bloodstream form Trypanosoma brucei depend upon multiple metacaspases associated with RAB11-positive endosomes, J Cell Sci (2006). https://doi.org/10.1242/jcs.02809.

[25] M. Laverrière, J.J. Cazzulo, V.E. Alvarez, Antagonic activities of Trypanosoma cruzi metacaspases affect the balance between cell proliferation, death and differentiation, Cell Death Differ (2012). https://doi.org/10.1038/cdd.2012.12.

[26] N. Watanabe, E. Lam, Calcium-dependent activation and autolysis of arabidopsis metacaspase 2d, Journal of Biological Chemistry (2011). https://doi.org/10.1074/jbc.M110.194340.

[27] G. Kosec, V.E. Alvarez, F. Agüero, D. Sánchez, M. Dolinar, B. Turk, V. Turk, J.J. Cazzulo, Metacaspases of Trypanosoma cruzi: Possible candidates for

programmed cell death mediators, Mol Biochem Parasitol 145 (2006). https://doi.org/10.1016/j.molbiopara.2005.09.001.

[28] Vandana, R. Dixit, R. Tiwari, A. Katyal, K.C. Pandey, Metacaspases: Potential Drug Target Against Protozoan Parasites, Front Pharmacol 10 (2019). https://doi.org/10.3389/FPHAR.2019.00790.

[29] E.M.G. Lourenço, J.F. Di Iório, F. da Silva, F.L.B. Fialho, M.M. Monteiro, A. Beatriz, R.T. Perdomo, E.G. Barbosa, J.P. Oses, C.C.P. de Arruda, W.A. de Souza Júdice, J. Rafique, D.P. de Lima, Flavonoid Derivatives as New Potent Inhibitors of Cysteine Proteases: An Important Step toward the Design of New Compounds for the Treatment of Leishmaniasis, Microorganisms 11 (2023). https://doi.org/10.3390/MICROORGANISMS11010225.

[30] R.M. Beteck, L.J. Legoabe, M. Isaacs, H.C. Hoppe, In vitro Anti-Trypanosomal Activities of Indanone-Based Chalcones, Drug Res 69 (2019) 337–341. https://doi.org/10.1055/A-0775-0737.

Supplementary Figure S1 – Molecular docking of the compound EM-1A against TbMCA2

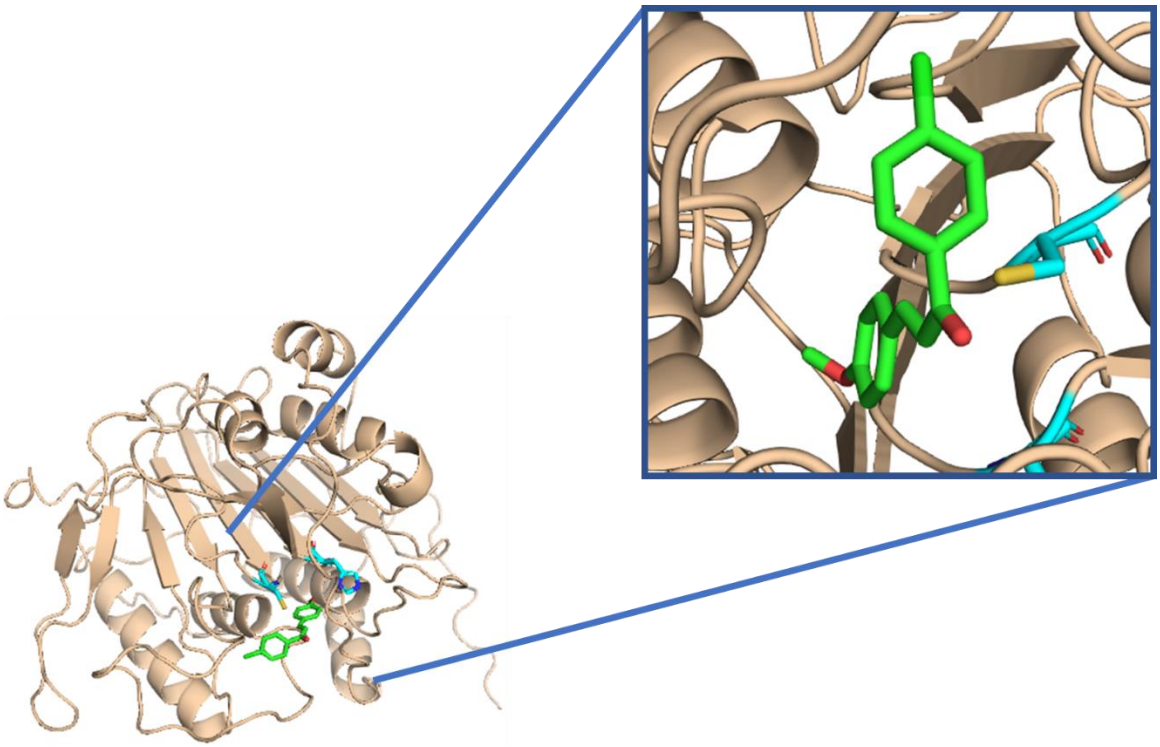

Supplementary Figure S2 – Molecular docking of the compound EM-1B against TbMCA2

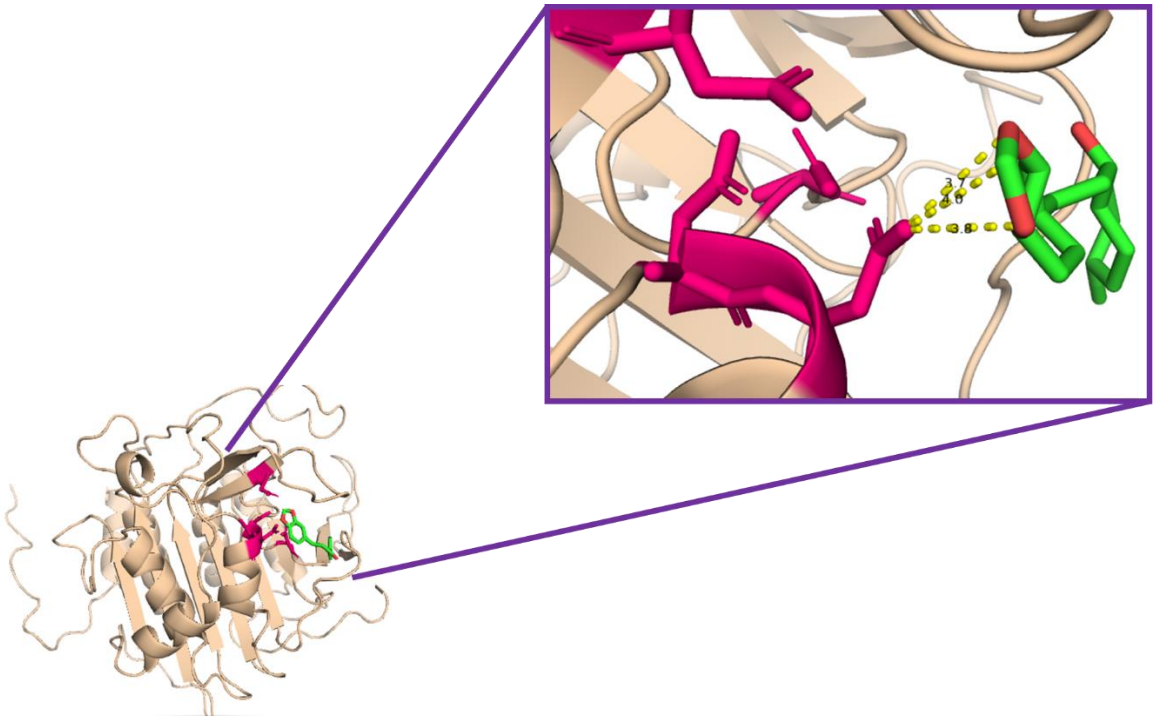

Supplementary Figure S3 – Molecular docking of the compound EM-1C against TbMCA2

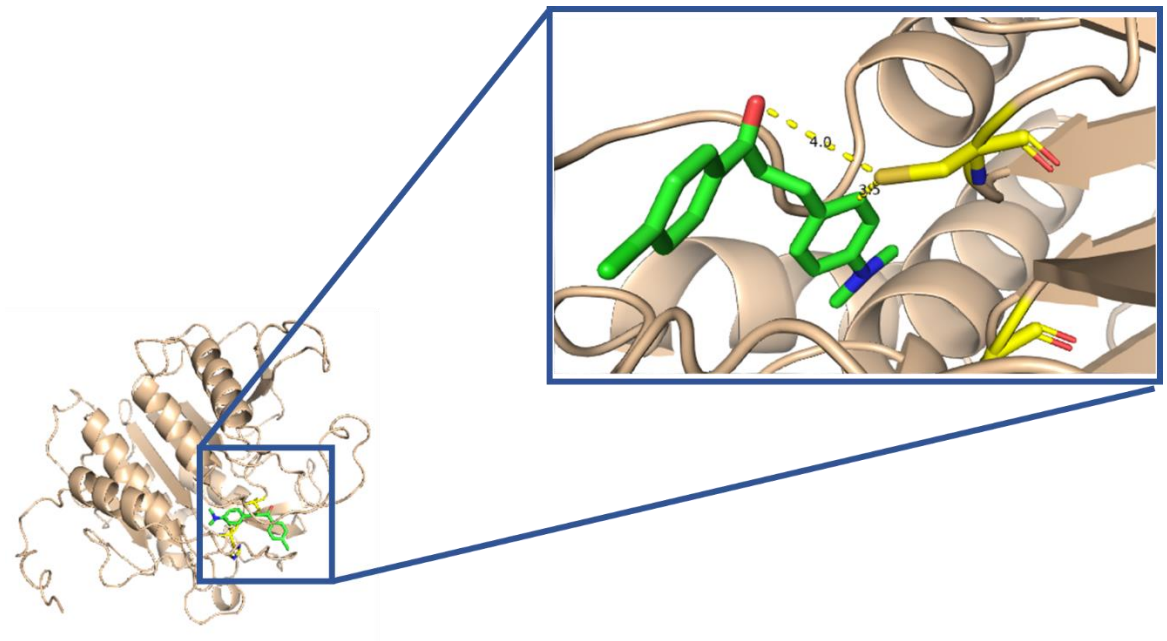

ANEXO I

Bioorg. Med. Chem. 46 (2021) 116365

Contents lists available at ScienceDirect

Bioorganic & Medicinal Chemistry

journal homepage: www.elsevier.com/locate/bmc

Cysteine proteases as potential targets for anti-trypanosomatid drug discovery

Wagner A.S. Judice [a,*], Letícia Silva Ferraz [b], Rayssa de Mello Lopes [b], Luan dos Santos Vianna [a], Fábio da Silva Siqueira [a], Juliana F. Di Iorio [a], Laura de Azevedo Maffeis Dalzoto [a], Mariana Nascimento Romero Trujilho [a], Taiz dos Reis Santos [a], Maurício F.M. Machado [a,*], Tiago Rodrigues [b,*]

[a] Centro Interdisciplinar de Investigação Bioquímica (CIIB), Universidade de Mogi das Cruzes (UMC), Mogi das Cruzes, SP, Brazil
[b] Centro de Ciências Naturais e Humanas (CCNH), Universidade Federal do ABC (UFABC), Santo André, SP, Brazil

ARTICLE INFO

Keywords:
Chagas disease
Chemotherapy
Cysteine proteases
Leishmaniasis
Neglected diseases

ABSTRACT

Leishmaniasis and trypanosomiasis are endemic neglected disease in South America and Africa and considered a significant public health problem, mainly in poor communities. The limitations of the current available therapeutic options, including the lack of specificity, relatively high toxicity, and the drug resistance acquiring, drive the constant search for new targets and therapeutic options. Advances in knowledge of parasite biology have revealed essential enzymes involved in the replication, survival, and pathogenicity of *Leishmania* and *Trypanosoma* species. In this scenario, cysteine proteases have drawn the attention of researchers and they are being proposed as promising targets for drug discovery of antiprotozoal drugs. In this systematic review, we will provide an update on drug discovery strategies targeting the cysteine proteases as potential targets for chemotherapy against protozoal neglected diseases.

1. Introduction

Neglected tropical diseases (NTDs) comprise a wide group of diseases with the highest prevalence in tropical and subtropical regions, specifically in underdeveloped or developing countries, since female vector flies use the decomposing organic materials and moist places for oviposition. NTDs affect over one billion people around the world with several social and economic impacts. The list of neglected diseases recognized by the World Health Organization (WHO) includes leishmaniasis - cutaneous (CL), mucocutaneous (MCL), and visceral (VL)) and trypanosomiasis (Chagas disease and sleeping sickness), which are caused by the infectious agents *Leishmania* spp., and *Trypanosoma cruzi* or *Trypanosoma brucei*, respectively [1,2]. Considering vaccines are not available yet for these diseases, preventive actions and pharmacological interventions are the current approaches to their treatment. However, the available drugs used to treat these diseases have several limitations, such as low efficacy, high toxicity, adverse reactions, long-course administration regimens, and also drug resistance [3]. Thus, several efforts have been made to discovery new therapeutic targets and novel drug candidates. In this review we discussed the potential of protozoal cysteine proteases as targets for the development new drugs for the treatment of leishmaniasis and trypanosomiasis.

2. Leishmaniasis and trypanosomiasis

Leishmania genus belongs to the Trypanosomatidae family. Approximately 53 species have already been identified, of which 31 species are known to parasite mammals and 20 species are pathogenic for human beings, causing leishmaniasis [4,5]. These parasites are transmitted by phlebotomine females of sand flies from Phlebotomus and Lutzomyia genera [6]. In Europe, Africa and Asia, the main vectors are *Phlebotomus* sp., while *Lutzomyia* sp. are the vectors in Americas and Oceania. The highest prevalence is observed in tropical and subtropical regions, mainly in underdeveloped or developing countries, since the female vector flies use the decomposing organic materials and moist places for oviposition. Around 70 countries are considered as endemic regions for leishmaniasis, although more than 90% of cases occur in Afghanistan, Algeria, Brazil, Pakistan, Peru, Saudi Arabia, and Syria [7,8]. Leishmaniasis is a neglected tropical disease considered as a global public health problem, occurring in about 98 countries with 1.3 million

* Corresponding authors.
E-mail addresses: wagneras@umc.br (W.A.S. Judice), mauriciomachado@umc.br (M.F.M. Machado), tiago.rodrigues@ufabc.edu.br (T. Rodrigues).

https://doi.org/10.1016/j.bmc.2021.116365
Received 27 May 2021; Received in revised form 2 August 2021; Accepted 4 August 2021
Available online 13 August 2021
0968-0896/© 2021 Elsevier Ltd. This article is made available under the Elsevier license (http://www.elsevier.com/open-access/userlicense/1.0/).

cases per year and 350 million people at risk of infection [9]. It is important to differentiate Leishmania species due to the epidemiologic and clinical issues. Their classification was based on geographical factors, clinical presentations of diseases, epidemiology, sandflies vectors, and animals as reservoirs [10]. The high diversity among the species results in different clinical presentations of the disease and immune response [11,12].

Although parasites alter their morphology depending on the environmental conditions, promastigote and amastigote are the main forms during the life cycle of *Leishmania* spp. Promastigote is the flagellated extracellular form, while the oval-shaped, non-flagellated amastigote form lives intracellularly in the definitive host [13]. During the infection, the infective promastigote forms of Leishmania are regurgitated and inoculated by the infected female sandflies into the human host blood vessel, being phagocytized by neutrophils and/or macrophages that are quickly recruited to the bite region due to the secretion of proteophosphoglycans by the parasites [14,15]. After recognition, promastigote forms are internalized by lipid pockets composed of cholesterol-rich microdomains and stored in phagolysosomes[16]. Inside the mammalian cells, promastigote transforms into amastigote form, which replicates by simple division until macrophage lysis, releasing more amastigotes that will infect others mononuclear phagocyte cells or another hematophagous female sandfly[17]. Leishmania parasite has several molecules to protect it from the oxidative damage and the hydrolytic activity within the phagolysosome, including lipophosphoglycans (LPG), which modulate the immune response by modifying the levels of produced cytokines[18], LPG glycosylinositol phospholipids, proteophosphoglycans, acid phosphatases, zinc-dependent metalloprotease GP63, and cysteine proteases [19,20].

The clinical manifestations of leishmaniasis are divided in cutaneous, mucocutaneous, and visceral. The first report of CL was provided by Lewis & Cunningham in 1876, being caused by *L. tropica*. Currently, Afghanistan, Pakistan, Iran, and Iraq are the main endemic areas [21,22]. MCL is a rare complication of CL that might arise in less than 5% of cases after cure and the cases are concentrated in Brazil, Peru and Bolivia [9]. Many species of the Leishmania genus are etiologic agents of CL, including *L. major*, *L. tropica*, *L. aethiopica*, *L. infantum*, and *L. archibaldi* in Eurasia and Africa, and *L. mexicana*, *L. venezuelensis*, *L. amazonensis*, *L. braziliensis*, *L. panamensis*, *L. chagasi*, *L. guyanensis*, and *L. peruviana* in South America. The infection might result in restricted primary skin lesions or parasitic metastasis to mucous membranes or reticuloendothelial system, depending on the genetic background of the host and the parasite specie [23]. It was reported that *L. donovani* caused mucosal damage, mainly in elderly and immunosuppressed people. Also, MCL often results in late destruction of mucosa and oronasopharyngeal cartilage, which is highly disfiguring and potentially fatal [24]. Moreover, VL, also known as kala-azar disease (black fever), is the most severe manifestation of leishmaniases, which can be fatal when not diagnosed in a timely manner and/or treated properly [24]. In eastern Africa and India this disease is caused by *L. donovani*, in Mediterranean by *L. infantum*, and in South America by *L. chagasi*, *L. amazonensis*, and *L. tropica* [25,26]. The parasites move by pleiotropism reaching the viscera and infecting Kupffer cells in the liver and reticular cells in the spleen, promoting hyperplasia of these organs (hepatosplenomegaly). They also might affect the bone marrow blocking the maturation of the granulocytic series and colonizing the hematopoietic system. The course of the infection depends on several factors related to the host immunity and the level of inflammatory response, determining the acute or chronic response [7].

Chagas disease (CD) is also considered a neglected and endemic disease with high prevalence in tropical and subtropical countries [27]. Regarding its morbidity and mortality, CD was considered one of the main public health problems in Latin America in the 90′s. CD is referred as a "disease of the poor", since the incidence is significant higher in regions with precarious houses, which are ideal for the development of the insect causative of the disease [28]. The life cycle of *T. cruzi* was described for the first time by Professor Carlos Chagas in 1909 [29]. The parasite is a kinetoplastid protozoan that infects vertebrate and invertebrate hosts during its life cycle [30,31]. The triatomine vector ingests the trypomastigote forms from the host during blood meals, which transforms in the epimastigotes in the medium intestine of the vector, differentiating into the infectious metacyclic trypomastigotes in the posterior intestine, being excreted in the feces of the triatomine. This form of the parasite enters through the bite wound or the mucosa of the mammalian host, invading different types of nucleated cells by a lysosomal-mediated mechanism [32], undergoing differentiation to the amastigote form in the cytoplasm, where it doubles every 12 h for 4 to 5 days. Subsequently, the trypomastigotes disrupt the cell membrane and reach the bloodstream and new cells, starting a new cycle or infecting other vectors during blood meal [33].

The symptoms depend on the phase of the disease, acute or chronic. Health system is focused on preventing the acute phase by controlling the vector. However, the complications occur in the chronic phase, and the organ damage led to the morbidity and mortality. During the chronic phase, the infection remains clinically silent in 60–70% of cases, characterizing the asymptomatic form of CD, also known as indeterminate [30]. Nevertheless, after 10–30 years, 30–40% of the asymptomatic patients develop clinical manifestations, such as neurological (rare), digestive (megacolon and megaesophagus syndromes), and cardiac or cardio digestive alerations [34]. The acute phase of CD is often ignored, since the symptoms might be confused with viruses and/or colds, including headache, muscle pain, apathy, and low and continuous fever [35]. The most prominent sign of the acute phase of the disease is the formation of a periorbital edema, popularly known as Romaña's sign, which consists of the ocular conjunctiva swelling, when the infection occurs through this route [36].

2.1. Current therapeutic options against leishmaniasis and trypanosomiasis

Many factors affect the treatment of leishmaniasis, including the parasite species, the form of the disease, the pre-existing comorbidities, among others. In the early 20th century, Gaspar Vianna showed that antimony and potassium tartrate could be effective against CL and VL. However, the use of these drugs was abandoned due to the severe side effects. In 1940, pentavalent antimonial (SbV) derivatives were developed and used in the treatment of leishmaniasis. Despite the relative lower toxicity of these pentavalent antimonial derivatives, some adverse effects were also described, including increased liver enzyme levels, heart toxicity, arthralgia, pancreatitis, joint stiffness, pancytopenia, and myalgia [37]. The proposed mechanism of action of antimonial is based on the inhibition of the trypanothione reductase (TR), a key enzyme to protect Leishmania from oxidative damage and consequently essential for its survival within the host [38]. Antimonial can only be administered by injectable form and adverse effects may vary from mild, as local allergic reaction, abdominal pain, gastrointestinal disturbances, edema, and headaches, to more severe effects, as pancreatitis and cardiac and renal toxicity, besides being more aggressive and lethal in HIV patients [39,40]. The arsenal of drugs available for VL treatment is limited to the antimonial sodium stibogluconate (SSG), meglumine antimoniate (MA), paromomycin (PM), oral miltefosine (MF), and amphotericin B in free deoxycholate form or lipid formulations (liposomal amphotericin B, LAB). Despite the variety of drugs, safer and innovative therapies with applicability in a large geographic area is still needed.

Besides the high toxicity, drug resistance is another major problem in the treatment of leishmaniasis. Several mechanisms of resistance have been described, such as increased intracellular thiol levels, overexpression of tryparedoxin peroxidase, decreased uptake of SbV by active form by amastigotes, changes in the thiol metabolism, and increased expression of drug efflux proteins (MRP1 and ABC transporters) [41–43]. For this reason, pentavalent antimonial drugs have become obsolete due to the loss of therapeutic efficacy [44] and

pentamidine (PMD) has been used instead. However, PMD was also abandoned due to high rate of resistance [45,46] and the severe side effects, such as irreversible diabetes mellitus [47]. Thereafter, amphotericin B (AmB) is currently the best therapeutic option for patients with antimonial-resistant leishmaniasis. Despite its efficacy, AmB also has high toxicity, such as acute nephrotoxicity, demanding the hospitalization of the patient, which can be a limiting factor in poor regions [48]. Also, reproductive toxicity was reported, thus AmB was contraindicated in pregnancy [49–52]. Moreover, AmB is a high-cost drug, since it must be inserted in a lipid-associated formulation to decrease its toxicity and extend the plasma half-life [53,54]. Despite the toxicity, both amphotericin B (AB) and the pharmaceutical liposomal formulation containing amphotericin B (LAB) showed high rates of definitive cure for leishmaniasis. LAB presented better tissue penetration, better efficacy at low doses, and lower toxicity [55–57].

Meanwhile, the search for new targets and drugs remains as the main approach to improve the treatment of leishmaniasis, with higher efficacy and lower toxicity. Several studies have been conducted to evaluate new potential targets for drug discovery, such as glycolytic pathway, polyamine biosynthesis, glyoxalase pathway, uptake and turnover of phospholipids/sphingolipids, microtubule biosynthesis, folate metabolism, and in these parasitic metabolic pathways the enzymes stand out [58–64]. Enzymes are crucial macromolecules that control the chemical reactions inside the cells, including the regulatory steps of the signaling and metabolic pathways. In this regard, several enzymes had already been studied as potential targets to chemotherapy, including nitric oxide synthase, DNA topoisomerase, trypanothione redutase, superoxide dismutase, hypoxanthine–guanine phosphoribosyltransferase [58], heme oxygenase-1 [65], ribose 5-phosphate isomerase B [66], dihydroorotate dehydrogenase [67], ornitine decarboxylases [68], Abl family kinases and phosphoinositide 3-kinase γ [69], spermidine synthase [70], and serine, cysteine, aspartic, threonine, and metallopeptidases.

Regarding Chagas' disease, the pharmacological treatment was restricted to the use of benznidazole and nifurtimox, two nitroheterocyclic drugs introduced in the 60–70 s [27]. Such therapeutic scheme required long-term administration of the drugs that were relatively toxic for adult patients. As nifurtimox was not available in Brazil anymore [27], benznidazole has been the first choice for CD treatment. Benznidazole seems to be effective only in the initial acute phase of CD, although a large-scale, multicenter, international clinical trial (BENEFIT project) proposed its use also at chronic stages, especially for patients with cardiovascular complications [71]. However, other studies aiming to correlate the trypanocidal effect of benznidazole and the clinical course of the disease are still scarce and inconclusive [72–74], and further clarification is needed. It is noteworthy the need for improvement of the early diagnosis and the treatment of patients with chronic indeterminate CD [75]. In this regard, Vallejo et al (2016) shown that benznidazole induced changes in the adaptive immune response in patients with indeterminate chronic CD, decreasing the inflammatory condition [76]. Moreover, new therapeutic regimens employing benznidazole in combination with other drugs, e.g., E1224 [77] or fosravuconazole [78], were proposed for the treatment of adults with chronic indeterminate CD. Current *in vitro* and preclinical studies aiming to develop new drugs to combat the infection with *T. cruzi* are based on the search for inhibitors of ergosterol metabolism, trypanothione, pyrophosphate, protein and purine synthesis, lysophospholipid analogues (LPAs), and also cysteine proteases [79].

Thereby, the available drugs for the treatment of leishmaniasis or trypanosomiasis have several limitations, including low effectiveness, toxicity, and development of drug resistance. To overcome these challenges, it is essential to improve the understanding of the genetic, molecular, and biochemistry features of these parasites and the parasite-host interactions, in order to make feasible the search for new therapeutic targets, allowing the design of new drugs for theses neglected diseases. Due to the recent advances in this field, some opportunities have arisen. In this scenario, cysteine protease inhibitors have emerged as a new potential class of drugs to treat leishmaniasis and trypanosomiasis.

3. Protozoal cysteine proteases

Cysteine proteases (CP) comprise one of the classes of proteolytic enzymes expressed in different organisms, which are involved in several physiological and pathological processes [80]. The first described enzyme of this class was papain, isolated from *Carica papaya* in 1937. After this, its three-dimensional structure was elucidated in 1968 and the presence of a catalytic triad formed by the residues of Cys^{25}, His^{159} and Ans^{175} was described. A conserved asparagine residue (Asn^{175}) in the vicinity of the catalytic histidine (His^{159}), creates a Cys-His-Asn triad, which is considered similar to the Ser-His-Asp triad found in serine proteases [81]. The histidine residue in the Cys-His-Asn triad of CPs acts as proton acceptor, enhancing the nucleophilicity of the cysteine residue [83]. According to the current classification of MEROPS database, the cysteine-proteases are grouped into 14 different clans based on their tertiary structure. Within each clan, proteases are grouped into families based on their structural similarity [82].

It was shown that protozoans from the genus Leishmania express a wide range of CPs. They are considered putative virulence factors, since the knockout of this protease family in *L. mexicana* affected its virulence [84]. Due to this, protozoal CPs have drawn considerable attention of researchers as possible targets to the development of inhibitors [85]. However, the effectiveness of CPs inhibitors seems to depend on the parasite species and life stage. *L. major* exhibited higher sensitivity to the inhibitors in the promastigote and amastigote forms [86], while in *L. mexicana* the promastigote form presented low sensitivity [84].

The most widely studied CPs are CPA, CPB, CPC, cathepsin L-like, and cathepsin B-like (Table 1). The expression of CPs in the amastigote form is higher than in promastigotes, suggesting that these enzymes are involved in the host-parasite interaction [87]. CPA and CPC genes are organized in a single copy, while CPB genes are arranged in tandem sequences, with 19 copies in *L. mexicana*, 8 in *L. major*, and 5 in *L. chagasi* [88]. In *L. mexicana*, CPBs hinder the action of macrophages by decreasing the Th1 immune response, increasing the production of IFN-γ, and inhibiting the IL-12 release by JNK and ERK cleavage. Conversely, CPAs inhibit the antigen presentation through the degradation of MHC class II complex molecules and CPCs control the expression of proteins that regulate the cell cycle in Leishmania species [89]. In order to improve the structural knowledge about CPs from *L. mexicana*, a study was conducted to investigate the effects of inhibitors on the activity of the rCPB2.8 enzyme and in rCPB3.0 and rH84Y isoforms, whose differences in the amino acid constitution are depicted in Table 2. The rCPB2.8 enzyme has Asn^{60}, Asp^{61}, Asp^{64} residues in the α-helices that form the wall of the active site cleft. Few negative charge modifications are observed in the CPB isoenzymes rCPB3.0 and rH84Y, conferring an array of hydrolytic activities and providing to the parasites a possibility of adaptation to pH, salinity, and temperature changes [90].

Glycosaminoglycans (GAGs) are molecules covalently linked to a protein core forming a dense network of negative charges in the extracellular matrix (ECM) available for the interaction of extracellularly

Table 1
Cysteine protease expression in *Leishmania* spp.

Species	Enzymes
L. amazonensis	CPA
L. panamensis	CPB
L. tropicalis	CPB
L. baziliensis	CPA, CPB, CPC
L. mexicana	CPA, CPB, CPC
L. major	CPA, CPB, CPC
L. donovani	CPA, CPB, CPC
L. chagasi	CPA, CPB, CPC
L. infantum	CPA, CPB, CPC

Table 2
Variation of the amino acid composition in rCPB2.8 and its isoforms (rCPB3.0 and rH84Y) in *L. mexicana*.

Enzymes	Amino acid position				
	18	*60*	*61*	*64*	*84*
rCPB2.8	Asp	Asn	Asp	Asp	His
rCPB3.0	Asp	Asp	Asn	Ser	His
rH84Y	Asp	Asp	Asn	Ser	Tyr

released CPBs during the infection [91]. In this regard, it was shown that *Leishmania* spp. secrete CPBs that bind to the ECM of host cells, promoting the proteolysis of fibronectin and parasitic infection [92]. The variation of the pH, temperature, and salt concentration conditions revealed that CPs contained in amastigotes and promastigote lysates from Leishmania have different behavior and ability to adapt to several environmental conditions during the parasite life cycle. Besides, the hydrolysis of the fluorogenic substrate of CPs Z-FR-MCA in Leishmania amastigotes was higher after preincubation with thapsigargin, an inhibitor of the sarco(endo)plasmic reticulum Ca^{2+}-ATPase (SERCA), which increases the cytosolic Ca^{2+} levels. This suggests that, at least part, the observed hydrolysis is related to Ca^{2+}-dependent cysteine peptidases, such as metacaspases [93]. Cysteine proteases from *T. cruzi* (cruzain) and *L. mexicana* (rCPB2.8) differ from other related mammalian peptidases because they are active over a broader pH range and both endo- and exopeptidase activities. These features probably drive the biological functions of these enzymes when exposed to different environmental conditions, depending on the location of the enzymes or the parasite development stage [94]. Thus, it highlights the potential of these enzymes as targets for drug development against these neglected diseases.

Around 2000′s, a new class of proteases, the metacaspases, was described as being a promising target for design for the anti-protozoa drugs. Belonging to caspase family, these enzymes are also cysteine proteases that, once activated, hydrolyze their substrates in order to activate a proteolytic cascade resulting in cell death [95]. Metacaspases belong to CD clan of C14 family and are homologous of caspases. Also found in plants, fungi, and protozoa, metacaspases cleave their substrates after basic residues at P_1 position and they are involved in the programed cell death (PCD) in these organisms [96–98]. After the discovery of this enzyme family, several efforts have been made to elucidate its roles in the apoptotic cell death program in mammals [99]. The first attempt to identify homologous caspases in fungi and protozoan eukaryotic cells were not successful, and then it was assumed that caspases were restricted to mammals [100]. Bioinformatic tools were used to identify a protease in lower eukaryotes with structural similarities compared to mammalian caspases. Such enzyme was named metacaspase and described in plants, fungi, and protozoa, but not in mammals [97]. Due to this, it was thought to be acquired by the lower eukaryotes through mitochondrial endosymbiosis [101]. As caspases, metacaspases present two domains called P_{10} and P_{20}; however, unlike caspases, metacaspases do not require dimerization to be activated. Additionally, caspases hydrolyze substrates after an aspartic acid residue at P_1 position, whereas metacaspases hydrolyze substrates after a basic residue (Arg or Lys) at P_1 position [102–104]. Moreover, metacaspases depend on Ca^{2+} for its activation [103,104]. Metacaspases exhibit some structural differences among them, being classified as type I, II, and III. Type I metacaspases have a *N*-terminal pro-domain containing a repeated sequence of proline, glutamine, and asparagine, besides a zinc finger motif. Type II metacaspases do not have the pro-domain but a linker between P_{10} and P_{20} subunits. At last, in contrast to type I and II, type III metacaspases have the P_{10} subunit before P_{20} [105,106].

Type I metacaspases are ubiquitously expressed in protozoa *Leishmania* spp. and *Trypanosoma* spp. In *T. brucei*, five metacaspases (TbMCA1 – TbMCA5) were found [107]. TbMCA2 and TbMCA3 exhibit a relatively high similarity in their amino acid sequence (89%). However, it is noteworthy the presence of a hydrophobic sequence in the *N*-terminal region of TbMCA3, whereas TbMCA5 has a characteristic central domain and an additional extension of C-terminal region. The other two metacaspases (TbMCA1 and TbMCA4) are expected to encode inactive enzymes, due to the presence of Ser and Tyr residues instead of His and Cys in the catalytic domain [108]. *T. cruzi* has two genes encoding metacaspases, TcMCA3 and TbMCA5, which are homologous to TbMCA2 and TbMCA5 of *T. brucei*, respectively. Such metacaspases, expressed during the parasite development, are thought to be implicated in the execution of PCD [109].

Two metacaspases are encoded in *L. donovani*, LdMC1 and LdMC2, which are involved in the oxidative stress-induced cell death. These metacaspases exhibit remarkable differences between them, e.g., LdMC1 has a higher rich proline domain in the C-terminal portion compared to LdMC2 [110]. The tridimensional structure of metacaspases from *Leishmania* spp. is similar to other metacaspases, with a P_{20} portion as central domain wherein the catalytic dyad (His-Cys) is found. Such dyad is conserved between both metacaspases from *L. donovani*. Also, a proline rich C-terminal domain is a common feature in type I metacaspases, as in TcMCA5 from *T. cruzi* and YCA1 from *S. cerevisiae* [111,112]. It was suggested that the *N*-terminal region of Leishmania metacaspases are cleaved independently of its autoprocessing activity [113]. Since their discovery, several evidences have suggested that metacaspases could act similarly to mammalian caspases in the PCD of unicellular eukaryotes. Particularly in Trypanosoma and Leishmania, metacaspases seem to be involved in stress-induced PCD [114,115]. However, unlike caspases that must be processed to exhibit catalytic activity, metacaspases do not need be processed by others to have catalytic activity, i.e., the autoprocessing allow them reaching maximal catalytic activity. Both catalytic and autoprocessing activities of metacaspases are strictly dependent on Ca^{2+} [102,116]. It was shown that, without autoprocessing, TbMCA2 is unable to exerted proteolytic activity [116]. Also, the overexpression of TbMCA4 on *Saccharomyces cerevisiae* inhibited the yeast growth and induced cell death, apparently due to the impairment of respiratory capacity. Nevertheless, it was proposed that TbMCA4 did not participate of the regulation of cell death in *T. brucei*, although its pseudo activity seems to be related to the production of virulence factors associated to the membrane [115]. Thus, *T. brucei* metacaspases (TbMCA2, −3, and −5) are involved in the cell cycle regulation and cell death program of this protozoa [115,117], as well as the metacaspase LmjMCA of *L. major* [118,119]. The LmjMCA expression is higher in the amastigote and procyclic promastigote forms and lower in metacyclic stages, regulating cell cycle progression and proliferation in *L. major* [118]. After autoprocessing, LmjMCA exhibited increased activity in *in vitro* assays [120].

3.1. Cysteine protease (CP) inhibitors as drug candidates

As mentioned before, CPs are involved in the life cycle and pathogenicity of several parasites, including Leishmania and Trypanosoma species. As these enzymes participates in the immune evasion, enzymatic activation, virulence, and tissue invasion, CPs are considered as potential targets to the development of new antileishmanial and trypanocidal drug candidates [121–124]. The antiparasitic effects of CP inhibitors from distinct chemical classes and with different targets in *Leishmania* and *Trypanosoma* have been reported, such as peptidomimetics (K11777, WRR-483, Cz007, Cz008), dipeptides (MDL28170), ketones (1,2,3-triazole-based tetrafluorophenoxymethyl ketone), benzophenones (1,2-substituted-1H-benzo[d]imidazole derivatives and benzophenone derivatives), quinolines (4-substituted quinoline HTI 15 and analogs of the 7-chloro-N-[3-(morpholin-4-yl)propyl]quinolin-4-amine compounds 1, 3 and 4), organic tellurium (RF07), aziridines (aziridine-2,3-dicarboxylate-Based compounds 13b and 13e), summarized in Table 3. Several efforts are ongoing to develop non-toxic and more specific inhibitors with improved biological half-lives and bioavailability [124]. In this regard, the oxalic acid-bis[[(2-hydroxy-1-naphthyl) methylene]hydrazide] derivatives (ZLIII43A and ZLIII115A) and

Table 3
Cysteine protease inhibitors with reported activity against *Leishmania* and *Trypanosoma* spp.

Compound class	Cysteine Protease Inhibitor	Target	Parasite
Peptidomimetic	K11777 or K777 [126]	Cruzain, Brucipain, LtCP	*T. cruzi*, *T. brucei*, *T. gambiense*, *L. tropica*
	WRR-483 [172]	Cruzain	*T. cruzi*
	Cz007, Cz008 [175]	Cruzipain	*T. cruzi*
Dipeptides	MDL28170 [177–179]	Calpain 1	*T. cruzi, L. amazonensis*
Ketones	1,2,3-triazole-based tetrafluorophenoxymethyl ketone [172]	Cruzain	*T. cruzi*
Benzophenones	1,2-substituted-1H-benzol [*d*]imidazole derivates (3aS, 4R, 4aR, 9bR, 9cR)-5-H; (9a-d) [132]	CPB 2.8ΔCTE	*L. mexicana*
	Benzophenone derivates (1c, 2c, 3a) [132]	Papain, rCPB2.8, rCPB 3.0, Cruzain	*L. amazonensis*, trypanosomatid *CP*
Quinolines	4-substituted quinoline (HTI 15)	Cathepsin B	*L. mexicana*
	Analogs of the 7-chloro-N0 [3-(*morpholin-4-yl*)*propyl*] quinoline-4-amine (Compounds 1, 3 and 4) [140]	Cruzain and rhodesain	*L. chagasi, L. amazonensis, T. cruzi*
Organic Tellurium	RF07 [139]	Cathepsin B	*L. chagasi*
Aziridines	Aziridine-2,3-Dicarboxylate-Based (13b and 13e) [169]	Cathepsin B and L, Rhodesain	*L. major, T. brucei*

pseudopeptide substrate analogue morpholine urea-phenylalanine-homophenylalanine-vinylsulfonyl-benzene (K11002) were assayed as reversible and irreversible CP inhibitors, respectively. They were able to kill Leishmania parasites *in vitro* at concentrations that did not affect mammalian host cells. The inhibition of Leishmania CP activity was accompanied by defects in the parasite's lysosomal/endosomal compartments, similar to those observed in lysosomal storage diseases [125]. *N*-methyl-piperazine-Phe-homoPhe-vinylsulfone phenyl 109 (K11777 or K777) is an orally bioavailable cruzain inhibitor with reasonable safety/toxicity profile included in pre-clinical studies for CD in mice [126], immunodeficient-mouse [127], and beagle dog models infected with *Trypanosoma cruzi* [128]. These drugs exhibited antiparasitic activity and decreased the size of the lesions in *L. tropica*-infected BALB/c mice by subcutaneous or intraperitoneal injections [129].

The search for CPs inhibitors in scientific databases revealed a wide range of compounds from different classes under evalutation. For example, eugenol ester derivatives, tested as leishmanicidal agents, inhibited the enzymatic activity of the cysteine protease rCPB2.8 from *L. mexicana*. The mechanism of inhibition involves the interaction of the glutamic acid residue (Glu^{205}) of the protein with the positively charged nitrogen group of the inhibitor [130]. Benzoxazole derivatives and their precursors inhibited *L. mexicana* CPs (rCPB2.8, and rCPB3.0) with relative lower toxicity when compared to standard drugs (pentamidine and amphotericin B) [129]. Also, benzophenone derivatives inhibited CPs from *L. mexicana* (CPBs) and *T. cruzi* (cruzain) and exhibited anti-leishmanial activity against the amastigote forms of *L. amazonensis* [131]. However, such effects were associated to cytotoxicity in murine macrophages. Alkylated benzophenone derivatives were also investigated and the 2-hydroxy-4-O-(3,3-dimethyl)-allylbenzophenone derivative inhibited rCPB 2.8, rCPB3.0, and cruzain, presenting IC_{50} values of 2.9, 4.3, and 1.6 μM, respectively. Although these compounds were less effective against amastigotes of *L. (L.) amazonensis* than amphotericin B, by comparing IC_{50} values, they exhibited lower toxicity than AmB. It was proposed that substitutions in the phenolic hydroxyl groups in benzophenone scaffold could modulate the toxicity and efficacy [132].

Natural bi-flavonoids isolated from *Garcinia brasilienses* and semi-synthetic derivatives exhibited potent activity against promastigote and amastigote forms of *L. (L.) amazonensis* and low cytotoxicity in mammalian cells *in vitro*. Such effects correlated with the potent inhibitory activity of CPs of *L. (L.) mexicana* [133]. Also, the leishmanicidal and tripanocidal activity of cyclopalladated complexes has been also investigated [134,135]. Despite their antitumor activity associated with the inhibition of cathepsin B, these compounds inhibited CPs of Leishmania *in vitro* [125,136]. Another biphosphinic palladacycle complex [Pd(*C*2,N—S(-)DMPA)(DPPE)]Cl (DPPE 1:2) was active against *L. amazonensis in vitro* and *in vivo* at nontoxic concentrations to the host [137]. After 24 h incubation, the drug (75 and 150 nM) inhibited the parasite growth by 84 and 96 %, respectively, and about 100 % of promastigotes, after 48 and 72 h. After 72 h of incubation, DPPE 1:2 presented lower EC_{50} (higher efficacy) compared to AmB and glucantime [138]. Another class of compounds derived from chalcogens has been evaluated. Hypervalent tellurium derivative 4-phenyl methyl ether (RF07) was effective against the *L. chagasi*, decreasing the infection by 85, 92.4, and 95.7% after 3, 5, and 7 days of treatment, respectively. The RF07 concentration that had leishmanicidal activity against intracellular amastigotes was 10-fold lower than that needed to cause toxicity to macrophages [139]. Lastly, quinoline is an important chemical moiety frequently used for the design and synthesis of large spectra of chemotherapeutic derivatives. A variety of biological and pharmacological activities were described for quinoline derivatives, including antimalarial, antifungal, and antibacterial properties. A recent study with novel 4-substituted quinoline derivatives (named HTI 1 to HTI 24) shown that HTI 15 exhibited the most potent inhibitory activity against cysteine proteases type B of *L. mexicana*, with IC_{50} of 3.6, 5.78, and 12.44 μM for rCPB2.8, rCPB3.0 and rH84Y, respectively. These findings pointed to the therapeutic potential of 4-substituted quinolines as promising antileishmanial drugs [140].

The therapeutic arsenal available for the treatment of *T. cruzi* infection has high toxicity and low safety in long term administration. Thus, several studies have pointing to cysteine proteases from *T. cruzi* as potential targets to drug development. The parasite encodes genes from four clans of CPs (CA, CD, CE, and CF). Clan CA includes the most abundant protease of this parasite, cruzain (cruzipain or GP57/51), a papain-like cathepsin L-like member of family C1. Cruzain is expressed with a typical pro-sequence, a catalytic domain, and an unusual C-terminal extension containing 100–130 amino acids, similar to that of *T. brucei* [141,142] and Leishmania CPs [141,143,144]. Studies employing irreversible inhibitors showed that cruzain is fundamental for the parasite survival in the intracellular environment [88,145,146]. Cruzain is expressed in epimastigote and trypomastigote forms in the blood stream and it was identified as the main antigen in infected individuals. Thus, it is considered a strong candidate as epitope for the vaccine development [147,148]. This protease has crucial functions in differentiation, metabolism, immune response evasion, and the invasive capacity of host cells [149–151]. Cruzain activity is associated with the presence of a cysteine (Cys^{25}) and histidine (His^{172}) residues in its active site and the type of the chemical bond formed between the ligand and the active site establishes the type of inhibition. As example, vinyl sulphones and chalcones bind covalently to Cys^{25}, acting as irreversible inhibitors [152]. It was shown that cruzain inhibitors healed mice infected with *T. cruzi* [153], preventing the proliferation of the parasite in its extracellular epimastigote and intracellular amastigote forms [153,154]. Thus, several cruzain inhibitors were reported, such as thiosemicarbazones [155,156], fluoromethyl ketones [157], triazoles [158], chalcones [159], benzamidazoles [160], pyrimidines [161], ureas [162], carbazones, carboxyamides, carboxylic acids, vinylsulfones, hydrozones, and others [163,164].

Dipeptidyl enoate derivatives were also investigated as CP inhibitors using rhodesain, cruzain, and falcipain-2 as models and these compounds presented an irreversible inhibitory effect [165,166]. Another class of potent inhibitors of *Trypanosoma* CPs is the dipeptidyl nitroalkenes, which exhibited a reversible interaction and inhibited rhodesain and cruzain [167]. A structure-based design using optimized substitutions at

the triazine nitrile moiety for the S_1, S_2, and S_3 pockets produced inhibitors that interact with rhodesain at a nanomolar range [168]. Another series of compounds based on aziridine-2,3-dicarboxylate moiety were synthetized and assayed for the inhibitory activity of a papain-like CP expressed in *T. brucei*. Such compounds inhibited rhodesain at a micromolar range [169] and impaired Leishmania promastigote growth at mid-micromolar concentrations [170]. It was shown that carbamoyl imidazoles can act as cruzain inhibitors. The most potent derivative exhibited an inhibition constant (K_i) about 20 nM, presenting activity against *T. cruzi in vitro* and *in vivo* [171]. Nonpeptidic tetrafluorophenoxymethyl ketones also inhibited cruzain and CD in an *in vivo* mouse model, exhibiting a great potential as antitrypanosomal drug candidates [172]. Moreover, the vinyl sulfones derivatives represented by K11777 showed great inhibitory potency against cruzain, presenting antitrypanosomal activity also *in vivo*. WRR-483, a K11777 analogue, exhibited good inhibitory potency against cruzain *in vitro* and eradicated parasitic infection in a mouse model of acute Chagas' disease. However, it was 20-fold less effective than its analog K11777 and exhibited sensitivity to pH [173,174]. The reversible and orally bioavailable cruzain inhibitors Cz007 and Cz008 were also effective against *T cruzi* trypomastigotes (IC_{50} 1.1 and 1.8 nM, respectively) [175]. The dipeptide MDL 28170, a potent cell-permeable inhibitor of calpain I, II, and III, also exhibited antileishmanial effects against *L. amazonensis* (LD_{50} 23.3 μM) [176]. Regarding *T. cruzi*, MDL 28,170 inhibited the growth of epimastigote (IC_{50} 31.7 μM) and trypomastigote forms (IC_{50} 20.4 μM), and also diminished the adhesion of parasites to the insect guts [177–179].

The widespread expression of metacaspases in *Leishmania* and *Trypanosoma* spp., differences with mammalian caspases, as well as their crucial role in several physiological processes during all life stages in these parasites enable them as promising targets for drug development. Thus, many studies have been conducted along the last years to find or develop specific inhibitors for parasite CPs. In this regard, a set of specific inhibitors for the metacaspases TbMCA2 and TbMCA3 was designed, considering mimetic substitutions at P_1 and chemical modifications at P_2 positions, in order to obtain higher specificity and potency [180]. All synthetized compounds exhibited a competitive inhibitory activity in *in vitro* assays. The best inhibitor was also tested against human caspase 3 and it did not inhibit it, showing a selectivity for metacaspases. However, despite the selective and potent inhibitory effect against TbMCA2 and TbMCA3 *in vitro*, they showed only a slight antiparasitic activity *in vivo* [181]. Procaspase-activating compound 1 (PAC-1), a procaspase 3 activator, was assayed against TcMCA3 of *T. cruzi* and it decreased the viability of epimastigote forms (but not metacyclic trypomastigotes), with an IC_{50} around 14 μM. Such effect was accompanied by mitochondrial transmembrane potential dissipation and phosphatidylserine externalization, suggesting the triggering of the apoptotic program. Interestingly, PAC-1 also decreased the viability of mammalian cells but with a 3-fold higher IC_{50} value, indicating distinct mode of action/affinity of this compound with caspases and metacaspases [181]. Thus, although metacaspases have the potential to constitute an excellent target for a development of new compounds, the development of specific and selective inhibitors with both *in vitro* and *in vivo* activities still remains a challenge.

4. Final remarks

The current evidences point to the protozoal CPs as potential targets to the development of selective and effective inhibitors to be considered as new drugs against leishmaniasis and trypanosomiasis. Modern tools applied in medicinal chemistry and biochemical/pharmacological studies, such as drug library high throughput screening and *in silico* analyses, combined with the *in vivo* assays certainly will contribute to the development of CPs inhibitors in a near future to be added to the therapeutic arsenal available to treat neglected diseases.

Funding

This research was funded by Fundação de Amparo à Pesquisa do Estado de São Paulo (FAPESP, 2016/25112–4; 2018/25747–5; 2019/05936–0), Conselho Nacional de Desenvolvimento Científico e Tecnológico (CNPq, 305672/2019–2; 312020/2019-8), and Coordenação de Aperfeiçoamento de Pessoal de Nível Superior (CAPES, Financial code 001).

CRediT authorship contribution statement

Wagner A.S. Judice: Writing - original draft. **Letícia Silva Ferraz:** Investigation, Writing - original draft. **Rayssa de Mello Lopes:** . **Luan dos Santos Vianna:** Investigation. **Fábio da Silva Siqueira:** Investigation. **Juliana F. Di Iorio:** Investigation. **Laura de Azevedo Maffeis Dalzoto:** Investigation, Writing - original draft. **Mariana Nascimento Romero Trujilho:** Investigation. **Taiz dos Reis Santos:** Investigation, Writing - original draft. **Maurício F.M. Machado:** Writing - original draft. **Tiago Rodrigues:** Conceptualization, Writing - review & editing, Supervision, Funding acquisition.

Declaration of Competing Interest

The authors declare that they have no known competing financial interests or personal relationships that could have appeared to influence the work reported in this paper.

References

1 Herwaldt BL. Leishmaniasis. *Lancet*. 1999;354:1191–1199. https://doi.org/10.1016/S0140-6736(98)10178-2.
2 Book Review: Working to Overcome the Global Impact of Neglected Tropical Diseases. Perspect Public Health. 2012;132(4):192–2. http://doi.org/10.1177/1757913912449575.
3 Akinsolu FT, Nemieboka PO, Njuguna DW, Ahadji MN, Dezso D, Varga O. Emerging resistance of neglected tropical diseases: A scoping review of the literature. *Int J Environ Res Public Health*. 2019;16. https://doi.org/10.3390/ijerph16111925.
4 Steverding D. The history of leishmaniasis. *Parasites Vectors*. 2017;10:1–10. https://doi.org/10.1186/s13071-017-2028-5.
5 Akhoundi M, Kuhls K, Cannet A, et al. A Historical Overview of the Classification, Evolution, and Dispersion of Leishmania Parasites and Sandflies. *PLoS Negl Trop Dis*. 2016;10. https://doi.org/10.1371/journal.pntd.0004349.
6 Killick-Kendrick R. The biology and control of Phlebotomine sand flies. *Clin Dermatol*. 1999;17:279–289. https://doi.org/10.1016/S0738-081X(99)00046-2.
7 Reithinger R, Dujardin JC, Louzir H, Pirmez C, Alexander B, Brooker S. Cutaneous leishmaniasis. *Lancet Infect Dis*. 2007;7:581–596. https://doi.org/10.1016/S1473-3099(07)70209-8.
8 World Helth Organization – Leishmaniasis: Vector control, 2018. - Pesquisa Google. Accessed March 23, 2021. https://www.google.com/search?q=World+Helth+Organization+–+Leishmaniasis%3A+Vector+control%2C+2018.&rlz=1C5CHFA_enBR824BR824&oq=World+Helth+Organization+–+Leishmaniasis%3A+Vector+control%2C+2018.&aqs=chrome..69i57.1161j0j9&sourceid=chrome&ie=UTF-8.
9 Burza S, Croft S, Boelaert M. Leishmaniasis. *Lancet*. 2018;392:951–970.
10 Lainson R, Shaw JJ. Evolution, classification and geographical distribution. In: The Leishmaniases in Biology and Medicine. Volume I. Biology and Epidemiology. ; 1987.
11 Arevalo J, Ramirez L, Adaui V, et al. Influence of Leishmania (Viannia) species on the response to antimonial treatment in patients with American tegumentary leishmaniasis. *J Infect Dis*. 2007;195:1846–1851. https://doi.org/10.1086/518041.
12 Andrade-Narváez FJ, Vargas-González A, Canto-Lara SB, Damián-Centeno AG. Clinical Picture of Cutaneous Leishmaniases Due to Leishmania (Leishmania) Mexicana in the Yucatan Peninsula Mexico. *Mem Inst Oswaldo Cruz*. 2001;96:163–167. https://doi.org/10.1590/S0074-02762001000200005.
13 Aransay AM, Scoulica E, Tselentis Y. Detection and identification of Leishmania DNA within naturally infected sand flies by seminested PCR on minicircle kinetoplastic DNA. *Appl Environ Microbiol*. 2000;66:1933–1938. https://doi.org/10.1128/AEM.66.5.1933-1938.2000.
14 Rogers M, Kropf P, Choi BS, et al. Proteophosophoglycans regurgitated by Leishmania-infected sand flies target the L-arginine metabolism of host macrophages to promote parasite survival. *PLoS Pathog*. 2009;5. https://doi.org/10.1371/journal.ppat.1000555.
15 Rogers ME, Corware K, Müller I, Bates PA. Leishmania infantum proteophosphoglycans regurgitated by the bite of its natural sand fly vector, Lutzomyia longipalpis, promote parasite establishment in mouse skin and skin-distant tissues. *Microbes Infect*. 2010;12:875–879. https://doi.org/10.1016/j.micinf.2010.05.014.

16 Rodríguez NE, Dixit UG, Allen L-AH, Wilson ME. Stage-Specific Pathways of Leishmania infantum chagasi Entry and Phagosome Maturation in Macrophages. Macrophages PLoS ONE. 2011;6(4):19000. http://doi.org/10.1371/journal.pone.0019000.

17 Serafim TD, Coutinho-Abreu IV, Oliveira F, Meneses C, Kamhawi S, Valenzuela JG. Sequential blood meals promote Leishmania replication and reverse metacyclogenesis augmenting vector infectivity. *Nat Microbiol*. 2018;3:548–555. https://doi.org/10.1038/s41564-018-0125-7.

18 Ramiro Assis R, Soares Noronha F, Turco SJ, et al. Molecular and Cellular Biochemistry Faculty Publications. *PLoS Negl Trop Dis*. 2012;6:44. https://doi.org/10.1371/journal.pntd.0001543.

19 Moradin N, Descoteaux A. Leishmania promastigotes: building a safe niche within macrophages. *Front Cell Infect Microbiol*. 2012;2:121. https://doi.org/10.3389/fcimb.2012.00121.

20 Olivier M, Atayde VD, Isnard A, Hassani K, Shio MT. Leishmania virulence factors: Focus on the metalloprotease GP63. *Microbes Infect*. 2012;14:1377–1389. https://doi.org/10.1016/j.micinf.2012.05.014.

21 Reithinger R, Mohsen M, Aadil K, Sidiqi M, Erasmus P, Coleman PG. Anthroponotic cutaneous leishmaniasis, Kabul Afghanistan. *Emerg Infect Dis*. 2003;9:727–729. https://doi.org/10.3201/eid0906.030026.

22 Brooker S, Mohammed N, Adil K, et al. Leishmaniasis in refugee and local Pakistani populations. *Emerg Infect Dis*. 2004;10:1681–1684. https://doi.org/10.3201/eid1009.040179.

23 Akilov OE, Khachemoune A. Clinical manifestations and classification of Old World cutaneous leishmaniasis Clinical trials in CTCL View project Empiric Treatment for Serious Bacterial Infections View project. *Artic Int J Dermatology Published online*. 2007. https://doi.org/10.1111/j.1365-4632.2007.03154.x.

24 Kima PE. The amastigote forms of Leishmania are experts at exploiting host cell processes to establish infection and persist. *Int J Parasitol*. 2007;37:1087–1096. https://doi.org/10.1016/j.ijpara.2007.04.007.

25 Desjeux P. Leishmaniasis: Current situation and new perspectives. *Comp Immunol Microbiol Infect Dis*. 2004;27:305–318. https://doi.org/10.1016/j.cimid.2004.03.004.

26 Guerin PJ, Olliaro P, Nosten F, et al. Malaria: Current status of control, diagnosis, treatment, and a proposed agenda for research and development. *Lancet Infect Dis*. 2002;2:564–573. https://doi.org/10.1016/S1473-3099(02)00372-9.

27 Sousa F das CA, Soares HVA, Lemos LEAS, Reis DM, Silva WC da, Rodrigues LA de S. Perfil epidemiológico de doenças negligenciadas de notificação compulsória no Brasil com análise dos investimentos governamentais nessa área. Res Soc Dev. 2020;9(1):e62911610. http://doi.org/10.33448/rsd-v9i1.1610.

28 Bilheiro AB, Da Rosa JA, De Oliveira J, et al. First report of natural infection with trypanosoma cruzi in rhodnius montenegrensis (Hemiptera, Reduviidae, Triatominae) in Western Amazon Brazil. *Vector-Borne Zoonotic Dis*. 2018;18:605–610. https://doi.org/10.1089/vbz.2018.2266.

29 Chagas C. Nova tripanozomiaze humana: estudos sobre a morfolojia e o ciclo evolutivo do Schizotrypanum cruzi n. gen., n. sp., ajente etiolojico de nova entidade morbida do homem. *Mem Inst Oswaldo Cruz*. 1909;1:159–218. https://doi.org/10.1590/s0074-02761909000200008.

30 Rassi A, Rassi A, Marin-Neto JA. Chagas disease. *Lancet*. 2010;375:1388–1402. https://doi.org/10.1016/S0140-6736(10)60061-X.

31 Tyler KM, Engman DM. The life cycle of Trypanosoma cruzi revisited. In: International Journal for Parasitology. Vol. 2001:472–81. http://doi.org/10.1016/S0020-7519(01)00153-9.

32 Burleigh BA, Andrews NW. The mechanisms of Trypanosoma cruzi invasion of mammalian cells. *Annu Rev Microbiol*. 1995;49:175–200. https://doi.org/10.1146/annurev.mi.49.100195.001135.

33 Bern C, Kjos S, Yabsley MJ, Montgomery SP. Trypanosoma cruzi and chagas' disease in the united states. *Clin Microbiol Rev*. 2011;24:655–681. https://doi.org/10.1128/CMR.00005-11.

34 Vago AR, Andrade LO, Leite AA, et al. Genetic characterization of Trypanosoma cruzi directly from tissues of patients with chronic chagas disease: Differential distribution of genetic types into diverse organs. *Am J Pathol*. 2000;156:1805–1809. https://doi.org/10.1016/S0002-9440(10)65052-3.

35 Barbosa-Ferreira JM, Guerra JA de O, Santana Filho FS de, Magalhães BML, Coelho LIARC, Barbosa M das GV. [Cardiac involvement in Acute Chagas' Disease cases in the Amazon region]. Arq Bras Cardiol. 2010;94(6). http://doi.org/10.1590/s0066-782x2010000600023.

36 Oliveira BG, Abreu MNS, Abreu CDG, da Costa Rocha MO, Ribeiro AL. Qualidade de vida relacionada à saúde na doença de Chagas. *Rev Soc Bras Med Trop*. 2011;44:150–156. https://doi.org/10.1590/S0037-86822011005000002.

37 Berbert TRN, De Mello TFP, Wolf Nassif P, et al. Pentavalent antimonials combined with other therapeutic alternatives for the treatment of cutaneous and mucocutaneous leishmaniasis: A systematic review. *Dermatol Res Pract*. 2018;2018. https://doi.org/10.1155/2018/9014726.

38 Turcano L, Torrente E, Missineo A, et al. Identification and binding mode of a novel Leishmania Trypanothione reductase inhibitor from high throughput screening. *PLoS Negl Trop Dis*. 2018;12. https://doi.org/10.1371/journal.pntd.0006969.

39 Oliveira LF, Schubach AO, Martins MM, et al. Systematic review of the adverse effects of cutaneous leishmaniasis treatment in the New World. *Acta Trop*. 2011;118:87–96. https://doi.org/10.1016/j.actatropica.2011.02.007.

40 Gasser RA, Magill AJ, Oster CN, Franke ED, Grögl M, Berman JD. Pancreatitis induced by pentavalent antimonial agents during treatment of leishmaniasis. *Clin Infect Dis*. 1994;18:83–90. https://doi.org/10.1093/clinids/18.1.83.

41 Maltezou HC. Drug resistance in visceral leishmaniasis. *J Biomed Biotechnol*. 2010;2010. https://doi.org/10.1155/2010/617521.

42 Singh N. Drug resistance mechanisms in clinical isolates of Leishmania donovani. Indian J Med Res. 2006;123(3):411-422. Accessed March 24, 2021. https://citeseerx.ist.psu.edu/viewdoc/download?doi=10.1.1.490.4804&rep=rep1&type=pdf.

43 Singh N, Chatterjee M, Sundar S. The overexpression of genes of thiol metabolism contribute to drug resistance in clinical isolates of visceral leishmaniasis (kala azar) in India. *Parasites Vectors*. 2014;7. https://doi.org/10.1186/s13071-014-0596-1.

44 Sundar S, More DK, Singh MK, et al. Failure of pentavalent antimony in visceral leishmaniasis in India: Report from the center of the Indian epidemic. *Clin Infect Dis*. 2000;31:1104–1107. https://doi.org/10.1086/318121.

45 Coelho AC, Messier N, Ouellette M, Cotrim PC. Role of the ABC transporter PRP1 (ABCC7) in pentamidine resistance in Leishmania amastigotes. *Antimicrob Agents Chemother*. 2007;51:3030–3032. https://doi.org/10.1128/AAC.00404-07.

46 Baker N, Glover L, Munday JC, et al. Aquaglyceroporin 2 controls susceptibility to melarsoprol and pentamidine in African trypanosomes. *Proc Natl Acad Sci USA*. 2012;109:10996–11001. https://doi.org/10.1073/pnas.1202885109.

47 Jha TK. Evaluation of diamidine compound (pentamidine isethionate) in the treatment of resistant cases of kala-azar occurring in North Bihar, India. *Trans R Soc Trop Med Hyg*. 1983;77:167–170. https://doi.org/10.1016/0035-9203(83)90058-5.

48 Moen MD, Lyseng-Williamson KA, Scott LJ. Liposomal amphotericin B: A review of its use as empirical therapy in febrile neutropenia and in the treatment of invasive fungal infections. *Drugs*. 2009;69:361–392. https://doi.org/10.2165/00003495-200969030-00010.

49 Croft SL, Neal RA, Pendergast W, Chan JH. The activity of alkyl phosphorylcholines and related derivatives against Leishmania donovani. *Biochem Pharmacol*. 1987;36:2633–2636. https://doi.org/10.1016/0006-2952(87)90543-0.

50 Kuhlencord A, Maniera T, Eibl H, Unger C. Hexadecylphosphocholine: Oral treatment of visceral leishmaniasis in mice. *Antimicrob Agents Chemother*. 1992;36:1630–1634. https://doi.org/10.1128/AAC.36.8.1630.

51 Sundar S, Rosenkaimer F, Makharia MK, et al. Trial of oral miltefosine for visceral leishmaniasis. *Lancet*. 1998;352:1821–1823. https://doi.org/10.1016/S0140-6736(98)04367-0.

52 Jha TK, Sundar S, Thakur CP, et al. Miltefosine, an Oral Agent, for the Treatment of Indian Visceral Leishmaniasis. *N Engl J Med*. 1999;341:1795–1800. https://doi.org/10.1056/nejm199912093412403.

53 Sundar S, Jaya J. Liposomal amphotericin B and leishmaniasis: Dose and response. *J Glob Infect Dis*. 2010;2:159. https://doi.org/10.4103/0974-777x.62886.

54 Wijnant GJ, Van Bocxlaer K, Yardley V, et al. Comparative efficacy, toxicity and biodistribution of the liposomal amphotericin B formulations Fungisome® and Am Bisome® in murine cutaneous leishmaniasis. *Int J Parasitol Drugs Drug Resist*. 2018;8:223–228. https://doi.org/10.1016/j.ijpddr.2018.04.001.

55 Adler-Moore J, Proffitt RT. Effect of tissue penetration on AmBisome efficacy. Curr Opin Investig Drugs. 2003;4(2):179-185. Accessed March 25, 2021. https://www.researchgate.net/publication/10828143.

56 Adler-Moore J, Proffitt RT. AmBisome: liposomal formulation, structure, mechanism of action and pre-clinical experience. J Antimicrob Chemother. 2002;49(suppl_1):21-30. Accessed March 25, 2021. https://academic.oup.com/jac/article-abstract/49/suppl_1/21/2473432.

57 Sundar S, Mehta H, Suresh AV, Singh SP, Rai M, Murray HW. Amphotericin B Treatment for Indian Visceral Leishmaniasis: Conventional versus Lipid Formulations. *Clin Infect Dis*. 2004;38:377–383. https://doi.org/10.1086/380971.

58 Melos JLR, Echevarria A. Trypanosomatids metabolic systems as potential chemotherapeutic targets. *Rev Virtual Quim*. 2012;4:374–392. https://doi.org/10.5935/1984-6835.20120029.

59 Dias LC, Dessoy MA, Silva JJN, Thiemann OH, Oliva G, Andricopulo AD. Quimioterapia da doença de Chagas: estado da arte e perspectivas no desenvolvimento de novos fármacos. *Quim Nova*. 2009;32:2444–2457. https://doi.org/10.1590/s0100-40422009000900038.

60 Roberts SC. Genetic Manipulation of Leishmania Parasites Facilitates the Exploration of the Polyamine Biosynthetic Pathway as a Potential Therapeutic Target. Adv Genet Reseach. 2013;10:29-54. Accessed March 25, 2021. http://commons.pacificu.edu/phrmfac.

61 Sousa Silva M, Gomes RA, Ferreira AEN, Ponces Freire A, Cordeiro C. The glyoxalase pathway: The first hundred years... and beyond. *Biochem J*. 2013;453:1–15. https://doi.org/10.1042/BJ20121743.

62 Zhang K, Beverley SM. Phospholipid and sphingolipid metabolism in Leishmania. *Mol Biochem Parasitol*. 2010;170:55–64. https://doi.org/10.1016/j.molbiopara.2009.12.004.

63 Abu-Mejdad N. Evaluation of therapeutic effects of vicine against leishmania donovani. in vitro. J Am Sci. 2013;9(5):115-20. Accessed March 25, 2021. http://www.jof.

64 Gangjee A, Jain H, Kurup S. Recent Advances in Classical and Non-Classical Antifolates as Antitumor and Antiopportunistic Infection Agents: Part II. *Anticancer Agents Med Chem*. 2008;8:205–231. https://doi.org/10.2174/187152008783497064.

65 Luz NF, Andrade BB, Feijó DF, et al. Heme Oxygenase-1 Promotes the Persistence of Leishmania chagasi Infection. *J Immunol*. 2012;188:4460–4467. https://doi.org/10.4049/jimmunol.1103072.

66 Kaur PK, Dinesh N, Soumya N, Kishore Babu N, Singh S. Identification and characterization of a novel Ribose 5-phosphate isomerase B from Leishmania donovani. *Biochem Biophys Res Commun*. 2012;421:51–56. https://doi.org/10.1016/j.bbrc.2012.03.107.

67 Cordeiro AT, Feliciano PR, Pinheiro MP, Nonato MC. Crystal structure of dihydroorotate dehydrogenase from Leishmania major. *Biochimie*. 2012;94:1739–1748. https://doi.org/10.1016/j.biochi.2012.04.003.

68 Silva AM, Tavares J, Silvestre R, Ouaissi A, Coombs GH, Cordeiro-da-Silva A. Characterization of Leishmania infantum thiol-dependent reductase 1 and evaluation of its potential to induce immune protection. *Parasite Immunol*. 2012;34: 345–350. https://doi.org/10.1111/j.1365-3024.2012.01361.x.

69 Rotella DP. Recent results in protein kinase inhibition for tropical diseases. *Bioorganic Med Chem Lett*. 2012;22:6788–6793. https://doi.org/10.1016/j.bmcl.2012.09.044.

70 Grover A, Katiyar SP, Singh SK, Dubey VK, Sundar D. A leishmaniasis study: Structure-based screening and molecular dynamics mechanistic analysis for discovering potent inhibitors of spermidine synthase. *Biochimica et Biophysica Acta - Proteins and Proteomics*. 1824;2012:1476–1483. https://doi.org/10.1016/j.bbapap.2012.05.016.

71 Antonio Marin-Neto J, Rassi A, Avezum A, Mattos AC, Rassi A. The Benefit trial: Testing the hypothesis that trypanocidal therapy is beneficial for patients with chronic Chagas heart disease. *Mem Inst Oswaldo Cruz*. 2009;104:319–324. https://doi.org/10.1590/s0074-02762009000900042.

72 Urbina JA. Recent clinical trials for the etiological treatment of chronic chagas disease: Advances, challenges and perspectives. *J Eukaryot Microbiol*. 2015;62. https://doi.org/10.1111/jeu.12184.

73 Canavaci AMC, Bustamante JM, Padilla AM, et al. In Vitro and In Vivo High-throughput assays for the testing of Anti-trypanosoma cruzi compounds. *PLoS Negl Trop Dis*. 2010;4. https://doi.org/10.1371/journal.pntd.0000740.

74 Moraes CB, Giardini MA, Kim H, et al. Nitroheterocyclic compounds are more efficacious than CYP51 inhibitors against Trypanosoma cruzi: Implications for Chagas disease drug discovery and development. Sci Rep. 2014;4. http://doi.org/10.1038/srep04703.

75 Urbina JA, Gascon J, Ribeiro I. Benznidazole for Chronic Chagas' Cardiomyopathy. *N Engl J Med*. 2016;374:188–190. https://doi.org/10.1056/nejmc1514453.

76 Vallejo A, Monge-Maillo B, Gutiérrez C, Norman FF, López-Vélez R, Pérez-Molina JA. Changes in the immune response after treatment with benznidazole versus no treatment in patients with chronic indeterminate Chagas disease. *Acta Trop*. 2016;164. https://doi.org/10.1016/j.actatropica.2016.09.010.

77 Torrico F, Gascon J, Ortiz L, et al. Treatment of adult chronic indeterminate Chagas disease with benznidazole and three E1224 dosing regimens: a proof-of-concept, randomised, placebo-controlled trial. *Lancet Infect Dis*. 2018;18. https://doi.org/10.1016/S1473-3099(17)30538-8.

78 Torrico F, Gascón J, Barreira F, et al. New regimens of benznidazole monotherapy and in combination with fosravuconazole for treatment of Chagas disease (BENDITA): a phase 2, double-blind, randomised trial. *Lancet Infect Dis Published online*. 2021. https://doi.org/10.1016/S1473-3099(20)30844-6.

79 Apt W. Current and developing therapeutic agents in the treatment of Chagas disease. *Drug Des Devel Ther*. 2010;4:243–253. https://doi.org/10.2147/DDDT.S8338.

80 Berti PJ, Storer AC. Alignment/phylogeny of the papain superfamily of cysteine proteases. *J Mol Biol*. 1995;246. https://doi.org/10.1006/jmbi.1994.0083.

81 Verma S, Dixit R, Pandey KC. Cysteine proteases: Modes of activation and future prospects as pharmacological targets. *Front Pharmacol*. 2016;7. https://doi.org/10.3389/fphar.2016.00107.

82 Coulombe R, Grochulski P, Sivaraman J, Ménard R, Mort JS, Cygler M. Structure of human procathepsin L reveals the molecular basis of inhibition by the prosegment. *EMBO J*. 1996;15. https://doi.org/10.1002/j.1460-2075.1996.tb00934.x.

83 Rawlings ND, Barrett AJ, Thomas PD, et al. and a comparison with peptidases in the PANTHER database. *Nucleic Acids Res Published online*. 2017;2018. https://doi.org/10.1093/nar/gkx1134.

84 Mottram JC, Souza AE, Hutchison JE, Carter R, Frame MJ, Coombs GH. Evidence from disruption of the lmcpb gene array of Leishmania mexicana that cysteine proteinases are virulence factors. *Proc Natl Acad Sci USA*. 1996;93. https://doi.org/10.1073/pnas.93.12.6008.

85 Matlashewski G. Leishmania infection and virulence. *Med Microbiol Immunol*. 2001; 190. https://doi.org/10.1007/s004300100076.

86 Selzer PM, Pingel S, Hsieh I, et al. Cysteine protease inhibitors as chemotherapy: Lessons from a parasite target. *Proc Natl Acad Sci USA*. 1999;96. https://doi.org/10.1073/pnas.96.20.11015.

87 North MJ, Coombs GH. Proteinases of Leishmania mexicana amastigotes and promastigotes: Analysis by gel electrophoresis. *Mol Biochem Parasitol*. 1981;3. https://doi.org/10.1016/0166-6851(81)90003-7.

88 Siqueira-Neto JL, Debnath A, McCall LI, et al. Cysteine proteases in protozoan parasites. *PLoS Negl Trop Dis*. 2018;12. https://doi.org/10.1371/journal.pntd.0006512.

89 De Souza Leao S, Lang T, Prina E, Hellio R, Antoine JC. Intracellular Leishmania amazonensis amastigotes internalize and degrade MHC class II molecules of their host cells. *J Cell Sci*. 1995;108.

90 Judice WAS, Mottram JC, Coombs GH, Juliano MA, Juliano L. Specific negative charges in cysteine protease isoforms of Leishmania mexicana are highly influential on the substrate binding and hydrolysis. *Mol Biochem Parasitol*. 2005;144. https://doi.org/10.1016/j.molbiopara.2005.07.004.

91 Judice WAS, Manfredi MA, Souza GP, et al. Heparin modulates the endopeptidase activity of Leishmania mexicana cysteine protease cathepsin L-like rCPB2.8. *PLoS ONE*. 2013;8. https://doi.org/10.1371/journal.pone.0080153.

92 Kulkarni MM, Jones EA, McMaster WR, McGwire BS. Fibronectin binding and proteolytic degradation by Leishmania and effects on macrophage activation. *Infect Immun*. 2008;76. https://doi.org/10.1128/IAI.01274-07.

93 Caroselli EE, Assis DM, Barbiéri CL, et al. Leishmania (L.) amazonensis peptidase activities inside the living cells and in their lysates. *Mol Biochem Parasitol*. 2012; 184. https://doi.org/10.1016/j.molbiopara.2012.04.012.

94 Judice WAS, Puzer L, Cotrin SS, et al. Carboxydipeptidase activities of recombinant cysteine peptidases Cruzain of Trypanosoma cruzi and CPB of Leishmania mexicana. *Eur J Biochem*. 2004;271. https://doi.org/10.1111/j.1432-1033.2004.04008.x.

95 Di Dai B, Wang Y, Li DD, et al. Hsp90 Is Involved in Apoptosis of Candida albicans by Regulating the Calcineurin-Caspase Apoptotic Pathway. *PLoS ONE*. 2012;7. https://doi.org/10.1371/journal.pone.0045109.

96 Klemenčič M, Funk C. Evolution and structural diversity of metacaspases. *J Exp Bot Published online*. 2019. https://doi.org/10.1093/jxb/erz082.

97 Uren AG, O'Rourke K, Aravind L, et al. Identification of paracaspases and metacaspases: Two ancient families of caspase-like proteins, one of which plays a key role in MALT lymphoma. *Mol Cell Published online*. 2000. https://doi.org/10.1016/s1097-2765(00)00094-0.

98 Sundström JF, Vaculova A, Smertenko AP, et al. Tudor staphylococcal nuclease is an evolutionarily conserved component of the programmed cell death degradome. *Nat Cell Biol Published online*. 2009. https://doi.org/10.1038/ncb1979.

99 Cerretti DP, Kozlosky CJ, Mosley B, et al. Molecular cloning of the interleukin-1β converting enzyme. *Science (80-)*. 1992;256. https://doi.org/10.1126/science.1373520.

100 Green DR, Kroemer G. The pathophysiology of mitochondrial cell death. *Science (80-)*. 2004;305. https://doi.org/10.1126/science.1099320.

101 Aravind L, Koonin EV. Classification of the caspase-hemoglobinase fold: Detection of new families and implications for the origin of the eukaryotic separins. *Proteins Struct Funct Genet*. 2002;46. https://doi.org/10.1002/prot.10060.

102 Machado MFM, Marcondes MF, Juliano MA, et al. Substrate specificity and the effect of calcium on Trypanosoma brucei metacaspase 2. *FEBS J*. 2013;280. https://doi.org/10.1111/febs.12248.

103 Vercammen D, De Cotte B Van, De Jaeger G, et al. Type II metacaspases Atmc4 and Atmc9 of Arabidopsis thaliana cleave substrates after arginine and lysine. J Biol Chem. Published online 2004. http://doi.org/10.1074/jbc.M406329200.

104 Moss CX, Westrop GD, Juliano L, Coombs GH, Mottram JC. Metacaspase 2 of Trypanosoma brucei is a calcium-dependent cysteine peptidase active without processing. *FEBS Lett*. 2007;581:5635–5639. https://doi.org/10.1016/j.febslet.2007.11.009.

105 Tsiatsiani L, Van Breusegem F, Gallois P, Zavialov A, Lam E, Bozhkov PV. *Metacaspases Cell Death Differ Published online*. 2011. https://doi.org/10.1038/cdd.2011.66.

106 Minina EA, Staal J, Alvarez VE, et al. Classification and Nomenclature of Metacaspases and Paracaspases: No More Confusion with Caspases. *Mol Cell Published online*. 2020. https://doi.org/10.1016/j.molcel.2019.12.020.

107 Mottram JC, Helms MJ, Coombs GH, Sajid M. Clan CD cysteine peptidases of parasitic protozoa. *Trends Parasitol Published online*. 2003. https://doi.org/10.1016/S1471-4922(03)00038-2.

108 Kosec G, Alvarez VE, Agüero F, et al. Metacaspases of Trypanosoma cruzi: Possible candidates for programmed cell death mediators. *Mol Biochem Parasitol*. 2006;145. https://doi.org/10.1016/j.molbiopara.2005.09.001.

109 Lee N, Gannavaram S, Selvapandiyan A, Debrabant A. Characterization of metacaspases with trypsin-like activity and their putative role in programmed cell death in the protozoan parasite Leishmania. *Eukaryot Cell Published online*. 2007. https://doi.org/10.1128/EC.00123-07.

110 Vercammen D, Belenghi B, van de Cotte B, et al. Serpin1 of Arabidopsis thaliana is a Suicide Inhibitor for Metacaspase 9. *J Mol Biol Published online*. 2006. https://doi.org/10.1016/j.jmb.2006.09.010.

111 McLuskey K, Rudolf J, Proto WR, et al. Crystal structure of a Trypanosoma brucei metacaspase. *Proc Natl Acad Sci USA Published online*. 2012. https://doi.org/10.1073/pnas.1200885109.

112 Wong AHH, Yan C, Shi Y. Crystal structure of the yeast metacaspase Yca1. *J Biol Chem Published online*. 2012. https://doi.org/10.1074/jbc.M112.381806.

113 Khademvatan S, Gharavi MJ, Saki J. Miltefosine induces metacaspase and PARP genes expression in Leishmania infantum. *Brazilian J Infect Dis Published online*. 2011. https://doi.org/10.1016/S1413-8670(11)70225-2.

114 Proto WR, Castanys-Munoz E, Black A, et al. Trypanosoma brucei metacaspase 4 is a pseudopeptidase and a virulence factor. *J Biol Chem Published online*. 2011. https://doi.org/10.1074/jbc.M111.292334.

115 Helms MJ, Ambit A, Appleton P, Tetley L, Coombs GH, Mottram JC. Bloodstream form Trypanosoma brucei depend upon multiple metacaspases associated with RAB11-positive endosomes. *J Cell Sci Published online*. 2006. https://doi.org/10.1242/jcs.02809.

116 Gilio JM, Marcondes MF, Ferrari D, et al. Processing of metacaspase 2 from Trypanosoma brucei (TbMCA2) broadens its substrate specificity. *Biochim Biophys Acta - Proteins Proteomics Published online*. 2017. https://doi.org/10.1016/j.bbapap.2017.01.002.

117 Debrabant A, Lee N, Bertholet S, Duncan R, Nakhasi HL. Programmed cell death in trypanosomatids and other unicellular organisms. *Int J Parasitol*. 2003;33. https://doi.org/10.1016/S0020-7519(03)00008-0.

118 Ambit A, Fasel N, Coombs GH, Mottram JC. An essential role for the Leishmania major metacaspase in cell cycle progression. *Cell Death Differ Published online*. 2008. https://doi.org/10.1038/sj.cdd.4402232.

119 Casanova M, Gonzalez IJ, Sprissler C, et al. Implication of different domains of the Leishmania major metacaspase in cell death and autophagy. *Cell Death Dis Published online*. 2015. https://doi.org/10.1038/cddis.2015.288.

120 González IJ, Desponds C, Schaff C, Mottram JC, Fasel N. Leishmania major metacaspase can replace yeast metacaspase in programmed cell death and has arginine-specific cysteine peptidase activity. *Int J Parasitol Published online*. 2007. https://doi.org/10.1016/j.ijpara.2006.10.004.

121 McKerrow JH, Engel JC, Caffrey CR. Cysteine protease inhibitors as chemotherapy for parasitic infections. *Bioorganic. Med Chem.* 1999;7. https://doi.org/10.1016/S0968-0896(99)00008-5.

122 McKerrow JH. Development of cysteine protease inhibitors as chemotherapy for parasitic diseases: Insights on safety, target validation, and mechanism of action. In: International Journal for Parasitology. Vol 29. ; 1999. http://doi.org/10.1016/S0020-7519(99)00044-2.

123 Freitas PG, Castilho TE, De Almeida L, et al. An in silico study of benzophenone derivatives as potential non-competitive inhibitors of trypanosoma cruzi and Leishmania amazonensis cysteine proteinases. *J Braz Chem Soc*. 2018;29. https://doi.org/10.21577/0103-5053.20170164.

124 Caffrey C, Scory S, Steverding D. Cysteine Proteinases of Trypanosome Parasites Novel Targets for Chemotherapy. *Curr Drug Targets*. 2005;1. https://doi.org/10.2174/1389450003349290.

125 Matsuo AL, Silva LS, Torrecilhas AC, et al. In vitro and in vivo trypanocidal effects of the cyclopalladated compound 7a, a drug candidate for treatment of Chagas' disease. *Antimicrob Agents Chemother*. 2010;54. https://doi.org/10.1128/AAC.00323-10.

126 Engel JC, Doyle PS, Hsieh I, McKerrow JH. Cysteine protease inhibitors cure an experimental Trypanosoma cruzi infection. *J Exp Med*. 1998;188. https://doi.org/10.1084/jem.188.4.725.

127 Doyle PS, Zhou YM, Engel JC, McKerrow JH. A cysteine protease inhibitor cures Chagas' disease in an immunodeficient-mouse model of infection. *Antimicrob Agents Chemother*. 2007;51. https://doi.org/10.1128/AAC.00436-07.

128 Barr SC, Warner KL, Kornreic BG, et al. A cysteine protease inhibitor protects dogs from cardiac damage during infection by Trypanosoma cruzi. *Antimicrob Agents Chemother*. 2005;49. https://doi.org/10.1128/AAC.49.12.5160-5161.2005.

129 Mahmoudzadeh-Niknam H, McKerrow JH. Leishmania tropica: Cysteine proteases are essential for growth and pathogenicity. *Exp Parasitol*. 2004;106. https://doi.org/10.1016/j.exppara.2004.03.005.

130 Sajid M, Robertson SA, Brinen LS, Cruzain McKerrow JH. The path from target validation to the clinic. *Adv Exp Med Biol*. 2011;712. https://doi.org/10.1007/978-1-4419-8414-2_7.

131 Coelho CM, Dos Santos T, Freitas PG, et al. Design, synthesis, biological evaluation and molecular modeling studies of novel eugenol esters as leishmanicidal agents. *J Braz Chem Soc Published online*. 2018. https://doi.org/10.21577/0103-5053.20170192.

132 Folquitto LRS, Nogueira PF, Espuri PF, et al. Synthesis, protease inhibition, and antileishmanial activity of new benzoxazoles derived from acetophenone or benzophenone and synthetic precursors. *Med Chem Res*. 2017;26. https://doi.org/10.1007/s00044-017-1824-y.

133 de Almeida L, Alves KF, Maciel-Rezende CM, et al. Benzophenone derivatives as cysteine protease inhibitors and biological activity against Leishmania(L.) amazonensis amastigotes. *Biomed Pharmacother*. 2015;75. https://doi.org/10.1016/j.biopha.2015.08.030.

134 Gontijo VS, Judice WAS, Codonho B, et al. Leishmanicidal, antiproteolytic and antioxidant evaluation of natural biflavonoids isolated from Garcinia brasiliensis and their semisynthetic derivatives. *Eur J Med Chem*. 2012;58. https://doi.org/10.1016/j.ejmech.2012.06.021.

135 Fricker SP, Mosi RM, Cameron BR, et al. Metal compounds for the treatment of parasitic diseases. *J Inorg Biochem*. 2008;102. https://doi.org/10.1016/j.jinorgbio.2008.05.010.

136 Navarro M, Betancourt A, Hernández C, Marchán E. Palladium polypyridyl complexes: Synthesis, characterization, DNA interaction and biological activity on Leishmania (L.) mexicana. *J Braz Chem Soc*. 2008;19. https://doi.org/10.1590/S0103-50532008000700018.

137 Bincoletto C, Tersariol ILS, Oliveira CR, et al. Chiral cyclopalladated complexes derived from N, N-dimethyl-1-phenethylamine with bridging bis (diphenylphosphine)ferrocene ligand as inhibitors of the cathepsin B activity and as antitumoral agents. *Bioorganic MedChem*. 2005;13. https://doi.org/10.1016/j.bmc.2005.01.057.

138 de Paladi CS, Pimentel IAS, Katz S, et al. In vitro and in vivo activity of a palladacycle complex on Leishmania (Leishmania) amazonensis. *PLoS Negl Trop Dis*. 2012;6. https://doi.org/10.1371/journal.pntd.0001626.

139 Pimentel IAS, Paladi C de S, Katz S, Júdice WA de S, Cunha RLOR, Barbiéri CL. In Vitro and In Vivo Activity of an Organic Tellurium Compound on Leishmania (Leishmania) chagasi. PLoS One. 2012;7(11). http://doi.org/10.1371/journal.pone.0048780.

140 Costa CA, Lopes RM, Ferraz LS, et al. Cytotoxicity of 4-substituted quinoline derivatives: Anticancer and antileishmanial potential. *Bioorganic Med Chem*. 2020;28. https://doi.org/10.1016/j.bmc.2020.115511.

141 Mottram JC, North MJ, Barry JD, Coombs GH. A cysteine proteinase cDNA from Trypanosoma brucei predicts an enzyme with an unusual C-terminal extension. *FEBS Lett*. 1989;258. https://doi.org/10.1016/0014-5793(89)81655-2.

142 Pamer EG, Davis CE, Eakin A, So M. Cloning and sequencing of the cysteine protease cDNA from Trypanosoma brucei rhodesiense. *Nucleic Acids Res*. 1990;18. https://doi.org/10.1093/nar/18.20.6141.

143 Souza AE, Waugh S, Coombs GH, Mottram JC. Characterization of a multi-copy gene for a major stage-specific cysteine proteinase of Leishmania mexicana. *FEBS Lett*. 1992;311. https://doi.org/10.1016/0014-5793(92)81382-V.

144 Traub-Cseko YM, Duboise M, Boukai LK, McMahon-Pratt D. Identification of two distinct cysteine proteinase genes of Leishmania pifanoi axenic amastigotes using the polymerase chain reaction. *Mol Biochem Parasitol*. 1993;57. https://doi.org/10.1016/0166-6851(93)90248-V.

145 Murta ACM, Persechini PM, Padron T de S, de Souza W, Guimarães JA, Scharfstein J. Structural and functional identification of GP57/51 antigen of Trypanosoma cruzi as a cysteine proteinase. Mol Biochem Parasitol. 1990;43(1). http://doi.org/10.1016/0166-6851(90)90127-8.

146 Campetella O, Henriksson J, Åslund U, Frasch ACC, Pettersson U, Cazzulo JJ. The major cysteine proteinase (cruzipain) from Trypanosoma cruzi is encoded by multiple polymorphic tandemly organized genes located on different chromosomes. *Mol Biochem Parasitol*. 1992;50. https://doi.org/10.1016/0166-6851(92)90219-A.

147 Scharfstein J, Schechter M, Senna M, Peralta JM, Mendonça-Previato L, Miles MA. Trypanosoma cruzi: Characterization and isolation of A 57/51,000 m.w. surface glycoprotein (GP57/51) expressed by epimastigotes and bloodstream trypomastigotes. *J Immunol*. 1986;137.

148 Duschak V, Couto A. Cruzipain, the Major Cysteine Protease of Trypanosoma cruzi: A Sulfated Glycoprotein Antigen as Relevant Candidate for Vaccine Development and Drug Target. A Review. *Curr Med Chem*. 2009;16. https://doi.org/10.2174/092986709788802971.

149 Cazzulo JJ, Stoka V, Turk V. Cruzipain, the major cysteine proteinase from the protozoan parasite Trypanosoma cruzi. *Biol Chem*. 1997;378. https://doi.org/10.1515/bchm.1997.378.1.1.

150 Franke de Cazzulo BM, Martínez J, North MJ, Coombs GH, Cazzulo JJ. Effects of proteinase inhibitors on the growth and differentiation of Trypanosoma cruzi. *FEMS Microbiol Lett*. 1994;124. https://doi.org/10.1111/j.1574-6968.1994.tb07265.x.

151 Meirelles MNL, Juliano L, Carmona E, et al. Inhibitors of the major cysteinyl proteinase (GP57/51) impair host cell invasion and arrest the intracellular development of Trypanosoma cruzi in vitro. *Mol Biochem Parasitol*. 1992;52. https://doi.org/10.1016/0166-6851(92)90050-T.

152 Herrera-Mayorga V, Lara-Ramírez EE, Chacón-Vargas KF, et al. Structure-based virtual screening and in vitro evaluation of new trypanosoma cruzi cruzain inhibitors. *Int J Mol Sci*. 2019;20. https://doi.org/10.3390/ijms20071742.

153 Gea S, Guiñazu N, Pellegrini A, et al. Cruzipain, a major Trypanosoma cruzi cystein protease in the host-parasite interplay. *Inmunologia*. 2006;25.

154 Ashall F, Angliker H, Shaw E. Lysis of trypanosomes by peptidyl fluoromethyl ketones. *Biochem Biophys Res Commun*. 1990;170. https://doi.org/10.1016/0006-291X(90)92179-4.

155 Andricopulo A, Guido R, Oliva G. Virtual Screening and Its Integration with Modern Drug Design Technologies. *Curr Med Chem*. 2008;15. https://doi.org/10.2174/092986708783330683.

156 Fujii N, Mallari JP, Hansell EJ, et al. Discovery of potent thiosemicarbazone inhibitors of rhodesain and cruzain. *Bioorganic Med Chem Lett*. 2005;15. https://doi.org/10.1016/j.bmcl.2004.10.023.

157 Gillmor SA, Craik CS, Fletterick RJ. Structural determinants of specificity in the cysteine protease cruzain. *Protein Sci*. 1997;6. https://doi.org/10.1002/pro.5560060801.

158 Brak K, Doyle PS, McKerrow JH, Ellman JA. Identification of a new class of nonpeptidic inhibitors of cruzain. *J Am Chem Soc*. 2008;130. https://doi.org/10.1021/ja710254m.

159 Borchhardt DM, Mascarello A, Chiaradia LD, et al. Biochemical evaluation of a series of synthetic chalcone and hydrazide derivatives as novel inhibitors of cruzain from trypanosoma cruzi. *J Braz Chem Soc*. 2010;21. https://doi.org/10.1590/S0103-50532010000100021.

160 Ferreira RS, Simeonov A, Jadhav A, et al. Complementarity between a docking and a high-throughput screen in discovering new cruzain inhibitors. *J Med Chem*. 2010;53. https://doi.org/10.1021/jm100488w.

161 Espíndola JWP, De Oliveira Cardoso MV, De Oliveira Filho GB, et al. Synthesis and structure-activity relationship study of a new series of antiparasitic aryloxyl thiosemicarbazones inhibiting Trypanosoma cruzi cruzain. *Eur J Med Chem*. 2015;101. https://doi.org/10.1016/j.ejmech.2015.06.048.

162 Du X, Hansell E, Engel JC, Caffrey CR, Cohen FE, McKerrow JH. Aryl ureas represent a new class of anti-trypanosomal agents. *Chem Biol*. 2000;7. https://doi.org/10.1016/S1074-5521(00)00018-1.

163 Roush WR, Hernandez AA, McKerrow JH, Selzer PM, Hansell E, Engel JC. Design, synthesis and evaluation of D-Homophenylalanyl epoxysuccinate inhibitors of the trypanosomal cysteine protease cruzain. In: Tetrahedron. Vol 56. ; 2000. http://doi.org/10.1016/S0040-4020(00)00882-6.

164 Beaulieu C, Isabel E, Fortier A, et al. Identification of potent and reversible cruzipain inhibitors for the treatment of Chagas disease. *Bioorganic Med Chem Lett*. 2010;20. https://doi.org/10.1016/j.bmcl.2010.10.015.

165 Royo S, Schirmeister T, Kaiser M, et al. Antiprotozoal and cysteine proteases inhibitory activity of dipeptidyl enoates. *Bioorganic Med Chem*. 2018;26:4624–4634. https://doi.org/10.1016/j.bmc.2018.07.015.

166 Royo S, Rodríguez S, Schirmeister T, Kesselring J, Kaiser M, González FV. Dipeptidyl Enoates As Potent Rhodesain Inhibitors That Display a Dual Mode of Action. *Chem Med Chem*. 2015;10. https://doi.org/10.1002/cmdc.201500204.

167 Latorre A, Schirmeister T, Kesselring J, et al. Dipeptidyl Nitroalkenes as Potent Reversible Inhibitors of Cysteine Proteases Rhodesain and Cruzain. *ACS Med Chem Lett*. 2016;7. https://doi.org/10.1021/acsmedchemlett.6b00276.

168 Ehmke V, Winkler E, Banner DW, et al. Optimization of Triazine Nitriles as Rhodesain Inhibitors: Structure-Activity Relationships, Bioisosteric Imidazopyridine Nitriles, and X-ray Crystal Structure Analysis with Human CathepsinL. *Chem Med Chem*. 2013;8. https://doi.org/10.1002/cmdc.201300112.

169 Vicik R, Hoerr V, Glaser M, et al. Aziridine-2,3-dicarboxylate inhibitors targeting the major cysteine protease of Trypanosoma brucei as lead trypanocidal agents. *Bioorganic Med Chem Lett*. 2006;16. https://doi.org/10.1016/j.bmcl.2006.02.026.

170 Ponte-Sucre A, Vicik R, Schultheis M, Schirmeister T, Moll H. Aziridine-2,3-dicarboxylates, peptidomimetic cysteine protease inhibitors with antileishmanial activity. *Antimicrob Agents Chemother*. 2006;50. https://doi.org/10.1128/AAC.01430-05.

171 De Souza ML, De Oliveira Rezende Junior C, Ferreira RS, et al. Discovery of Potent, Reversible, and Competitive Cruzain Inhibitors with Trypanocidal Activity: A Structure-Based Drug Design Approach. J Chem Inf Model. 2020;60(2). http://doi.org/10.1021/acs.jcim.9b00802.

172 Brak K, Kerr ID, Barrett KT, et al. Nonpeptidic tetrafluorophenoxymethyl ketone cruzain inhibitors as promising new leads for chagas disease chemotherapy. *J Med Chem*. 2010;53. https://doi.org/10.1021/jm901633v.

173 Chen YT, Brinen LS, Kerr ID, et al. In vitro and in vivo studies of the trypanocidal properties of WRR-483 against Trypanosoma cruzi. *PLoS Negl Trop Dis*. 2010;4. https://doi.org/10.1371/journal.pntd.0000825.

174 Jones BD, Tochowicz A, Tang Y, et al. Synthesis and Evaluation of Oxyguanidine Analogues of the Cysteine Protease Inhibitor WRR-483 against Cruzain. *ACS Med Chem Lett*. 2016;7. https://doi.org/10.1021/acsmedchemlett.5b00336.

175 Ndao M, Beaulieu C, Black WC, et al. Reversible cysteine protease inhibitors show promise for a chagas disease cure. *Antimicrob Agents Chemother*. 2014;58. https://doi.org/10.1128/AAC.01855-13.

176 d'Avila-Levy CM, Marinho FA, Santos LO, Martins JL, Santos ALS, Branquinha MH. Antileishmanial activity of MDL 28170, a potent calpain inhibitor. *Int J Antimicrob Agents*. 2006;28. https://doi.org/10.1016/j.ijantimicag.2006.03.021.

177 Sangenito LS, Ennes-Vidal V, Marinho FA, et al. Arrested growth of Trypanosoma cruzi by the calpain inhibitor MDL28170 and detection of calpain homologues in epimastigote forms. *Parasitology*. 2009;136. https://doi.org/10.1017/S0031182009005629.

178 Ennes-Vidal V, Menna-Barreto RFS, Santos ALS, Branquinha MH, d'Avila-Levy CM. Effects of the calpain inhibitor MDL28170 on the clinically relevant forms of Trypanosoma cruzi in vitro. *J Antimicrob Chemother*. 2010;65. https://doi.org/10.1093/jac/dkq154.

179 Ennes-Vidal V, Menna-Barreto RFS, Santos ALS, Branquinha MH, d'Avila-Levy CM. MDL28170, a calpain inhibitor, affects Trypanosoma cruzi metacyclogenesis, ultrastructure and attachment to Rhodnius prolixus midgut. *PLoS ONE*. 2011;6. https://doi.org/10.1371/journal.pone.0018371.

180 Berg M, Van der Veken P, Joossens J, et al. Design and evaluation of Trypanosoma brucei metacaspase inhibitors. *Bioorganic Med Chem Lett Published online*. 2010. https://doi.org/10.1016/j.bmcl.2010.01.099.

181 de Castro E, Reus TL, de Aguiar AM, Ávila AR, de Arruda Campos Brasil de Souza T. Procaspase-activating compound-1 induces apoptosis in Trypanosoma cruzi. Apoptosis. 2017;22(12). http://doi.org/10.1007/s10495-017-1428-5.

ANEXO II

Biochemical and Biophysical Research Communications 687 (2023) 149185

Contents lists available at ScienceDirect

Biochemical and Biophysical Research Communications

journal homepage: www.elsevier.com/locate/ybbrc

Metacaspase of *Saccharomyces cerevisiae* (ScMCA-Ia) presents different catalytic cysteine in a processed and non-processed form

Laura de Azevedo Maffeis Dalzoto [a,1], Mariana Nascimento Romero Trujilho [a,1], Taiz dos Reis Santos [a], João Pedro Martins Silva Costa [a], Ane Caroline Moreira Duarte [b], Wagner Alves de Souza Judice [a], Marcelo Ferreira Marcondes [c], Maurício Ferreira Marcondes Machado [a,b,*]

[a] *Interdisciplinary Center for Biochemical Research, University of Mogi das Cruzes, Av Dr. Cândido Xavier de Almeida e Souza, 200, 08780-991, Mogi das Cruzes, Brazil*
[b] *Technological Research Center, University of Mogi das Cruzes, Av Dr. Cândido Xavier de Almeida e Souza, 200, 08780-991, Mogi das Cruzes, Brazil*
[c] *Department of Biophysics, São Paulo Federal University, Rua Pedro de Toledo, 669, 7° floor, 04039-032, São Paulo, Brazil*

ARTICLE INFO

Keywords:
Metacaspase
Catalytic cysteine
Mutants
Autoprocessing

ABSTRACT

Metacaspases are cysteine proteases belonging to the CD clan of the C14 family. They possess important characteristics, such as specificity for cleavage after basic residues (Arg/Lys) and dependence on calcium ions to exert their catalytic activity. They are defined by the presence of a large subunit (p20) and a small subunit (p10) and are classified into types I, II, and III. Type I metacaspases have a characteristic pro-domain at the N-terminal of the enzyme, preceding a region rich in glutamine and asparagine. In the yeast *Saccharomyces cerevisiae*, a type I metacaspase is found. This organism encodes a single metacaspase that participates in the process of programmed cell death by apoptosis. The study focuses on cloning, expressing, and mutating Saccharomyces cerevisiae metacaspase (ScMCA-Ia). Mutations in Cys^{155} and Cys^{276} were introduced to investigate autoprocessing mechanisms. Results revealed that Cys^{155} plays a crucial role in autoprocessing, initiating a conformational change that activates ScMCA-Ia. Comparative analysis with TbMCA-IIa highlighted the significance of the N-terminal region in substrate access to the active site. The study proposes a two-step processing mechanism for type I metacaspases, where an initial processing step generates the active form, followed by a distinct intermolecular processing step. This provides new insights into ScMCA-Ia's activation and function. The findings hold potential implications for understanding cellular processes regulated by metacaspases. Overall, this research significantly advances knowledge in metacaspase biology.

1. Introduction

Metacaspases belong to the CD clan of the C14 protease family and share structural similarities with mammalian caspases [1]. Caspases are aspartate-specific proteases that cleave substrate containing aspartic acid at the P_1 position. Most proteins in the C14 family are expressed in a zymogen form and become activated through proteolysis, forming an active dimer [2,3]. Metacaspases are present in plant, fungi, and protozoa, but absent in metazoans [2,4].

Metacaspases are cysteine proteases that were discovered in a simple eukaryotic cell, which shows structural similarity with a mammal's caspase, known as metacaspase [1]. Three types of metacaspases have been described: type I metacaspase, which contains an N-terminal pro-domain rich in proline, asparagine, and glutamine; type II metacaspase, which lacks an N-terminal pro-domain; and type III metacaspase, which presents the p10 subunit before the p20 [3,5,6].

While metacaspases share structural similarities with caspase, they exhibit biochemical differences. Metacaspases have a P_1 specifity for basic residues (Arg or Lys) [7] and are expressed as active monomers, requiring an autoprocessing event for activation and substrate selection

Abreviations: ScMCA-Ia, *Saccharomyces cerevisiae* metacaspase; TbMCA-IIa, *Trypanosoma brucei* metacaspase 2.

* Corresponding author. Interdisciplinary Center for Biochemical Research, University of Mogi das Cruzes, Av. Dr. Cândido Xavier de Almeida e Souza, 200, 08780-991, Mogi das Cruzes, Brazil.
E-mail address: mauriciomachado@umc.br (M.F.M. Machado).

[1] Both authors contributed equally to this work.

https://doi.org/10.1016/j.bbrc.2023.149185
Received 19 October 2023; Accepted 29 October 2023
Available online 31 October 2023
0006-291X/© 2023 Elsevier Inc. All rights reserved.

[2,4,8]. The activity of *Trypanosoma brucei* metacaspase 2 (TbMCA-IIa) is calcium-dependen, and autoprocessing occurs at two sites: one at the N-terminal after the Lys55 residue, and another at the C-terminal after the Lys288 residue, resulting in a three-peptide chain that remains associated [9]. The three-dimensional structure of TbMCA-IIa was obtained using inactive mutants (C213 A/G) to prevent autoprocessing of the active full-length recombinant enzyme. This was crucial because even the non-processed form of TbMCA-IIa could undergo non-specific autoproccessing/degradation [2].

Autoprocessing and activity od metacaspases are intrinsically correlated with Ca2+ concentration and have two dissociation constants. One with higher affinity as important for the autoprocessing event, while another with lower affinity is crucial for substrate specificity [4].

Saccharomyces cerevisiae is a yeast that encodes only one metacaspase, known as Yeast Caspase-1 (ScMCA-Ia) [10]. ScMCA-Ia is a type I metacaspase directly associated with programmed cell death, cell cycle regulation and elimination of a protein aggregates [10–13]. The crystallographic structure of ScMCA-Ia reveals that this enzyme consists of a large subunit (P_{20}) and a small subunit (P_{10}), and the autoprocessing occurs after the residues Lys^{331} and/or Lys^{334} [14].

When compared with TbMCA-IIa, the structure of ScMCA-Ia reveals some similarities, such as the arrangement of calcium binding site residues, the catalytic dyad, and the lysine where autoprocessing occurs at C-terminal [2,14]. Interestingly, the structure of ScMCA-Ia was elucidated with a truncated enzyme, ScMCA-Ia was treated with V8 protease which removes 86 amino acids from the N-terminal [14].

The crystallographic structure of TbMCA-IIa has been resolved with its N-terminal region, revealing that it surrounds the protein, obstructing access to the Cys/His catalytic dyad [2,4]. It has been suggested that another cysteine may act as a catalytic residue in a non-processed form of TbMCA-IIa [2]. Some data indicate that the autoprocessing event is crucial to relocating the N-terminal region, exposing residues at the catalytic site, and thereby enhancing the proteolytic activity of TbMCA-IIa [8].

The N-terminal amino acids of ScMCA-Ia, rich in glutamine and asparagine, have a capacity to promote the precipitation of this enzyme. Consequently, biochemical assays with ScMCA-Ia are very challenging due to protein aggregation; the N-terminal of ScMCA-Ia act as a modulator, causing the protein to become insoluble [14,15]. In this study, we produced both forms of ScMCA-Ia: the complete form and a form without 86 amino acids residues from the N-terminal (truncated ScMCA-Ia – t-ScMCA-Ia).

In this work, we produced both forms of ScMCA-Ia forms (complete and truncated) each containing a site direct mutagenesis in a catalytic cysteine (Cys^{276}) [14]. The aim was to analyze the effect of calcium in ScMCA-Ia. However, curiously, mutation of this Cys by Ala (C276A) could not halt the autoprocessing event of ScMCA-Ia in either form. To further evaluate whether ScMCA-Ia possesses a second cysteine involved in its autoprocessing event, we aligned sequences of TbMCA-IIa and ScMCA-Ia, and subsequently generated a mutant in Cys^{155}, ScMCA-Ia C155A mutant does not present autoprocessing event,

These findings demonstrate that this enzyme possesses two catalytic cysteines, and the autoprocessing event induces a conformational change that alters the configuration of the catalytic domain.

2. Experimental procedures

2.1. Cloning of ScMCA-Ia complete and truncated form

From *S. cerevisiae* strain BY4742 plated on YPD medium (1 % yeast extract, 2 % dextrose, 2 % peptone and 2 % agar), PCR was performed using a Pfu polymerase (Thermo). For the complete ScMCA-Ia (ScMCA-Ia), the forward primer (5′-GGTGGTGGATCCATGTATCCAGGTAGTG-GACGTTAC-3′) and reverse primer (5′-ACCACCCTCGAGTTACATAA-TAAATTGCAGATTTACGTC-3′) were utilized. The amplified sequence was inserted into the BamHI and XhoI sites of pET28(a)+ (Novagen).

For truncated form of ScMCA-Ia (t-ScMCA-IA), PCR was performed using a Pfu polymerase (Thermo) with ScMCA-Ia as a template. The forward primer (5′–ATTTGCTAGCCCCCCTATGGCTTATAA–3′) and reverse primer (5′–ATCTGCAATTTATTATGTAGGAATTCGCGC–3′) were used. The amplified sequence was inserted in to the NheI and EcorRI sites of pET28(a)+ (Novagen). Both ScMCA-Ia and t-ScMCA-Ia enzymes are encoding with N-terminal His-tag (6X-His).

2.2. Site direct mutagenesis of ScMCA-Ia

To introduce site-direct mutagenesis in ScMCA-Ia and t-ScMCA-Ia (Table 1), we followed a protocol developed by Ho et al. (1989) with modifications [16]. All PCRs were carried out using Pfu polymerase (Thermo) with a specific primers. The PCR products of insert and pet28 (a)+ were treated with 10 U/mL of T5 exonuclease in a buffer containing 500 mM Tris, 50 mM $MgCl_2$, 50 mM DTT, 0,25 g/mL PEG 800, at pH 7.0. The vector/insert proportion was 1:4 [17], and the reaction was incubated at 37 °C for 3 h. The resulting reactions were then transformed into BL21(DE3) pLysS *Escherichia coli*.

2.3. Expression of ScMCA-Ia WT and Mutants

Bacteria containing ScMCA-Ia wild type (WT) and mutants, as well as t-ScMCA-Ia WT, were initially grown in 10 mL Luria broth medium supplemented with kanamycin (50 μg/mL) and incubated at 37 °C overnight (approximately 16 h) with shaking at 150 rpm. The overnight cultures were then transferred to 1 L of LB medium at 37 °C and grown until the culture density reached an A_{600} of 0.4. The temperature was them reduced to 20 °C until the cell density reached an A_{600} of 0.6–0.7. Isopropyl-b-D-1-thiogalactopyranoside was added to a final concentration of 0.5 mM, and the cells were incubated at 20 °C for 14–16 h before being harvested by centrifugation at 4000×*g* for 10 min at 4 °C. The pellet was subsequently stored at −70 °C until needed.

The cell pellet was resuspended in 20 mL of 50 mM sodium phosphate pH 8.0, 500 mM NaCl, 20 mM imidazole, 1 mg/mL lysozyme. It was then incubated on ice for 30 min before the addition of 5 μg/mL RNase, 5 μg/mL DNase and 0.02 % Triton X-100. The solution was further incubated for 30 min on ice before being centrifuged at 26,000×*g* for 20 min at 4 °C and the supernatant was recovered. Lysates were centrifuged and filtered through in 0.45 μM membrane.

2.4. Purification of ScMCA-Ia WT and Mutants

The cell pellet was resuspended in 20 mL of solution containing 50 mM sodium phosphate at pH 8.0, 500 mM NaCl, 20 mM imidazole, and 1 mg/mL lysozyme. This mixture was incubated on ice for 30 min before the addition of 5 μg/mL RNase, 5 μg/mL DNase and 0.02 % Triton X-100. After an additional 30-min incubation on ice, the solution was centrifuged at 26,000×*g* for 20 min at 4 °C, and the supernatant was collected. Lysates were then centrifuged and filtered through a 0.45 μM membrane.

The resulting material was loaded onto a HisTrap Ni^{2+} Sepharose column (GE Healthcare) connected to an AKTA-Start chromatograph (GE Healthcare). The column had been previously equilibrated with a binding buffer consisting of 50 mM Tris at pH 7.5 and 100 mM NaCl,

Table 1
Primers to produced ScMCA-Ia and t-ScMCA-Ia mutants.

Mutant		Primer
C155A	Forward	5′ AAATCAACTGCGTGGT**GCT**ATCAATGATGCTC 3′
	Reverse	5′ GAGCATCATTGAT**AGC**ACCACGCAGTTGATTT 3′
C276A	Forward	5′ ACAGCATTGTTTGACTCT**GCT**CATTCGGGTACAGTGTTG 3′
	Reverse	5′ CAACACTGTACCCGAATG**AGC**AGAGTCAAACAATGCTGT 3′

with a flow rate of 1.0 mL/min. The column was washed with 5 mL of binding buffer, and recombinant ScMCA-Ia WT and mutants were purified and eluted using a step gradient of imidazole concentrations (50, 100, 200, 300 and 500 mM) in the same buffer. The recombinant ScMCA-Ia WT and mutants were found to elute between 200 and 300 mM imidazole (as confirmed by SDS/PAGE analysis), and the protein were combined.

To desalt the pooled protein, it was loaded onto a HiTrap 26/10 Desalting size-exclusion column, 5 mL (GE Healthcare) and equilibrated in a buffer containing 50 mM Tris at pH 7.4 and 100 mM NaCl (NaCl/Tris buffer). Elution fractions were analyzed using SDS/PAGE, and the fractions containing pure recombinant ScMCA-Ia were collected. These fractions were stored in NaCl/Tris buffer containing 30 % glycerol at −20 °C. To avoid any decrease in ScMCA-Ia activity, repeated freeze-thaw cycles were consequently avoided.

2.5. Western blotting of ScMCA-Ia WT and Mutants

To confirm the presence of ScMCA-Ia in both processed and non-processed forms, a western blotting assay was conducted using a 6x-His-tag antibody (MA1-21315-HRP – Thermo). The SDS-PAGE gel was the transferred onto a PVDF membrane (Bio-Rad) for 5 min a Trans-Blot Turbo (Bio-Rad) following the manufacturer's instructions.

The PVDF membrane was subsequently washed with a PBS buffer (10 mM Na_2HPO_4, 150 mM NaCl – pH 7.4) with the addiction of 5 % BSA and 0.01 % Tween 20 and left to incubate for 1 h with agitation at room temperature. Following this, mebrane was washed three times with PBS, and then incubated with 6x-His-tag antibody (Thermo), which was diluted to ratio of 1:30,000 in PBS with 5 % BSA and 0.01 % Tween 20. This incubation took place for 18 h at 4 °C with constant agitation.

After the antibody incubation, the membrane was washed with PBS and subsequently developed SuperSignal-West Pico (Thermo) in a photodocumentator ChemiDoc MP Imaging System (Bio-Rad).

3. Results and discussion

SDS-PAGE analysis reveals that ScMCA-Ia WT, after the desalination process, exhibits a lower concentration of protein (Fig. 1A). This is because after its autoprocessing event, this enzyme can self-degrade very rapidly, resulting in the observation of a small fragment of around 14 kDa. A similar effect has been observed with other metacaspases [2,18]. Interestingly, western blotting shows that ScMCA-Ia WT exhibits a small concentration of the non-processed form (Fig. 1B).

Analysis of ScMCA-Ia C276A reveal the presence of two fragments around 43 kDa (Fig. 1). These fragments are described to correspond to the processed form of ScMCA-Ia. Interestingly Cys^{276} serve as the catalytic cysteine for this enzyme [14]. It has been suggested that other metacaspases like TbMCA-IIa of *T.brucei* and metacaspase 9 of *A. thaliana*, may have a second cysteine could play role in the activation of these enzymes [2,19].

TbMCA-IIa possesses a cysteine at position 92, which is located in the N-terminal region. Interestingly, ScMCA-Ia also contains a conserved cysteine in the same region (Cys^{155}), although it is not present in the N-terminal of this enzyme. When we examined the three-dimensional structure of ScMCA-Ia (PDB 4F6O), we found that the distance of Cys^{276} and the catalytic histidine (His^{220}) is 9.6 Å, whereas Cys^{155} has just 7.2 Å (Fig. 2) [14].

With the knowledge that the crystal-defined structure of ScMCA-Ia lacks the first 86 N-terminal amino acids, we aimed to assess how these amino acids might interact with the enzyme's catalytic site. For this purpose, we overlaid the ctructures of ScMCA-Ia (PDB: 4F6O) and TbMCA-IIa (PDB: 4AFR), which was crystallized using an inactive mutant, allowing for the visualization on the N-terminal region encompassing 70 amino acids. In Fig. 3, ScMCA-Ia structure is depicted in gray, while TbMCA-IIa structure is shown in brown, with its N-terminal segment highlighted in purple.

This generated image reveals an intriguing feature of TbMCA-IIa N-terminal region it envelops the entire protein and extends through the active site of the enzyme. This positioning obstructs the interaction necessary for catalysis between the cysteine and histidine of the catalytic dyad.

To assess whether Cys^{155} participates in autoprocessing event of ScMCA-Ia, we created a C155A mutant. Indeed SDS-PAGE analysis demonstrate that this mutant does not undergo an autoprocessed event, providing further support for our hypothesis that this cysteine is crucial for the initial processing of ScMCA-Ia.

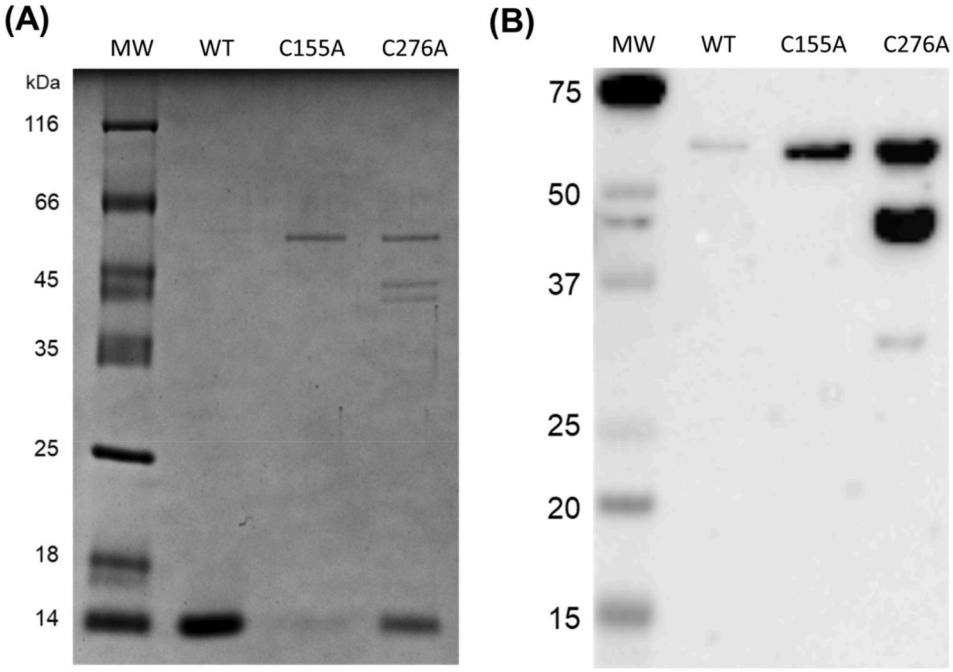

Fig. 1. Analyses of ScMCA-Ia. (A) SDS-PAGE of ScMCA-Ia WT, ScMCA C155A and ScMCA-Ia C276A and (B) Western blotting with 6X-His-tag antibody of ScMCA-Ia WT, ScMCA C155A and ScMCA-Ia C276A.

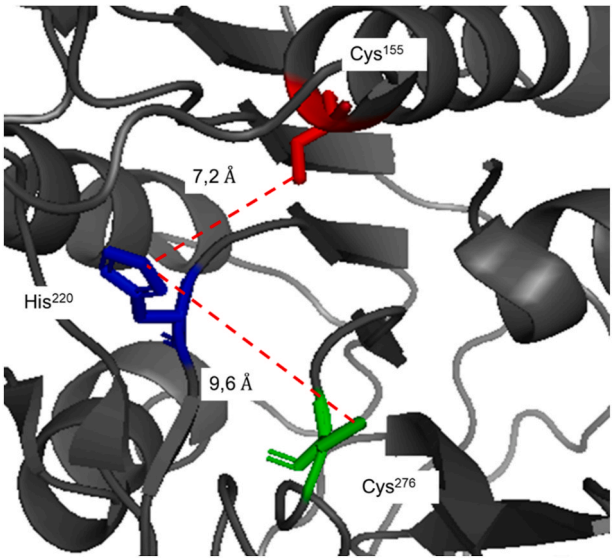

Fig. 2. Three-dimensional structure of ScMCA-Ia showing the catalytic site. Three-dimensional structure of ScMCA-Ia approaching the catalytic site, highlighting the amino acids that compose it and the distance in angstrom (Å) between them. In red, cysteine 155; in blue histidine 220; and in green cysteine 276. The distance between Cys^{155} and His^{220} is established as 7.2 Å, and the distance between Cys^{276} and His^{220} is established as 9.6 Å. (For interpretation of the references to colour in this figure legend, the reader is referred to the Web version of this article.)

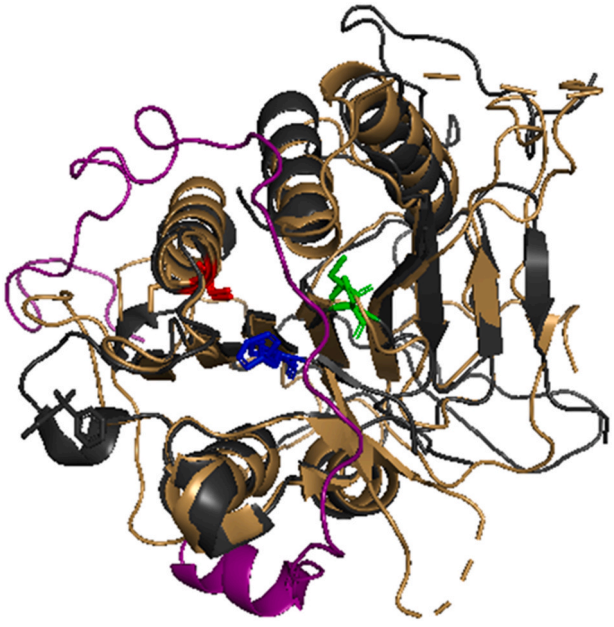

Fig. 3. Three-dimensional structure of ScMCA-Ia and TbMCA-IIa, superimposed, highlighting the catalytic sites. Three-dimensional structures of ScMCA-Ia (PDB: 4F6O [14]), in gray, and TbMCA-IIa (PDB 4AFR [2]), in brown, superimposed. In TbMCA-IIa, the N-terminal is highlighted, in purple, consisting of 70 amino acids. For both, the amino acids that make up the catalytic site stand out. In ScMCA-Ia, in red is Cys^{155}, in blue is His^{220}, and in green is Cys^{276}. For TbMCA-IIa, in red is Cys^{92}, in blue is His^{158}, and in green is Cys^{213}. (For interpretation of the references to colour in this figure legend, the reader is referred to the Web version of this article.)

The ScMCA-Ia in its complete form has been described above to undergo a self-degradation process. It has been noted that this form also undergoes precipitation (data do not show), likely due to the presence of an N-terminal region rich in glutamine and asparagine, rendering it hydrophobic [14,15]. To generate a soluble ScMCA-Ia, we expressed a truncated form with deletion of 86 amino acids from the N-terminal (t-ScMCA-Ia), building upon prior work by Wong et al. (2012) who treated ScMCA-Ia with V8 protease [14] (See Fig. 2).

Unlike ScMCA-Ia, t-ScMCA-Ia does not undergo a self-degradation process and cannot precipitated (Fig. 4). This enhances the stability of the enzyme significantly, t-ScMCA-Ia presents same molecular weight of processed ScMCA-Ia (43 kDa). It is noteworthy that this enzyme continues to undergo autoprocessing, although it was described that the initial processing of ScMCA-Ia occurs after Arg^{72} and Lys^{86} residues, both of which have been deleted in truncated form [14].

However, both cysteine mutants t-ScMCA-Ia C276A and t-ScMCA-Ia C155A continue to undergo processing, but in the C-terminal region. Studies on others metacaspases have shown that in *T.brucei*, TbMCA-IIIa is capable of processing TbMCA-IVa, providing evidence of proteolytic activation similar to caspases [3,20].

Western blotting data reveals that the ScMCA-Ia C276A mutant does not undergo self-degradation, corroborating that this residue acts as a catalytic. After autoprocessing coordinated by Cys^{155}, a third fragment around 33 kDa was noted. This is the same size as the processing observed with t-ScMCA-Ia. Since our antibody recognizes the histidine tail present at the N-terminal, this second processing occurs in C-terminal. As described for metacaspase of *Candida glabrata*, autoprocessing occurs, and the processed enzyme can process another metacaspase, which is a time-consuming event [21].

These data demonstrate that once autoprocessed, ScMCA-Ia is capable of performing intermolecular processing of other ScMCA-Ia molecules, generating an active form of this enzyme.

4. Conclusions

The investigation into ScMCA-Ia has provided significant insights into its autoprocessing and activation mechanisms. The desalination process revealed a lower concentration of ScMCA-Ia WT due to its rapid self-degradation following autoprocessing. Interestingly, traces of the

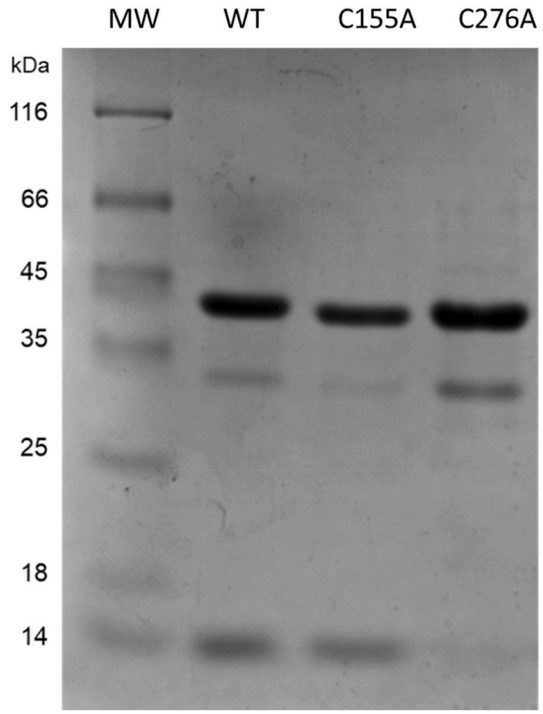

Fig. 4. Analyses of t-ScMCA-Ia WT and mutants. SDS-PAGE of ScMCA-Ia WT, ScMCA C155A and ScMCA-Ia C276A and.

non-processed form were detected through western blotting.

The analysis of the C276A mutant showcased two fragments around 43 kDa, indicating the processed form of ScMCA-Ia, reinforcing the pivotal role of Cys276 as the catalytic cysteine. This aligns with suggestions that second cysteines may play a role in activating similar enzymes.

Obtaining the mutants was important for us to elucidate and deepen the knowledge surrounding the activation of ScMCA-Ia, that surfers processing steps to release its active form, capable of cleaving protein substrates. The mutation in the Cys^{155} residue demonstrated the presence of a second catalytic cysteine in the structure of ScMCA-Ia, which is crucial in the enzyme's autoprocessing. Proposing that initially the action of Cys^{155} directly impacts the action of catalytic cysteine (Cys^{276}), since the first autoprocessing must occur to generate the active form of ScMCA-Ia, where the active site composed of the catalytic dyad (Cys^{276} and His^{220}) is free for interaction with the substrate.

Interestingly, t-ScMCA-Ia exhibited stability and molecular weight similar to the processed ScMCA-Ia. Both cysteine mutants, t-ScMCA-Ia C276A and t-ScMCA-Ia C155A, demonstrated processing in the C-terminal region. This aligns with studies on other metacaspases, indicating proteolytic activation akin to caspases.

Comparative analysis of the structure of ScMCA-Ia showed that in theory, the N-terminal is like that of TbMCA-IIa, located around the enzyme and directly influencing the access of the substrate to the active site. Confirming our hypothesis that Cys^{155} interacts primarily with His^{220}, carrying out autoprocessing so that a conformational change occurs at the N-terminal and the release of the enzyme's active site, that is, its active form.

Our data provided a different perspective on the autoprocessing that occurs in type I metacaspases, such as ScMCA-Ia. Pointing out that a first processing occurs generating the active form of ScMCA-Ia, which will subsequently undergo a second processing, however this is not autoprocessing, but rather intermolecular processing between metacaspases.

These findings underscore the ability of autoprocessed ScMCA-Ia to intermolecularly process other ScMCA-Ia molecules, generating an active enzyme form. This study enhances our understanding of the intricate regulatory pathways governing programmed cell death and cellular homeostasis.

CRediT authorship contribution statement

Laura de Azevedo Maffeis Dalzoto: Formal analysis, Investigation, Resources. **Mariana Nascimento Romero Trujilho:** Formal analysis, Investigation, Methodology. **Taiz dos Reis Santos:** Investigation, Methodology. **João Pedro Martins Silva Costa:** Investigation, Methodology, Resources. **Ane Caroline Moreira Duarte:** Investigation, Methodology. **Wagner Alves de Souza Judice:** Data curation, Writing – original draft. **Marcelo Ferreira Marcondes:** Resources, Validation, Visualization, Writing – original draft. **Maurício Ferreira Marcondes Machado:** Conceptualization, Funding acquisition, Project administration, Supervision, Writing – original draft, Writing – review & editing.

Declaration of competing interest

The authors declare that they have no known competing financial interests or personal relationships that could have appeared to influence the work reported in this paper.

Acknowledgements

This work was supported by FAPESP grant 2022/06394-0 to MFMM, FAPESP grant 2019/27813-8 to MFM and FAPESP grant 2021/01503-2 to WASJ.

References

[1] A.G. Uren, K. O'Rourke, L. Aravind, M.T. Pisabarro, S. Seshagiri, E.V. Koonin, V. M. Dixit, Identification of paracaspases and metacaspases: two ancient families of caspase-like proteins, one of which plays a key role in MALT lymphoma, Mol. Cell (2000), https://doi.org/10.1016/s1097-2765(00)00094-0.

[2] K. McLuskey, J. Rudolf, W.R. Proto, N.W. Isaacs, G.H. Coombs, C.X. Moss, J. C. Mottram, Crystal Structure of a Trypanosoma Brucei Metacaspase, Proc Natl Acad Sci U S A., 2012, https://doi.org/10.1073/pnas.1200885109.

[3] E.A. Minina, N.S. Coll, H. Tuominen, P.V. Bozhkov, Metacaspases versus caspases in development and cell fate regulation, Cell Death Differ. (2017), https://doi.org/10.1038/cdd.2017.18.

[4] M.F.M. Machado, M.F. Marcondes, M.A. Juliano, K. McLuskey, J.C. Mottram, C. X. Moss, L. Juliano, V. Oliveira, Substrate specificity and the effect of calcium on Trypanosoma brucei metacaspase 2, FEBS J. (2013), https://doi.org/10.1111/febs.12248.

[5] M. Klemenčič, C. Funk, Evolution and structural diversity of metacaspases, J. Exp. Bot. (2019), https://doi.org/10.1093/jxb/erz082.

[6] E.A. Minina, J. Staal, V.E. Alvarez, J.A. Berges, I. Berman-Frank, R. Beyaert, K. D. Bidle, F. Bornancin, M. Casanova, J.J. Cazzulo, C.J. Choi, N.S. Coll, V.M. Dixit, M. Dolinar, N. Fasel, C. Funk, P. Gallois, K. Gevaert, E. Gutierrez-Beltran, S. Hailfinger, M. Klemenčič, E.V. Koonin, D. Krappmann, A. Linusson, M.F. M. Machado, F. Madeo, L.A. Megeney, P.N. Moschou, J.C. Mottram, T. Nyström, H. D. Osiewacz, C.M. Overall, K.C. Pandey, J. Ruland, G.S. Salvesen, Y. Shi, A. Smertenko, S. Stael, J. Ståhlberg, M.F. Suárez, M. Thome, H. Tuominen, F. Van Breusegem, R.A.L. van der Hoorn, A. Vardi, B. Zhivotovsky, E. Lam, P.V. Bozhkov, Classification and nomenclature of metacaspases and paracaspases: No more confusion with caspases, Mol. Cell (2020), https://doi.org/10.1016/j.molcel.2019.12.020.

[7] S.M. Hill, T. Nyström, The dual role of a yeast metacaspase: what doesn't kill you makes you stronger, Bioessays (2015), https://doi.org/10.1002/bies.201400208.

[8] J.M. Gilio, M.F. Marcondes, D. Ferrari, M.A. Juliano, L. Juliano, V. Oliveira, M.F. M. Machado, Processing of metacaspase 2 from Trypanosoma brucei (TbMCA2) broadens its substrate specificity, Biochim. Biophys. Acta, Proteins Proteomics 1865 (2017), https://doi.org/10.1016/j.bbapap.2017.01.002.

[9] C.X. Moss, G.D. Westrop, L. Juliano, G.H. Coombs, J.C. Mottram, Metacaspase 2 of Trypanosoma brucei is a calcium-dependent cysteine peptidase active without processing, FEBS Lett. (2007), https://doi.org/10.1016/j.febslet.2007.11.009.

[10] A. Shrestha, S. Brunette, W.L. Stanford, L.A. Megeney, The metacaspase Yca1 maintains proteostasis through multiple interactions with the ubiquitin system, Cell Discov (2019), https://doi.org/10.1038/s41421-018-0071-9.

[11] F. Madeo, E. Herker, C. Maldener, S. Wissing, S. Lächelt, M. Herlan, M. Fehr, K. Lauber, S.J. Sigrist, S. Wesselborg, K.U. Fröhlich, A caspase-related protease regulates apoptosis in yeast, Mol. Cell (2002), https://doi.org/10.1016/S1097-2765(02)00501-4.

[12] L. Tsiatsiani, F. Van Breusegem, P. Gallois, A. Zavialov, E. Lam, P.V. Bozhkov, Metacaspases, Cell Death Differ. (2011), https://doi.org/10.1038/cdd.2011.66.

[13] R.E.C. Lee, L.G. Puente, M. Kærn, L.A. Megeney, A non-death role of the yeast metacaspase: yca1p alters cell cycle dynamics, PLoS One (2008), https://doi.org/10.1371/journal.pone.0002956.

[14] A.H.H. Wong, C. Yan, Y. Shi, Crystal structure of the yeast metacaspase Yca1, J. Biol. Chem. (2012), https://doi.org/10.1074/jbc.M112.381806.

[15] M. Erhardt, R.D. Wegrzyn, E. Deuerling, Extra N-terminal residues have a profound effect on the aggregation properties of the potential yeast prion protein Mca1, PLoS One (2010), https://doi.org/10.1371/journal.pone.0009929.

[16] S.N. Ho, H.D. Hunt, R.M. Horton, J.K. Pullen, L.R. Pease, Site-directed mutagenesis by overlap extension using the polymerase chain reaction, Gene 77 (1989) 51–59, https://doi.org/10.1016/0378-1119(89)90358-2.

[17] Y. Xia, K. Li, J. Li, T. Wang, L. Gu, L. Xun, T5 exonuclease-dependent assembly offers a low-cost method for efficient cloning and site-directed mutagenesis, Nucleic Acids Res. 47 (2019), https://doi.org/10.1093/nar/gky1169.

[18] M. Klemenčič, C. Funk, Type III metacaspases: calcium-dependent activity proposes new function for the p10 domain, New Phytol. (2018), https://doi.org/10.1111/nph.14660.

[19] B. Belenghi, M.C. Romero-Puertas, D. Vercammen, A. Brackenier, D. Inzé, M. Delledonne, F. Van Breusegem, Metacaspase activity of Arabidopsis thaliana is regulated by S-nitrosylation of a critical cysteine residue, J. Biol. Chem. (2007), https://doi.org/10.1074/jbc.M608931200.

[20] W.R. Proto, E. Castanys-Munoz, A. Black, L. Tetley, C.X. Moss, L. Juliano, G. H. Coombs, J.C. Mottram, Trypanosoma brucei metacaspase 4 is a pseudopeptidase and a virulence factor, J. Biol. Chem. (2011), https://doi.org/10.1074/jbc.M111.292334.

[21] L. Conchou, B. Doumèche, F. Galisson, S. Violot, C. Dugelay, E. Diesis, A. Page, A. L. Bienvenu, S. Picot, N. Aghajari, L. Ballut, Structural and molecular determinants of Candida glabrata metacaspase maturation and activation by calcium, Commun. Biol. 5 (2022), https://doi.org/10.1038/S42003-022-04091-4.

ANEXO III

Biochemical and Biophysical Research Communications 735 (2024) 150657

Contents lists available at ScienceDirect

Biochemical and Biophysical Research Communications

journal homepage: www.elsevier.com/locate/ybbrc

Oximic compounds as potential inhibitors of metacaspase-2 (TbMCA2) of *Trypanosoma brucei*

Laura Helena Araujo [a], Thaynan Aparecida Bueno Chagas [b], Taiz Reis [a], João Ricardo Bueno de Morais Borba [b], Mariana Nascimento Romero Trujilho [a], Laura de Azevedo Maffeis Dalzoto [a], Marcelo Ferreira Marcondes [c], Maria Aparecida Juliano [c], Wagner Alves de Souza Júdice [a], Márcia Paranho Veloso [b], Maurício Ferreira Marcondes Machado [a,*]

[a] *Interdisciplinary Center for Biochemical Research, University of Mogi das Cruzes, Av Dr. Càndido Xavier de Almeida e Souza, 200, 08780-991, Mogi das Cruzes, Brazil*
[b] *Pharmaceutical Science Department, Alfenas Federal University, Rua Gabriel Monteiro da Silva, 700, 37130-001, Alfenas, Brazil*
[c] *Department of Biophysics, São Paulo Federal University, Rua Pedro de Toledo, 669, 7° floor, 04039-032, São Paulo, Brazil*

ARTICLE INFO

Keywords:
Metacaspase
Inhibition
Oximic compounds
Inhibition mechanism

ABSTRACT

Metacaspases are a distinct class of cysteine proteases predominantly found in plants, fungi, and protozoa, crucial for regulating programmed cell death (PCD). They possess unique structural features and differ markedly from caspases in their activation mechanisms and substrate specificities, with a notable preference for binding basic residues in substrates. In this study, we introduced vanillin-derived oximic compounds to explore their pharmaceutical potential. We evaluated these compounds for their inhibitory effects on TbMCA2, a metacaspase in *Trypanosoma brucei*, identifying **AO-7**, **AO-12**, and **EO-20** as promising inhibitors. **AO-12** showed significant potential as a non-competitive inhibitor with notable IC_{50} values. Molecular docking studies were also conducted to evaluate the binding affinity of these compounds for TbMCA2. This research is particularly relevant given the urgent need for more effective and less toxic treatments for trypanosomiasis, a parasitic disease caused by trypanosomes. The absence of available vaccines and the limitations imposed by drug toxicity underscore the importance of these findings. Our study represents a significant advancement in developing therapeutic agents targeting metacaspases in trypanosomatids and highlights the necessity of understanding metacaspase regulation across various species. It provides valuable insights into inhibitor sensitivity and potential species-specific therapeutic strategies. In conclusion, this research opens promising avenues for novel therapeutic agents targeting metacaspases in trypanosomatids, addressing a critical gap in combating neglected diseases associated with these pathogens. Further research is essential to refine the efficacy and safety profiles of these compounds, aiming to deliver more accessible and effective therapeutic solutions to populations afflicted by these debilitating diseases.

1. Introduction

Human African trypanosomiasis (HAT), commonly known as sleeping sickness, remains a significant public health issue across 36 nations in sub-Saharan Africa, with approximately 60 million individuals at risk of infection. This neglected tropical disease is caused by protozoan parasites belonging to the genus *Trypanosoma*, transmitted through the bites of tsetse flies from the genus *Glossina*. The geographical distribution of HAT is restricted to latitudes between 14° North and 29° South. The disease presents in two primary forms: the West African variant, caused by *Trypanosoma brucei gambiense*, which accounts for approximately 95 % of reported cases, and the East African form, caused by *Trypanosoma brucei rhodesiense*, responsible for the remaining 5 %. The progression of the rhodesiense variant is more rapid compared to the gambiense variant, with the former progressing over approximately 6–12 weeks and the latter extending over several months to years, likely due to the parasite's enhanced adaptation to its host. Without appropriate treatment, HAT is usually fatal, and many of the available

* Corresponding author.
E-mail address: mauriciomachado@umc.br (M.F.M. Machado).

https://doi.org/10.1016/j.bbrc.2024.150657
Received 9 May 2024; Received in revised form 20 August 2024; Accepted 3 September 2024
Available online 5 September 2024
0006-291X/© 2024 Elsevier Inc. All rights are reserved, including those for text and data mining, AI training, and similar technologies.

medications for advanced stages of the disease are highly toxic [1,2].

There is a clear distinction between the early stage of the disease, known as the haemolymphatic phase (Stage 1), where the parasites proliferate throughout the blood, lymphatic system, and peripheral organs, and the late stage, termed the encephalitic phase (Stage 2), characterized by the breach of the blood-brain barrier leading to central nervous system involvement. Accurate staging of the disease is crucial for appropriate treatment but remains challenging. Recent years have witnessed significant advancements in our understanding and management of HAT, including progress in epidemiology, recognition of clinical diversity, improved diagnostic methods, innovative treatments, understanding of neuropathogenesis, and future outlooks [3–5].

Parasite proteases represent a large and diverse group of enzymes that, having vital roles in nutrition and pathogenicity, offer great potential for drug development. In the past few years, extensive research has been dedicated to a unique family of enzymes called metacaspases, these enzymes, which are associated with crucial cellular events in trypanosomes, are absent in the human host, thus arising as attractive drug targets [6,7].

Metacaspases are cysteine proteases classified within the CD clan of the C14 family. These enzymes are homologous to caspases and are found in plants, fungi, and protozoa. Metacaspases cleave their substrates after basic residues at the P_1 position and are involved in the regulation of programmed cell death (PCD) in these organisms [1–3]. They are categorized into three types based on the arrangement of their p10 and p20 subunits: Type I metacaspases, prevalent in plants, fungi, and protozoa, are characterized by a proline-rich sequence at the N-terminal, which may also include a preceding zinc-finger motif. Type II metacaspases have a linker region between the p20 and p10 subunits and are found in plants and protozoa, respectively. Type III metacaspases are specific to phytoplankton, with the p10 subunit located at the N-terminal [8,9].

Metacaspases differ from caspases in that they do not require dimerization for their activity and possess a monomeric structure consisting of six parallel and two anti-parallel β-sheets [10]. Activation of metacaspases occurs through an auto-processing event induced by calcium ions. In type II metacaspases, this event occurs within a specific region between the p20 and p10 subunits, analogous to caspase activation [8]. In contrast, type I metacaspases undergo auto-processing at the N-terminal and/or C-terminal regions, as observed in metacaspase-2 of *T. brucei* [11].

The nomenclature "metacaspase" might lead to misconceptions regarding the substrate specificity of these enzymes. While "caspase" stands for "Cysteine-ASpartate-ProteASE," metacaspases exhibit a preference for substrates with a basic residue (Arg or Lys) at the P_1 position. Therefore, a new classification and nomenclature system has been proposed. The revised nomenclature uses the root symbol MCA, preceded by the abbreviated Latin name of the species, followed by a Latin numeral representing the type of metacaspase, and a small alpha character indicating the homologous number of metacaspases in the genome [9]. For instance, the type I metacaspase-2 of *T. brucei*, previously known as TbMCA2, has been officially reclassified as TbMCA2.

In the *T. brucei* genome, five metacaspase genes have been identified, exhibiting sequence identities ranging from 40 % to 89 %, along with variations in catalytic activity [12,13]. TbMCA1 and TbMCA4 possess a serine residue in place of a catalytic cysteine, rendering them catalytically inactive pseudo-peptidases. Despite the lack of catalytic activity in TbMCA4 [14,15], this enzyme plays a crucial role in the virulence and proliferation of *T. brucei*. Metacaspases 2, -3, and -5 of *T. brucei* contain a Cys/His catalytic dyad and are enzymatically active [15].

Given that metacaspases are calcium-dependent enzymes, their activity relies on structural modifications induced by auto-processing events. These stimuli promote programmed cell death [8,16–18]. The activity of TbMCA2 depends on calcium, with activation triggering auto-processing events at Lys^{55} and Lys^{268}. Following this event, the resulting three peptide chains remain associated in the activated form of TbMCA2 [11]. The crystal structure of TbMCA2 was elucidated using an inactive mutant (C213A) due to difficulties in producing diffraction-quality crystals of the activated form [10]. The three-dimensional structure of TbMCA2 reveals its monomeric form, where the N-terminal region surrounds the protein and extends over the active site, obstructing the S_1 pocket. Despite this obstruction, a TbMCA2 mutant (K55/268G) exhibits activity in the non-processed form [11,17].

Crystallographic analysis of TbMCA2 reveals a calcium-binding site consisting of four aspartate residues (Asp^{173}, Asp^{189}, Asp^{190}, and Asp^{220}). These residues are highly conserved in metacaspases across various organisms, distinguishing them from caspases and accounting for their calcium-dependent nature [10]. Studies using a mutant of the calcium-binding site, TbMCA2 D189/190A, confirm the critical role of these aspartic acid residues in calcium binding and subsequently in TbMCA2 activity. This is evidenced by the lack of detectable activity against a synthetic substrate (Z-GGR-AMC) and the absence of auto-processing events [10].

Oxime are widely used in the pharmaceutical field due to their anti-inflammatory, anti-tumoral, and anti-parasitic properties [19–21]. Vanillin is extensively utilized in pharmaceutical product manufacturing [22,23]. While vanillin is traditionally extracted from vanilla, various synthetic methods, including chemical synthesis via oximation, have been developed for its production [24,25]. Oxime derivatives synthesized from vanillin have shown promise as antimicrobial, cytotoxic, and antioxidant agents [26].

In this study, we evaluated a series of 17 oxime compounds as potential modulators of TbMCA2 activity. Among these, three compounds - ACYL OXIME (7), ACYL OXIME (12), and ETER OXIME (20) - demonstrated robust enzyme inhibition. Furthermore, we elucidated the inhibition mechanisms, revealing that compounds 7 and 20 exhibited mixed inhibition behavior, while compound 12 displayed non-competitive behavior.

Experiments conducted with the processed form of TbMCA2, monitoring intrinsic fluorescence changes with increasing Ca^{2+} concentration, revealed the presence of two Ca^{2+} binding sites. One site exhibited high affinity (K_D of 3 μM), crucial for TbMCA2 activity, while the other demonstrated low-affinity calcium binding (K_D of 900 μM), influencing the substrate specificity of TbMCA2 [15]. The non-processed form of TbMCA2 displayed the capacity to hydrolyze small synthetic substrates, whereas hydrolysis of larger substrates was contingent on the auto-processing event, which displaced the N-terminal blockage of the active site, facilitating interaction with these substrates [17].

Compound 12 was assessed for its interaction with the calcium-binding site of TbMCA2. Intrinsic fluorescence experiments conducted with TbMCA2 wild type (TbMCA2 WT) and the mutant with calcium-binding site aspartates (Asp^{189} and Asp^{190}) mutated (TbMCA2 D189/190A) demonstrated that compound 12 induced changes in intrinsic fluorescence in TbMCA2 WT as its concentration increased. The dissociation constant ($K_D = 2.6 \pm 0.2$ μM) was closely aligned with the K_i observed for this compound ($K_i = 2.6 \pm 0.1$ μM). Interestingly, no such changes were observed in the intrinsic fluorescence of TbMCA2 D189/190A.

These findings suggest that compound 12 is a promising molecule for inhibiting TbMCA2 activity. Compound 12 exerts its inhibitory effect by disrupting the interaction with calcium, a pivotal element for TbMCA2 function.

2. Experimental procedures

2.1. Production of recombinant TbMCA2

The TbMCA2 clone was generously provided by Prof. Dr. Jeremy C. Mottram of York University. The expression of TbMCA2, which includes an N-terminal His-tag, has been previously describe [11].

Plasmids containing the TbMCA2 WT and TbMCA2 D189/190A

genes were introduced into chemically competent *Escherichia coli* BL21 (DE3) pLysS cells (Novagen, Darmstadt, Germany). Initially, the cells were cultured in 20 mL of Luria broth medium supplemented with 50 μg/mL of kanamycin (supplemented LB, sLB) and incubated at 37 °C for approximately 16 h with shaking at 1500×*g*. The pre-inoculum was then transferred to 1 L of sLB medium at 37 °C and grown until the culture reached an OD_{600} of 0.4. At this point, the temperature was reduced to 20 °C, and isopropyl-β-D-1-thiogalactopyranoside (IPTG) was added to a final concentration of 0.5 mM. The cells were incubated for an additional 16 h before being harvested by centrifugation at 3000×*g* for 20 min at 4 °C. The pellet was subsequently stored at −80 °C until needed.

2.2. Purification of recombinant TbMCA2 WT and TbMCA2 D189/190A

The cell pellet was resuspended in 20 mL of PBS (50 mM NaH_2PO_4, pH 8.0, 150 mM NaCl), supplemented with 20 mM imidazole and 1 mg/mL lysozyme, and incubated on ice for 30 min. Following this, 5 μg/mL RNase, 5 μg/mL DNase, and 0.02 % Triton X-100 were added. The solution was further incubated on ice for an additional 30 min before centrifugation at 15,000×*g* for 20 min at 4 °C, and the supernatant was collected.

The supernatant was loaded onto a 1 mL HisTrap Ni^{2+} Sepharose column (GE Healthcare, Amersham, UK) pre-equilibrated with a binding buffer consisting of 20 mM NaH_2PO_4 (pH 8.0), 150 mM NaCl, and 20 mM imidazole, using a flow rate of 1.0 mL/min. The column was then washed with 5 mL of the binding buffer, and the recombinant TbMCA2 was eluted using a step gradient with 5 mL of 50, 150, 300, and 500 mM imidazole in the same buffer. TbMCA2 was eluted with 300 mM imidazole, as confirmed by SDS-PAGE analysis, and the collected fractions were pooled. To desalt and further purify the protein, the pooled sample was loaded directly onto a Sephadex G-75 size-exclusion column prepacked with 100 mL of resin (GE Healthcare, Amersham, UK) and equilibrated with TBS buffer (50 mM Tris, pH 7.4, 150 mM NaCl). Elution fractions were analyzed by SDS-PAGE, and those containing recombinant TbMCA2 were collected. The pure TbMCA2 was stored in TBS buffer containing 30 % glycerol at −80 °C.

2.3. Peptide synthesis

FRET peptides with the sequence Abz-peptidyl-Gln-EDDnp, where Abz denotes the fluorescent group *ortho*-aminobenzoic acid and EDDnp is the C-terminal quencher moiety N-(2,4-dinitrophenyl)-ethylenediamide, were synthesized using solid-phase synthesis (as detailed in Ref. [27]) with a bench-top automated solid-phase peptide synthesizer PSSM-8 (Shimadzu, Tokyo, Japan). The molecular mass and purity of the peptides were verified by analytical HPLC using a Shimadzu 10AVP system (Shimadzu, Tokyo, Japan) and by MALDI-TOF MS using a Microflex LT system (Bruker Daltonics, Bremen, Germany). Stock solutions of the peptide substrates were prepared in distilled water, and their concentrations were determined spectrophotometrically at 365 nm using the molar extinction coefficient of the Dnp group, which is 17,300 M^{-1} cm^{-1}.

2.4. Compounds synthesis

2.4.1. Synthesis of (E)-3,4-dimethoxylbenzaldehyde oxime (2)

To a solution of 2 g (13 mmol) of 4-hydroxy-3-methoxybenzaldehyde in acetone, 1.8 g (13 mmol) of potassium carbonate was added. After 20 min, 1.62 mL (26 mmol) of iodomethane was introduced into the resulting suspension, which was stirred at room temperature for 6 h. The reaction was monitored by TLC until completion. The acetone was then removed, and 30 mL of water was added to the mixture, which was extracted with ethyl acetate (3 × 20 mL). The organic layer was dried with anhydrous sodium sulfate and concentrated to yield 2 g of 3,4-dimethoxybenzaldehyde. Subsequently, 2 g (1.2×10^{-2} mol) of 3,4-dimethoxybenzaldehyde, 16.3 g (1.2×10^{-1} mol) of sodium acetate, and 8.3 g (1.2×10^{-1} mol) of hydroxylamine hydrochloride were added to a mixture of methanol and water (8:2, 30 mL). This mixture was stirred at 80 °C for 24 h. After this period, 40 mL of water was added, and the mixture was extracted with dichloromethane (3 × 30 mL). The organic layer was washed with saturated sodium chloride solution (2 × 60 mL), dried with anhydrous sodium sulfate, and concentrated to obtain 1.8 g (82 % yield) of product 2.

2.5. General procedure for synthesis of acyl oxime 3-12

1-Ethyl-3-(3-dimethylaminopropyl)carbodiimide (EDAC, 1.5 equiv.) and the corresponding carboxylic acid (1.5 equiv.) were dissolved in dichloromethane (15 mL), and the mixture was stirred at room temperature for 15 min. After this time, the solution was cooled to 0 °C, and compound 2 (1.0 equiv.) along with 4-dimethylaminopyridine (DMAP, 0.1 equiv.) were added. The resulting mixture was stirred at room temperature overnight. The mixture was then washed with 1 M HCl (3 × 30 mL), saturated $NaHCO_3$ (3 × 20 mL), and water (2 × 50 mL). The organic layer was concentrated to yield the acyl oximes 3–12, which were purified by column chromatography.

2.5.1. (E)-3,4-Dimethoxyphenyl-(O-benzoyl)oxime (AO-3)

This product was obtained as yellow crystals in 51 % yield after chromatography (hexane/ethyl acetate 90:10 to 80:20). The melting point was 116–117 °C; IR ($\bar{\upsilon}$/cm^{-1}): 3066, 3029, 2972, 2936, 2842, 1734, 1595, 1570, 1510. ^{1}H NMR (300 MHz, $CDCl_3$) δ: 8.47 (1H, s, oxime), 8.11 (2H, dd, Ar–H, $J^3 = 8.4$ Hz, $J^4 = 1.3$ Hz), 7.63–7.57 (1H, m, Ar–H), 7.50–7.45 (3H, m, Ar–H), 7.18 (1H, dd, Ar–H, $J^3 = 8.3$ Hz, $J^4 = 1.9$ Hz), 7.39 (1H, d, Ar–H, $J^3 = 8.3$ Hz), 3.95 (3H, s, OCH_3), 3.92 (3H, s, OCH_3). ^{13}C NMR (75 MHz, $CDCl_3$) δ: 164.1 (1C, C═O), 156.6 (1C, C═N), 152.3 (1C, ar.), 149.4 (1C, ar.), 133.3 (1C, ar.), 129.6 (2C, ar.), 128.7 (1C, ar.), 128.5 (2C, ar.), 124.1 (1C, ar.), 122.7 (1C, ar.), 110.5 (1C, ar.), 108.7 (1C, ar.), 56.1 (1C, OCH_3), 55.9 (1C, OCH_3).

2.5.2. (E)-3,4-Dimethoxyphenyl-[O-(4-chloro)benzoyl]oxime (AO-4)

This product was obtained as yellow oil in 71 % yield after chromatography (hexane/ethyl acetate 90:10 to 80:20). The melting point was 130–132 °C; IR ($\bar{\upsilon}$/cm^{-1}): 3090, 3006, 2922, 2848, 1736, 1589, 1573, 1509. ^{1}H NMR (300 MHz, $CDCl_3$) δ: 8.46 (1H, s, oxime), 8.06 (2H, d, Ar–H, $J^3 = 8.8$ Hz), 7.48–7.45 (3H, m, Ar–H), 7.18 (1H, dd, Ar–H, $J^3 = 8.3$ Hz, $J^4 = 1.6$ Hz), 6.90 (1H, d, Ar–H, $J^3 = 8.3$ Hz), 3.96 (3H, s, OCH_3), 3.93 (3H, s, OCH_3). ^{13}C NMR (75 MHz, $CDCl_3$) δ: 163.3 (1C, C═O), 156.9 (1C, C═N), 152.4 (1C, ar.), 149.5 (1C, ar.), 139.8 (1C, ar.), 131.0 (2C, ar.), 128.9 (2C, ar.), 127.1 (1C, ar.), 124.2 (1C, ar.), 122.6 (1C, ar.), 110.6 (1C, ar.), 108.7 (1C, ar.), 56.1 (1C, OCH_3), 55.9 (1C, OCH_3).

2.5.3. (E)-3,4-Dimethoxyphenyl-[O-(4-nitro)benzoyl]oxime (AO-5)

This product was obtained as yellow crystals in 80 % yield after chromatography (hexane/ethyl acetate 90:10 to 80:20). The melting point was 151–152 °C; IR ($\bar{\upsilon}$/cm^{-1}): 3078, 2940, 2847, 1730, 1593, 1569, 1512. ^{1}H NMR (300 MHz, $CDCl_3$) δ: 8.49 (1H, s, oxime), 8.35–8.27 (4H, m, Ar–H), 7.47 (1H, d, Ar–H, $J^4 = 1.9$ Hz), 7.19 (1H, dd, Ar–H, $J^3 = 8.6$ Hz, $J^4 = 1.9$ Hz), 6.91 (1H, d, Ar–H, $J^3 = 8.3$ Hz), 3.95 (3H, s, OCH_3), 3.93 (3H, s, OCH_3). ^{13}C NMR (75 MHz, $CDCl_3$) δ: 162.2 (1C, C═O), 157.5 (1C, C═N), 152.6 (1C, ar.), 150.6 (1C, ar.), 149.5 (1C, ar.), 134.2 (1C, ar.), 130.7 (2C, ar.), 124.4 (1C, ar.), 123.6 (2C, ar.), 122.2 (1C, ar.), 110.6 (1C, ar.), 108.7 (1C, ar.), 56.1 (1C, OCH_3), 55.9 (1C, OCH_3).

2.5.4. (E)-3,4-Dimethoxyphenyl-[O-(4-trifluoromethyl)benzoyl]oxime (AO-6)

This compound was obtained as white crystals in 55 % yield after purification by chromatography (hexane/ethyl acetate 90:10 to 80:20). The melting point was 121–122 °C; IR ($\bar{\upsilon}$/cm^{-1}): 3051, 2943, 2916, 1754, 1735, 1599, 1574, 1513. ^{1}H NMR (300 MHz, $CDCl_3$) δ: 8.49 (1H, s, oxime), 8.23 (2H, d, Ar–H, $J^3 = 8.8$ Hz), 7.75 (2H, d, Ar–H, $J^3 = 8.8$ Hz),

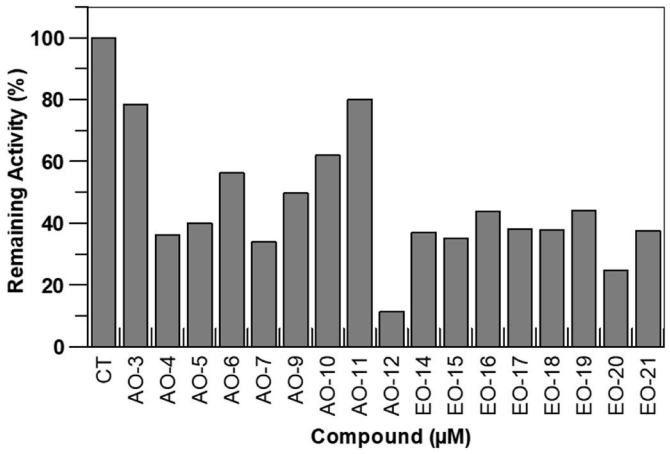

Fig. 1. *Screening of Oximic Compounds Against TbMCA2.* Residual activity of TbMCA2 after incubation with 10 μM of (A) acyl oxime compounds and (B) ether oxime compounds for 10 min.

Table 1
Structural characteristics and inhibitory potentials (IC50 values) of AO-7, AO-12, and EO-20.

COMPOUND	STRUCTURE	IC_{50} (μM)
AO-7	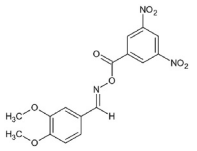	3.31 ± 0.25
AO-12	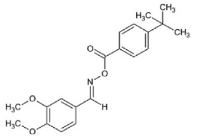	2.52 ± 0.19
EO-20	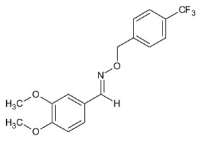	5.23 ± 0.83

7.48 (1H, d, Ar–H, $J^4 = 1.9$Hz), 7.19 (1H, dd, Ar–H, $J^3 = 8.3$ Hz, $J^4 = 1.9$ Hz), 6.90 (1H, d, Ar–H, $J^3 = 8.3$ Hz), 3.96 (3H, s, O$\underline{C}H_3$), 3.93 (3H, s, O$\underline{C}H_3$). ^{13}C NMR (75 MHz, $CDCl_3$) δ: 162.9 (1C, C═O), 157.2 (1C, C═N), 152.5 (1C, ar.), 149.5 (1C, ar.), 132.0 (1C, ar.), 130.0 (3C, ar.), 125.6 (1C, ar.), 125.5 (2C, ar.), 124.3 (1C, ar.), 122.4 (1C, CF_3), 110.6 (1C, ar.), 108.7 (1C, ar.), 56.1 (1C, O$\underline{C}H_3$), 55.9 (1C, O$\underline{C}H_3$).

2.5.5. (E)-3,4-Dimethoxyphenyl-[O-(3,5-dinitro)benzoyl]oxime (AO-7)

This compound was obtained as yellow crystals in 48 % yield with a melting point of 138–139 °C; IR ($\bar{\upsilon}$/cm^{-1}): 3113, 3096, 3013, 2920, 2848, 1760, 1598, 1575, 1534. ^{1}H NMR (300 MHz, $CDCl_3$) δ: 9.28–9.24 (3H, m, Ar–H); 8.57 (1H, s, oxime), 7.47 (1H, d, Ar–H, $J^4 = 1.9$ Hz), 6.93 (2H, d, Ar–H, $J^3 = 8.3$ Hz), 3.97 (3H, s, O$\underline{C}H_3$), 3.95 (3H, s, O$\underline{C}H_3$). ^{13}C NMR (75 MHz, $CDCl_3$) δ: 160.1 (1C, C═O), 158.2 (1C, C═N), 153.0 (1C, ar.), 149.6 (1C, ar.), 148.7 (2C, ar.), 132.6 (1C, ar.), 129.4 (2C, ar.), 124.7 (1C, ar.), 122.7 (1C, ar.), 121.7 (1C, ar.), 110.7 (1C, ar.), 108.8 (1C, ar.), 56.2 (1C, O$\underline{C}H_3$), 56.0 (1C, O$\underline{C}H_3$).

2.5.6. (E)-3,4-Dimethoxyphenyl-[O-(4-methyl)benzoyl]oxime (AO-9)

This compound was obtained as yellow crystals in 56 % yield after purification by chromatography (dichloromethane/hexane 70:30), with a melting point of 139–141 °C; IR ($\bar{\upsilon}$/cm^{-1}): 2955, 2921, 2849, 2839, 1735, 1607, 1598, 1574, 1508. ^{1}H NMR (300 MHz, $CDCl_3$) δ: 2.36 (3H, s, Ar-C$\underline{H}_3$), 3.85 (3H, s, O$\underline{C}H_3$), 3.88 (3H, s, O$\underline{C}H_3$), 6.82 (1H, d, Ar–$\underline{H}$, ^3J = 8.3 Hz), 7.11 (1H, dd, Ar–$\underline{H}$, $^3J = 8.2$, $^4J = 1.8$ Hz), 7.21 (2H, d, Ar–$\underline{H}$, ^3J = 8.4 Hz), 7.42 (1H, d, Ar–$\underline{H}$, $^3J = 1.7$ Hz), 7.94 (2H, d, Ar–$\underline{H}$, $^3J = 8.2$ Hz), 8.39 (1H, s, -C$\underline{H}$═N-). ^{13}C NMR (75 MHz, $CDCl_3$) δ: 21.8 (1C, Ar-$\underline{C}H_3$), 56.1 (1C, -O$\underline{C}H_3$), 56.3 (1C, -O$\underline{C}H_3$), 108.9 (1C, ar.), 110.8 (1C, ar.), 123.1 (1C, ar.), 124.2 (2C, ar.), 126.1 (2C, ar.), 129.4 (1C, ar.), 129.8 (1C, ar.), 144.3 (1C, ar.), 149.6 (1C, ar.), 152.4 (1C, ar.), 156.7 (1C, $\underline{C}$═N), 164.4 (1C, $\underline{C}$═O).

2.5.7. (E)-3,4-Dimethoxyphenyl-[O-(4-methoxy)benzoyl]oxime (AO-10)

This compound was obtained as brown crystals in 72 % yield after purification by chromatography (dichloromethane/hexane 70:30 and 80:20), with a melting point of 112–114 °C; IR ($\bar{\upsilon}$/cm^{-1}): 2953, 2924, 2843, 1738, 1683, 1601, 1575, 1509. ^{1}H NMR (300 MHz, $CDCl_3$) δ: 3.87 (3H, s, Ar-O$\underline{C}H_3$), 3.92 (3H, s, O$\underline{C}H_3$), 3.95 (3H, s, O$\underline{C}H_3$), 6.89 (1H, d, Ar–$\underline{H}$, $^3J = 8.3$ Hz), 6.96 (2H, d, Ar–$\underline{H}$, $^3J = 8.9$ Hz), 7.17 (1H, dd, Ar–$\underline{H}$, $^3J = 8.3$, $^4J = 1.9$ Hz), 7.49 (1H, d, Ar–$\underline{H}$, $^3J = 1.8$ Hz), 8.08 (2H, d, Ar–$\underline{H}$, $^3J = 8.9$ Hz), 8.45 (1H, s, -C$\underline{H}$═N-). ^{13}C NMR (75 MHz, $CDCl_3$) δ: 55.6 (1C, Ar-O$\underline{C}H_3$), 56.1 (1C, -O$\underline{C}H_3$), 56.3 (1C, -O$\underline{C}H_3$), 108.9 (1C, ar.), 110.7 (1C, ar.), 113.9 (2C, ar.), 121.1 (1C, ar.), 123.1 (2C, ar.), 124.2 (1C, ar.), 131.9 (1C, ar.), 149.6 (1C, ar.), 152.4 (1C, ar.), 156.5 (1C, $\underline{C}$═N), 163.8 (1C, Ar-O$\underline{C}H_3$), 164.1 (1C, $\underline{C}$═O).

2.5.8. (E)-3,4-Dimethoxyphenyl-[O-(4-fluoro)benzoyl]oxime (AO-11)

This compound was obtained as yellow crystals in 38 % yield after purification by chromatography (dichloromethane/hexane 50:50 and 70:30), with a melting point of 120–124 °C; IR ($\bar{\upsilon}$/cm^{-1}): 2954, 2917, 2848, 1599, 1573,1509. ^{1}H NMR (300 MHz, $CDCl_3$) δ: 3.83 (3H, s, O$\underline{C}H_3$), 3.86 (3H, s, O$\underline{C}H_3$), 6.83 (1H, d, Ar–$\underline{H}$, $^3J = 8.4$ Hz), 7.01 (1H, d, Ar–$\underline{H}$, $^3J = 1.9$ Hz), 7.07 (2H, d, Ar–$\underline{H}$, $^3J = 8.5$ Hz), 7.10 (2H, d, Ar–$\underline{H}$, $^3J = 8.4$ Hz), 7.14–7.30 (2H, m, Ar–$\underline{H}$), 8.08 (1H, s, -C$\underline{H}$═N-). ^{13}C NMR (75 MHz, $CDCl_3$) δ: 56.3 (2C, -O$\underline{C}H_3$), 111.4 (1C, ar.), 114.1 (1C, ar.), 115.7 (2C, ar.), 116.0 (1C, ar.), 125.7 (2C, ar.), 126.6 (1C, ar.), 132.9 (1C, ar.), 133.1 (1C, ar.), 149.4 (1C, ar.), 153.0 (1C, $\underline{C}$═N), 164.8 (1C, $\underline{C}$═O), 168.2 (1C, ar.).

2.5.9. (E)-3,4-Dimethoxyphenyl-[O-(4-tert-butil)benzoyl]oxime (AO-12)

This compound was obtained as yellow crystals in a 28 % yield after purification by chromatography (dichloromethane/hexane, 70:30). The melting point was observed at 121–123 °C; IR ($\bar{\upsilon}$/cm^{-1}): 2951, 2921, 2876, 2844, 1598, 1571, 1508.^{1}H NMR (300 MHz, $CDCl_3$) δ: 1.35 (9H, s, C(C$\underline{H}_3$)$_3$), 3.93 (3H, s, O$\underline{C}H_3$), 3.96 (3H, s, O$\underline{C}H_3$), 6.90 (1H, d, Ar–H, J^3 = 8.3 Hz), 7.18 (1H, dd, Ar–H, $J^3 = 8.3$ Hz, $J^4 = 1.9$ Hz), 7.26–7.50 (3H, m, Ar–H), 8.05 (2H, dd, Ar–H, $J^3 = 8.3$ Hz, $J^4 = 1.9$ Hz), 8.47 (1H, s, oxime). ^{13}C NMR (75 MHz, $CDCl_3$) δ: 31.1 (3C, C(C$\underline{H}_3$)$_3$, 35.2 (1C, $\underline{C}$(CH$_3$)$_3$), 56.0 (1C, O$\underline{C}H_3$), 56.2 (1C, O$\underline{C}H_3$), 108.8 (1C, ar.), 110.6 (1C, ar.), 122.9 (1C, ar.), 124.1 (1C, ar.), 125.6 (2C, ar), 125.9 (1C, ar.), 129.6 (2C, ar), 149.5 (1C, ar.), 152.0 (1C, ar.), 156.5 (1C, $\underline{C}$═N), 157.1 (1C, ar.), 164.2 (1C, $\underline{C}$═O).

2.6. General procedure for synthesis of oxime ethers 14-21

To a solution of dimethyl sulfoxide/water (8:2), sodium hydroxide (13 equivalents) and oxime 2 (1 equivalent) were added, and the mixture was stirred at room temperature for 30 min. Subsequently, the corresponding benzyl chloride (6 equivalents) was added, and the reaction mixture was stirred at room temperature for an additional 30 min, until TLC analysis indicated the reaction had reached completion. The mixture was then diluted with water (30 mL) and extracted with ethyl acetate (4 × 20 mL). The combined organic layers were washed with water (2 × 20 mL), dried over anhydrous sodium sulfate, and concentrated. The resulting crude product was purified by column chromatography to yield oxime ethers **14**–**21**.

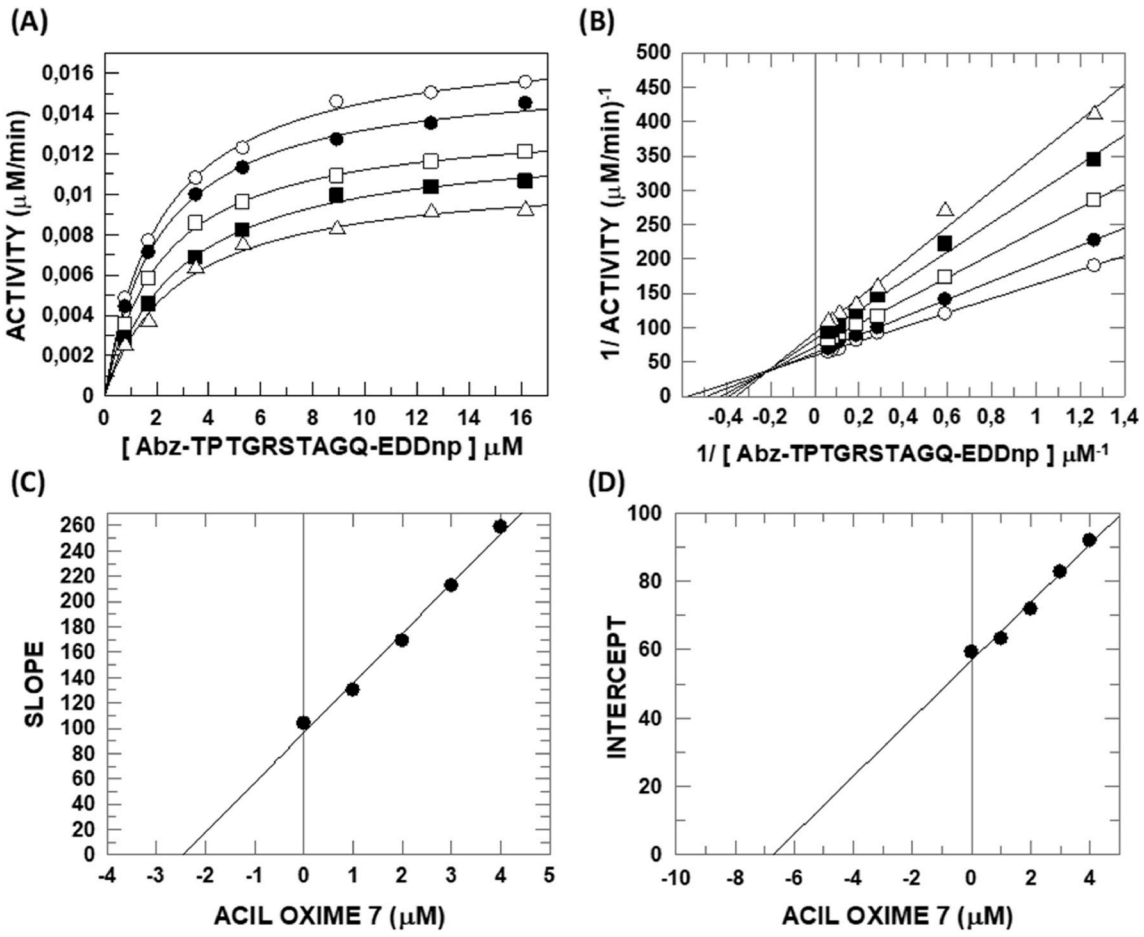

Fig. 2. *Inhibitory Kinetic Profiles of AO-7 on TbMCA2.* (A) Michaelis-Menten plot showing the hyperbolic rectangular curve, (B) Lineweaver-Burk plot indicating mixed inhibition, (C) Slope replot for determining inhibition constants, and (D) Intercept replot for detailed kinetic analysis.

2.6.1. (E)-3,4-Dimethoxyphenyl-[O-(4-chloro)benzyl]oxime (EO-14)

This compound was obtained as yellow crystals in a 41 % yield after purification by chromatography (hexane/ethyl acetate 95:5 to 90:10). The melting point was observed at 72–73 °C; IR ($\bar{\upsilon}$/cm^{-1}): 3068, 3000, 2990, 2968, 2931, 2855, 2833, 1605, 1575, 1511. ^{1}H NMR (300 MHz, $CDCl_3$) δ: 8.06 (1H, s, oxime), 7.33 (4H, s, Ar–H), 7.21 (1H, d, Ar–H, J^3 = 1.9 Hz), 7.00 (1H, dd, Ar–H, J^3 = 8.3 Hz, J^4 = 1.9 Hz), 6.83 (1H, d, Ar–H, J^3 = 8.3 Hz), 5.14 (2H, s, methylene), 3.91 (3H, s, $OC\underline{H}_3$), 3.89 (3H, s, $OC\underline{H}_3$). ^{13}C NMR (75 MHz, $CDCl_3$) δ: 150.7 (1C, C═N), 149.2 (1C, ar.), 149.1 (1C, ar.), 136.1 (1C, ar.), 133.6 (1C, ar.), 129.5 (2C, ar.), 128.5 (2C, ar.), 124.8 (1C, ar.), 121.7 (1C, ar.), 110.6 (1C, ar.), 108.0 (1C, ar.), 75.2 (methylene), 55.8 (2C, $O\underline{C}H_3$).

2.6.2. (E)-3,4-Dimethoxyphenyl-[O-(4-methyl)benzyl]oxime (EO-15)

This compound was obtained as yellow crystals in a 64 % yield after purification by chromatography (hexane/ethyl acetate 95:5 to 90:10). The melting point was observed at 53–54 °C; IR ($\bar{\upsilon}$/cm^{-1}): 3057, 3008, 2962, 2928, 2861, 2835, 1595, 1571, 1512. ^{1}H NMR (300 MHz, $CDCl_3$) δ: 8.06 (1H, s, oxime), 7.32 (2H, d, Ar–H, J^3 = 8.0 Hz), 7.24 (1H, d, Ar–H, J^4 = 1.9 Hz), 7.17 (2H, d, Ar–H, J^3 = 8.0 Hz), 7.00 (1H, dd, Ar–H, J^3 = 8.4 Hz, J^4 = 1.9 Hz), 6.83 (1H, d, Ar–H, J^3 = 8.4 Hz), 5.16 (2H, s, methylene), 3.92 (3H, s, $OC\underline{H}_3$), 3.89 (3H, s, $OC\underline{H}_3$), 2.35 (3H, s, methyl). ^{13}C NMR (75 MHz, $CDCl_3$) δ: 150.6 (1C, C═N), 149.2 (1C, ar.), 148.7 (1C, ar.), 136.7 (1C, ar.), 134.4 (1C, ar.), 129.0 (2C, ar.), 128.4 (2C, ar.), 125.1 (1C, ar.), 121.6 (1C, ar.), 110.6 (1C, ar.), 108.0 (1C, ar.), 76.1 (methylene), 55.8 (2C, $O\underline{C}H_3$), 21.1 (1C, Ar-$\underline{C}H_3$).

2.6.3. (E)-3,4-Dimethoxyphenyl-[O-(4-tert-butil)benzyl]oxime (EO-16)

This compound was obtained as yellow crystals in a 51 % yield after purification by chromatography (hexane/ethyl acetate 95:5 to 90:10). The melting point was observed at 69–71 °C; IR ($\bar{\upsilon}$/cm^{-1}): 3078, 3029, 2998, 2947, 2901, 2877, 2840, 1599, 1573, 1508. ^{1}H NMR (300 MHz, $CDCl_3$) δ: 8.07 (1H, s, oxime), 7.42–7.37 (4H, m, Ar–H), 7.25 (1H, s, Ar–H), 7.01 (1H, dd, Ar–H, J^3 = 8.3 Hz, J^4 = 1.9 Hz), 6.83 (1H, d, Ar–H, J^3 = 8.3 Hz), 5.17 (2H, s, methylene), 3.92 (3H, s, $OC\underline{H}_3$), 3.89 (3H, s, $OC\underline{H}_3$), 1.32 (9H, s, $C(C\underline{H}_3)_3$). ^{13}C NMR (75 MHz, $CDCl_3$) δ: 150.9 (1C, C═N), 150.6 (1C, ar.), 149.2 (1C, ar.), 148.7 (1C, ar.), 134.4 (1C, ar.), 128.2 (2C, ar.), 125.3 (2C, ar.), 125.1 (1C, ar.), 121.6 (1C, ar.), 110.6 (1C, ar.), 108.0 (1C, ar.), 76.1 (methylene), 55.8 (2C, $O\underline{C}H_3$), 34.5 (1C, $\underline{C}(CH_3)_3$), 31.3 (3C, $C(\underline{C}H_3)_3$).

2.6.4. (E)-3,4-Dimethoxyphenyl-[O-(4-methoxy)benzyl]oxime (EO-17)

This compound was obtained as yellow crystals in a 82 % yield after purification by chromatography (hexane/ethyl acetate 90:0 to 80:20). The melting point was observed at 79–80 °C; IR ($\bar{\upsilon}$/cm^{-1}): 3042, 3011, 2960, 2916, 2876, 2845, 1612, 1601, 1510. ^{1}H NMR (300 MHz, $CDCl_3$) δ: 8.05 (1H, s, oxime), 7.36 (2H, d, Ar–H, J^3 = 8.7 Hz), 7.24 (1H, d, Ar–H, J^4 = 1.9 Hz), 7.00 (1H, dd, Ar–H, J^3 = 8.3 Hz, J^4 = 1.9 Hz), 6.90 (2H, d, Ar–H, J^3 = 8.7 Hz), 6.83 (1H, d, Ar–H, J^3 = 8.3 Hz), 5.13 (2H, s, methylene), 3.92 (3H, s, $OC\underline{H}_3$), 3.89 (3H, s, $OC\underline{H}_3$), 3.81 (3H, s, $OC\underline{H}_3$). ^{13}C NMR (75 MHz, $CDCl_3$) δ: 159.4 (1C, ar.), 150.6 (1C, C═N), 149.2 (1C, ar.), 148.7 (1C, ar.), 130.0 (2C, ar.), 129.5 (1C, ar.), 125.1 (1C, ar.), 121.6 (1C, ar.), 113.8 (2C, ar.), 110.6 (1C, ar.), 108.0 (1C, ar.), 75.9 (methylene), 55.8 (2C, $O\underline{C}H_3$), 55.2 (1C, $O\underline{C}H_3$).

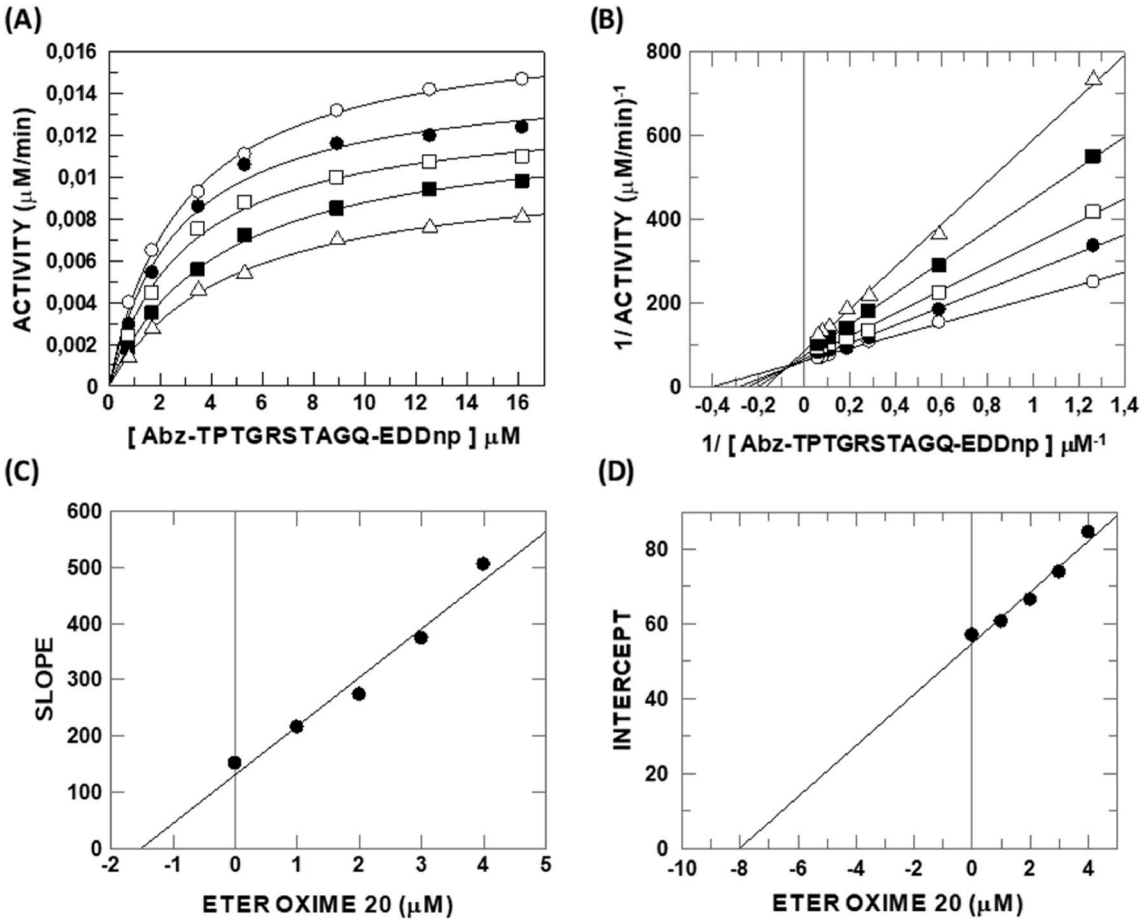

Fig. 3. *Inhibitory Kinetic Profiles of EO-20 on TbMCA2.* (A) Michaelis-Menten plot showing the hyperbolic rectangular curve, (B) Lineweaver-Burk plot indicating mixed inhibition, (C) Slope replot for determining inhibition constants, and (D) Intercept replot for detailed kinetic analysis.

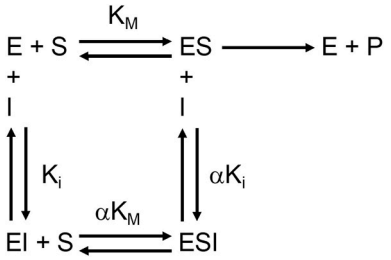

Fig. 4. *Proposed Inhibition Mechanism of TbMCA2 by AO-7 and EO-20.* Schematic representation of the mixed inhibition mechanism of TbMCA2 by AO-7 and EO-20, highlighting the parameter α, which indicates the degree to which inhibitor binding influences enzyme-substrate affinity. For $\alpha > 1$, the inhibition mechanism is mixed. The figure also illustrates the non-competitive inhibition mechanism of AO-12 against TbMCA2, where $\alpha = 1$.

2.6.5. (E)-3,4-Dimethoxyphenyl-[O-(4-nitro)benzyl]oxime (EO-18)

This compound was obtained in a 54 % yield as brown crystals after purification by chromatography (hexane/ethyl acetate 90:10). The melting point was recorded at 87–90 °C; IR ($\bar{\upsilon}$/cm^{-1}): 3040, 3008, 2951, 2845, 1730, 1602, 1511. ^{1}H NMR (300 MHz, $CDCl_3$) δ: 8.22 (2H, d, Ar–H, $J^3 = 8.0$ Hz), 8.22 (1H, s, oxime), 7.55 (2H, d, Ar–H, $J^3 = 8.0$ Hz), 7.21 (1H, m, Ar–H), 7.00 (1H, d, Ar–H, $J^4 = 8.2$ Hz), 6.84 (1H, d, Ar–H, $J^3 = 8.2$ Hz), 5.27 (2H, s, methylene), 3.90 (6H, s, O$\underline{C}$H$_3$). ^{13}C NMR (75 MHz, $CDCl_3$) δ: 151.0 (1C, ar.), 149.8 (1C, C═N), 149.3 (1C, ar.), 145.6 (1C, ar.), 128.3 (2C, ar.), 124,6 (1C, ar.), 123.7 (2C, ar.), 121.9 (1C, ar.), 110.8 (1C, ar.), 108.2 (1C, ar.), 74.6 (methylene), 55.9 (2C, O$\underline{C}$H$_3$).

2.6.6. (E)-3,4-Dimethoxyphenyl-[O-(4-bromo)benzyl]oxime (EO-19)

This compound was obtained in a 62 % yield as white crystals after purification by chromatography (hexane/ethyl acetate 90:10). The melting point was recorded at 93–95 °C; IR ($\bar{\upsilon}$/cm^{-1}): 2989, 2965, 2933, 2832, 1607, 1575, 1511. ^{1}H NMR (300 MHz, $CDCl_3$) δ: 3.90 (3H, s, -OC$\underline{H}_3$), 3.91 (3H, s, OC$\underline{H}_3$), 5.13 (2H, s, -*O*-C$\underline{H}_2$-Ar), 6.84 (1H, d, Ar–$\underline{H}$, $^3J = 8.3$ Hz), 7.01 (1H, dd, Ar–$\underline{H}$, $^3J = 8.3$, $^4J = 1.9$ Hz), 7.22 (1H, d, Ar–H, $^3J = 1.8$ Hz), 7.29 (2H, d, Ar–H, $^3J = 8.4$ Hz), 7.49 (2H, d, Ar–$\underline{H}$, $^3J = 8.4$ Hz), 8.06 (1H, s, C$\underline{H}$═N). ^{13}C NMR (75 MHz, $CDCl_3$) δ: 56.1 (2C, -O$\underline{C}$H$_3$), 75.5 (1C, -O$\underline{C}$H$_2$-Ar), 108.3 (1C, ar.), 110.9 (1C, ar.), 121.9 (1C, ar.), 121.9 (1C, ar.), 125.0 (1C, ar.), 130.0 (2C, ar.), 131.7 (2C, ar.), 136.9 (1C, ar.), 149,3 (1C, $\underline{C}$═N), 159,4 (1C, ar.), 150,9 (1C, ar.).

2.6.7. (E)-3,4-Dimethoxyphenyl-[O-(4-trifluoromethyl)benzyl]oxime (EO-20)

This compound was obtained in a 64 % yield as a yellow oil after purification by chromatography (hexane/ethyl acetate 80:20). The melting point was recorded at 88–91 °C; IR ($\bar{\upsilon}$/cm^{-1}): 3032, 3001, 2954, 2914, 2868, 2840, 1606, 1599. ^{1}H NMR (300 MHz, $CDCl_3$) δ: 3.90 (3H, s, -OC$\underline{H}_3$), 3.91 (3H, s, OC$\underline{H}_3$), 5.24 (2H, s, -*O*-C$\underline{H}_2$-Ar), 6.83 (1H, d, Ar–$\underline{H}$, $^3J = 8.2$ Hz), 7.02 (1H, d, Ar–$\underline{H}$, $^3J = 8.2$), 7.24 (1H, d, Ar–H, $^3J = 1.7$ Hz), 7.52 (2H, d, Ar–H, $^3J = 8.2$ Hz), 7.62 (2H, d, Ar–$\underline{H}$, $^3J = 8.2$ Hz), 8.09 (1H, s, C$\underline{H}$═N). ^{13}C NMR (75 MHz, $CDCl_3$) δ: 55.9 (2C, -O$\underline{C}$H$_3$), 75.2 (1C, -O$\underline{C}$H$_2$-Ar), 108.2 (1C, ar.), 110.7 (1C, ar.), 121.8 (2C, ar.), 124.8 (1C, ar.), 125.3 (1C, ar.), 128.1 (2C, ar.), 141.9 (1C, ar.), 149.4 (1C, $\underline{C}$═N), 150,9 (1C, ar.).

2.6.8. (E)-3,4-Dimethoxyphenyl-[O-(4-fluoro)benzyl]oxime (EO-21)

This compound was obtained in a 59 % yield as a yellow oil after

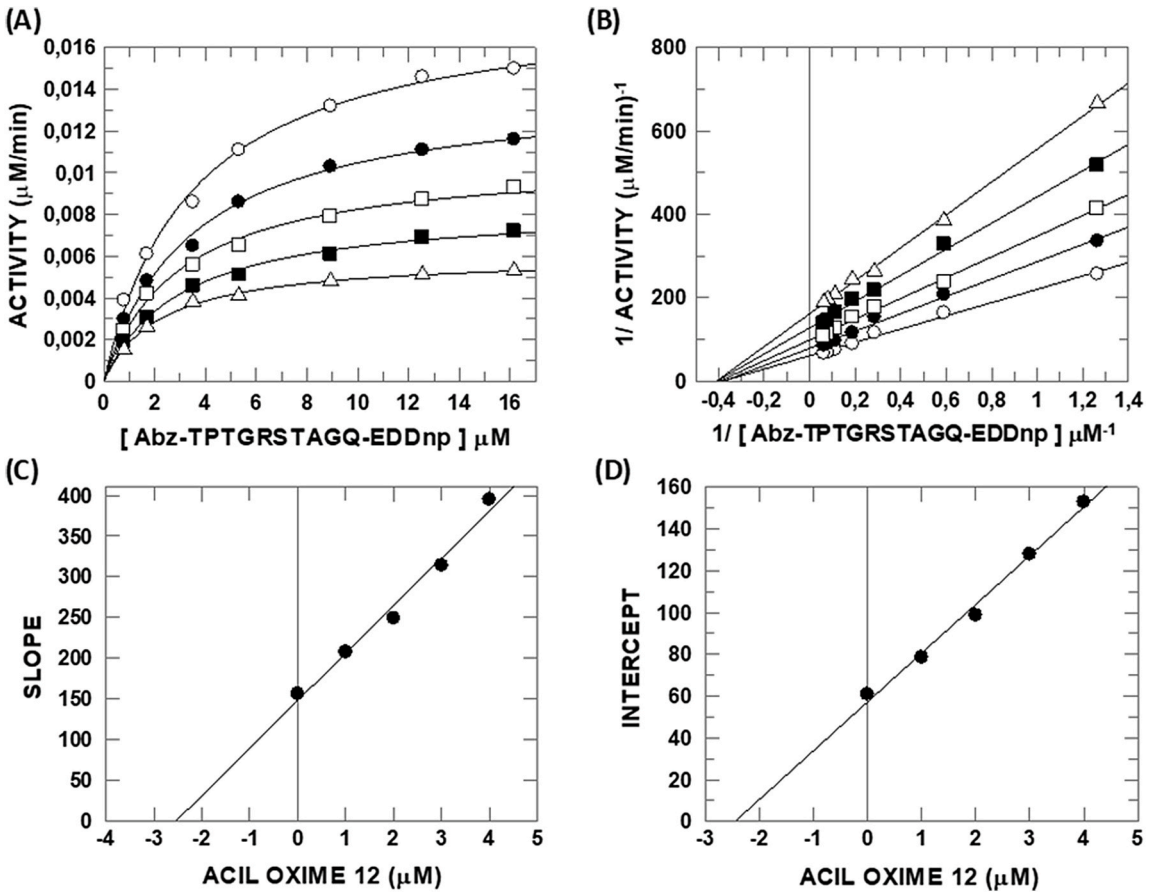

Fig. 5. *Inhibitory Kinetic Profiles of AO-12 on TbMCA2.* (A) Michaelis-Menten plot showing the hyperbolic rectangular curve, (B) Lineweaver-Burk plot indicating non-competitive inhibition, (C) Slope replot for determining inhibition constants, and (D) Intercept replot for detailed kinetic analysis.

purification by chromatography (hexane/ethyl acetate 90:10); IR ($\bar{\upsilon}$/cm^{-1}): 2956, 2931, 2872, 2839, 1600, 1577, 1508. ^{1}H NMR (300 MHz, $CDCl_3$) δ: 3.90 (3H, s, -OC$\underline{H}_3$), 3.92 (3H, s, OC$\underline{H}_3$), 5.15 (2H, s, -*O*-C$\underline{H}_2$-Ar), 6.84 (1H, d, Ar–$\underline{H}$, ^3J = 8.3 Hz), 7.01 (1H, dd, Ar–$\underline{H}$, ^3J = 8.1 Hz, ^4J = 1.9 Hz), 7.05 (2H, d, Ar–$\underline{H}$, ^3J = 8.7 Hz), 7.23 (1H, d, Ar–$\underline{H}$, ^3J = 1.9 Hz), 7.39 (2H, dd, Ar–$\underline{H}$, ^3J = 8.7 Hz, ^4J = 5.5 Hz), 8.06 (1H, s, -C$\underline{H}$═N-). ^{13}C NMR (75 MHz, $CDCl_3$) δ: 56.1 (2C, -O$\underline{C}H_3$), 75.6 (1C, -O$\underline{C}H_2$-Ar), 108.3 (1C, ar.), 110.9 (1C, ar.), 115.3 (2C, ar.), 115.6 (2C, ar.), 121.9 (1C, ar.), 125.1 (1C, ar.), 130.4 (1C, ar.), 148.2 (1C, $\underline{C}$═N), 149.4 (1C, ar.), 150.9 (1C, ar.), 164.3 (1C, ar.).

2.7. Screening of oximic compounds as a TbMCA2 modulator

The screening of compounds was conducted using a Hitachi F-2700 spectrofluorometer (Tokyo, Japan) with a cuvette possessing a 1 cm path length, containing a final volume of 1 mL of 50 mM Tris/HCl buffer, pH 7.4, supplemented with 100 mM NaCl and 1 mM $CaCl_2$. The reaction mixture was placed in a temperature-controlled chamber for 5 min. Following this, TbMCA2 was pre-incubated with 2.5 mM dithiothreitol (DTT) and 10 μM of the test compound for 5 min. The FRET substrate Abz-KARSSAQ-EDDnp was then added (5 μM final concentration), and hydrolysis was monitored with excitation and emission wavelengths set at 320 nm and 420 nm, respectively. The increase in fluorescence was recorded as arbitrary fluorescence units per minute (AFU/min). The substrate hydrolysis rate without the compound was set as 100 %, and the effects of the oximic compounds were expressed as a percentage of this reference rate.

2.8. Determination of IC_{50} values for inhibitor

TbMCA2 activity was assayed in a standard reaction buffer containing 50 mM Tris/HCl at pH 7.4, 100 mM NaCl, and 1 mM $CaCl_2$. The enzyme was incubated with 2.5 mM DTT for 5 min at 25 °C in a final volume of 1 mL under constant stirring. Enzyme activity was monitored using the FRET substrate Abz-KARSSAQ-EDDnp, with fluorescence increases measured over time. Selected compounds, namely **AO-7** (ACYL OXIME 7), **AO-12** (ACYL OXIME 12), and **EO-20** (ETHER OXIME 20), were evaluated for their inhibitory effects on TbMCA2 through a spectrofluorometric method, using excitation and emission wavelengths of 320 nm and 420 nm, respectively. Enzyme inhibition was quantified by the compound concentration that resulted in a 50 % decrease in enzyme activity, represented as IC_{50} values. The IC_{50} values were determined using non-linear regression analysis, based on dose-response curves obtained by testing the inhibitors at various concentrations. Data analysis was performed using Grafit 5.0 software (Erithacus, UK) with the equation [$y = \text{Range}/(1 + (x/IC_{50})^s)$], where "Range" is the fitted uninhibited value and "s" is the slope factor, assuming that y decreases with increasing x.

2.9. Enzyme kinetics and mechanism determination

Kinetic studies of TbMCA2 inhibition were performed with varying concentrations of the substrate Abz-TPTGRSTAGQ-EDDnp, ranging from 0 to 20 μM, in the absence and presence of oximic compounds (1, 2, 3, and 4 μM, respectively). The reactions were monitored using a Hitachi F-2700 spectrofluorometer (Hitachi, Tokyo, Japan) with excitation and emission wavelengths set at 320 and 420 nm, respectively. For all kinetic measurements, the compound was pre-incubated with TbMCA2 for 10

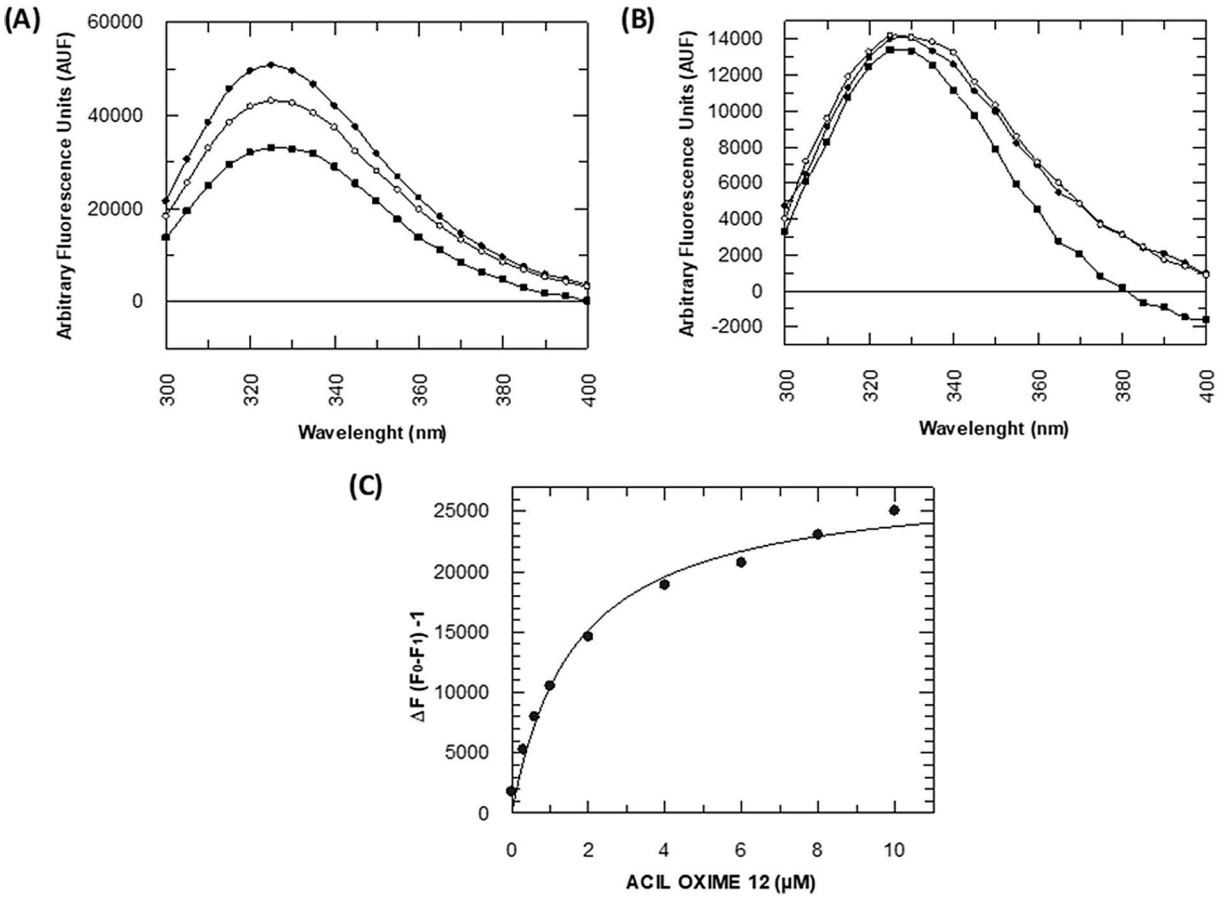

Fig. 6. *Effects of AO-12 on the TbMCA2 Structure.* (A) Effect of AO-12 on the intrinsic fluorescence of TbMCA2 WT, showing fluorescence intensity changes without compound (●), with 2 μM of AO-12 (○), and with 10 μM of AO-12 (□). (B) Effect of AO-12 on the TbMCA2 D189/190A mutant, showing fluorescence intensity changes without compound (●), with 2 μM of AO-12 (○), and with 10 μM of AO-12 (□). (C) Changes in maximum fluorescence intensity at an emission wavelength of 330 nm with increasing AO-12 concentration.

min before substrate addition. All assays were conducted in triplicate. Inhibition constants (K_i) were determined using different equations depending on the inhibition mechanism. The activity rate and substrate concentration data generated rectangular hyperbolic profiles, which were linearized using Lineweaver-Burk (double reciprocal) plots. Replotting the slope vs. [inhibitor] and intercept vs. [inhibitor] provided the K_i and αK_i parameters, respectively.

2.10. The effect of ACYL OXIME 12 on the intrinsic fluorescence of TbMCA2 WT and TbMCA2 D189/190A

Structural changes in both wild-type TbMCA2 (WT) and the D189/190A mutant were investigated by monitoring intrinsic fluorescence. Experiments were conducted in a buffer containing 50 mM Tris/HCl at pH 8.5, with varying concentrations of compound 12 (ranging from 0.3 to 10 μM) and a final protein concentration of 2 μM. Emission spectra were recorded between 300 and 400 nm at 25 °C, using a fixed excitation wavelength of 280 nm, with both excitation and emission slit widths set to 2.5 nm. Data were analyzed using the one-site interaction equation, which models the binding of ligands to a single receptor site. Analysis was performed with Grafit 5.0 software.

2.11. Molecular docking methodology

The three-dimensional (3D) structures of compound **AO-12** were drawn and optimized using MarvinSketch v21.20 software. Ionization states at pH 7.4 were generated using the OpenBabel v3.1.1 tool, which also facilitated the conversion of files from *.mol2 to *.pdbqt format.

The 3D structure of *Trypanosoma brucei* metacaspase-2 (TbMCA2) was obtained from the RCSB Protein Data Bank (PDB ID: 4AF8). Using AutoDock Tools v1.5.7 software, water molecules and other non-relevant entities were removed from TbMCA2 to prevent bias due to these entities in the binding site. Kollman charges and polar hydrogen atoms were added, and the protein target was saved in *.pdbqt format.

Molecular docking assays were performed using AutoDock Vina software. To ensure specific interaction with the TbMCA2 binding region, docking calculations were confined to a 3D grid box. Vina's search algorithms explored different ligand conformations to identify the most favorable binding mode with the protein target. The grid box parameters were defined based on the following coordinates and sizes: center values x = 58.306, y = 44.611, z = −36.549; sizes x = 25.0 Å, y = 25.0 Å, z = 25.0 Å, encompassing the TbMCA2 Ca^{2+} binding site, specifically the residues Asp^{173}, Asp^{189}, Asp^{190}, and Asp^{220} [8,14,15].

Results were analyzed from the perspective of binding affinity energy (in kcal/mol), considering variations in rotational, translational, and conformational positions to identify the most stable protein-ligand complex. Results were sorted by increasing energy values (from most negative to most positive) to determine the best interaction profiles. Subsequently, the top-ranked conformations of each ligand were visualized in association with the TbMCA2 protein using PyMOL v2.5.2 software (Schrödinger, LLC, San Diego, CA, USA). Interaction profiles were further analyzed using Discovery Studio Client v21.1.0.20298 software, enabling the identification of intermolecular forces such as hydrogen bonds (H-bonds) through 2D ligand-protein interaction diagrams and 3D representations.

Table 2
Binding affinity energies, hydrogen bonds, and intermolecular interactions of AO-7, AO-12, and EO-20 ligands with TbMCA2.

Ligand	Affinity (Kcal.mol^{-1})	H-bonds (number/residues)	Other intermolecular interactions
AO-7 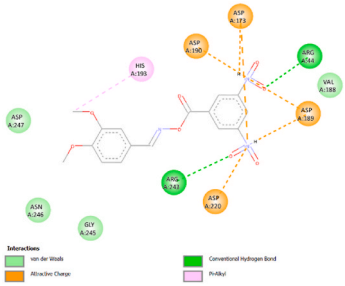	−7.0	2/Arg^{44}; Arg^{243}	Attractive charge Pi-Alkyl van der Waals
AO-12 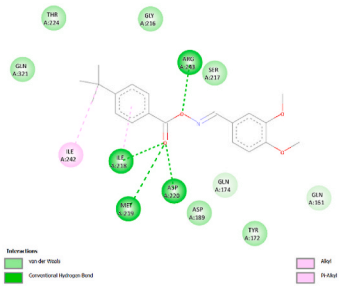	−6.3	4/Ile^{218}; Met^{219}; Asp^{220}; Arg^{243}	Alkyl Pi-Alkyl van der Waals
EO-20 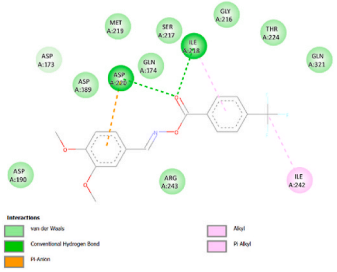	−6.1	2/Ile^{218}; Asp^{220}	Pi-Anion Alkyl Pi-Alkyl van der Waals

3. Results

3.1. Screening for the inhibitory activity of oxime compounds

TbMCA2 was fully processed following the purification procedures as described in previous studies by our group [16]. All compounds tested in this screening were dissolved in dimethyl sulfoxide (DMSO), and the activity of TbMCA2 was evaluated at different concentrations of DMSO, confirming that this solvent does not affect TbMCA2 activity (data not shown). The screening of the effect of 17 oxime compounds on TbMCA2 activity was conducted at a concentration of 10 μM for each compound. It was observed that at concentrations higher than 30 μM, oxime compounds precipitated; therefore, the screening was conducted at 10 μM for all oxime compounds, with each experiment performed in triplicate. All compounds were capable of inhibiting TbMCA2 activity (Fig. 1), and those compounds that inhibited 65 % or more of TbMCA2 activity were selected for more detailed analysis. Specifically, compounds **AO-7** (65 % inhibition), **AO-12** (88 % inhibition), and **EO-20** (75 % inhibition) were chosen for determining IC$_{50}$ values and analyzing the inhibition mechanism.

3.2. Inhibitory concentration (IC_{50})

The inhibitory concentration (IC$_{50}$) of compounds **AO-7**, **AO-12**, and **EO-20** was evaluated using various concentrations. The decrease in TbMCA2 activity was measured using a HITACHI F-2700 spectrofluorometer. Each concentration of the compounds was pre-incubated with TbMCA2 for 10 min at 25 °C, with activity measurements taken at each concentration. The IC$_{50}$ values for **AO-7**, **AO-12**, and **EO-20** were determined to be 3.31 ± 0.25 μM, 2.52 ± 0.19 μM, and 5.3 ± 0.83 μM, respectively (Table 1).

3.3. Inhibition mechanism of TbMCA2 by oximic compounds

Due to the lower IC$_{50}$ values observed for compounds **AO-7**, **AO-12**, and **EO-20**, we further investigated their inhibition mechanisms and determined the values of K_i and αK_i.

Screening and IC$_{50}$ experiments were conducted with the FRET peptide Abz-KARSSAQ-EDDnp ($K_M = 0.5$ μM and $k_{cat} = 0.5$ s^{-1}) [15]. For inhibition mechanism studies, we used the FRET peptide Abz-TPTGRSTAGQ-EDDnp ($K_M = 5.5$ μM and $k_{cat} = 0.1$ s^{-1}), selected due to its higher K_M and slower k_{cat}, which allowed for a more precise comparison of kinetic parameters in TbMCA2 experiments involving different compounds.

The Michaelis-Menten plot for compound **AO-7** is depicted in Fig. 2A. According to the Lineweaver-Burk plot (Fig. 2B), this compound alters both kinetic parameters, K_M and k_{cat}, as evidenced by the intersection of the lines in the second quadrant. Upon re-evaluating the intercept and slope parameters from the Lineweaver-Burk plot, it became evident that the replot of both slope vs. [inhibitor] and intercept

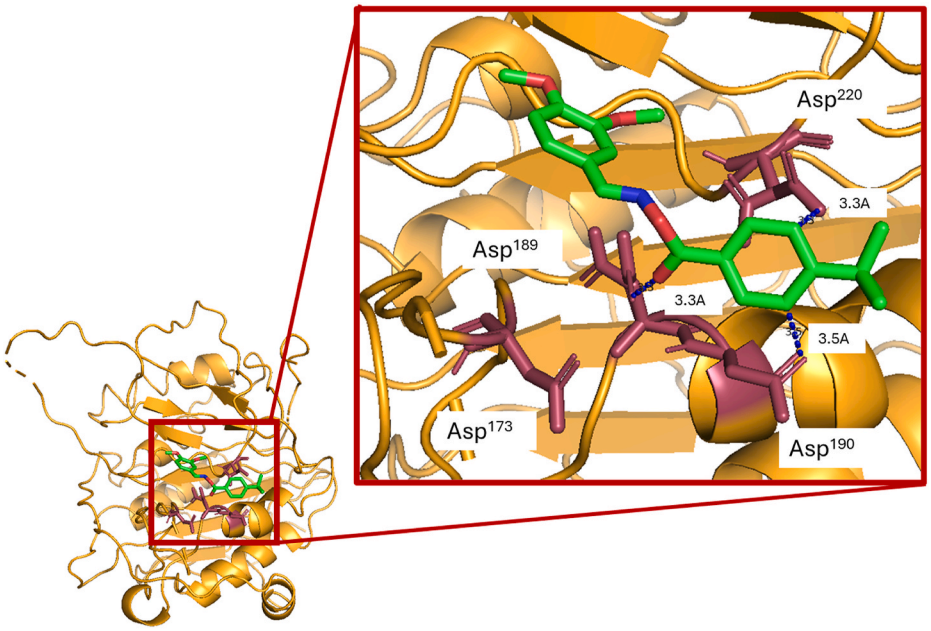

Fig. 7. *Molecular Docking of AO-12 Against TbMCA2.* 3D representation of the binding interactions between AO-12 and the calcium-binding site of TbMCA2, which includes Asp173, Asp189, Asp190, and Asp220 residues.

vs. [inhibitor] exhibited linear behavior, allowing the determination of K_i and αK_i values through linear regression. The calculated values were $K_i = 2.45 \pm 0.14$ μM and $\alpha K_i = 6.72 \pm 0.21$ μM, with $\alpha = 2.74$. A similar pattern was observed with compound **EO-20**, where the inhibition kinetics yielded $K_i = 1.51 \pm 0.25$ μM and $\alpha K_i = 8.02 \pm 0.27$ μM, with $\alpha = 5.31$. Both compounds **AO-7** and **EO-20** exhibited a non-competitive mixed inhibition mechanism (Fig. 3), suggesting that these compounds interact with both the active site and the enzyme-substrate (ES) complex in an allosteric manner, presenting two pathways for inhibiting TbMCA2. The α parameters indicate that compounds **AO-7** and **EO-20** have a significantly higher affinity, approximately 3–5 times greater, for the free enzyme E compared to the ES complex.

Compound **AO-12** displayed a distinctive behavior compared to **AO-7** and **EO-20**. Examination of the Michaelis-Menten plot reveals that **AO-12** exclusively impacts V_{max} (Fig. 5A). This observation is reinforced by the Lineweaver-Burk plot, which shows the plots converging on the X-axis, indicating that **AO-12** specifically affects the k_{cat} of TbMCA2 (Fig. 5B). Replotting the intercept vs. [inhibitor] and slope vs. [inhibitor] displayed a linear pattern, enabling the calculation of $K_i = 2.53 \pm 0.18$ μM and $\alpha K_i = 2.44 \pm 0.14$ μM (Fig. 5C and D). These data emphasize that the $K_i/\alpha K_i$ ratio is close to 1.0, leading to the conclusion that the inhibition mechanism of **AO-12** is non-competitive, with the compound binding with equal affinity to both the free enzyme E and the ES complex (Fig. 4).

3.4. Interaction at ACYL OXIME 12 with calcium binding site of TbMCA2

To evaluate whether compound **AO-12** interacts allosterically with the calcium-binding site of TbMCA2, composed of residues Asp^{173}, Asp^{189}, Asp^{190}, and Asp^{220}, we examined its impact on the intrinsic fluorescence of TbMCA2. The intrinsic fluorescence of TbMCA2 was known to be modified upon interaction with calcium, a principle we used to assess the effect of **AO-12** on both wild-type TbMCA2 and the calcium-binding site mutant TbMCA2 D189/190A. This analysis was carried out using both the wild-type enzyme and the catalytically inactive TbMCA2 D189A/D190A mutant, which lacks the calcium-binding site. Interestingly, compound **AO-12** modulates the intrinsic fluorescence of wild-type TbMCA2 in a dose-dependent manner, with a dissociation constant (K_D) closely approximating the K_i value, at approximately 2.6 ± 0.21 μM (Fig. 6A). The modification observed in intrinsic fluorescence was similar to that observed with calcium interaction [15]. However, **AO-12** did not elicit any change in the intrinsic fluorescence of the TbMCA2 D189A/D190A mutant, which lacks the calcium-binding site (Fig. 6B).

3.5. Molecular docking studies

To verify the affinity of oxime derivatives that showed promising inhibitory potential against *Trypanosoma brucei* metacaspase-2 (TbMCA2), molecular docking studies were conducted for these compounds, with affinity energy results presented in Table 2. Compound **AO-7** exhibited the best affinity energy value of −7.0 kcal/mol. The main intermolecular interactions observed between the ligand and TbMCA2 included two hydrogen bond interactions with residues Arg^{44} and Arg^{243}, salt bridge interactions with residues Asp^{173}, Asp^{189}, Asp^{190}, and Asp^{220}, as well as a Pi-Alkyl interaction with residue His^{193}. Compound **AO-12** showed an affinity energy value of −6.3 kcal/mol, with four hydrogen bond interactions with amino acid residues Ile^{218}, Met^{219}, Asp^{220}, and Arg^{243}, along with a Pi-Alkyl interaction with residue Ile^{218} and an Alkyl interaction with residue Ile^{242}. Compound **EO-20** exhibited a binding energy of −6.1 kcal/mol, forming two hydrogen bond interactions with residues Ile^{218} and Asp^{220}. Additionally, it demonstrated a Pi-anion interaction with residue Asp^{220} and an Alkyl interaction with residue Ile^{242}, illustrating a diverse and robust binding profile. Fig. 7 highlights the principal ligand-enzyme interactions in TbMCA2, underscoring how the observed affinity could potentially translate into inhibitory activity.

4. Discussion

Trypanosomatids belong to the Kinetoplastida order, with certain species acting as pathogens responsible for neglected diseases such as Chagas disease, sleeping sickness, and various forms of leishmaniasis. Despite the availability of chemotherapies for these diseases for many years, no vaccines are available against these protozoa. However, these drugs have limitations, as they can be toxic and may cause unpleasant side effects [7,28–30].

Numerous efforts have been made to identify novel therapeutic

targets, with proteolytic enzymes emerging as potential candidates for developing new drugs aimed at treating trypanosomiasis [31,32]. In recent years, metacaspases have proven significant in various cellular processes within trypanosomatid parasites. These enzymes play crucial roles in cell cycle progression, differentiation, and homeostasis, all of which are vital for cell survival and development [11,13,33–36]. Initial evidence highlighting the involvement of metacaspases in a programmed cell death pathway was observed in yeast [31]. Given their role in cell death pathways, metacaspases are an appealing target in the realm of medically significant trypanosomatids.

It has been reported that *Trypanosoma brucei* harbors five metacaspase genes (TbMCA1 – TbMCA5), with three of these metacaspases being essential for the survival of the bloodstream form of the parasite [13].

A set of 17 synthetic oximic compounds was tested at a concentration of 10 μM against TbMCA2. All compounds demonstrated the ability to inhibit TbMCA2 activity (Fig. 1), with **AO-7**, **AO-12**, and **EO-20** exhibiting over 65 % inhibition of enzyme activity. These compounds were further assessed and displayed IC_{50} values of 3.31 ± 0.25 μM, 2.52 ± 0.19 μM, and 5.30 ± 0.83 μM, respectively (Table 1). Notably, these values were lower than those reported by Pérez et al., whose study indicated an IC_{50} of 49.2 μM for HTS01959, which exhibits non-competitive inhibition against TbMCA2 [32].

We are the first to describe micromolar inhibitors for *T. brucei* metacaspase and to test the inhibition mechanisms for these compounds. **AO-7** and **EO-20** exhibit a mixed inhibition mechanism, with an αK_i value higher than the K_i value, suggesting that TbMCA2 prefers to interact with the enzyme-substrate complex. Notably, TbMCA2 is a cytosolic metacaspase in *T. brucei*, and its activity is calcium-dependent. Calcium activation could lead to TbMCA2 processing after two lysine residues (Lys^{55} and Lys^{268}), with the residues formed during processing remaining associated in the autoprocessed form of TbMCA2 [9,14]. The structure of TbMCA2 shows that its N-terminal region encircles the protein and crosses over the active site, obstructing the S_1 pocket [10]. Therefore, our data suggest that **AO-7** and **EO-20** interact with the processed form of TbMCA2. There is no data indicating that *T. cruzi* metacaspases undergo any autoprocessing *in vivo* or *in vitro* [26]. TbMCA2, similar to *T. cruzi* metacaspases, has not been detected undergoing processing *in vivo*, which is intriguing because, as noted above, *in vitro*, the autoprocessing of TbMCA2 is readily detected [11].

In contrast, compound **AO-12** exhibits a non-competitive inhibition mechanism, and this compound preferentially interacts with the free enzyme form in an allosteric manner. In a study using the processed form of TbMCA2, we observed intrinsic fluorescence changes based on added Ca^{2+} concentrations [16]. This titration assay revealed at least two Ca^{2+} binding sites on TbMCA2: a high-affinity calcium binding site (K_D μM) essential for TbMCA2 activity and a low-affinity calcium binding site (K_D mM) that appears to modulate TbMCA2 substrate specificity.

Here, we assessed the effect of **AO-12** on intrinsic fluorescence in TbMCA2 WT, noting that **AO-12** affects TbMCA2 with a K_D of 2.6 ± 0.2 μM, which is very similar to the K_i (Fig. 6A). To determine if this compound interacts with a calcium binding site, we examined the effect of **AO-12** on intrinsic fluorescence in the TbMCA2 D189/190A mutant. This mutant was inactive because metacaspases are highly dependent on calcium [10]. **AO-12** does not affect the intrinsic fluorescence of this mutant, indicating that the compound interacts with the free enzyme, preventing calcium from interacting with TbMCA2 and activating it (Fig. 6B). These data were corroborated by molecular docking, which showed that **AO-12** interacts with the four aspartates of the calcium binding site (Fig. 7).

5. Conclusions

In conclusion, this research represents a significant advancement in the search for potential inhibitors targeting TbMCA2, a metacaspase found in *Trypanosoma brucei*, the causative agent of African sleeping sickness. Compounds **AO-7**, **AO-12**, and **EO-20** have demonstrated considerable inhibitory potential against TbMCA2, with IC_{50} values lower than those previously reported in the literature. Notably, **AO-12** exhibited a non-competitive inhibition mechanism, suggesting a preference for allosteric interactions with the free enzyme.

Furthermore, these findings provide valuable insights into the regulation of TbMCA2 activity by calcium ions, enhancing our understanding of the fundamental interactions critical for metacaspase activation. The identification and characterization of these compounds represent key milestones in the quest for more effective therapies with reduced adverse effects for trypanosomiasis. This approach holds promise as a therapeutic strategy in a field lacking viable options, where existing treatments often face limitations due to toxicity and undesirable side effects.

Additionally, this study clarifies the complexities of metacaspase regulation across various trypanosomatid species, such as *Trypanosoma cruzi*, highlighting significant differences in autoproteolytic processing compared to TbMCA2. Understanding these distinctions is crucial for grasping variations in inhibitor sensitivity and may inform species-specific therapeutic strategies.

Overall, the findings presented here offer promising prospects for the development of novel therapeutic agents targeting metacaspases in trypanosomatids, marking a critical step forward in the fight against neglected diseases associated with these pathogens. Continued research in this area is essential to refine the efficacy and safety profiles of these compounds, with the ultimate aim of providing more accessible and effective therapeutic solutions to populations affected by these debilitating diseases.

CRediT authorship contribution statement

Laura Helena Araujo: Resources, Methodology, Investigation, Formal analysis, Data curation. **Thaynan Aparecida Bueno Chagas:** Methodology, Investigation, Formal analysis, Data curation. **Taiz Reis:** Methodology, Investigation. **João Ricardo Bueno de Morais Borba:** Methodology, Investigation, Formal analysis, Data curation. **Mariana Nascimento Romero Trujilho:** Methodology, Investigation, Formal analysis, Data curation. **Laura de Azevedo Maffeis Dalzoto:** Investigation, Data curation. **Marcelo Ferreira Marcondes:** Supervision, Project administration, Methodology, Investigation, Conceptualization. **Maria Aparecida Juliano:** Resources, Formal analysis, Data curation, Conceptualization. **Wagner Alves de Souza Júdice:** Validation, Supervision, Resources, Project administration. **Márcia Paranho Veloso:** Validation, Methodology, Data curation, Conceptualization. **Maurício Ferreira Marcondes Machado:** Writing – review & editing, Writing – original draft, Resources, Project administration, Funding acquisition, Formal analysis, Data curation, Conceptualization.

Declaration of competing interest

The authors declare that they have no known competing financial interests or personal relationships that could have appeared to influence the work reported in this paper.

Acknowledgements

This work was supported by FAPESP grants 2022/06394-0 to MFMM, 2019/27813-8 to MFM, and 2021/01503-2 to WASJ. LHA, TRS, and MNRT were supported by CAPES scholarships. We would like to acknowledge Prof. Jeremy C. Mottram from The Wellcome Trust Centre for Molecular Parasitology for providing the TbMCA2 WT and TbMCA2 D189/190A samples.

References

[1] M. Rottenberg, S. Magez, M. Duszenko, P.G.E. Kennedy, J. Rodgers, Clinical and neuropathogenetic aspects of human african trypanosomiasis, Frontiers in Immunology | Www.Frontiersin.Org 1 (2019) 39, https://doi.org/10.3389/fimmu.2019.00039.

[2] P.G.E. Kennedy, Clinical features, diagnosis, and treatment of human African trypanosomiasis (sleeping sickness), Lancet Neurol. 12 (2013) 186–194, https://doi.org/10.1016/S1474-4422(12)70296-X.

[3] P.G.E. Kennedy, Human African trypanosomiasis of the CNS: current issues and challenges, J. Clin. Invest. 113 (2004) 496–504, https://doi.org/10.1172/JCI200421052.

[4] P.G.E. Kennedy, The continuing problem of human African trypanosomiasis (sleeping sickness), Ann. Neurol. 64 (2008) 116–126, https://doi.org/10.1002/ANA.21429.

[5] D. Sudarshi, S. Lawrence, W.O. Pickrell, V. Eligar, R. Walters, S. Quaderi, A. Walker, P. Capewell, C. Clucas, A. Vincent, F. Checchi, A. MacLeod, M. Brown, Human African trypanosomiasis presenting at least 29 years after infection–what can this teach us about the pathogenesis and control of this neglected tropical disease? PLoS Negl Trop Dis 8 (2014) https://doi.org/10.1371/JOURNAL.PNTD.0003349.

[6] B. Pérez, L.A. Bouvier, J.J. Cazzulo, F. Agüero, E. Salas-Sarduy, V.E. Alvarez, Screening and identification of metacaspase inhibitors: evaluation of inhibition mechanism and trypanocidal activity, Antimicrob. Agents Chemother. 65 (2021), https://doi.org/10.1128/AAC.01330-20.

[7] W.A.S. Judice, L.S. Ferraz, R. de M. Lopes, L. dos S. Vianna, F. da S. Siqueira, J.F. Di Iorio, L. de A.M. Dalzoto, M.N.R. Trujilho, T. dos R. Santos, M.F.M. Machado, T. Rodrigues, Cysteine proteases as potential targets for anti-trypanosomatid drug discovery, Bioorg. Med. Chem. 46 (2021) 116365, https://doi.org/10.1016/J.BMC.2021.116365.

[8] D. Vercammen, B. Van De Cotte, G. De Jaeger, D. Eeckhout, P. Casteels, K. Vandepoele, I. Vandenberghe, J. Van Beeumen, D. Inzé, F. Van Breusegem, Type II metacaspases Atmc4 and Atmc9 of Arabidopsis thaliana cleave substrates after arginine and lysine, J. Biol. Chem. (2004), https://doi.org/10.1074/jbc.M406329200.

[9] E.A. Minina, J. Staal, V.E. Alvarez, J.A. Berges, I. Berman-Frank, R. Beyaert, K. D. Bidle, F. Bornancin, M. Casanova, J.J. Cazzulo, C.J. Choi, N.S. Coll, V.M. Dixit, M. Dolinar, N. Fasel, C. Funk, P. Gallois, K. Gevaert, E. Gutierrez-Beltran, S. Hailfinger, M. Klemenčič, E.V. Koonin, D. Krappmann, A. Linusson, M.F. M. Machado, F. Madeo, L.A. Megeney, P.N. Moschou, J.C. Mottram, T. Nyström, H. D. Osiewacz, C.M. Overall, K.C. Pandey, J. Ruland, G.S. Salvesen, Y. Shi, A. Smertenko, S. Stael, J. Ståhlberg, M.F. Suárez, M. Thome, H. Tuominen, F. Van Breusegem, R.A.L. van der Hoorn, A. Vardi, B. Zhivotovsky, E. Lam, P.V. Bozhkov, Classification and nomenclature of metacaspases and paracaspases: No more confusion with caspases, Mol Cell (2020), https://doi.org/10.1016/j.molcel.2019.12.020.

[10] K. McLuskey, J. Rudolf, W.R. Proto, N.W. Isaacs, G.H. Coombs, C.X. Moss, J. C. Mottram, Crystal structure of a Trypanosoma brucei metacaspase, Proc Natl Acad Sci U S A (2012), https://doi.org/10.1073/pnas.1200885109.

[11] C.X. Moss, G.D. Westrop, L. Juliano, G.H. Coombs, J.C. Mottram, Metacaspase 2 of Trypanosoma brucei is a calcium-dependent cysteine peptidase active without processing, FEBS Lett. (2007), https://doi.org/10.1016/j.febslet.2007.11.009.

[12] J.C. Mottram, M.J. Helms, G.H. Coombs, M. Sajid, Clan CD cysteine peptidases of parasitic protozoa, Trends Parasitol. (2003), https://doi.org/10.1016/S1471-4922(03)00038-2.

[13] M.J. Helms, A. Ambit, P. Appleton, L. Tetley, G.H. Coombs, J.C. Mottram, Bloodstream form Trypanosoma brucei depend upon multiple metacaspases associated with RAB11-positive endosomes, J. Cell Sci. (2006), https://doi.org/10.1242/jcs.02809.

[14] A. Szallies, B.K. Kubata, M. Duszenko, A metacaspase of Trypanosoma brucei causes loss of respiration competence and clonal death in the yeast Saccharomyces cerevisiae, FEBS Lett. 517 (2002) 144–150, https://doi.org/10.1016/S0014-5793(02)02608-X.

[15] W.R. Proto, E. Castanys-Munoz, A. Black, L. Tetley, C.X. Moss, L. Juliano, G. H. Coombs, J.C. Mottram, Trypanosoma brucei metacaspase 4 is a pseudopeptidase and a virulence factor, J. Biol. Chem. (2011), https://doi.org/10.1074/jbc.M111.292334.

[16] M.F.M. Machado, M.F. Marcondes, M.A. Juliano, K. McLuskey, J.C. Mottram, C. X. Moss, L. Juliano, V. Oliveira, Substrate specificity and the effect of calcium on Trypanosoma brucei metacaspase 2, FEBS J. 280 (2013), https://doi.org/10.1111/febs.12248.

[17] J.M. Gilio, M.F. Marcondes, D. Ferrari, M.A. Juliano, L. Juliano, V. Oliveira, M.F. M. Machado, Processing of metacaspase 2 from Trypanosoma brucei (TbMCA2) broadens its substrate specificity, Biochim Biophys Acta Proteins Proteom 1865 (2017), https://doi.org/10.1016/j.bbapap.2017.01.002.

[18] L. de A.M. Dalzoto, M.N.R. Trujilho, T. dos R. Santos, J.P.M.S. Costa, A.C. M. Duarte, W.A. de S. Judice, M.F. Marcondes, M.F.M. Machado, Metacaspase of Saccharomyces cerevisiae (ScMCA-Ia) presents different catalytic cysteine in a processed and non-processed form, Biochem. Biophys. Res. Commun. (2023) 149185, https://doi.org/10.1016/J.BBRC.2023.149185.

[19] R. Prichard, C. Ménez, A. Lespine, Moxidectin and the avermectins: consanguinity but not identity, Int J Parasitol Drugs Drug Resist (2012), https://doi.org/10.1016/j.ijpddr.2012.04.001.

[20] C.M. Coelho, T. Dos Santos, P.G. Freitas, J.B. Nunes, M.J. Marques, C.G. D. Padovani, W.A.S. Júdice, I. Camps, N.J.F. Da Silveira, D.T. Carvalho, M. P. Veloso, Design, synthesis, biological evaluation and molecular modeling studies of novel eugenol esters as leishmanicidal agents, J. Braz. Chem. Soc. (2018), https://doi.org/10.21577/0103-5053.20170192.

[21] I. Cortés, T.S. Kaufman, A.B.J. Bracca, A convenient and eco-friendly cerium(III) chloride-catalysed synthesis of methoxime derivatives of aromatic aldehydes and ketones, R. Soc. Open Sci. (2018), https://doi.org/10.1098/rsos.180279.

[22] J.D.P. Araújo, C.A. Grande, A.E. Rodrigues, Vanillin production from lignin oxidation in a batch reactor, Chem. Eng. Res. Des. (2010), https://doi.org/10.1016/j.cherd.2010.01.021.

[23] A.F.M. Cláudio, M.G. Freire, C.S.R. Freire, A.J.D. Silvestre, J.A.P. Coutinho, Extraction of vanillin using ionic-liquid-based aqueous two-phase systems, Sep. Purif. Technol. (2010), https://doi.org/10.1016/j.seppur.2010.07.007.

[24] D. Jadhav, R. BN, P.R. Gogate, V.K. Rathod, Extraction of vanillin from vanilla pods: a comparison study of conventional soxhlet and ultrasound assisted extraction, J. Food Eng. (2009), https://doi.org/10.1016/j.jfoodeng.2009.02.007.

[25] B.R. Torres, B. Aliakbarian, P. Torre, P. Perego, J.M. Domínguez, M. Zilli, A. Converti, Vanillin bioproduction from alkaline hydrolyzate of corn cob by Escherichia coli JM109/pBB1, Enzyme Microb Technol (2009), https://doi.org/10.1016/j.enzmictec.2008.10.003.

[26] M. Sirajuddin, S. Ali, F.A. Shah, M. Ahmad, M.N. Tahir, Potential bioactive Vanillin-Schiff base di- and tri-organotin(IV) complexes of 4-((3,5-dimethylphenylimino)methyl)-2-methoxyphenol: synthesis, characterization and biological screenings, J. Iran. Chem. Soc. (2014), https://doi.org/10.1007/s13738-013-0301-x.

[27] I.Y. Hirata, M.H. Sedenho Cezari, C.R. Nakaie, P. Boschcov, A.S. Ito, M.A. Juliano, L. Juliano, Internally quenched fluorogenic protease substrates: solid-phase synthesis and fluorescence spectroscopy of peptides containing ortho-aminobenzoyl/dinitrophenyl groups as donor-acceptor pairs, Lett. Pept. Sci. (1995), https://doi.org/10.1007/BF00119771.

[28] E. Schwartz, Tropical diseases in travelers, J Travel Med 17 (2010), https://doi.org/10.1111/J.1708-8305.2010.00459.X, 432–432.

[29] M.P. Barrett, R.J.S. Burchmore, A. Stich, J.O. Lazzari, A.C. Frasch, J.J. Cazzulo, S. Krishna, The trypanosomiases, Lancet 362 (2003) 1469–1480, https://doi.org/10.1016/S0140-6736(03)14694-6.

[30] B.L. Herwaldt, Leishmaniasis, Lancet 354 (1999) 1191–1199, https://doi.org/10.1016/S0140-6736(98)10178-2.

[31] F. Madeo, E. Herker, C. Maldener, S. Wissing, S. Lächelt, M. Herlan, M. Fehr, K. Lauber, S.J. Sigrist, S. Wesselborg, K.U. Fröhlich, A caspase-related protease regulates apoptosis in yeast, Mol Cell (2002), https://doi.org/10.1016/S1097-2765(02)00501-4.

[32] B. Pérez, L.A. Bouvier, J.J. Cazzulo, F. Agüero, E. Salas-Sarduy, V.E. Alvarez, Screening and identification of metacaspase inhibitors: evaluation of inhibition mechanism and trypanocidal activity, Antimicrob. Agents Chemother. 65 (2021), https://doi.org/10.1128/AAC.01330-20.

[33] M. Laverrière, J.J. Cazzulo, V.E. Alvarez, Antagonic activities of Trypanosoma cruzi metacaspases affect the balance between cell proliferation, death and differentiation, Cell Death Differ. (2012), https://doi.org/10.1038/cdd.2012.12.

[34] N. Watanabe, E. Lam, Calcium-dependent activation and autolysis of arabidopsis metacaspase 2d, J. Biol. Chem. (2011), https://doi.org/10.1074/jbc.M110.194340.

[35] G. Kosec, V.E. Alvarez, F. Agüero, D. Sánchez, M. Dolinar, B. Turk, V. Turk, J. J. Cazzulo, Metacaspases of Trypanosoma cruzi: possible candidates for programmed cell death mediators, Mol. Biochem. Parasitol. 145 (2006), https://doi.org/10.1016/j.molbiopara.2005.09.001.

[36] R. Dixit Vandana, R. Tiwari, A. Katyal, K.C. Pandey, Metacaspases: potential drug target against Protozoan parasites, Front. Pharmacol. 10 (2019), https://doi.org/10.3389/FPHAR.2019.00790.

ANEXO IV

N-terminal of metacaspase of *Candida albicans* as essential for calcium interaction.

Taiz dos Reis Santos [a,#], Mariana Nascimento Romero Trujilho [a,#], João Pedro Martins Silva Costa [a], Laura de Azevedo Maffeis Dalzoto [a], Ane Caroline Moreira Duarte [b], Ana Júlia de Oliveira Machado [c], Laura Helena Araujo [a], Vitória Caroline Domingues Rios [a], Tatiane Faustino de Moraes [a], Wagner Alves de Souza Judice [a], Marcelo Ferreira Marcondes [c] and Maurício Ferreira Marcondes Machado [a, b, *].

[a] Interdisciplinary Center for Biochemical Research, University of Mogi das Cruzes, Av Dr. Cândido Xavier de Almeida e Souza, 200, 08780-991, Mogi das Cruzes, Brazil.

[b] Technological Research Center, University of Mogi das Cruzes, Av Dr. Cândido Xavier de Almeida e Souza, 200, 08780-991, Mogi das Cruzes, Brazil.

[c] Department of Biophysics, São Paulo Federal University, Rua Pedro de Toledo, 669, 7º floor, 04039-032, São Paulo. Brazil.

[#] Both authors contribute equally for this work

***Corresponding author:**

Maurício Ferreira Marcondes Machado, Ph.D.

Mail address: mauriciomachado@umc.br

Interdisciplinary Center for Biochemical Research

University of Mogi das Cruzes

Av. Dr. Cândido Xavier de Almeida e Souza, 200 - 08780-991 - Mogi das Cruzes, Brazil.

Author contributions:

TRS, MNRT, JPMSC, MFM and AJOM – cloning expression and purification of CaMCA-Ia and CaMCA-Ia-ΔN86

TRS, MNRT, LAMD, LHA and VCDR – autoprocessing experiments

WASJ, ACMD and TFM – analysis of intrinsic fluorescence

MFMM – design of experimental procedures and writing the manuscript.

ABSTRACT

Metacaspases are of CD clan members and share structural similarities with mammalian caspases but possess unique features. This study delves into Candida albicans metacaspase CaMCA-Ia, a type I metacaspase. CaMCA-Ia demonstrates Ca^{2+}-dependent autoprocessing and presents on the hydrophobic N-terminal different from type II metacaspases. Truncated CaMCA-Ia (CaMCA-Ia-ΔN86), lacking 86 N-terminal amino acids, undergoes gradual self-processing and intermolecular processing. Calcium addition induces multistep processing, leading to maturation. Like mammalian caspases, CaMCA-Ia-ΔN86 can activate others, indicating intermolecular activation and accelerating maturation. Distinct binding sites for full-length and truncated forms in CaMCA-Ia interaction with Ca^{2+} underscore the N-terminal role in altering calcium affinity. These findings enhance understanding of metacaspases intricate activation and maturation dynamics, offering insights into potential drug targets for pathogenic fungi. The CaMCA mutants D252A, D268A, D299A, and D268/269A display varied responses to calcium, while the corresponding CaMCA-Ia-ΔN86 mutants exhibit different processing patterns. The D268/299A mutant showed processing after 48 h of incubation with calcium. Alterations in CaMCA structure and function, such as deletion of the N-terminus and changes in aspartates at the calcium site, provide important insights into how CaMCA enzymatic activity and autoprocessing are regulated.

Keywords: Metacaspase, N-terminal, Mutants, Autoprocessing, Calcium interaction

Running Title: Calcium interaction depends on presence of N-terminal at CaMCA-Ia.

Abreviations: CaMCA-Ia – *Candida albicans* metacaspase; TbMCA-IIa – *Trypanosoma brucei* metacaspase 2.

1. INTRODUCTION

Metacaspases are proteases found in simple eukaryotic cells; these enzymes are cysteine proteases belonging to the CD clan of C14 proteases [1]. Metacaspases presents two subdomains: a small one (P_{10}) and a large one (P_{20}), and they don't have any additional domains [2]. Interestingly, these enzymes are structural closely related with mammalian caspases and feature a Cys/His catalytic dyad. However, they exhibit an affinity for basic residues (Arg or Lys) at the P_1 position [3–5].

Structural differences are observed among metacaspases, classifying them into type I, II or III. Yeast metacaspases belong to type I, characterized by a N-terminal pro-domain rich in glutamine and arginine, along with a repeated sequence of proline [1,2,6]. Metacaspases are a calcium-dependent enzymes, and this ion plays a crucial role in both auto-processing events and the catalytic activity of these enzymes [5,7–9].

While metacaspases share structural similarities with caspases, they display distinctive biochemical characteristics. Metacaspases exhibit a P_1 specificity for basic residues (Arg or Lys) [10] and are expressed as active monomers, necessitating an autoprocessing event for both activation and substrate selection [5,8,9]. The calcium-dependent activity of *Trypanosoma brucei* metacaspase 2 (TbMCA-IIa) involves autoprocessing at two distinct sites: one at the N-terminal following the Lys^{55} residue and another at the C-terminal after the Lys^{288} residue. This results in a three-peptide chain that remains associated [7].

The intrinsic correlation between autoprocessing and the activity of metacaspases is associated with the concentration of Ca^{2+} and is characterized by two dissociation constants. One, with higher affinity, is crucial for the autoprocessing event, while the other, with lower affinity, plays a pivotal role in substrate specificity [5,9]. Calcium as important to release the autoprocessing of metacaspases, to reorder the N-terminal and C-terminal [7,9].

Since of the discovery of metacaspases, these enzymes have been shown to essential for physiological and pathological conditions in simple eukaryotic cells [1,2]. The metacaspase of *Saccharomyces cerevisiae* (YCA1 or ScMCA-Ia) is the most studied among metacaspases. The initial description indicates that this enzyme participates in the programmed cell death (PCD), as is also crucial for regulating the cell cycle of *S. cerevisiae*, and their inactivation stretches the G_1 phase [11].

YCA1 as involved in the remodeling of insoluble protein aggregates [12], and the overexpression of this enzyme reduces protein aggregates, prolonging the lifetime of this yeast [10]. The metacaspase of *S.cerevisiae* presents two cysteine residues that, in response to structural modifications induced by calcium, act in auto-processing events [13].

Candida albicans metacaspase (CaMCA-Ia) is very similar to YCA1, as observed with this enzyme, CaMCA-Ia participates in PCD in response to different stimulus such as exposure to hydrogen peroxide, acetic acid, and amphotericin B [14–18]. Numerous research demonstrates that certain antifungal and another pharmacological drug classes activate intracellular metacaspases in *C. albicans*, indicating that this enzyme is an interestingly target for new drugs discovery [17,19–22].

Investigation of the expression and maturation dynamics of Candida albicans metacaspase CaMCA-Ia, a type I metacaspase, was observed that unprocessed CaMCA-Ia transforms into processed forms during purification, reaching its mature state after a second processing event triggered by $CaCl_2$. Indee, metacaspase of *Candida glabrata* shows is calcium dependent and this is a slower and gradual process, that occurs after 8 days of incubation with calcium for CgMCA-Ia be completed process [23].

The Ca^{2+}-dependent autoprocessing of CaMCA-Ia involves both faster and slower events. A distinctive feature of type I metacaspases is the hydrophobic N-terminal, in this study we produced a truncated form of CaMCA-Ia without 86 aminoacids (CaMCA-Ia-ΔN86), this enzyme undergoes self-processing, with calcium inducing multiple processing steps, culminating in the mature form. Notably, CaMCA-Ia-ΔN86 exhibits intermolecular processing, suggesting a cascade of activation like mammalian caspases.

Distinct binding sites for full-length and truncated forms in CaMCA-Ia interaction with Ca^{2+} underscore the N-terminal role in altering calcium affinity. These findings enhance understanding of metacaspases' intricate activation and maturation dynamics, offering insights into potential drug targets for pathogenic fungi. The CaMCA mutants D252A, D268A, D299A, and D268/269A display varied responses to calcium, while the corresponding CaMCA-Ia-ΔN86 mutants exhibit different processing patterns.

The study also delves into the calcium interaction of full-length and truncated CaMCA-Ia, revealing differences in binding sites and dissociation constants. The findings contribute to understanding the complex activation and

maturation mechanisms of metacaspases, providing insights into potential drug targets for pathogenic fungi.

2. EXPERIMENTAL PROCEDURES

2.1. Cloning of CaMCA-Ia complete and truncated form

From a synthetic gene (Invitrogen), PCR was performed using a Pfu polymerase (Thermo). For the complete CaMCA-Ia, the forward primer (5'-ATATGCTAGCATGTTTCCTGGTCAGGGTCGTCATACCTATG -3') and reverse primer (5'-ATAGCTGAATTCTTAAAAAATAAATTGCAAGTTGGTGTCT-3') were utilized. The amplified sequence was inserted into the NheI and EcorRI sites of pET28(a)+ (Novagen).

For truncated form of CaMCA-Ia (CaMCA-Ia-ΔN86-Ia), PCR was performed using a Pfu polymerase (Thermo) with CaMCA-Ia as a template. The forward primer (5'– ATTTGCTAGCACCGATAGCCAGAGCTT TG –3') and reverse primer (5'-ATAGCTGAATTCTTAAAAAATAAATTGCAAGTTGGTGTCT-3') were used. The amplified sequence was inserted into the NheI and EcorRI sites of pET28(a)+ (Novagen). Both CaMCA-Ia and CaMCA-Ia-ΔN86 enzymes are encoding with N-terminal His-tag (6X-His).

2.2. Site direct mutagenesis of CaMCA-Ia and CaMCA-Ia-ΔN86

To introduce site-directed mutagenesis in CaMCA-Ia and CaMCA-Ia-ΔN86 (Table 1), we followed a protocol developed by Ho et al. (1989) with modifications [24]. All PCRs were carried out using Pfu polymerase (Thermo) with specific primers. The PCR products of the insert and pet28(a)+ vector was treated with 10 U/mL of T5 exonuclease in a buffer containing 500 mM Tris, 50 mM $MgCl_2$, 50 mM DTT, 0.25 g/mL PEG 800, at pH 7.0. The vector/insert proportion was 1:4 [25], and the reaction was incubated at 37°C for 3 hours. The resulting reactions were then transformed into BL21(DE3) pLysS *Escherichia coli*.

2.3. Expression of CaMCA-Ia and CaMCA-Ia-ΔN86 WT, and mutants

Bacteria containing CaMCA-Ia, as well as CaMCA-Ia-ΔN86, were initially grown in 10 mL Luria broth medium supplemented with kanamycin (50 μg/mL) and incubated at 37°C overnight (approximately 16 hours) with shaking at 150 rpm. The overnight cultures were then transferred to 1 L of LB medium at 37°C and grown until the culture density reached an A_{600} of 0.4. The temperature was them reduced to 20°C until the cell density reached an A_{600} of 0.6–0.7. Isopropyl-b-D-1-thiogalactopyranoside was added to a final concentration of 0.5 mM, and the cells were incubated at 20°C for 14–16 h before being harvested by centrifugation at 4000 x g for 10 min at 4°C. The pellet was subsequently stored at -70°C until needed.

The cell pellet was resuspended in 20 mL of 50 mM sodium phosphate pH 8.0, 500 mM NaCl, 20 mM imidazole, 1 mg/mL lysozyme. It was then incubated on ice for 30 min before the addition of 5 μg/mL RNase, 5 μg/mL DNase and 0.02% Triton X-100. The solution was further incubated for 30 min on ice before being centrifuged at 26,000 × g for 20 min at 4°C and the supernatant was recovered. Lysates were centrifuged and filtered through in 0.45 μM membrane.

2.4. Purification of CaMCA-Ia and CaMCA-Ia-ΔN86-Ia

The cell pellet was resuspended in 20 mL of solution containing 50 mM sodium phosphate at pH 8.0, 500 mM NaCl, 20 mM imidazole, and 1 mg/mL lysozyme. This mixture was incubated on ice for 30 min before the addition of 5 μg/mL RNase, 5 μg/mL DNase and 0.02% Triton X-100. After an additional 30-minute incubation on ice, the solution was centrifuged at 26,000 × g for 20

minutes at 4°C, and the supernatant was collected. Lysates were then centrifuged and filtered through a 0.45 µM membrane.

The resulting material was loaded onto a HisTrap Ni^{2+} Sepharose column (GE Healthcare) connected to an AKTA-Start chromatograph (GE Healthcare). The column had been previously equilibrated with a binding buffer consisting of 50 mM Tris at pH 7.5 and 100 mM NaCl, with a flow rate of 1.0 mL/min. The column was washed with 5 mL of binding buffer, and recombinant CaMCA-Ia and t-CaMCA-Ia were purified and eluted using a step gradient of imidazole concentrations (50, 100, 200, 300 and 500 mM) in the same buffer. The recombinant CaMCA-Ia and CaMCA-Ia-ΔN86 were found to elute between 200- and 300-mM imidazole (as confirmed by SDS/PAGE analysis), and the protein were combined.

To desalt the pooled protein, it was loaded onto a HiTrap 26/10 Desalting size-exclusion column, 5 mL (GE Healthcare) and equilibrated in a buffer containing 50 mM Tris at pH 7.4 and 100 mM NaCl (NaCl/Tris buffer). Elution fractions were analyzed using SDS/PAGE, and the fractions containing pure recombinant CaMCA-Ia were collected. These fractions were stored in NaCl/Tris buffer containing 30% glycerol at −20 °C. To avoid any decrease in CaMCA-Ia activity, repeated freeze-thaw cycles were consequently avoided.

2.5. Western blotting of CaMCA-Ia and CaMCA-Ia-ΔN86, WT and Mutants

CaMCA-Ia and CaMCA-Ia-ΔN86 purification and ion experiments were submitted to a western blotting assay was performed using a 6x-His-tag antibody (MA1-21315-HRP – Thermo). The SDS-PAGE gel was then transferred onto a PVDF membrane (Bio-Rad) for 5 minutes using a Trans-Blot Turbo (Bio-Rad)

following the manufacturer's instructions. The PVDF membrane was subsequently washed with a PBS buffer (10 mM Na_2HPO_4, 150 mM NaCl – pH 7.4) with the addition of 5% BSA and 0.01% Tween 20 and left to incubate for 1 hour with agitation at room temperature. Following this, the membrane was washed three times with PBS and then incubated with the 6x-His-tag antibody (Thermo), which was diluted to a ratio of 1:30,000 in PBS with 5% BSA and 0.01% Tween 20. This incubation took place for 18 hours at 4°C with constant agitation. After the antibody incubation, the membrane was washed with PBS and subsequently developed using SuperSignal-West Pico (Thermo) in a photodocumentator ChemiDoc MP Imaging System (Bio-Rad).

2.6. Calcium effects on autoprocessing of CaMCA-Ia and CaMCA-Ia-ΔN86, WT and mutants

For this assay, CaMCA-Ia and CaMCA-Ia-ΔN86, along with their respective mutants, were incubated with different concentrations calcium (0 to 15 mM) and 5 mM dithiothreitol at 25 °C in a 50 mM TRIS buffer containing 150 mM NaCl, pH 7.4, for 96 hours, aliquots were collected every 24 hours, and were analyzed the protease maturation capacity across different salt concentrations using 15% SDS-PAGE electrophoresis. As a control, we incubated the protease in the presence of 5 mM EGTA and the protease alone in assay buffer without additional calcium. We analyzed the protease maturation capacity across different Ca^{2+} concentrations using 15% SDS-PAGE electrophoresis

2.7. The effect $CaCl_2$ on the intrinsic fluorescence of CaMCA-Ia and CaMCA-Ia-ΔN86-Ia

Structural changes in CaMCA-Ia and CaMCA-Ia-ΔN86 at final concentrations of 2 µM were studied by monitoring the intrinsic fluorescence in 50 mM Tris/HCl at pH 8.5 with the addition of varying concentrations of $CaCl_2$ (10 µM – 30 mM). The emission spectra were collected in the range of 300-400 nm at 25ºC using a fixed excitation wavelength of 280 nm (2.5-nm slit width for both excitation and emission). These data were analyzed using the 1-site interaction equation that describes the binding of ligands to a single site on a receptor through Grafit 5.0 software.

3. RESULTS AND DISCUSSION

In the SDS-PAGE of CaMCA-Ia expression (Figure 1A), we observed that the unprocessed form of CaMCA-Ia appears at 55 kDa (E1), while its processed form is evident at 40 kDa (E2). During purification, the protease is predominantly in its intermediate form (~40 kDa), indicating that maturation begins during the expression and purification process. However, it only reaches its mature form after a second processing event (E3) (Figure 1B), which we could only observe after incubation with 5 mM $CaCl_2$ for 72 hours (Figure 1C). The enzyme was incubated in the presence of EGTA as a negative control, and under this condition, no processing was observed even after 96 hours of incubation, indicating that maturation is dependent on Ca^{2+}.

In these data we can observed that CaMCA-Ia presents two different autoprocessing events, one faster and another slower, but both are Ca^{2+}-dependent (Figure 1C). Similar effect was demonstrated that the maturation of CgMCA-I from *Candida glabrata* is dependent on the calcium ion, and this process is slow and gradual, taking up to 8 days for the complete maturation of

the protease [23]. Other studies had already shown the importance of calcium in the activation and maturation process of type I metacaspase [8,26,27].

One of the most striking differences between metacaspases type I when compared to metacaspases type II, is the presence of the hydrophobic N-terminal [1,2]. As type I metacaspases in Arabidopsis, as well as CaMCA and YCA1, are synthesized as inactive proenzymes and are activated through self-processing. However, type II metacaspases in Arabidopsis undergo activation like effector caspases in mammals [4,28].

The N-terminal portion of the YCA1 metacaspase from the yeast S. cerevisiae holds a significant influence on the precipitation capability of this protease, given that this region is rich in glutamine and asparagine [29]. Evaluating the constitution of the N-terminal region of CaMCA-Ia, we observe that it shares important characteristics of the N-terminal region with YCA1. Faced with these facts, we charted a new path to obtain the recombinant protein with the deletion of this region (deletion of 86 amino acids at N-terminal), called truncated CaMCA-Ia (CaMCA-Ia-ΔN86) allowing us to obtain a soluble enzyme.

Processing is a typical characteristic of both caspases and metacaspases when expressed in bacteria [4]. Both type I and type II metacaspases undergo self-processing [30]. Was suggested that recombinant metacaspases may exhibit lower catalytic activity and can initiate a cascade of peptidolytic processes. Thus, when two pro-enzyme molecules are close, a slightly active pro-enzyme can cleave a second molecule [26].

It is described that mammalian caspases convert their inactive proenzymes into active peptidases through processing. Metacaspases from *Leishmania major* [31], *Arabidopsis thaliana* [4], and *S. cerevisiae* [32] also

require prior processing to be active. Metacaspases, through interaction with calcium, can self-process; however, this self-processing is not a prerequisite for their enzymatic activity [7,9]. It has been demonstrated in the metacaspase-2 of T. brucei that self-processing is an essential step in which the N-terminal is structurally relocated, exposing the catalytic residues, and favoring the action of metacaspase on protein substrates, not just on oligopeptides [9].

CaMCA-Ia-ΔN86 undergoes self-processing, which occurs slowly and gradually (72 hours), indicating that once the protease reaches maturation, it can perform intermolecular processing so that maturation occurs in others, indicating an intrinsic ability of the protease to undergo self-lytic modifications over time. With the addition of calcium (0.5 – 15 mM), CaMCA-Ia-ΔN86 seems to undergo self-processing to remove amino acid residues from the N-terminal portion, becoming more evident at 10 and 15 mM, generating bands of ~43 and ~33 kDa, with the latter being the intermediate form of the protease. The second processing of CaMCA-Ia-ΔN86 occurs after 72 hours of incubation, generating a band of ~30 kDa. This processing occurs at all concentrations of Ca^{2+}, but only at 5 mM does it occur completely, and CaMCA-Ia-ΔN86 undergoes a third self-processing, giving rise to a band of 25 kDa, which represents the mature form of CaMCA-Ia-ΔN86 (Figure 2).

Our data show that, like mammalian caspases, CaMCA-Ia-ΔN86 may undergo a cascade of activation, so that when one molecule is active, it can activate others, accelerating the protease maturation process [33]. This is an intermolecular process, different from the initial self-processing, which is an auto-processing. CaMCA-Ia-ΔN86-Ia, after self-processing, is capable of processing

other as-yet-unprocessed enzymes. A similar event was observed for the metacaspase of *Candida glabrata* [23].

CaMCA-Ia-ΔN86, after self-processing, can process other as-yet-unprocessed enzymes reinforces the idea of cooperative regulation among active molecules. This interaction between proteases may result in a coordinated activation mechanism, providing efficiency and speed in the maturation of CaMCA-Ia-ΔN86. The analogy with the event observed in the metacaspase of *Candida glabrata* [23]. The convergent data between the current study and the results obtained in a similar context strengthen the plausibility of this intermolecular activation and processing mechanism like observed with mecaspases of *C.glabrata* and *S.cerevisiae* [13,23].

To assess the interaction of CaMCA-Ia with Ca^{2+}. It has been described that TbMCA2 has two Ca^{2+} interaction sites, a high-affinity site responsible for auto-processing of TbMCA2 and a low-affinity site responsible for an allosteric effect on the enzyme structure, affecting its affinity for different substrates. Like what was observed for TbMCA2, the full-length CaMCA-Ia showed two inflection points: one of high affinity (K_{D1} = 7 μM) and one of low affinity (K_{D2} = 7.65 mM) (Figure 3A). Interestingly, we found that after the addition of 30 mM ethylene-glycol-bis(β-aminoethyl)-tetra-acetic acid (EGTA), a specific calcium chelator, the effect of this ion on the structure of full-length CaMCA-Ia was completely reversed (Figure 3B). The reversal of the Ca^{2+} effect on metacaspase structure by a chelating agent for this ion has been described for various metacaspases. Therefore, this data supports that full-length CaMCA-Ia was expressed in a structured form [5,9,34].

For CaMCA-Ia-ΔN86-Ia, unlike what was observed for TbMCA2 and full-length CaMCA-Ia, CaMCA-Ia-ΔN86 showed only the low-affinity calcium binding site (K_D = 5.08 mM) (Figure 4A). The addition of 30 mM ethyleneglycol-bis(β-aminoethyl)-tetraacetic acid (EGTA), a specific calcium chelator, did not completely reverse the effect of this ion on the structure of CaMCA-Ia-ΔN86 (Figure 4B). The notable difference in K_D values between full-length CaMCA-Ia and CaMCA-Ia-ΔN86 can be justified by the removal of the N-terminal portion through truncation of CaMCA. This removal can directly influence the protein's affinity for calcium ions, leading to differences in dissociation constants.

This removal may have caused a change in the exposure of Ca^{2+} binding sites due to alterations in the three-dimensional arrangement of amino acid residues comprising the Ca^{2+} binding site. It could have resulted in changes in interactions with calcium ions and, consequently, in CaMCA-Ia-ΔN86-Ia response to the presence of these ions. It is worth noting that since the removal of the N-terminal can also affect the ability of CaMCA-Ia-ΔN86 to undergo allosteric changes in response to calcium ion binding, this would justify the differences in the reversal of effects by EGTA between full-length CaMCA-Ia and CaMCA-Ia-ΔN86-Ia.

In comparison with YCA1 structure, CaMCA-Ia presents four asparagine residues conserved of calcium binding site on YCA1 Asp^{236}, Asp^{252}, Asp^{253} and Asp^{283}, that corresponds to CaMCA-Ia Asp^{252}, Asp^{268}, Asp^{269} and Asp^{299}, we produced mutants for these residues changed by alanine for both enzymes CaMCA-Ia and CaMCA-Ia-ΔN86, and a double mutant D268/269A cause the experiments for YCA1 shows that deletion of these two residues inactivated this metacaspase [27].

Each mutated amino acid had a distinct impact on CaMCA-Ia autoprocessing. Mutants at residues Asp^{268}, Asp^{299}, and the double mutant $Asp^{268/269}$ of CaMCA-Ia showed a negative influence on CaMCA-Ia activation capacity, evidenced by reduced protease autoprocessing ability. Only the Asp^{268} mutant and the $Asp^{268/269}$ double mutant exhibited a ~14 kDa fragment not observed in CaMCA-Ia WT (Figure 5A). This phenomenon becomes even more evident when comparing the band profiles of mutants with intact CaMCA. Only the Asp^{269} mutant displayed an activation and autoprocessing process like intact CaMCA-Ia. Despite a noticeable decrease in activation and autoprocessing capacity, the Asp^{252} mutant exhibited a processing profile with low molecular weight bands (Figure 5A).

The effect of mutations on CaMCA-Ia-ΔN86 autoprocessing was more evident. Mutants D268A, D252A, D299A, and D268/268A showed a greater reduction in autoprocessing, evidenced by decreased formation of the processed fragment (~33 kDa). Meanwhile, the D269A mutant exhibited a processing profile like that of CaMCA-Ia-ΔN86 (Figure 5B). Like the D268A mutant and the D268/269 double mutant of CaMCA-Ia (Figure 5A), mutants in CaMCA-Ia-ΔN86 (D268A, D269A, D252A, and D299A) also displayed a low molecular weight fragment (~14 kDa - Figure 5B).

The results obtained from Western blot analysis revealed that mutations in the aspartate residues affected CaMCA-Ia and CaMCA-Ia-ΔN86 autoprocessing differently (Figure 5C and 5D). All mutants showed both processed and unprocessed fractions, indicating autoprocessing occurred at the C-terminal. However, CaMCA-Ia-ΔN86 D268A did not exhibit the detected processed fraction, suggesting that the initial processing in this mutant occurred

at the N-terminal of the protein, as evidenced by the visible fragment on SDS-PAGE (Figure 5B and 5D).

The effect of Ca^{2+} on CaMCA-Ia autoprocessing and activation was tested in the presence of Ca^{2+} (5mM) over 96 hours, resulting in the formation of a ~30 kDa molecular weight fragment. This indicates protein activation and processing, confirming a direct relationship between Ca^{2+} presence and CaMCA-Ia activation (Figure 6). Initially, the CaMCA-Ia D252A mutant did not respond to Ca^{2+} stimulation during the initial incubation time. However, after 96 hours, activation occurred, resulting in a smaller fragment (~30 kDa), like what is observed for CaMCA-Ia WT. The reduced response time of the D252A mutant to Ca^{2+} may be due to structural or functional changes caused by the mutation. Initially, the mutated CaMCA-Ia may not effectively interact with Ca^{2+}, resulting in a lack of response during the initial incubation period. However, prolonged exposure may lead to structural reorganization, allowing activation like on intact CaMCA-Ia. Mutants D268A, D299A, and D268/269A did not exhibit processing in the presence of Ca^{2+}, indicating a failure in activation in response to Ca^{2+} stimulation.

This highlights the critical role of Asp^{268}, Asp^{299}, and the interaction between Asp^{268} and Asp^{269} in CaMCA-Ia ability to respond to Ca^{2+} stimuli. The data demonstrate that asparagines at positions 268 and 299 are in regions crucial for Ca^{2+} binding (Figure 6). These data shows that CaMCA-Ia are different of TbMCA2 (Asp^{189} and Asp^{190}) and YCA1 (Asp^{252} and Asp^{253}), that presents residues corresponding to Asp^{268} and Asp^{269} as crucial for a calcium binding, indeed Asp^{269} at CaMCA-Ia does not affect the interaction of calcium with this enzyme (Figure 5A and 5C) [8,27].

Tests with the variation of $CaCl_2$ concentration were conducted to evaluate the effect of mutations; the mutants were incubated in a range from 0 to 15 mM of $CaCl_2$, using EGTA as a negative control. The effect of Ca^{2+} on autoprocessing was assessed in 15% SDS-PAGE (Figure 6). The D252A mutant (Figure 6A) did not show any effect from Ca^{2+} at the initial incubation time; however, after 96 hours, this mutant underwent autoprocessing, resulting in a smaller fragment (~30 kDa) like what is observed for CaMCA-Δ86 after 24 hours of incubation with Ca^{2+} (Figures 5B and 5D). Although processing occurred in the positive control, this effect was less pronounced compared to the presence of Ca^{2+}. Processing occurred at all concentrations of Ca^{2+}. The mutants D268A, D299A, and D268/269A (Figure 6) did not show processing in the presence of Ca^{2+}, while the D269A mutant was completely degraded after the initial addition of Ca^{2+} (data not shown).

Were observed that the effect of $CaCl_2$ with the mutants of CaMCA-Ia-Δ86, mutant D252A showed immediate processing (zero incubation time) at concentrations of 10 and 15 mM of Ca^{2+}, like what was observed for CaMCA-Ia-Δ86 at the same incubation time. After 72 hours, we confirmed processing at all tested concentrations of Ca^{2+}, with evidence of both the first and second processing (Figure 7). The D269A mutant demonstrated processing at the start of incubation, being observed only in the presence of 15 mM of Ca^{2+}. After 72 hours of incubation, processing was observed at all tested concentrations of Ca^{2+}, being more evident at higher concentrations (10 and 15 mM), indicating a clear dependence on the concentration of Ca^{2+}. This processing profile remained stable up to 96 hours of incubation (Figure 7). The mutants D268A and D299A did not show processing at any of the tested concentrations of Ca^{2+}, even after

96 hours of incubation (Figure 7). The double mutant (D268/269A) did not demonstrate processing at the initial incubation time, and after 72 hours, the observed profile resembled that described for the D269A mutant; this profile was maintained until 96 hours (Figure 7).

The metacaspase-2 of *T.brucei* (TbMCA2) shows different responses to calcium depending on its structure. It is described that the regulation of the processing of this enzyme is time/calcium-dependent, and that its processing alters this relationship [9]. As TbMCA2 does not have a long N-terminal and processes simultaneously at both ends (N-terminal and C-terminal), it does not undergo intermolecular processing like YCA1 and the metacaspase of *C.glabrata* [13,23]. Interestingly, the data obtained with CaMCA-Ia demonstrate the participation of asparagines (252, 268, 269, and 299) in the interaction with Ca^{2+} and subsequent autoprocessing. However, the results observed with CaMCA-Ia-ΔN86 show a different behavior from that observed with CaMCA-Ia, where we see that the processing occurs more slowly and requires more time and concentration of Ca^{2+}, which resembles the data presented by Gilio *et al.* (2017) for TbMCA2.

We evaluated the interference of calcium on the mutants of CaMCA-Ia and CaMCA-Ia-ΔN86. The CaMCA-Ia D252A mutant did not show a change in intrinsic fluorescence, despite the processing data, although we observed bands resulting from self-processing in the presence of calcium, with a notable difference between the positive and negative controls, strengthening the hypothesis that the processing of CaMCA-Ia is both an intra- and intermolecular event, as observed for CgMCA-Ia [23]. However, the CaMCA-Ia mutants D268A, D269A, D268/269A, and D299A did not show a different pattern of fluorescence

in response to the variation in Ca^{2+} concentration; these mutants present only one inflection point showing only one dissociation constant, demonstrating that these residues are important for the low-affinity calcium constant (Table 2).

Interestingly, the data on the effect of calcium on the self-processing of CaMCA-Ia demonstrates that for this enzyme to process itself, it requires high concentrations of Ca^{2+} (10 mM), showing that the residues of the calcium site are important for a more effective binding of calcium and that the Asp^{252} residue is essential for the activation and self-processing of this enzyme.

The CaMCA-ΔN86 D252A, D268A, and D299A mutants exhibit only the high-affinity dissociation constant, which is curious since the CaMCA-ΔN86 WT enzyme presents only the high-affinity constant (Table 3). Therefore, after the first processing, a conformational change must occur that makes the entry of calcium into its interaction site difficult, and with the removal of these residues, the diameter of the calcium site increases, facilitating the interaction of this ion.

Interestingly, the CaMCA-ΔN86 D269A mutant has its processing completely inhibited, and conversely, the CaMCA-ΔN86 D268/269A mutant presents two inflection points, showing both dissociation constants lower than those observed for the CaMCA-Ia WT. These data suggest that after processing, the Asp^{268} and Asp^{269} residues play a fundamental role in the activation of CaMCA-Ia, as described for TbMCA2, which does not have a long and hydrophobic N-terminal [5,9].

CONCLUSIONS

In conclusion, our investigation into CaMCA-Ia reveals a complex maturation process influenced by calcium ions. The protein undergoes multiple

processing events, with an intermediate form dominating during expression and purification, culminating in its mature form after prolonged incubation with $CaCl_2$. The Ca^{2+}-dependent autoprocessing events in both fast and slow modes highlight the intricate regulatory role of calcium in the activation and maturation of CaMCA-Ia. The distinct N-terminal features shared with YCA1, and the successful generation of a truncated variant (CaMCA-Ia-ΔN86) underscore the importance of this region in modulating the enzyme's solubility and activation. The observed intermolecular self-processing capability and the cooperative regulation among active molecules further contribute to understanding the dynamic activation mechanisms of metacaspases. Additionally, the differential calcium binding characteristics between full-length and truncated forms emphasize the structural influence of the N-terminal truncation on calcium interactions.

The CaMCA-Ia mutants revealed distinct responses to calcium. The D252A mutant showed activation after 96 hours of incubation, while the D268A, D299A, and D268/269A mutants did not demonstrate any effect of calcium. The CaMCA-Ia-ΔN86 mutants also exhibited different processing patterns in response to calcium. The D252A mutant demonstrated immediate processing with 10 and 15 mM of calcium and at all concentrations after 96 hours, while the D269A mutant showed initial processing with 15 mM of calcium, remaining at all concentrations after 86 hours. The D268A and D299A mutants did not show processing, while the D268/269A mutant resembled the D269A after 96 hours.

Thes findings highlight the complex regulation of CaMCA-Ia by the presence of calcium and by the protein structure, including the N-terminal and the calcium-binding sites. The self-processing of CaMCA-Ia, influenced by calcium, is a key process that affects its enzymatic activity. We observed

differentiated responses among the mutants, indicating an interaction between specific residues and calcium. Overall, our findings shed light on the nuanced interplay between calcium, autoprocessing, and N-terminal regulation in the activation and maturation of CaMCA-Ia.

Acknowledgements

This work was supported by FAPESP grant 2022/06394-0 to MFMM, FAPESP grant 2019/ 27813-8 to MFM and FAPESP grant 2021/01503-2 to WASJ. LHA, TRS, JPMSC and MNRT was supported by CAPES scholar fellowship.

REFERENCES

[1] A.G. Uren, K. O'Rourke, L. Aravind, M.T. Pisabarro, S. Seshagiri, E. V. Koonin, V.M. Dixit, Identification of paracaspases and metacaspases: Two ancient families of caspase-like proteins, one of which plays a key role in MALT lymphoma, Mol Cell (2000). https://doi.org/10.1016/s1097-2765(00)00094-0.

[2] L. Tsiatsiani, F. Van Breusegem, P. Gallois, A. Zavialov, E. Lam, P. V. Bozhkov, Metacaspases, Cell Death Differ (2011). https://doi.org/10.1038/cdd.2011.66.

[3] J.C. Mottram, M.J. Helms, G.H. Coombs, M. Sajid, Clan CD cysteine peptidases of parasitic protozoa, Trends Parasitol (2003). https://doi.org/10.1016/S1471-4922(03)00038-2.

[4] D. Vercammen, B. Van De Cotte, G. De Jaeger, D. Eeckhout, P. Casteels, K. Vandepoele, I. Vandenberghe, J. Van Beeumen, D. Inzé, F. Van Breusegem, Type II metacaspases Atmc4 and Atmc9 of Arabidopsis thaliana cleave substrates after arginine and lysine, Journal of Biological Chemistry (2004). https://doi.org/10.1074/jbc.M406329200.

[5] M.F.M. Machado, M.F. Marcondes, M.A. Juliano, K. McLuskey, J.C. Mottram, C.X. Moss, L. Juliano, V. Oliveira, Substrate specificity and the effect of calcium on Trypanosoma brucei metacaspase 2, FEBS Journal 280 (2013). https://doi.org/10.1111/febs.12248.

[6] E.A. Minina, J. Staal, V.E. Alvarez, J.A. Berges, I. Berman-Frank, R. Beyaert, K.D. Bidle, F. Bornancin, M. Casanova, J.J. Cazzulo, C.J. Choi, N.S. Coll, V.M. Dixit, M. Dolinar, N. Fasel, C. Funk, P. Gallois, K. Gevaert, E. Gutierrez-Beltran, S. Hailfinger, M. Klemenčič, E. V. Koonin, D.

Krappmann, A. Linusson, M.F.M. Machado, F. Madeo, L.A. Megeney, P.N. Moschou, J.C. Mottram, T. Nyström, H.D. Osiewacz, C.M. Overall, K.C. Pandey, J. Ruland, G.S. Salvesen, Y. Shi, A. Smertenko, S. Stael, J. Ståhlberg, M.F. Suárez, M. Thome, H. Tuominen, F. Van Breusegem, R.A.L. van der Hoorn, A. Vardi, B. Zhivotovsky, E. Lam, P. V. Bozhkov, Classification and Nomenclature of Metacaspases and Paracaspases: No More Confusion with Caspases, Mol Cell (2020). https://doi.org/10.1016/j.molcel.2019.12.020.

[7] C.X. Moss, G.D. Westrop, L. Juliano, G.H. Coombs, J.C. Mottram, Metacaspase 2 of Trypanosoma brucei is a calcium-dependent cysteine peptidase active without processing, FEBS Lett (2007). https://doi.org/10.1016/j.febslet.2007.11.009.

[8] K. McLuskey, J. Rudolf, W.R. Proto, N.W. Isaacs, G.H. Coombs, C.X. Moss, J.C. Mottram, Crystal structure of a Trypanosoma brucei metacaspase, Proc Natl Acad Sci U S A (2012). https://doi.org/10.1073/pnas.1200885109.

[9] J.M. Gilio, M.F. Marcondes, D. Ferrari, M.A. Juliano, L. Juliano, V. Oliveira, M.F.M. Machado, Processing of metacaspase 2 from Trypanosoma brucei (TbMCA2) broadens its substrate specificity, Biochim Biophys Acta Proteins Proteom 1865 (2017). https://doi.org/10.1016/j.bbapap.2017.01.002.

[10] S.M. Hill, T. Nyström, The dual role of a yeast metacaspase: What doesn't kill you makes you stronger, BioEssays (2015). https://doi.org/10.1002/bies.201400208.

[11] R.E.C. Lee, L.G. Puente, M. Kærn, L.A. Megeney, A non-death role of the yeast metacaspase: Yca1p alters cell cycle dynamics, PLoS One (2008). https://doi.org/10.1371/journal.pone.0002956.

[12] R.E.C. Lee, S. Brunette, L.G. Puente, L.A. Megeney, Metacaspase Yca1 is required for clearance of insoluble protein aggregates, Proc Natl Acad Sci U S A (2010). https://doi.org/10.1073/pnas.1006610107.

[13] L. de A.M. Dalzoto, M.N.R. Trujilho, T. dos R. Santos, J.P.M.S. Costa, A.C.M. Duarte, W.A. de S. Judice, M.F. Marcondes, M.F.M. Machado, Metacaspase of Saccharomyces cerevisiae (ScMCA-Ia) presents different catalytic cysteine in a processed and non-processed form, Biochem Biophys Res Commun (2023) 149185. https://doi.org/10.1016/J.BBRC.2023.149185.

[14] Y.Y. Cao, S. Huang, B. Di Dai, Z.Y. Zhu, H. Lu, L.L. Dong, Y.B. Cao, Y. Wang, P.H. Gao, Y.F. Chai, Y.Y. Jiang, Candida albicans cells lacking CaMCA1-encoded metacaspase show resistance to oxidative stress-induced death and change in energy metabolism, Fungal Genetics and Biology (2009). https://doi.org/10.1016/j.fgb.2008.11.001.

[15] B. Di Dai, Y. Wang, D.D. Li, Y. Xu, R.M. Liang, L.X. Zhao, Y.B. Cao, J.H. Jia, Y.Y. Jiang, Hsp90 Is Involved in Apoptosis of Candida albicans by Regulating the Calcineurin-Caspase Apoptotic Pathway, PLoS One 7 (2012). https://doi.org/10.1371/journal.pone.0045109.

[16] H. Lu, Z.Y. Zhu, L.L. Dong, X.M. Jia, X.R. Sun, L. Yan, Y.F. Chai, Y.Y. Jiang, Y.Y. Cao, Lack of trehalose accelerates H2O2-induced Candida albicans apoptosis through regulating Ca2+ signaling pathway and

caspase activity, PLoS One (2011). https://doi.org/10.1371/journal.pone.0015808.

[17] A.J. Phillips, I. Sudbery, M. Ramsdale, Apoptosis induced by environmental stresses and amphotericin B in Candida albicans, Proc Natl Acad Sci U S A 100 (2003) 14327. https://doi.org/10.1073/PNAS.2332326100.

[18] A.J. Phillips, J.D. Crowe, M. Ramsdale, Ras pathway signaling accelerates programmed cell death in the pathogenic fungus Candida albicans, Proc Natl Acad Sci U S A 103 (2006) 726. https://doi.org/10.1073/PNAS.0506405103.

[19] B. Hao, S. Cheng, C.J. Clancy, M.H. Nguyen, Caspofungin kills Candida albicans by causing both cellular apoptosis and necrosis, Antimicrob Agents Chemother (2013). https://doi.org/10.1128/AAC.01366-12.

[20] F. Shirazi, D.P. Kontoyiannis, Micafungin triggers caspase-dependent apoptosis in Candida albicans and Candida parapsilosis biofilms, including caspofungin non-susceptible isolates, Virulence (2015). https://doi.org/10.1080/21505594.2015.1027479.

[21] X. Chen, J. Wu, L. Sun, J. Nie, S. Su, S. Sun, Antifungal Effects and Potential Mechanisms of Benserazide Hydrochloride Alone and in Combination with Fluconazole Against Candida albicans, (2021). https://doi.org/10.2147/DDDT.S336667.

[22] C. Zhang, P. Gong, R. Wei, S. Li, X. Zhang, Y. Yu, Y. Wang, The metacaspase gene family of Vitis vinifera L.: Characterization and differential expression during ovule abortion in stenospermocarpic seedless grapes, Gene (2013). https://doi.org/10.1016/j.gene.2013.06.062.

[23] L. Conchou, B. Doumèche, F. Galisson, S. Violot, C. Dugelay, E. Diesis, A. Page, A.L. Bienvenu, S. Picot, N. Aghajari, L. Ballut, Structural and molecular determinants of Candida glabrata metacaspase maturation and activation by calcium, Commun Biol 5 (2022). https://doi.org/10.1038/S42003-022-04091-4.

[24] S.N. Ho, H.D. Hunt, R.M. Horton, J.K. Pullen, L.R. Pease, Site-directed mutagenesis by overlap extension using the polymerase chain reaction, Gene 77 (1989) 51–59. https://doi.org/10.1016/0378-1119(89)90358-2.

[25] Y. Xia, K. Li, J. Li, T. Wang, L. Gu, L. Xun, T5 exonuclease-dependent assembly offers a low-cost method for efficient cloning and site-directed mutagenesis, Nucleic Acids Res 47 (2019). https://doi.org/10.1093/nar/gky1169.

[26] N. Watanabe, E. Lam, Arabidopsis metacaspase 2d is a positive mediator of cell death induced during biotic and abiotic stresses, Plant Journal (2011). https://doi.org/10.1111/j.1365-313X.2011.04554.x.

[27] A.H.H. Wong, C. Yan, Y. Shi, Crystal structure of the yeast metacaspase Yca1, Journal of Biological Chemistry (2012). https://doi.org/10.1074/jbc.M112.381806.

[28] P. V. Bozhkov, M.F. Suarez, L.H. Filonova, G. Daniel, A.A. Zamyatnin, S. Rodriguez-Nieto, B. Zhivotovsky, A. Smertenko, Cysteine protease mcII-Pa executes programmed cell death during plant embryogenesis, Proc Natl Acad Sci U S A (2005). https://doi.org/10.1073/pnas.0506948102.

[29] M. Erhardt, R.D. Wegrzyn, E. Deuerling, Extra N-terminal residues have a profound effect on the aggregation properties of the potential yeast prion

protein Mca1, PLoS One (2010). https://doi.org/10.1371/journal.pone.0009929.

[30] A. Acosta-Maspons, E. Sepúlveda-García, L. Sánchez-Baldoquín, J. Marrero-Gutiérrez, T. Pons, M. Rocha-Sosa, L. González, Two aspartate residues at the putative p10 subunit of a type II metacaspase from Nicotiana tabacum L. may contribute to the substrate-binding pocket, Planta (2014). https://doi.org/10.1007/s00425-013-1975-0.

[31] I.J. González, C. Desponds, C. Schaff, J.C. Mottram, N. Fasel, Leishmania major metacaspase can replace yeast metacaspase in programmed cell death and has arginine-specific cysteine peptidase activity, Int J Parasitol (2007). https://doi.org/10.1016/j.ijpara.2006.10.004.

[32] F. Madeo, E. Herker, C. Maldener, S. Wissing, S. Lächelt, M. Herlan, M. Fehr, K. Lauber, S.J. Sigrist, S. Wesselborg, K.U. Fröhlich, A caspase-related protease regulates apoptosis in yeast, Mol Cell (2002). https://doi.org/10.1016/S1097-2765(02)00501-4.

[33] E.A. Minina, N.S. Coll, H. Tuominen, P. V. Bozhkov, Metacaspases versus caspases in development and cell fate regulation, Cell Death Differ (2017). https://doi.org/10.1038/cdd.2017.18.

[34] M. Klemenčič, C. Funk, Evolution and structural diversity of metacaspases, J Exp Bot (2019). https://doi.org/10.1093/jxb/erz082.

Table 1. Forward and reverse primers used for the point mutations in the gene encoding CaMCA-WT.

MUTATION	SEQUENCE
D252A	**5'** TGA GGA TGA TGG CTA TGC CGA AGT GAT TTA TC **3'**
D269A	**5'** CTT TAT TAT CGA TGC TCT GCT GCA TAC CAT GA **3'**
D268A	**5'** CGG CTT TAT TAT CGC TGA TCT GCT GCA TAC CA **3'**
D268/269A	5' CGG CTT TAT TAT CGC TGC TCT GCT GCA TAC CA 3'
D299A	**5'** CGG TAG CGT TCT GGC TCT GCC GTA TAT GTA TA **3'**
C292A	**5'** CAC TGT TTG ATA GCG CTC ATA GCG GTA GCG TT **3'**

Table 2. KD values for CaMCA-Ia WT and mutants

Enzyme	K_{D1}	K_{D2}
CaMCA-Ia	7.0 μM	9.3 mM
D252A	**ND**	**ND**
D269A	3.0 μM	**ND**
D268A	0.5 μM	**ND**
D299A	1.0 μM	**ND**
D268/269A	2.3 μM	**ND**

Table 3. KD values for CaMCA-Ia-ΔN86 WT and mutants

Enzyme	K_{D1}	K_{D2}
CaMCA-Δ86	**ND**	4.0 mM
D252A	1.3 μM	**ND**
D269A	**ND**	**ND**
D268A	1.7 μM	**ND**
D299A	1.4 μM	**ND**
D268/269A	0.2 μM	2.6 mM

FIGURE LEGENDS

Figure 1. Maturation process of full-length CaMCA. (A) CaMCA-Ia purified; (B) Schematic representation of intermediate maturation forms of CaMCA-Ia starting from the unmatured form (E1), after the first cleavage (E2), and the mature form (E3); (C) Maturation of full-length CaMCA-Ia in the presence of 5 mM $CaCl_2$.

Figure 2. Maturation of CaMCA-Ia-ΔN86 in the presence of calcium. SDS-PAGE of CaMCA-Ia-ΔN86 in the presence of Ca^{2+} (0 – 15 mM) and EGTA, where (A) before incubation and (B) after 72 hours of incubation.

Figure 3. Influence of Ca^{2+} on the intrinsic fluorescence of CaMCA-Ia. (A) The graph shows changes in the maximum intensity of the fluorescence emission peak (emission wavelength of 330 nm) with increasing and (B) Fluorescence emission spectra of CaMCA-Ia (λex = 280 nm) in the absence (o) or in the presence (•) of 1 mM $CaCl_2$ or in the presence of 10 mM $CaCl_2$ (□)or in a presence of 10 mM EGTA (■).

Figure 4. Influence of Ca^{2+} on the intrinsic fluorescence of CaMCA-Ia-ΔN86. (A) The graph shows changes in the maximum intensity of the fluorescence emission peak (emission wavelength of 330 nm) with increasing and (B) Fluorescence emission spectra of CaMCA-Ia-ΔN86 (λex = 280 nm) in the absence (o) or in the presence (•) of 1 mM $CaCl_2$ or in the presence of 10 mM $CaCl_2$ (□) or in a presence of 10 mM EGTA (■).

Figure 5. Effect of mutations of calcium binding site asparagine residues (252, 268, 269 and 299) on autoprocessing at CaMCA-Ia and CaMCA-IaΔN86 WT and mutants. (A) SDS-PAGE of CaMCA-Ia WT and mutants, (B) SDS-PAGE of CaMCA-Ia-ΔN86 WT and mutants, (C) western blotting of CaMCA-Ia WT and mutants and (D) western blotting of CaMCA-Ia-ΔN86 WT and mutants.

Figure 6. Effect of calcium on autoprocessing at CaMCA-Ia D252A, D268A, D299A and D268/269A. SDS-PAGE of CaMCA-Ia mutants in different $CaCl_2$ concentrations (0-15 mM) and 30 mM of EGTA as negative control at 0 and 96 hours.

Figure 7. Effect of calcium on autoprocessing at CaMCA-Ia-ΔN86 D252A, D268A, D269A, D299A and D268/269A. SDS-PAGE of CaMCA-Ia-ΔN86 mutants in different $CaCl_2$ concentrations (0-15 mM) and 30 mM of EGTA as negative control at 0 and 96 hour